Rate-Adaptive Schemes and Capacity Issues in Wireless Systems

Sébastien de la Kethulle de Ryhove

A Dissertation Submitted in Partial Fulfillment
of the Requirements for the Degree of

DOCTOR OF PHILOSOPHY

Department of Electronics and Telecommunications
Norwegian University of Science and Technology

2007

Norwegian University of Science and Technology
Department of Electronics and Telecommunications
N-7491 Trondheim
Norway

Abstract

The present dissertation consists of a collection of five papers and an introduction. The papers are dedicated firstly to the analysis and design of efficient wireless communication systems operating over fading channels, and secondly to the information theoretic characterisation of fading channels under different sets of assumptions.

The wireless systems that are considered operate over frequency-flat, block-fading channels under the assumption that perfect channel state information (CSI) is available both at the transmitter and at the receiver. One of the issues that is addressed is the energy-efficient design of constant power link adaptation schemes in which circuit energy consumption is included in the total energy budget, and in which the system's instantaneous bit-error rate must never exceed a predefined threshold. This is done assuming that a number of different transmission schemes are available for use, and that the objective is to maximise the system's average spectral efficiency (ASE). Another issue is how to optimally choose the rates of a given finite number of capacity-achieving codes in order to maximise the ASE of dual-branch multiple-input multiple-output (MIMO) systems (that is to say, MIMO systems with either two transmit or two receive antennæ). Yet another is the derivation of expressions for the signal-to-noise ratio (SNR) distributions of the independent subchannels which can be obtained by decoupling a dual-branch MIMO channel using linear precoding and decoding, assuming that the available power is distributed among these subchannels in accordance with the *water-filling* solution. It is also shown that the knowledge of the subchannel SNR distributions can be very helpful when optimising MIMO communication systems.

The information theoretic characterisation of fading channels under different sets of assumptions is the other main concern of this thesis. The first channel that is considered from this perspective is the frequency-flat block-fading channel discussed above. The power adaptation strategy that maximises the average information rate that can be reliably transmitted over such a channel assuming the availability of perfect transmitter and re-

ceiver CSI, assuming that any transmitted codeword spans a single fading block, and assuming the input signal is subject to both average and peak power constraints is characterised by means of a theorem and numerically computed in different scenarios.

The next channel that is considered is the memoryless noncoherent Rayleigh fading channel, in which the channel state is assumed to change on a symbol-by-symbol basis. Closed-form expressions for the mutual information between the output and the input of this channel when the input magnitude distribution is discrete and restricted to having two mass points are derived, and it is shown how these expressions can be used to obtain closed-form expressions for the capacity of this channel for SNR values of up to approximately 0 dB.

The final channels to be examined are noncoherent Rayleigh-fading channels with memory, in which the channel state is once again assumed to change on a symbol-by-symbol basis, but where the fading process has memory which is modelled by an autoregressive process of arbitrary order. For such channels, it is shown that for any input magnitude distribution, it is optimum from a capacity perspective to choose the phase of the input independent and identically distributed, with a distribution which is uniform over the interval $[0, 2\pi)$.

Preface

This dissertation is submitted in partial fulfilment of the requirements for the degree of *Philosophiae Doctor* (PhD) at the Department of Electronics and Telecommunications, Norwegian University of Science and Technology (NTNU). My advisors have been Professor Geir E. Øien and Associate Professor Lars Lundheim, both of whom are with the Department of Electronics and Telecommunications, NTNU.

The studies have been carried out in the period from January 2004 to April 2007. The work includes the equivalent of half a year of full-time course studies and approximately nine months of teaching duties. The latter included being a teaching assistant in several graduate courses, as well as being an advisor for students working on their master theses or term projects.

As a doctoral student, I have had the opportunity – from October 2005 to September 2006 – to visit the research group headed by Professor Seiichi Sampei at Osaka University, Osaka, Japan.

The work included in this thesis has been funded by the Co-optimised Ubiquitous Broadband Access Networks (CUBAN) project and by the Department of Electronics and Telecommunications, NTNU; whereas the teaching assistantship has been funded by the Department of Electronics and Telecommunications, NTNU.

Acknowledgements

I would first and foremost like to express my warmest thanks to Professor Geir E. Øien for having been such a wonderful advisor all along the realisation of this PhD dissertation. He has always been very kind and friendly, invariably knew how to proceed in difficult situations, and constantly provided me with encouragement and support. He also is a unique researcher brimming with brilliant ideas; I benefited immensely from our numerous

discussions. The writing of this PhD dissertation certainly would not have been possible without him.

I also wish to thank to Professor Seiichi Sampei for allowing me to be part of his research group at Osaka University. I would moreover like to thank PhD candidate Hironobu Hatamoto from Osaka University for helping me with many practical matters during my stay there.

I greatly valued the discussions I had with Associate Professor Lars Lundheim, with Professor Ralf R. Müller, with Professor Nils Holte, and with Professor Mohamed-Slim Alouini. I wish to express my gratitude to them all.

I wish to thank my friends and colleagues at the Signal Processing Group of NTNU, who not only never failed to provide a foreigner like myself with much needed help and advice, but also made my stay here a real pleasure. I am particularly indebted to Øystein Birkenes, Bojana Gajič, Anders Gjendemsjø, Vegard Hassel, Fredrik Hekland, Greg Håkonsen, Anna Kim, Vidar Markhus, and Saeeid Tahmasbi Oskuii. I also greatly enjoyed and learnt from our many technical discussions.

I am in addition grateful to Frode Bøhagen for a collaboration from which we both benefited, and to Mrs. Kirsten Ekseth who is the secretary at our group and has always been prepared to provide her help. I furthermore wish to thank Professor Tor Ramstad for the heart-warming smile which never leaves his face and the interesting conversations we had together.

I would like to thank my dear friends Charles-Antoine Louët and Jean-Chalres Delvenne for our numerous mathematical discussions, and for their encouragement all along the writing of this PhD dissertation.

Finally, I wish to thank my treasured mother Elena for always being there for me, and my sweet Akiko for her love and encouragement.

Trondheim, February 2007
Sébastien de la Kethulle de Ryhove

Contents

Abbreviations

AR	Autoregressive process
AR(1)	First order autoregressive process
AR(p)	Autoregressive process of order p
ASE	Average spectral efficiency
AWGN	Additive white Gaussian noise
BER	Bit-error rate
BLAST	Bell Labs layered space-time
CFSQP	C code for feasible sequential quadratic programming
CSI	Channel state information
CSNR	Channel signal-to-noise ratio
dB	Decibel
FSK	Frequency shift keying
i.i.d.	independent identically distributed
IF	Intermediate frequency
KKT	Karush-Kuhn-Tucker
LDPC	Low-density parity-check
LOS	Line-of-sight
MFCQ	Mangasarian-Fromovitz constraint qualification
MIMO	Multiple-input multiple-output
MISO	Multiple-input single-output
OFDM	Orthogonal frequency-division multiplexing
PSK	Phase shift keying
QAM	Quadrature amplitude modulation
RF	Radio Frequency
SIMO	Single-input multiple-output
SISO	Single-input single-output
SNR	Signal-to-noise ratio

Part I

Introduction

Introduction

This dissertation is devoted to the study of single-user wireless communication links. Radio signals propagate from the transmitter to the receiver of such links across a transmission medium (or *wireless channel*), and encounter different obstacles on their way. The manner in which these obstacles affect the transmitted radio signal depends on the obstacles' characteristics and on the nature of the propagating electromagnetic wave, and can be attributed to three main propagation mechanisms: reflection, diffraction, and scattering [Rap02; Stü01].

Reflection takes place when an incident wave arrives upon a surface with dimensions which are much larger than the wavelength of the incident wave. Diffraction occurs when an obstacle with sharp edges lies in the radio path between the transmitter and the receiver, which results in the transmitted waves bending around the obstacle. Scattering arises when an electromagnetic wave impinges on an object whose dimensions are small compared to the wavelength of the propagating wave, resulting in the energy of the wave to be smeared across a wide range of different directions [Rap02; Stü01].

The presence of natural or man-made obstacles along the transmission medium will consequently cause multiple copies of the transmitted signal to arrive at the receiver via different paths; with random delays, attenuations, and phase shifts – which is a phenomenon known as *multipath propagation*. The position and orientation of the transmitter, receiver, and physical objects in the transmission path will influence the delays, attenuations, and phase shifts; and determine whether these multiple copies add up constructively or destructively. Modifications in the wireless channel will hence cause fluctuations in the received signal power, commonly referred to as *fading*.

Fading can be *slow* or *fast*, and *frequency-flat* or *frequency-selective*. The channel *coherence time* T_c [s] measures the period of time after which the correlation function of two samples of the channel impulse response taken at the same frequency but different time instants drops below a certain pre-

determined threshold [SA01]. It thus indicates roughly for how long the channel impulse response remains in essence the same, and is related to the notions of slow and fast fading. If the channel coherence time is smaller than the symbol duration T_s [s], the channel response varies during the transmission of one symbol, and the fading is said to be fast. On the other hand, if the channel remains essentially the same for at least a few consecutive symbols, the fading is said to be slow – which is an assumption that will be made in a large portion of this dissertation. Frequency-flat and frequency-selective fading are concepts which are related to the channel *coherence bandwidth* B_c [Hz] and to the bandwidth B_s [Hz] of the transmitted signal. The coherence bandwidth measures the difference in frequency beyond which the correlation function of two samples of the channel impulse response taken at the same time but different frequencies drops below a certain predetermined threshold [SA01]. It can be thought of as a measure of the range of frequencies over which the channel response can considered to remain constant. The fading is said to be frequency-flat (or simply flat) if the signal bandwidth B_s is significantly smaller than the channel coherence bandwidth B_c; otherwise it is said to be frequency-selective.

We will assume the fading to be frequency-flat throughout this dissertation. This is for example realistic in narrowband communication systems, or when modelling one single subchannel in so-called *orthogonal frequency-division multiplexing* (OFDM) systems, where communication is performed by separating a wideband channel into several different narrowband subchannels [San96; Lin06]. The flatness of the fading allows us to model the effect of the channel by a single multiplicative complex coefficient $h = \alpha e^{i\beta}$ rather than by an impulse response with many taps, rendering wireless systems operating over flat-fading channels more amenable to analysis. *Channel state information* (CSI) is respectively said to be available at the transmitter and the receiver when the value of h (or channel state) is known to the transmitter and when the value of h is known to the receiver.

The statistical distribution of the fading amplitude α – which modulates the received carrier amplitude – directly influences the capacity and performance of wireless systems. Different models for the statistics of α have been proposed depending on the characteristics of the propagation environment. One among these is the probability distribution introduced by Lord Rayleigh [Ray80] and which now bears his name,

$$f_\alpha(\alpha) = \frac{2\alpha}{\Omega} \exp\left(-\frac{\alpha^2}{\Omega}\right); \qquad \alpha \geq 0, \tag{1}$$

where $\Omega = E[\alpha^2]$ is the expected value of α^2. It can be derived by assuming that there is no line-of-sight between the transmitter and the receiver,

and that the received signal consists of a number of independent, identically distributed (i.i.d.) reflected and scattered components arriving from different angles which is sufficiently large for the central limit theorem to apply. The in-phase and quadrature components of the received signal are then zero mean i.i.d. Gaussian random variables, and the magnitude of the received signal can be shown to have the distribution (1).

In the presence of a line-of-sight between the transmitter and the receiver, the random reflected and scattered components are superimposed to a dominant stationary signal. The in-phase and quadrature components of the received signal become non-zero mean Gaussian random variables, and the law according to which the received signal magnitude is distributed reads [Stü01]

$$f_\alpha(\alpha) = \frac{2\alpha}{\Omega} \exp\left(-\frac{\alpha^2 + s^2}{\Omega}\right) I_0\left(\frac{2\alpha s}{\Omega}\right); \qquad \alpha, s \geq 0, \tag{2}$$

where s^2 is the sum of the squares of the means of the Gaussian random variables respectively corresponding to the received in-phase and quadrature components, and $I_0(\cdot)$ denotes the modified Bessel function of the first kind of order zero [GR00]. The probability distribution (2) is most commonly referred to as the Rice distribution [Rap02; Stü01], although it also sometimes is called the Nakagami-n distribution [Nak60; SA01]. It is moreover customary to speak of the Ricean factor $K = s^2/\Omega$, which is the ratio between the power of the deterministic signal and the average total power of the multipath components [Rap02; Stü01].

The Nakagami-m distribution [Nak60]

$$f_\alpha(\alpha) = \frac{2m^m \alpha^{2m-1}}{\Gamma(m)\Omega^m} \exp\left(-\frac{m\alpha^2}{\Omega}\right); \qquad \alpha \geq 0, m \geq \tfrac{1}{2}, \tag{3}$$

where $\Gamma(\cdot)$ denotes the Gamma function [GR00], is yet another model for the statistics of α. It was inferred by Nakagami in 1943 after large-scale experiments on rapid fading in long-distance high frequency channels [Nak60]. It has the advantages of providing a better fit for some empirical data than the Rayleigh and Rice distributions, of including the Rayleigh distribution as the special case $m = 1$, and approaching a channel without fading (constant α) as $m \to \infty$. It is furthermore easy to manipulate due to its simple form without special functions such as the modified Bessel function from the Rice distribution appearing in (2).

In addition to the fluctuations in received signal power brought about by multipath propagation, the received signal is also corrupted by additive noise, which may arise from interference during the transmission or from

thermal noise introduced primarily by electronic components and amplifiers at the receiver [Pro01]. In the latter case, the noise can be statistically characterised as a Gaussian process, which is a model that is widely adopted due to its mathematical tractability and to the broad range of physical channels it applies to. It is also mathematically convenient to model the additive noise process as white (meaning that the knowledge of the noise process up to time t provides no information whatever on its future values); and it is therefore usual to speak of *additive white Gaussian noise* (AWGN) channels [Pro01]. However, as its name suggests, this term has been reserved for channels that are only corrupted by additive white Gaussian noise and *do not* suffer from fading and multipath propagation.

This dissertation – which is largely based on a collection of five papers – is concerned firstly with the analysis and design of efficient wireless communication systems operating over the fading channels just described, and secondly with the information theoretic characterisation of these fading channels. We now give a brief introduction to the discipline of information theory, and subsequently present some of the main ideas and techniques which lie at the heart of the papers that can be found in this thesis. This is followed by a summary of the contributions of each one of those papers, some suggestions for further research, and a succinct outline of three additional papers to which the author also contributed but which are not formally included this thesis.

1 Information Theory

The Oxford English Dictionary [OED89] defines information theory as "the quantitative theory, based on a precise definition of information and on the theory of probability, of the coding and transmission of signals and information". It is generally accepted that the theory originated with Shannon's 1948 paper entitled "A mathematical theory of communication" [Sha48].

One of the major successes of information theory is proving that there exists a maximum rate at which information can be sent and recovered through a communication channel with arbitrarily low probability of error (this maximum rate is known as the channel *capacity*). Perhaps the most well-known and celebrated example of channel capacity calculations is that of the calculation of the capacity of an AWGN channel subject to an average power constraint. The knowledge of such bounds has proved to be of great help for the design of communication systems since their discovery. Finding capacity-achieving codes (viz. a means of encoding and decoding the information that is to be transmitted in such a way that the

capacity is attained) for AWGN channels has for example long been one of the chief concerns of coding theory, culminating with the obtainment of turbo codes [BGT93] and low-density parity-check (LDPC) codes [Gal63]. These codes, while keeping the probability of error remarkably low, can achieve information rates that are so close to the AWGN channel capacity (also called the *Shannon bound*) that they can be deemed capacity-achieving for all practical purposes. Intimately woven with the notion of capacity is also that of *capacity-achieving input distribution*, which for a given channel is the probability distribution of the channel input which maximises the mutual information [CT91] between the channel input and output. (The mutual information between two random variables X and Y is formally defined as the Kullback Leibler distance [CT91] between the joint distribution $f_{X,Y}(x,y)$ and the marginal distributions $f_X(x)$ and $f_Y(y)$, to wit

$$I(X;Y) = \int f_{X,Y}(x,y) \log \frac{f_{X,Y}(x,y)}{f_X(x) f_Y(y)} \,\mathrm{d}x \,\mathrm{d}y, \tag{4}$$

and can be thought of as the amount of information regarding one of the variables contained in the other.) This maximum mutual information in reality is nothing more than the capacity of the channel [CT91].

The capacity of fading channels has been the object of extensive investigations in recent years. Depending on the assumptions that are made regarding the quality and presence of CSI at the transmitter and the receiver, those that are made regarding the properties of the fading process, and the type of power constraint that is considered, one can obtain problems (and solutions) of radically different natures. Although significant progress has been made in a number of cases of practical relevance – such as that with perfect receiver CSI and perfect, imperfect, or absent transmitter CSI [GV97; CS99]; that with no transmitter or receiver CSI and an i.i.d. Rayleigh- or Ricean-fading process [TE97; AFTS01; LM03; GPV05a; GPV05b]; that with no transmitter or receiver CSI and a Rayleigh-fading process with *memory* (i.e. a situation where knowledge of the fading process up to a certain time allows one to predict future values of the fading process with a certain accuracy) [LM03; CHM04; Zha05] – many open questions still remain. A large portion of this thesis is dedicated to the study of a few of these questions.

One among the many criteria that can be used to describe the performance of a communication system is the power that is required to achieve a certain *spectral efficiency* [bits/s/Hz] (viz. the number of information bits that can be reliably transmitted per Hertz of available bandwidth during a time of one second) subject to a given bit-error rate (BER) requirement.

(In some theoretical studies, including one that can be found in this thesis, the availability of capacity-achieving codes is assumed – in which case the BER requirement ceases to be relevant.) It is common to normalise the available power by the average power of the additive noise corrupting the transmitted symbols. If one chooses to do so, the communication system performance can be described in terms of the *signal-to-noise ratio* (SNR) that is required to achieve a given spectral efficiency.

2 Link Adaptation

One possible way to guarantee the reliable performance of a wireless communication system operating over a fading channel is to dimension it for the worst-case scenario of the channel, which corresponds to the situation where the received signal power is close to its lowest overall value; a circumstance also frequently referred to as a *deep fade*. This however results in an inefficient use of the channel when the received signal power is high – but is the only way of avoiding frequent *outages* (viz. service interruptions) in constant rate and constant power wireless systems.

Substantial increases in spectral efficiency without any extra power costs are possible if one adapts to the time-varying channel by changing the channel codes, modulation constellations, and transmitted power. This is a technique which is known as *link adaptation* (including in particular *adaptive coded modulation*), and has received considerable attention in recent years [GV97; AG97; GC97; HHØ00; KG00; CG01; FSES04; GØO06]. Designing and finding the performance limits of link adaptation schemes under different settings are topics which are considered in several of the papers that can be found in this dissertation.

An assumption we will find convenient to make when analysing link adaptation schemes is that the wireless channel is i.i.d. *block-fading* [BCT01; SB04; ZV04; LLC04; Kim06], i.e. that the channel fading coefficient h remains constant for a block consisting of several symbols (often called a *frame*) and that the sequence of channel coefficients corresponding to different frames is i.i.d., with magnitude α for example distributed according to the law given in (1), (2), or (3). The wireless fading channel can hence be regarded as an AWGN channel without fading during the duration of each frame – which is often assumed to be sufficiently long [GØH05; Kim06] for the information theoretic arguments used to establish coding theorems [CT91] to be of application, although it is imperative that it remain short compared to the channel coherence time T_c if the block-fading model is to be an accurate representation of the fading channel under considera-

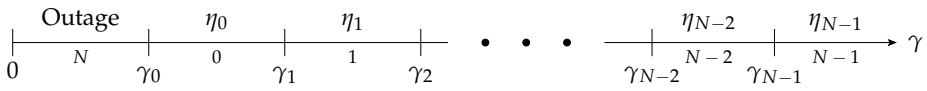

FIGURE 1: Division of the CSNR range $[0, \infty)$ into $N + 1$ bins, which are numbered in such a way that $\gamma \in [\gamma_0, \gamma_1)$ in bin 0, $\gamma \in [\gamma_1, \gamma_2)$ in bin 1, ..., $\gamma \in [\gamma_{N-1}, \infty)$ in bin $N - 1$, and $\gamma \in [0, \gamma_0)$ in bin N.

tion.

In order to be able to adapt to the time-varying channel, the availability of CSI at the transmitter becomes necessary. A reliable estimate of h can for example be obtained at the receiver by transmitting a known sequence of pilot symbols at the beginning of each frame. The transmitter can thereafter be informed of the outcome of this estimation via a *feedback channel*. Some important issues regarding the acquisition of CSI are the quality of the estimate obtained at the receiver, the possible presence of delay or errors on the feedback channel, and the capacity of the feedback channel. In this thesis we do not address any of these potential problems and assume an ideal situation where the receiver *perfectly* estimates the channel coefficient h, and the feedback channel is delay- and error-free in addition to having the required – albeit maybe infinite – capacity. (The interested reader is invited to set her or his eyes upon e.g. [FSES04; ØHH04; LLC04; Duo06] for detailed discussions regarding some of these matters.)

A scenario without the restriction to block-fading (where the channel coefficient h could vary on a symbol-by-symbol basis) but still with perfect transmitter and receiver CSI could also be considered [GV97; CS99]. Although it is highly probable that most of the results presented in this thesis where the block-fading assumption has been made would continue to hold under this less restrictive scenario, we have chosen not to investigate this case because then CSI estimation as described above becomes more difficult, and in our opinion the perfect CSI assumption becomes less realistic.

Link adaptation is usually performed by dividing the range $[0, \infty)$ of possible *channel signal-to-noise* (CSNR) values γ that can be observed at the receiver into a number $N + 1$ of non overlapping quantisation intervals (or *bins*), for example as depicted in Fig. 1, and using a transmission scheme with a suitable spectral efficiency η_n when the CSNR falls in the nth bin ($n \in \{0, \ldots, N - 1\}$). The spectral efficiencies of the transmission schemes are chosen so that $0 < \eta_0 < \eta_1 < \cdots < \eta_{N-1}$. When $\gamma \in [0, \gamma_0)$, no transmission is performed and the system experiences an outage. The system's

resulting *average spectral efficiency* (ASE) η can then be written

$$\eta = \sum_{n=0}^{N-1} \eta_n \int_{\gamma_n}^{\gamma_{n+1}} f_\gamma(\gamma) \mathrm{d}\gamma, \tag{5}$$

where $f_\gamma(\gamma)$ is the received CSNR probability distribution, $\int_{\gamma_n}^{\gamma_{n+1}} f_\gamma(\gamma)\mathrm{d}\gamma$ hence corresponds to the probability that transmission scheme n be used, and the convention $\gamma_N = \infty$ has been adopted for convenience. The different transmission schemes will consist of different channel codes and/or modulation constellations, and the power at the transmitter can moreover also be adapted as a function of the received CSNR γ.

It is also worth mentioning that, for a fixed transmit power S and a given noise power σ^2, the relation between the received CSNR γ and the channel fading coefficient $h = \alpha e^{i\beta}$ is simply given by $\gamma = \frac{S}{\sigma^2}\,\alpha^2$. The CSNR probability distribution $f_\gamma(\gamma)$ can then be obtained from that of $f_\alpha(\alpha)$ via a simple mathematical transformation. In the case of Nakagami-m fading, this for instance yields

$$f_\gamma(\gamma) = \left(\frac{m}{\bar{\gamma}}\right)^m \frac{\gamma^{m-1}}{\Gamma(m)} \exp\left(-m\frac{\gamma}{\bar{\gamma}}\right), \tag{6}$$

where $\bar{\gamma} = \frac{S}{\sigma^2}\,\Omega$ is the average CSNR.

3 Short-Range Wireless Communications

In any wireless communication system, in addition to the energy which is required for the information-bearing electromagnetic waves that are to be transmitted (*transmission energy*), a certain amount of energy will always be needed for the operation of the transmitter and receiver circuitry (*circuit energy*). When the distance between the transmitter and the receiver of a wireless link is long (typically more than 100 m. [CGB05]) transmission energy consumption is considerably larger than circuit energy consumption, and optimising wireless communication systems based on transmission energy alone is a valid approach. The reason for the dominance of transmission energy is that the *path loss*, or attenuation undergone by electromagnetic waves as they propagate from the transmitter to the receiver of a wireless link (which is characterised using a *path loss exponent*), is quite significant [Rap02]; and for long transmission distances large transmission powers hence become necessary if sufficient power is to remain present in the information-bearing electromagnetic waves at the instant they reach the receiver.

On the other hand, for short transmission distances the attenuation due to path loss is much less significant, and circuit energy consumption becomes comparable to and can even dominate transmission energy consumption [CGB05]. Including circuit energy consumption in the global energy budget when designing a short-distance wireless communication system then becomes a matter of paramount importance if the system's overall energy consumption is to be minimised. Indeed, optimising short-range wireless systems based on both transmission and circuit energy or on transmission energy alone can lead to completely different design strategies. This has been the subject of significant investigation under a number of different settings [CGB04; CMGL05; CGB05; KØ05], and also is a topic that is addressed in one of the papers that has been included in this dissertation. One of the chief difficulties regarding the design and optimisation of short-range wireless systems where circuit energy consumption is included in the overall energy budget is that the actual energy consumption of the different circuit components is highly implementation-dependent, and finding circuit energy consumption models which are both relevant and mathematically tractable consequently is a particularly challenging problem.

4 Multiple-Antenna Systems

In its simplest configuration, a wireless system possesses a single antenna at the transmitter and a single antenna at the receiver – in which case the epithet "SISO" (for *single-input single-output*) is sometimes used to unequivocably stress this fact. Traditionally, multiple antennæ were used either at the transmitter or the receiver in order to enhance the performance of wireless systems using techniques such as *beamforming*, by means of which the link quality can be improved by increasing the gain in the direction of the signal that is to be sent or received, and such as *spatial diversity*, which helps mitigate the effects of multipath propagation by making several independently fading copies of the same signal available to the receiver. Wireless systems with respectively a single antenna at the transmitter and multiple antennæ at the receiver, and with multiple antennæ at the transmitter and a single antenna at the receiver are known as *single-input multiple-output* (SIMO) and *multiple-input single-output* (MISO) systems.

Wireless systems with multiple antennæ both at the transmitter and the receiver are classified as *multiple-input multiple-output* (MIMO) systems. Denoting by N the number of antennæ at the transmitter and by M the number of antennæ at the receiver, we see that there are NM different possible ways of forming transmitter-receiver antenna pairs. The fading

channel corresponding to each one of these pairs will be characterised by a potentially different channel coefficient; and a *matrix* $\mathbf{H} \in \mathbb{C}^{M \times N}$, the entry in row i and column j of which is given by the coefficient h_{ij} describing the condition of the fading channel between transmit antenna j and receive antenna i, is hence needed to fully describe the state of the MIMO channel. In the case of MIMO systems, we thus speak of perfect receiver CSI if the channel matrix $\mathbf{H}$ is perfectly known to the receiver, a similar definition being also applicable in the case of transmitter CSI. Note that obtaining CSI is more expensive in the case of MIMO systems than in that of SISO systems since more channel coefficients need to be estimated.

Considerable interest in MIMO systems arose after it was shown in information theoretic work by Telatar [Tel95] (see also Foschini [Fos96] and Foschini and Gans [FG98]) that the *ergodic* capacity (that is to say, the channel capacity averaged over all possible realisations of $\mathbf{H}$) of a MIMO wireless system with perfect receiver CSI, and with the entries of the channel matrix $\mathbf{H}$ i.i.d. with Rayleigh-distributed magnitude α_{ij} and phase β_{ij} uniformly distributed and independent of α_{ij}, grows linearly with the minimum $\min\{N, M\}$ of the number of antennæ.[1] Indeed, this capacity augmentation at the cost of no extra bandwidth or power (only the complexity of the transceiver increases) has been identified as a potential means to help satisfy the ever growing demand for data-intensive applications in a world where bandwidth is exceedingly scarce and strict regulations on the maximum radiated power have to be respected.

The situation of a channel matrix $\mathbf{H}$ with zero mean i.i.d. circularly symmetric complex Gaussian entries corresponds to a scenario where there is no line-of-sight between the transmitter and the receiver, and each one of the NM channels between the transmitter and receiver arrays fades independently. The independence assumption between the elements of a non line-of-sight matrix $\mathbf{H}$ is verified if the inter-element separation at the transmitter and receiver arrays is sufficiently large (the actual distance requirement is highly dependent on the number of scatterers, and can vary from as little half a wavelength in the case of infinitely many scatterers [SFGK00] to significantly more if less scatterers are present [CTKV02]). It therefore can happen that the elements of $\mathbf{H}$ be correlated due to insufficient antenna spacing or the presence of a few dominant scatterers, which can lead to capacity reductions [CTKV02].

Research concerning MIMO systems has focused in two main direc-

[1] When the entries of the channel matrix $\mathbf{H}$ are i.i.d. with Rayleigh-distributed magnitude α_{ij} and phase β_{ij} uniformly distributed and independent of α_{ij}, it is often said that the entries h_{ij} are zero mean i.i.d. circularly symmetric complex Gaussian random variables.

tions: increasing spectral efficiency via a technique known as *spatial multiplexing*, and combating multipath fading by providing the receiver with as many independently fading copies of the transmitted signal as possible – which is the object of *diversity* schemes [BP02]. Some examples of work in the former direction include the family of BLAST (for *Bell Labs Layered Space-Time*) algorithms [Fos96; GFVW99]; whereas the field of *space-time coding* [Ala98; TSC98; TJC99] is concerned with achieving the maximum possible diversity in MIMO wireless systems without transmitter CSI. It was later shown [ZT03] that a certain amount of *both* the diversity and the multiplexing gains can be obtained simultaneously, but that there is a fundamental trade-off between how much of one gain can be exchanged for the other, and that the *full* diversity and multiplexing gains cannot be simultaneously achieved.

One of the papers included in this manuscript will explore the spectral efficiency maximisation of a MIMO system with full transmitter and receiver CSI, an i.i.d. block-fading scenario, and a channel matrix $\mathbf{H}$ having zero mean i.i.d. circularly symmetric complex Gaussian entries. In this case, the capacity-achieving scheme (if capacity-achieving codes for AWGN channels of any SNR in the range $[0, \infty)$ are available) is to decompose the MIMO channel into a set of independent subchannels and distribute the available power between the different subchannels in accordance with the so-called *water-filling* solution [Tel95; CT91; SSP01]. This will be done in the case of *dual-branch* MIMO systems (viz. MIMO systems with two antennæ at the transmitter or the receiver).

For a more detailed overview of the extensive number of publications concerned with MIMO systems that have emerged during the past decade and for further particularities regarding the principles behind MIMO technology we refer the interested reader to the excellent tutorial by Gesbert et al. [GSS$^+$03].

5 Power Constraints in Wireless Channels

In wireless communication systems, a constraint on the power of the transmitted signal is always present; be it for instance due to limited battery lifetime, to radiated power regulations, or to hardware constraints such as nonlinear power amplifiers. (Nonlinear power amplifiers are less power-hungry than linear power amplifiers, but produce out-of-band emissions requiring the use of expensive filters at the transmitter front end if the distortions introduced by the nonlinearity are compensated for at the receiver [AR03].)

The most commonly used input constraint is the *average* power constraint [Sha48; GV97] – where the average power of the input signal is constrained to remain below a certain value. Another power constraint which is often used is the *peak* power constraint [Smi71; SBD95], in which case the power of the input signal must remain below a certain value at all times.

When choosing to model a wireless fading channel as a block-fading channel (see Sec. 2), it is common to speak of *short-term* and *long-term* power constraints [CTB99]. In the case of a short-term power constraint, the average power which is allocated to the symbols (or symbol vectors in the case of MIMO systems) within any one given symbol frame[2] must be kept below a given constant during the transmission of each and every symbol frame. The long-term power constraint is less restrictive: the transmitter is then allowed to allocate different (possibly sometimes extremely large) average powers to the symbols (or symbol vectors) within different symbol frames as long as the average allocated power over multiple symbol frames does not exceed the available power budget.[3] The former scenario is for example relevant in systems where the transmitted power must be kept below a certain level due to e.g. power regulations or limitations in the dynamic range of the power amplifier, whereas the latter scenario is for instance of relevance in systems where the priority is to minimise the total power consumption, or where battery lifetime is an important design parameter.

Link adaptation schemes in which the average power allocated to the symbols in any one given symbol frame is kept constant are referred to in the literature using terms such as "constant power signalling" [KG00] or "constant power transmission scheme" [GØO06]; whereas link adaptation schemes where the average power allocated to the symbols in a given symbol frame can vary from frame to frame are referred to for instance using the appellation "variable power transmission scheme" [GØO06].

The terminology that is used in the various papers of this dissertation to describe the nature of the different power constraints that are considered sometimes changes from one paper to another; chiefly because the timespan over which these papers have been written was relatively long and the problems addressed in the various papers have different properties. Our assumptions are however clearly detailed in each paper.

[2]One symbol frame always spans exactly one fading block in the papers in this dissertation where the block-fading assumption is made.

[3]It actually is the same thing to consider that the transmitter simply is subject to the previously described average power constraint in this case.

6 Noncoherent Communications

Although tracking the state of a fading channel using, for instance, pilot symbols is possible with sufficient accuracy if the channel coherence time T_c is significantly longer than the symbol duration T_s, this can become expensive – or even infeasible – when this ceases to be the case. For example [MH99], a mobile terminal moving at a speed v of 60 miles per hour and operating at $f_0 = 1.9\,\mathrm{GHz}$ has a maximum *Doppler shift* (or maximum apparent change in frequency) [Rap02] of approximately

$$f_m = \frac{v}{c} f_0 \approx \frac{26.82\,\mathrm{m/s}}{2.998 \times 10^8\,\mathrm{m/s}} \times 1.9 \times 10^9\,\mathrm{Hz} \approx 170\,\mathrm{Hz} \tag{7}$$

(here, the speed of light in air has been approximated by the speed c of light in a vacuum), which would give a coherence time of more or less [Rap02, Eq. (5.40.c)]

$$T_c \approx \frac{0.423}{f_m} \approx 2.5\,\mathrm{ms}, \tag{8}$$

which for a symbol rate of 30 kHz corresponds to roughly only 75 symbol periods.

This motivates the study of *noncoherent* fading channels, which is the literature term for fading channels in which the CSI is unknown to both the receiver and the transmitter. Notwithstanding the considerable amount of attention such channels have recently been receiving due to their theoretical and practical importance [TE97; MH99; AFTS01; ZT02; LM03; LV04; CHM04; Zha05], they currently still are notably less well understood than coherent channels, in which the channel state is known to the receiver (and sometimes also the transmitter). The reader whose curiosity has been piqued is referred to the introduction of paper E in this dissertation for an overview of some of the main recent results in the area of noncoherent communications.

We would now like to introduce and discuss the practical relevance of the two different channel models that are utilised in the papers in this dissertation which are concerned with noncoherent communications. This is done with SISO channels in mind.

The first among these is the memoryless, discrete-time noncoherent Rayleigh fading channel, examined in [TE97; AFTS01; LM03]. Here, the channel state h is assumed to change on a symbol-by-symbol basis, there being no relation whatever between the different realisations of h; that is to say, the fading process is memoryless. Although upon inspection of (7) and (8) one might be led to believe that this could be a valid model in case

either the mobile velocity or carrier frequency is sufficiently high (or in case the symbol rate is sufficiently low) for the inequality $T_c < T_s$ to be satisfied, in such a situation the fading is *fast*, the bandwidth of the received signal is significantly larger than that of the transmitted signal, and one must *oversample* the time-continuous received signal in order to capture the changes in the fast-fading channel as also pointed out in [KD00; AFTS01]. This hence does not lead to the memoryless fading channel under consideration.

On the other hand, this model befits the situation where a narrowband signal would be hopped rapidly over an extensive set of largely spaced frequencies, one symbol per hop, in order to gain security [AFTS01]. This model would also be applicable when successive symbols are sent over a slowly fading channel at widely separated time instants. This might be done when using an extremely long interleaver in a communication system where delay is not of particular concern in order to guarantee that no one transmitted codeword is lost due to the possible presence of prolonged deep fades, or in order for all the transmitted codewords to experience similar channel conditions.

The second is the discrete-time, noncoherent Rayleigh-fading channel with memory, in which memory is modelled by an *autoregressive* (AR) process [BJR94] of arbitrary order $p \in \mathbb{Z}^+$; viz. we now have

$$H_k = -\sum_{j=1}^{p} \alpha_j H_{k-j} + W_k, \tag{9}$$

where $k \in \mathbb{Z}^+$ is the discrete time index, H_k is a random variable representing the state of the fading channel at time k, $\{W_k\}$ is a sequence of i.i.d. zero mean circularly symmetric complex Gaussian random variables of variance σ_w^2 (the so-called *driving noise* process), and $\{\alpha_1, \alpha_2, \ldots, \alpha_p\}$ are complex coefficients. The special case where $p = 1$ was investigated in e.g. [CHM04; Zha05]. The channel state h is thus again assumed to change on a symbol-by-symbol basis, but the presence of memory now allows for correlation between the realisations of the fading process at different time instants. This channel model is highly relevant in a wide variety of scenarios. Indeed, the coefficients $\{\alpha_1, \ldots, \alpha_p\}$ and σ_w^2 can be chosen such that the autocorrelation function of the process $\{H_k\}$ matches any other desired autocorrelation function up to lag p [BJR94]. Furthermore, the strictly bandlimited Rayleigh-fading process can be modelled with arbitrary accuracy provided that the order p of the AR process is taken sufficiently large [BB04]. (Note that after passing through the channel a pure sine wave of frequency f_0 will only generate spectral components at the

receiver within the range $[f_0 - f_m, f_0 + f_m]$, where f_m is the previously discussed maximum Doppler shift. This is the reason why the equivalent baseband fading process representing the channel can only have nonzero spectral components in the range $[-f_m, f_m]$, and is therefore said to be strictly bandlimited.)

It is moreover to be expected that representing a channel with state h which varies continuously in time – and with a fading process possessing for example Jakes' [Jak74] or Clarke and Khoo's [CK97] autocorrelation properties – utilising the continuously fading channel model under consideration will result in a better approximation than when attempting to represent such a channel utilising the previously discussed piecewise-constant block-fading channel model. It is for example observed in [CHM04] that even though the latter model is considered to be a good approximation for a channel with state h which varies continuously in time, the approximation seems to deteriorate for increasing SNR values.

Papers D and E in this dissertation contribute to the information theoretic understanding of the two different channel models presented above by addressing respectively actual capacity calculations and the structure of the capacity-achieving input distribution under different scenarios. Progress in this area is important since capacity values provide fundamental transmission limits, whereas capacity-achieving input distributions suggest practical signalling schemes.

7 Main Contributions of the Papers Included in This Thesis

Paper A – An Efficient Design Methodology for Constant Power Link Adaptation Schemes

Sébastien de la Kethulle de Ryhove, Geir E. Øien, and Lars Lundheim; under review for possible publication in *IEEE Transactions on Vehicular Technology* at the time of writing of this dissertation. The results are also partially published in *Proc. 2006 IEEE International Conference on Communications (ICC)*, Istanbul, June 2006.

In paper A, the design of constant power link adaptation schemes operating over slowly-varying flat-fading SISO wireless channels in which perfect CSI is available both at the transmitter and the receiver is considered. It is assumed that the distance between the transmitter and the receiver is short. Circuit energy consumption is therefore included in the total energy budget in order to correctly account for the system's overall energy con-

sumption. It is furthermore assumed that the system's instantaneous bit-error rate must never exceed a predefined threshold, that N transmission schemes (consisting of different error-correcting codes and/or modulation constellations) of varying spectral efficiencies are available for use, and that the system's average power consumption is constrained to lie below a certain level.

The main contribution of this paper is a methodology showing how, in numerous cases of practical importance, the $N + 1$-dimensional nonlinear optimisation problem that needs to be solved in order to maximise the average spectral efficiency of such link adaptation schemes can be reduced to a one-dimensional optimisation problem. An example illustrating the design methodology is given in the paper.

Paper B – On the Statistics and Spectral Efficiency of Dual-Branch MIMO Systems with Link Adaptation and Power Control

Sébastien de la Kethulle de Ryhove, Geir E. Øien, and Frode Bøhagen; under review for possible publication in *IEEE Transactions on Vehicular Technology* at the time of writing of this dissertation. The results are also partially published in *Proc. 2005 IEEE/ITG International Workshop on Smart Antennas (WSA),* Duisburg, April 2005, and *Proc. seventh IEEE International Workshop on Signal Processing Advances in Wireless Communications (SPAWC),* Cannes, July 2006.

As mentioned in Sec. 4, the capacity of MIMO systems with perfect transmitter and receiver CSI operating under an i.i.d. block-fading scenario can be attained (provided that capacity-achieving codes for AWGN channels of any SNR in the range $[0, \infty)$ are available and that the block-fading frames are long enough for these to be applied) by decoupling the MIMO channel into a set of independent subchannels, and distributing the power among these subchannels in accordance with the water-filling solution. The first contribution of paper B lies in the derivation of expressions for the SNR distributions of the subchannels which arise when decoupling a dual-branch MIMO system according to the above principle; this being done both in the case of short- and long-term transmitter power constraints, and in a Rayleigh-fading environment.

Achieving capacity using the above scheme (decomposition of the MIMO system into independent subchannels and water-filling for power allocation) on a time-varying channel requires however continuous rate adaptation, that is to say the ability to implement any rate within the continuum covered by the statistical distribution of the channel realisations, as

mentioned above. This is unfortunately not feasible in any practical system. Indeed, although it is realistic to assume that capacity-achieving codes for AWGN channels of any desired rate can be designed thanks to advances in coding theory (concerning mainly turbo codes [BGT93] and low-density parity-check codes [Gal63]), only a finite number of such codes – and thus rates – will be available in any practical system due to memory and complexity constraints.

The second contribution of paper B therefore consists in showing how to maximise the ASE of dual-branch MIMO systems which have perfect transmitter and receiver CSI, which operate under a i.i.d. block-fading scenario, and which are subject to a short-term power constraint assuming a given *finite* number of capacity-achieving codes for AWGN channels of different rates are available for use. This maximum ASE is compared to the system's ergodic capacity, which is found using the subchannel SNR distributions derived in the first part of the paper, and to the maximum ASE that can be attained with discrete rate adaptation if the available power is distributed among the different subchannels in accordance with the water-filling solution although the number of available rates is finite and this hence is suboptimal. Knowledge of the subchannel SNR distributions proves necessary to perform this analysis, demonstrating how valuable the knowledge of the subchannel SNR distributions can be for the design of MIMO communication links. The results show that it is possible to come very close to the ergodic capacity with only a few optimal codes, provided that the power distribution is done in an optimal way. Furthermore, they indicate that water-filling is significantly suboptimal when the number of available rates is small.

Paper C – Rate-Optimal Power Adaptation in Average and Peak Power Constrained Fading Channels

Sébastien de la Kethulle de Ryhove and Geir E. Øien; accepted for publication in *Proc. 2007 IEEE Wireless Communications & Networking Conference (WCNC),* Hong Kong, March 2007.

In paper C, SISO frequency-flat block-fading wireless channels in which perfect CSI is available both at the transmitter and the receiver, in which any transmitted codeword spans a single fading block, and in which the transmitted signal is subject to both an average (long-term) and a peak power constraint are considered. (The average transmitted power is thus constrained to lie below a given maximum level, and the peak symbol power also must remain below a certain threshold.)

The main contributions of this paper consist firstly in a theorem which characterises the power adaptation strategy that maximises the average information rate that can be transmitted over such channels with an arbitrarily low probability of error, and secondly in numerical simulations which reveal that this optimal power allocation strategy is strikingly different from the rate-optimal power allocation strategy for block-fading channels where the input is subject to an average power constraint only. The latter strategy is also the capacity-achieving power allocation strategy for the stationary and ergodic fading channel studied in [GV97; CS99] (and mentioned in Sec. 2 of the present introduction) as shown in the paper.

Paper D – On the Capacity and Mutual Information of Memoryless Noncoherent Rayleigh-Fading Channels

Sébastien de la Kethulle de Ryhove, Ninoslav Marina, and Geir E. Øien; under review for possible publication in *IEEE Transactions on Information Theory* at the time of writing of this dissertation.

The discrete-time memoryless SISO noncoherent Rayleigh-fading channel, in which the channel state varies on a symbol-by-symbol basis but where successive realisations of the fading process are mutually independent – and which was presented in Sec. 6 of the present introduction – is considered in this paper. When the input to this channel is subject to an average power constraint, it was rigorously established [AFTS01] that the magnitude of the capacity-achieving input distribution is discrete with a finite number of mass points, one of these mass points being necessarily located at the origin. By using numerical optimisation algorithms, it was also empirically found [AFTS01] that a magnitude distribution with two mass points is capacity-achieving for low SNR values, and that the number of mass points in the capacity-achieving magnitude distribution increases monotonously with the SNR.

The most important contribution of this paper consists in the rigorous derivation of closed-form expressions for the mutual information of this channel when the input magnitude distribution is discrete and restricted to having two mass points. For low SNR values (of up to approximately 0 dB) and an average power constrained input, in which case the capacity-achieving magnitude distribution is discrete with two mass points, these closed-form expressions additionally make it possible to write the channel capacity as a function of a single parameter which can be obtained via numerical root-finding algorithms. This capacity expression also becomes a tight capacity lower bound when the SNR takes values between 0 dB and

10 dB.

We also discuss in this paper how the mutual information expressions we provide can be simplified in a special case, how the hypergeometric functions [GR00] appearing in these expressions can be rewritten in terms of the incomplete beta function [GR00], and how to obtain analytical expressions for the derivative of these expressions with respect to parameters of interest.

Paper E – Capacity-Achieving Input Phase Distributions for Noncoherent Rayleigh-Fading Channels with Memory

Sébastien de la Kethulle de Ryhove, Ralf R. Müller, and Geir E. Øien; under review for possible publication in *IEEE Transactions on Information Theory* at the time of writing of this dissertation. The results are also partially published in *Proc. seventh IEEE International Workshop on Signal Processing Advances in Wireless Communications (SPAWC),* Cannes, July 2006.

In paper E, discrete-time SISO noncoherent Rayleigh-fading channels, in which the channel state varies on a symbol-by-symbol basis and the memory is modelled by an autoregressive process of arbitrary order p – as also presented in Sec. 6 of the present introduction – are considered. A contribution is made to the understanding of such channels by showing that, for any given input magnitude distribution, it is optimum from a capacity perspective to choose the phase of the input i.i.d., with a distribution which is uniform over the interval $[0, 2\pi)$. We would like to emphasise that this is a somewhat unexpected property, since because of the memory characterising the fading process it at first sight would appear natural to believe that the phase values of the successive input symbols should exhibit correlation in order to maximise the information carried by the input signal.

The problem of finding the capacity-achieving input distribution of such channels under a given set of constraints on the magnitude of the input signal is thus reduced to finding the capacity-achieving magnitude distribution (which to the best of the author's knowledge remains a difficult open problem).

It is also observed in this paper that although the input phase distribution can be chosen independently of the input magnitude distribution in order to maximise the information that is carried by the input signal, it seems that one has to take into account the maximisation of the information carried by the phase of the input signal when seeking the capacity-achieving magnitude distribution.

8 Some Suggestions for Further Research

In the following list, we bring forth some ideas for further research that might be of interest.

- In paper A, it is shown how the dimensionality of the nonlinear optimisation problem associated with the design of constant power link adaptation schemes can be reduced from $N+1$ (N denoting the number of available transmission schemes) to one in numerous cases of practical importance. Finding out whether a given scenario is covered by one of the cases in paper A is straightforward. It therefore could be useful to try to find more cases that are practically relevant in which the dimensionality of this nonlinear optimisation problem can be reduced in a similar way. For example, considering average BER constraints instead of instantaneous BER constraints is a possible extension.
- One of the contributions of paper B consists in showing how to maximise the ASE of dual-branch MIMO systems with perfect transmitter and receiver CSI which are subject to a short-term power constraint assuming a given finite number of capacity-achieving codes for AWGN channels are available for use. It could be useful to investigate how to maximise the ASE of similar dual-branch MIMO systems which are subject to a *long-term* power constraint instead of a short-term power constraint – and compare the resulting maximum ASE to the system's ergodic capacity. This would show how close one can expect to come to the ergodic capacity of dual-branch MIMO systems which are subject to a long-term power constraint with only a given finite number of capacity-achieving codes, and could additionally result in practical design rules for how the rates of these capacity-achieving codes ought to be chosen in order to maximise the ASE of such a system.
- Paper C reveals that the power adaptation strategy that must be used to maximise the average rate that can be reliably transmitted over average and peak power constrained block-fading channels with perfect transmitter and receiver CSI significantly differs from that which must be used to maximise the average rate that can be reliably transmitted in similar average power constrained only block-fading channels. It is therefore the author's belief that it could be of relevance to find simpler and better ways of computing (approximations to) the power adaptation strategy calculated in paper C, or to find analytical expressions approximately describing its behaviour. Moreover, investigating what the power allocation strategy calculated in paper C

would become in the case of imperfect transmitter or receiver CSI is another possible topic for future research.

- The closed-form expressions for the mutual information between the input and the output of the memoryless SISO noncoherent Rayleigh-fading channel considered in paper D are valid only when the input magnitude distribution is discrete and restricted to having two mass points. A possible topic for further research is therefore trying to find analytical expressions for the mutual information between the input and the output of this channel when the input magnitude distribution possesses *more* than two mass points. In addition, another idea for further investigation would be trying to find a simple criterion allowing to calculate the number of mass points in the capacity-achieving input distribution as a function of the SNR.
- In paper E we prove that, for SISO noncoherent Rayleigh-fading channels in which the memory is modelled by an autoregressive process of arbitrary order $p \in \mathbb{Z}^+$ and in which the magnitude of the input signal is constrained in an arbitrary manner, it is optimum from a capacity perspective to choose the input phase i.i.d. and independent of the input magnitude, with a distribution which is uniform over the interval $[0, 2\pi)$. Investigating whether or not this property continues to hold under even more general assumptions is yet another possible subject for future research. For example, the case of Ricean fading and that of SIMO systems could be worthy of consideration.

9 Additional Papers

In addition to papers A-E the author also actively participated to the writing of the following three papers, which are not formally part of this dissertation.

Paper 1 – Energy-Optimised Coded Modulation for Short-Range Wireless Communications on Nakagami-m Fading Channels

Sébastien de la Kethulle de Ryhove and Geir E. Øien; in *Proc. 2005 Norwegian Signal Processing Symposium (NORSIG)*, Stavanger, September 2005.

When the distance between the transmitter and the receiver of a wireless communication link is sufficiently short, circuit energy consumption and transmission energy consumption become comparable, and substantial energy savings can be achieved by making use of a transmission

scheme which takes into account total energy consumption instead of transmission energy alone. In this paper, a trellis coded system operating on a Nakagami-*m* fading channel is considered, and the manner in which the trade-off between transmission energy and circuit energy consumption is affected by the value of the fading parameter *m* is investigated.

Paper 2 – Scheduling Algorithms for Increased Throughput Guarantees in Wireless Networks

Vegard Hassel, Sébastien de la Kethulle de Ryhove, and Geir E. Øien; in preparation at the time of writing of this dissertation.

For cellular wireless networks carrying real-time traffic, it is in the interest of both network operators and customers that throughput guarantees can be offered. In this paper, an optimisation problem which aims at maximising the throughput that can be guaranteed to the mobile users is formulated. By building on results obtained by Borst and Whiting [BW03] and by assuming that the distributions of the users' carrier-to-noise ratios are known, the solution to this problem for users with different channel quality distributions is found, both for the scenario where all the users have the same throughput guarantee, and for the scenario where all the users have different throughput guarantees. To improve the short-term performance, an adaptive version of this algorithm that performs significantly better than other well-known scheduling algorithms is proposed.

Paper 3 – Exact Capacity Expressions for Dual-Branch Ricean MIMO Channels

Frode Bøhagen, Pål Orten, Geir E. Øien, and Sébastien de la Kethulle de Ryhove; to be published in *IEEE Transactions on Communications.* The results are also partially published in *Proc. sixth IEEE International Workshop on Signal Processing Advances in Wireless Communications (SPAWC),* New York, June 2005.

In this paper, exact expressions for the mutual information probability density function and the mutual information cumulative distribution function of dual-branch MIMO systems communicating over a Ricean channel with no constraint on the rank of the line-of-sight channel matrix are derived. This is done both for the case where the channel is only known at the receiver, and for the case where the channel is known both at the transmitter and the receiver. For the sake of completeness, exact expressions

for the average mutual information of dual-branch MIMO systems – utilising the simplifications that are made possible thanks to the dual-branch assumption – are presented. As an example to evaluate the expressions, uniform linear arrays are employed, and expressions for the eigenvalues of the line-of-sight channel matrix for the dual-branch case are given.

References

[AFTS01] I. Abou-Faycal, M. Trott, and S. Shamai (Shitz). The capacity of discrete-time memoryless Rayleigh-fading channels. *IEEE Transactions on Information Theory*, 47(4):1290–1301, May 2001.

[AG97] M.-S. Alouini and A. Goldsmith. Adaptive M–QAM modulation over Nakagami fading channels. In *Proc. 1997 IEEE Global Communications Conference (Globecom)*, pages 218–223, Phoenix, November 1997.

[Ala98] S. M. Alamouti. A simple transmit diversity technique for wireless communications. *IEEE Journal on Selected Areas in Communications*, 16(8):1451–1458, October 1998.

[AR03] E. Aschbacher and M. Rupp. Modelling and identification of a nonlinear power-amplifier with memory for nonlinear digital adaptive pre-distortion. In *Proc. fourth IEEE Workshop on Signal Processing Advances in Wireless Communications (SPAWC)*, pages 658–662, Rome, June 2003.

[BB04] K. E. Baddour and N. C. Beaulieu. Autoregressive modeling for fading channel simulation. *IEEE Transactions on Wireless Communications*, 4(4):1650–1662, July 2004.

[BCT01] E. Biglieri, G. Caire, and G. Taricco. Limiting performance of block-fading channels with multiple antennas. *IEEE Transactions on Information Theory*, 47(4):1273–1289, May 2001.

[BGT93] C. Berrou, A. Glavieux, and P. Thitimajshima. Near Shannon limit error-correcting coding and decoding: Turbo-codes. In *Proc. 1993 IEEE International Conference on Communications (ICC)*, pages 1064–1070, Geneva, May 1993.

[BJR94] G. E. P. Box, G. M. Jenkins, and G. C. Reinsel. *Time Series Analysis: Forecasting and Control*. Prentice Hall, third edition, 1994.

[BP02] H. Bölcskei and A. Paulraj. Multiple-input multiple-output (MIMO) wireless systems. Chapter in *The Communications Handbook*, J. Gibson, editor, second edition, CRC Press, pages 90.1 – 90.14, 2002.

[BW03] S. Borst and P. Whiting. Dynamic channel-sensitive scheduling algorithms for wireless data throughput optimization. *IEEE Transactions on Vehicular Technology*, 52(3):569–586, May 2003.

[CG01] S. T. Chung and A. Goldsmith. Degrees of freedom in adaptive modulation: a unified view. *IEEE Transactions on Communications*, 49(9):1561–1571, September 2001.

[CGB04] S. Cui, A. Goldsmith, and A. Bahai. Energy-efficiency of mimo and cooperative MIMO in sensor networks. *IEEE Journal on Selected Areas in Communications*, 22(6), August 2004.

[CGB05] S. Cui, A. Goldsmith, and A. Bahai. Energy-constrained modulation optimization. *IEEE Transaction on Wireless Communications*, 4(5):2349–2360, September 2005.

[CHM04] R. Chen, B. Hajek, and U. Madhow. On fixed input distributions for noncoherent communication over high-SNR Rayleigh-fading channels. *IEEE Transactions on Information Theory*, 50(12):3390–3396, December 2004.

[CK97] R. H. Clarke and W. L. Khoo. 3-D mobile radio channel statistics. *IEEE Transactions on Vehicular Technology*, 46(3):798–799, August 1997.

[CMGL05] S. Cui, R. Madan, A. J. Goldsmith, and S. Lall. Joint routing, MAC, and link layer optimization in sensor networks with energy constraints. In *Proc. 2005 IEEE International Conference on Communications (ICC)*, Seoul, May 2005.

[CS99] G. Caire and S. Shamai (Shitz). On the capacity of some channels with channel state information. *IEEE Transactions on Information Theory*, September 1999.

[CT91] T. Cover and J. Thomas. *Elements of Information Theory*. John Wiley & Sons, first edition, 1991.

[CTB99] G. Caire, G. Taricco, and E. Biglieri. Optimum power control over fading channels. *IEEE Transactions on Information Theory*, 45(5):1468–1489, July 1999.

[CTKV02] C.-N. Chuah, D. N. C. Tse, J. M. Kahn, and R. A. Valenzuela. Capacity scaling in MIMO wireless systems under correlated fading. *IEEE Transactions on Information Theory*, 48(3):637–650, March 2002.

[Duo06] D. V. Duong. *Analysis and optimization of pilot-aided adaptive coded modulation under noisy channel state information and antenna diversity*. PhD thesis, Norwegian University of Science and Technology, 2006.

[FG98] G. J. Foschini and M. J. Gans. On limits of wireless communications in a fading environment when using multiple antennas. *Wireless Personal Communications*, 6:311–335, March 1998.

[Fos96] G. J. Foschini. Layered space-time architecture for wireless communication in a fading environment when using multiple antennas. *Bell Labs Technical Journal*, 1(2):41–59, Autumn 1996.

[FSES04] S. Falahati, A. Svensson, T. Ekman, and M. Sternad. Adaptive modulation systems for predicted wireless channels. *IEEE Transactions on Communications*, 52(2):307–316, February 2004.

[Gal63] R. Gallager. *Low-density parity-check codes*. PhD thesis, MIT Press, Cambridge, MA, 1963.

[GC97] A. J. Goldsmith and S.-G. Chua. Variable-rate variable-power MQAM for fading channels. *IEEE Transactions on Communications*, 45(10):1218–1230, October 1997.

[GFVW99] G. D. Golden, C. J. Foschini, R. A. Valenzuela, and P. W. Wolniansky. Detection algorithm and initial laboratory results using V-BLAST space-time communication architecture. *Electronics Letters*, 35(1), January 1999.

[GØH05] A. Gjendemsjø, G. E. Øien, and H. Holm. Optimal power control for discrete-rate link adaptation schemes with capacity-approaching coding. In *Proc. 2005 IEEE Global Telecommunications Conference (Globecom)*, St. Louis, Missouri, November 2005.

[GØO06] A. Gjendemsjø, G. E. Øien, and P. Orten. Optimal discrete-level power control for adaptive modulation schemes with capacity-approaching component codes. In *Proc. 2006 IEEE International Conference on Communications (ICC)*, Istanbul, June 2006.

[GPV05a] M. C. Gursoy, V. Poor, and S. Verdú. The noncoherent Rician fading channel—Part I: Structure of the capacity-achieving input. *IEEE Transactions on Wireless Communications*, 4(5):2193–2206, September 2005.

[GPV05b] M. C. Gursoy, V. Poor, and S. Verdú. The noncoherent Rician fading channel—Part II: Spectral efficiency in the low-power regime. *IEEE Transactions on Wireless Communications*, 4(5):2207–2221, September 2005.

[GR00] I. S. Gradshteyn and I. M. Ryzhik. *Table of Integrals, Series, and Products*. Academic Press, sixth edition, 2000.

[GSS+03] D. Gesbert, M. Shafi, D. Shiu, P. J. Smith, and A. Nayguib. From theory to practice: An overview of MIMO space-time coded wireless systems. *IEEE Journal on Selected Areas in Communications*, 21(3):281–302, April 2003.

[GV97] A. J. Goldsmith and P. P. Varaiya. Capacity of fading channels with channel side information. *IEEE Transactions on Information Theory*, November 1997.

[HHØ00] K. J. Hole, H. Holm, and G. E. Øien. Adaptive multidimensional coded modulation over flat fading channels. *IEEE Journal on Selected Areas in Communications*, 18(7):1153–1158, July 2000.

[Jak74] W. C. Jakes. *Microwave Mobile Communications*. Wiley, 1974.

[KD00] J. H. Kotecha and P. M. Djurić. Sequential Monte Carlo sampling for Rayleigh fast-fading channels. In *Proc. 2000 IEEE International Conference on Acoustics, Speech, and Signal Processing (ICASSP)*, pages 61–64, Istanbul, June 2000.

[KG00] C. Köse and L. Goeckel. On power adaptation in adaptive signaling systems. *IEEE Transactions on Communications*, 48(11):1769–1773, November 2000.

[Kim06] T. T. Kim. *Quantized feedback for slow fading channels*. Licentiate Thesis, Royal Institute of Technology (KTH), Stockholm, Sweden, 2006.

[KØ05] S. de la Kethulle de Ryhove and G. E. Øien. Energy-optimised coded modulation for short-range wireless communications on Nakagami-*m* fading channels. In *Proc. Norwegian Signal Processing Symposium (NORSIG)*, Stavanger, September 2005.

[Lin06] G. Lin. *On the design and optimization of OFDM Systems*. PhD thesis, Norwegian University of Science and Technology, 2006.

[LLC04] V. K. N. Lau, Y. Liu, and T.-A. Chen. Capacity of memoryless channels and block-fading channels with designable cardinality-constrained channel state feedback. *IEEE Transactions on Information Theory*, 50(9):2038–2049, September 2004.

[LM03] A. Lapidoth and S. Moser. Capacity bounds via duality with applications to multiple-antenna systems on flat-fading channels. *IEEE Transactions on Information Theory*, 49(10):2426–2467, October 2003.

[LV04] Y. Liang and V. Veeravalli. Capacity of noncoherent time-selective Rayleigh-fading channels. *IEEE Transactions on Information Theory*, 50(12):3095–3110, December 2004.

[MH99] T. Marzetta and B. Hochwald. Capacity of a mobile multiple-antenna communication link in Rayleigh flat fading. *IEEE Transactions on Information Theory*, 45(1):139–157, January 1999.

[Nak60] M. Nakagami. The *m*-distribution – a general formula of intensity distribution of rapid fading. In *Statistical Methods in Radio Wave Propagation*, pages 3–36. Pergamon Press, 1960.

[OED89] *The Oxford English Dictionary*. Clarendon Press, second edition, 1989.

[ØHH04] G. E. Øien, H. Holm, and K. J. Hole. Impact of channel prediction on adaptive coded modulation performance in Rayleigh fading. *IEEE Transactions on Vehicular Technology*, 53(3):758–769, May 2004.

[Pro01] J. Proakis. *Digital Communications*. McGraw-Hill, fourth edition, 2001.

[Rap02] T. S. Rappaport. *Wireless Communications Principles and Practice*. Prentice Hall, second edition, 2002.

[Ray80] J. W. S. Rayleigh. On the resultant of a large number of vibrations of the same pitch and of arbitrary phase. *Philosophical Magazine*, 10:73–78, August 1880.

[SA01] M. K. Simon and M. S. Alouini. *Digital Communication over Fading Channels*. Wiley Series in Telecommunications and Signal Processing, first edition, 2001.

[San96] M. Sandell. *Degign and analysis of estimators for multicarrier modulation and ultrasonic imaging*. PhD thesis, Luleå University of Technology, 1996.

[SB04] Y. Song and S. D. Blostein. Adaptive modulation for MIMO systems with imperfect channel knowledge. In *Proc. 22nd Biennial Symposium on Communications, Kingston, Canada*, pages 428–430, May/June 2004.

[SBD95] S. Shamai (Shitz) and I. Bar-David. The capacity of average and peak-power-limited quadrature Gaussian channels. *IEEE Transactions on Information Theory*, 41(4):1060–1071, July 1995.

[SFGK00] D. Shiu, G. J. Foschini, M. J. Gans, and J. M. Kahn. Fading correlation and its effect on the capacity of multielement antenna systems. *IEEE Transactions on Communications*, 48(3):502–513, March 2000.

[Sha48] C. E. Shannon. A mathematical theory of communication. *Bell System Technical Journal*, 27:379–423, 623–656, July, October 1948.

[Smi71] J. Smith. The information capacity of amplitude- and variance-constrained scalar Gaussian channels. *Information and Control*, 18(3):203–219, April 1971.

[SSP01] H. Sampath, P. Stoica, and A. Paulraj. Generalized linear precoder and decoder design for MIMO channels using the weighted MMSE criterion. *IEEE Transactions on Communications*, 49(12):2198–2206, December 2001.

[Stü01] G. L. Stüber. *Principles of Mobile Communication*. Kluwer Academic Publishers, second edition, 2001.

[TE97] G. Taricco and M. Elia. Capacity of fading channel with no side information. *Electronics Letters*, 33(16):1368–1370, July 1997.

[Tel95] E. Telatar. Capacity of multi-antenna Gaussian channels. Technical report, AT&T Bell Laboratories, June 1995.

[TJC99] V. Tarokh, H. Jafarkhani, and A. R. Calderbank. Space-time block codes from orthogonal designs. *IEEE Transactions on Information Theory*, 45(5):1456–1467, July 1999.

[TSC98] V. Tarokh, N. Seshadri, and A. Calderbank. Space-time codes for high data rate wireless communications: Performance criterion and code construction. *IEEE Transactions on Information Theory*, 44(2):744–765, March 1998.

[Zha05] J. Zhang. On the bounds of the non-coherent capacity of Gauss-Markov fading channels. In *Proc. 2005 IEEE International Conference on Acoustics, Speech, and Signal Processing (ICASSP)*, pages 757–760, Philadelphia, March 2005.

[ZT02] L. Zheng and D. Tse. Communication on the Grassmann manifold: A geometric approach to the noncoherent multiple-antenna channel. *IEEE Transactions on Information Theory*, 48(2):359–383, February 2002.

[ZT03] L. Zheng and D. N. C. Tse. Diversity and multiplexing: a fundamental tradeoff in multiple antenna channels. *IEEE Transactions on Information Theory*, 49(5):1073–1096, May 2003.

[ZV04] Z. Zhou and B. Vucetic. Design of adaptive modulation using imperfect CSI in MIMO systems. *Electronics Letters*, 40(17):1073–1075, August 2004.

Part II

Included papers

Paper A

An Efficient Design Methodology for Constant Power Link Adaptation Schemes

Sébastien de la Kethulle de Ryhove, Geir E. Øien, and Lars Lundheim

Under review for possible publication in *IEEE Transactions on Vehicular Technology* at the time of writing of this dissertation.

Abstract

The energy-efficient design of short-distance wireless communication systems requires the inclusion of circuit energy consumption in the system's total energy budget. We consider the design of constant power link adaptation schemes in which circuit energy consumption is included in the total energy budget, and in which the system's instantaneous bit-error rate (BER) must never exceed a predefined threshold. We show how – in numerous cases of practical importance – the dimensionality of the associated nonlinear optimisation problem can be reduced from $N + 1$ to one, where N denotes the number of available transmission schemes. The main contribution, a methodology which significantly simplifies the design of such constant power link adaptation schemes, is then illustrated by an example.

S. de la Kethulle de Ryhove, G. E. Øien, and L. Lundheim are with the Department of Electronics and Telecommunications, Norwegian University of Science and Technology, N–7491 Trondheim, Norway (e-mails: {delaketh, oien, lundheim}@iet.ntnu.no).

The material in this letter was presented in part at the 2006 International Conference on Communications (ICC '06), Istanbul, Turkey, 2006.

1 Introduction

Including circuit energy consumption in the global energy budget when designing a short-distance wireless communication system has been shown to be a matter of paramount importance if the communication system's overall energy consumption is to be minimised [CGB05; KØ05; CGB04; CMGL05]. The reason for this is that when the distance between the transmitter and the receiver of a communication link becomes sufficiently short, circuit energy consumption and transmission energy consumption become comparable, and substantial energy savings can be achieved by making use of a transmission scheme which takes into account total energy consumption instead of transmission energy alone [CGB05; KØ05; CGB04; CMGL05]. In such scenarios, including circuit energy consumption in the global energy budget is thus essential for maximising the lifetime of energy-constrained wireless devices, which nowadays have to meet ever more stringent requirements.

In this correspondence, we apply the above ideas to the energy-efficient design of wireless communication systems that make use of link adaptation, which is a promising technique to improve the average spectral efficiency of wireless communication systems that are affected by fading. The underlying concept is adaptation to a time-varying channel through variation of channel codes, modulation constellations, and transmitted power [GV97; HHØ00; GC97; CG01; KG00; FSES04; AG97; GØO06].

We will exclusively consider the design of link adaptation schemes in which the average power of every transmitted symbol frame is kept constant [KG00; AG97; FSES04; CG01; GØO06]. Such schemes are referred to in the literature using terms such as "constant power signalling" [KG00] or "constant power transmission scheme" [GØO06]. It is however imperative to bear in mind that when using such a phrase, it is the average power of every transmitted symbol frame – rather than the power of each one of the symbols within a frame – which is constrained to remain constant.

Constant power link adaptation schemes are attractive for a variety of reasons. Firstly, the practical implementation of constant power link adaptation schemes is easier than that of variable power link adaptation schemes, among others because the latter require more feedback bandwidth [FSES04] and hardware complexity [CG01]. Constant power schemes can in addition be desirable in multiuser systems to reduce variations in interference power [CG01], and also offer the advantage of less severe requirements on the power amplifier's dynamic range. Information theoretic arguments provide yet another motivation for the study of constant power link adaptation schemes: when the transmission rate can be adapted con-

tinuously and the channel state is known to both the transmitter and the receiver, it has been shown [GV97] that power adaptation only provides a negligible increase in capacity. Nonetheless, when only a finite set of rates can be used, power adaptation can considerably increase the system's average spectral efficiency [GØO06; CG01] – although the penalty for not performing power adaptation becomes less and less significant as the number of available rates becomes larger, and is described as "not very large" in [CG01]. Constant power link adaptation schemes therefore unquestionably provide an option which is worthy of consideration when designing a wireless communication system.

We will examine the energy-efficient design of constant power link adaptation schemes in which circuit energy consumption is included in the total energy budget and in which the system's instantaneous bit-error rate (BER) must never exceed a predefined threshold; and separately analyse systems where the available signal constellations have a constant peak to average power ratio (e.g. PSK or FSK modulations), and systems where the available signal constellations have a varying peak to average power ratio (e.g. QAM modulation). After showing in detail how – in numerous cases of practical importance – the associated $N+1$-dimensional optimisation problem can be reduced to a one-dimensional optimisation problem (N denoting the number of available component transmission schemes), we will apply our design method to an example system. Related work on a similar problem can also be found in [SS03].

The remainder of this correspondence is organised as follows: the system model is presented in Sec. 2, the design problem we consider being introduced in Sec. 3. After analysing some of its properties in Sec. 4, we respectively show in Secs. 5 and 6 how – in many cases of practical importance – it can be reduced to a one-dimensional optimisation problem in the case of signal constellations of constant and varying peak to average power ratios. Our design method is subsequently applied to an example problem in Sec. 7, and we draw some conclusions in Sec. 8.

2 System Model

We consider a slowly varying, frequency-flat fading discrete-time channel with stationary and ergodic time-varying channel gain denoted by $\sqrt{g(i)}$ at time $i \in \{1,2,\ldots\}$. Let the transmitted signal have complex baseband representation $x(i)$. The received baseband signal is then given by $y(i) = \sqrt{g(i)}x(i) + w(i)$, where $w(i)$ denotes complex AWGN. The real and imaginary parts of $w(i)$ are assumed to be statistically independent with

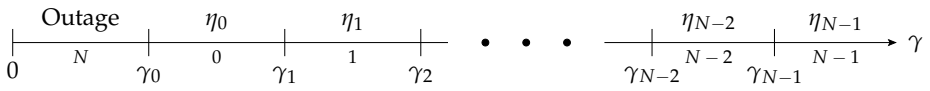

FIGURE A.1: Division of the CSNR range $[0, \infty)$ into $N + 1$ quantisation intervals.

variance $BN_0/2$, where B is the received signal bandwidth and $N_0/2$ is the two-sided noise power spectral density.

Let S_t denote the constant transmit signal power. The instantaneous channel signal-to-noise ratio (CSNR) of the system is given by $\gamma(i) = S_t g(i)/(N_0 B)$, and its expected value is $\bar{\gamma} = S_t \bar{g}/(N_0 B)$, where $\bar{g}$ denotes the average channel power gain. For the sake of notational simplicity, we henceforth omit the time index i in $\gamma(i)$ and $g(i)$.

The non-negative, real-valued channel gain $\sqrt{g}$ is modelled as a continuous stochastic variable in the range $[0, \infty)$. The distribution of the instantaneous received CSNR γ depends on the distribution of $\sqrt{g}$ and is denoted by $f(\gamma)$, with $\gamma \in [0, \infty)$ and mean value $\bar{\gamma}$. (Note that $f(\gamma)$ is independent of i since the channel gain $\sqrt{g}$ is stationary.) We assume that the received CSNR distribution results from one of the standard channel fading models used in the literature on communication theory (e.g. Rayleigh, Rice, or Nakagami-m [Nak60]), and we will thus say that $f(\gamma)$ is a "practical received CSNR distribution". All subsequent statements regarding "practical received CSNR distributions" can be formally verified for each one of the CSNR distributions $f(\gamma)$ arising from one of the channel fading models mentioned above.

We assume that the communication channel is slowly varying. The channel gain $\sqrt{g}$ therefore changes at a rate much slower than the symbol rate, and we can assume that $\sqrt{g}$ remains constant during any given symbol frame. We assume ideal estimation of $\sqrt{g}$ is performed at the receiver (high-quality estimates can for example be achieved by the transmission of a known sequence of pilot symbols), and that a zero-delay, zero-error feedback channel exists between the receiver and the transmitter.

Let the set $[0, \infty)$ of possible CSNR values be divided into $N + 1$ non overlapping quantisation intervals (or *bins*), as depicted in Fig. A.1. We assume $\gamma \in [\gamma_0, \gamma_1)$ in bin 0, $\gamma \in [\gamma_1, \gamma_2)$ in bin 1, ..., $\gamma \in [\gamma_{N-1}, \infty)$ in bin $N - 1$, and $\gamma \in [0, \gamma_0)$ in bin N – with $\gamma_0 \leq \gamma_1 \leq \cdots \leq \gamma_{N-1}$. Once the CSNR estimation has been performed at the receiver, the corresponding bin number is fed back to the transmitter. When the estimation of the CSNR γ yields a value belonging to the interval $[\gamma_n, \gamma_{n+1})$, the communication channel may be viewed, during the transmission of the subsequent symbol frame, as an AWGN channel of CSNR $\geq \gamma_n$. We will assume in this

work that the system's BER must be maintained below a predetermined threshold value BER_0 during the transmission of each and every symbol frame. (Such systems are said to be subject to an "instantaneous BER constraint" in the literature [CG01; FSES04].) A transmission scheme designed to achieve a BER $\leq \mathrm{BER}_0$ on AWGN channels of CSNR $\geq \gamma_n$ can hence be selected for the transmission of this symbol frame.

We assume thus that a set of N different transmission schemes, numbered from $n = 0$ to $n = N - 1$, of increasing spectral efficiencies $0 < \eta_0 < \eta_1 < \cdots < \eta_{N-1}$ has been designed and is available for use. The nth transmission scheme, of spectral efficiency η_n and peak to average power ratio ξ_n, is to be used when the CSNR $\gamma \in [\gamma_n, \gamma_{n+1})$ (i.e. the CSNR is in the nth bin). When $\gamma \in [0, \gamma_0)$, no transmission is performed and the system experiences an *outage*. Note that this can also be interpreted as transmission at zero-rate and zero-power; we implicitly allow for this possibility when speaking of constant power transmission schemes.

We will assume throughout this correspondence that $\xi_0 \leq \xi_1 \leq \cdots \leq \xi_{N-1}$. This is the case both for PSK and FSK modulations, where we have $\xi_n = 1$ for all n, and also for square QAM modulations as long as $M_0 \leq M_1 \leq \cdots \leq M_{N-1}$, where M_n denotes the number of points in the nth signal constellation. The latter statement can be verified by using the expression [CGB05] $\xi_n = 3\frac{\sqrt{M_n}-1}{\sqrt{M_n}+1}$ for the peak to average power ratio of a square QAM signal constellation with M_n points.

Our modelling of circuit power consumption is inspired by [CGB05]. We invite the reader to examine this reference for details on how this modelling can be done, for more elaborate particularities on the meaning of the different parameters involved in this modelling, and for a thorough discussion on why it is of utmost importance to include circuit power consumption in the overall energy budget when designing short-distance wireless communication systems. We conclude this section by providing a short summary of the manner in which circuit power consumption is modelled in [CGB05], this being necessary for the understanding of the remainder of this correspondence.

The power consumption of baseband signal processing blocks (e.g. source coding, pulse shaping, and digital modulation) is neglected, a generic Low-IF transceiver structure is assumed, and it is assumed that the transceiver circuitry works on a multimode basis: the circuits work in active mode when there is a signal to transmit, in sleep mode when there is no signal to transmit (i.e. when there is an outage), and in transient mode when switching from sleep mode to active mode. As explained in [CGB05], although the transient duration from active mode to sleep mode is short

enough to be neglected, the start-up process from sleep mode to active mode may be slow due to the finite phase lock loop settling time in the frequency synthesisers. This settling time is denoted by T_{tr}.

Circuit power consumption in active mode is denoted by S_{c}, and it includes both circuit power consumption in active mode at the transmitter S_{ct} and circuit power consumption in active mode at the receiver S_{cr}. The amplifier power consumption when using the nth transmission scheme is modelled according to $S_{\text{amp},n} = \alpha_n S_{\text{t}}$ [CGB05], where $\alpha_n = \frac{\xi_n}{\nu} - 1$ with ν the drain efficiency of the power amplifier. The amplifier power consumption $S_{\text{amp},n}$ does not include the transmit power S_{t}.

The power consumption in sleep mode S_{sp} is neglected because it is much smaller than the power consumption in active mode if the circuitry is properly designed; we thus set $S_{\text{sp}} = 0$ [CGB05]. The power consumption during the transient mode S_{tr} only needs to include that of the frequency synthesisers, since no power is consumed by the other circuit components while they wait for these to settle down [CGB05]. Finally, the total power consumption in active mode when using the nth transmission scheme $S_{\text{on},n}$ is given by $S_{\text{c}} + (1 + \alpha_n) S_{\text{t}}$, i.e. the sum of circuit power consumption, transmit power consumption, and losses due to the power amplifier.

The average channel gain $\bar{g}$ is also modelled as in [CGB05]. It can be expressed as $\bar{g} = 1/(N_{\text{f}} G_d)$, where N_{f} is the receiver noise figure, and $G_d \triangleq G_1 d^r M_{\text{link}}$ with d the transmitter-receiver separation, r the path loss exponent, M_{link} the link margin compensating the hardware process variations and other additive background noise or interference, and G_1 the gain factor at $d = 1$ m which is defined by the antenna gain, carrier frequency, and other system parameters.

3 Problem Setting

The problem we consider is that of designing a communication system with constant power link adaptation, assuming a set of N different predefined transmission schemes (which could for instance be predefined due to the choice of a certain protocol, and therefore be beyond the designer's control) is available. The parameters defined in Sec. 2, namely N_0, B, BER_0, S_{ct}, S_{cr}, ν, N_{f}, G_1, d, r, M_{link}, S_{tr}, and T_{tr}, as well as the peak to average power ratios of the N signal constellations $\xi_0, \ldots, \xi_{N-1}$, the channel fading model (e.g. Rayleigh, Rice, or Nakagami-m), and the duration T_{f} of a symbol frame are assumed to be known.

Our objective is then to find – for the given N predefined transmission schemes and system parameters – the values of $\gamma_0, \ldots, \gamma_{N-1}$, and S_{t} which

maximise the system's average spectral efficiency subject to requirements on the target instantaneous bit-error rate (BER $\leq$ BER$_0$), and the average and peak power consumptions. The system's average spectral efficiency η is given by

$$\eta = \sum_{n=0}^{N-1} \eta_n \int_{\gamma_n}^{\gamma_{n+1}} f(\gamma) \mathrm{d}\gamma, \tag{A.1}$$

where η_n corresponds to the spectral efficiency of the nth transmission scheme ($0 < \eta_0 < \eta_1 < \cdots < \eta_{N-1}$), $\int_{\gamma_n}^{\gamma_{n+1}} f(\gamma)\mathrm{d}\gamma$ is the probability that transmission scheme n be used, and we have defined $\gamma_N = \infty$ for convenience. Note that both the resulting constant transmit power S_t and the resulting CSNR subdivision specified by $\gamma_0, \ldots, \gamma_{N-1}$ will *only* be optimal for the given set of transmission schemes and system parameters.

Now, for a given transmission scheme $n \in \{0, \ldots, N-1\}$ operating over an AWGN channel, the BER obviously being a monotonously decreasing function of the SNR, the requirement BER $\leq$ BER$_0$ can be rewritten $\gamma_n \geq \gamma_n^*$, where γ_n^* is the SNR value for which a bit-error rate of BER$_0$ is achieved when using transmission scheme n over an AWGN channel. The transmission schemes $0, \ldots, N-1$ being of increasing spectral efficiencies, we will also have $\gamma_0^* < \ldots < \gamma_{N-1}^*$. Remember in addition that $\gamma_0 \leq \ldots \leq \gamma_{N-1}$.[1]

Using S to denote the maximum permitted average power consumption, the average power constraint can be written

$$\sum_{n=0}^{N-1} [S_\mathrm{c} + S_\mathrm{t}(1+\alpha_n)] \int_{\gamma_n}^{\gamma_{n+1}} f(\gamma)\mathrm{d}\gamma + S_\mathrm{tr}\frac{T_\mathrm{tr}}{\kappa T_\mathrm{f}} \int_0^{\gamma_0} f(\gamma)\mathrm{d}\gamma \leq S. \tag{A.2}$$

Here, the terms in the sum correspond to the power consumption in active mode when using transmission scheme n multiplied by the probability that transmission scheme n be used ($n \in \{0, \ldots, N-1\}$), while the second term corresponds to the power consumption that results from sleep mode to active mode transitions. The expected number of consecutive outage frames is denoted κ, and is included because the system remains in sleep mode when consecutive outages occur. Although strictly speaking κ is a function of the outage probability, we neglect this dependency here and make

[1] It is common to set $\gamma_n = \gamma_n^*$ for all $n \in \{0, \ldots, N-1\}$ in the literature on link adaptation (see e.g. [HHØ00]), since it is straightforward to show that – for a given power budget – doing so maximises the average spectral efficiency of constant power link adaptation schemes if transmission energy only is taken into account. However, this is not always the case anymore when circuit energy consumption is also included in the global energy budget, as illustrated by the example presented in Sec. 7.

the approximation $\kappa \approx 1$ (Note that since in general $T_{\text{tr}} \ll T_{\text{f}}$, the influence of the second term will be close to negligible anyway.) If one defines $S' = S - S_{\text{tr}}T_{\text{tr}}/(\kappa T_{\text{f}})$ and $S'_{\text{c}} = S_{\text{c}} - S_{\text{tr}}T_{\text{tr}}/(\kappa T_{\text{f}})$, (A.2) can be rewritten

$$\sum_{n=0}^{N-1} \left[S'_{\text{c}} + S_{\text{t}}(1+\alpha_n)\right] \int_{\gamma_n}^{\gamma_{n+1}} f(\gamma)\mathrm{d}\gamma \leq S'. \tag{A.3}$$

In the remainder of this letter, we will assume this has been done and assume an average power constraint of the form (A.3), replacing however S'_{c} by S_{c} and S' by S for notational simplicity.

A peak power constraint will be present in any practical communication system: the maximum power consumption at the transmitter cannot exceed the maximum available power at the transmitter S_{maxt}, and likewise at the receiver. Since as a consequence of $\xi_0 \leq \xi_1 \leq \cdots \leq \xi_{N-1}$ we must have $\alpha_0 \leq \alpha_1 \leq \cdots \leq \alpha_{N-1}$, and since the transmitter circuit power consumption is maximum in active mode, this will result in a constraint of the form

$$S_{\text{ct}} + (1+\alpha_{N-1})S_{\text{t}} \leq S_{\text{maxt}}, \tag{A.4}$$

i.e. the total power consumption at the transmitter when using the $(N-1)$th transmission scheme must be less than or equal to S_{maxt}. If we make use of the relation $S_{\text{t}} = N_0 B\bar{\gamma}/\bar{g}$, the peak power constraint (A.4) can be rewritten

$$\bar{\gamma} \leq \frac{\bar{g}}{N_0 B}\,\frac{S_{\text{maxt}} - S_{\text{ct}}}{1+\alpha_{N-1}} \triangleq \bar{\gamma}^*. \tag{A.5}$$

We thus wish to solve the following optimisation problem (referred to as problem P in the remainder of this document): find $\underline{\gamma} = (\gamma_0, \ldots, \gamma_{N-1}, \bar{\gamma})$ such that

$$J(\underline{\gamma}) = -\sum_{n=0}^{N-1} \eta_n \int_{\gamma_n}^{\gamma_{n+1}} f(\gamma)\mathrm{d}\gamma \tag{A.6}$$

is minimum, under the constraints

$$c_n(\underline{\gamma}) = \gamma_n - \gamma_n^* \geq 0, \qquad n = 0, \ldots, N-1 \tag{A.7}$$

$$c_N(\underline{\gamma}) = S - \sum_{n=0}^{N-1} \left[S_{\text{c}} + \rho\bar{\gamma}(1+\alpha_n)\right] \int_{\gamma_n}^{\gamma_{n+1}} f(\gamma)\mathrm{d}\gamma \geq 0, \tag{A.8}$$

$$c'_n(\underline{\gamma}) = \gamma_{n+1} - \gamma_n \geq 0, \quad n = 0, \ldots, N-2, \tag{A.9}$$

$$c'_N(\underline{\gamma}) = \bar{\gamma}^* - \bar{\gamma} \geq 0, \tag{A.10}$$

where we have made the definition $\rho \triangleq \frac{N_0 B}{\bar{g}}$ for convenience. The minus sign in (A.6) is included in order to state the problem as a minimi-

sation problem, which is standard practice in optimisation theory literature [NW99]. Note also that the optimisation variable $\bar{\gamma}$ is being used instead of S_t.

4 Problem Analysis

The analysis of problem P will be based on the Karush-Kuhn-Tucker (KKT) theorem, which is a central theorem in constrained optimisation (see e.g. [NW99], Ch. 12). The KKT equations of problem P read

$$\begin{cases} \lambda_0 - \lambda_0' + \lambda_N \left[\rho\bar{\gamma}(1+\alpha_0) + S_c\right] f(\gamma_0) = \eta_0 \, f(\gamma_0) \\ \lambda_1 + \lambda_0' - \lambda_1' + \lambda_N \rho\bar{\gamma} \, (\alpha_1 - \alpha_0) \, f(\gamma_1) = (\eta_1 - \eta_0) \, f(\gamma_1) \\ \lambda_2 + \lambda_1' - \lambda_2' + \lambda_N \rho\bar{\gamma} \, (\alpha_2 - \alpha_1) \, f(\gamma_2) = (\eta_2 - \eta_1) \, f(\gamma_2) \\ \qquad\qquad\qquad\qquad\qquad\qquad \vdots \\ \lambda_{N-2} + \lambda_{N-3}' - \lambda_{N-2}' + \lambda_N \rho\bar{\gamma} \, (\alpha_{N-2} - \alpha_{N-3}) \, f(\gamma_{N-2}) \\ \qquad\qquad\qquad\qquad\qquad\qquad = (\eta_{N-2} - \eta_{N-3}) \, f(\gamma_{N-2}) \\ \lambda_{N-1} + \lambda_{N-2}' + \lambda_N \rho\bar{\gamma} \, (\alpha_{N-1} - \alpha_{N-2}) \, f(\gamma_{N-1}) \\ \qquad\qquad\qquad\qquad\qquad\qquad = (\eta_{N-1} - \eta_{N-2}) \, f(\gamma_{N-1}) \\ \lambda_N \dfrac{\partial}{\partial\bar{\gamma}} \left[S - \displaystyle\sum_{n=0}^{N-1} \left[S_c + \rho\bar{\gamma}(1+\alpha_n)\right] \int_{\gamma_n}^{\gamma_{n+1}} f(\gamma) \mathrm{d}\gamma \right] - \lambda_N' \\ \qquad\qquad\qquad\qquad\qquad\qquad = \; - \displaystyle\sum_{n=0}^{N-1} \eta_n \frac{\partial}{\partial\bar{\gamma}} \int_{\gamma_n}^{\gamma_{n+1}} f(\gamma) \mathrm{d}\gamma, \end{cases} \tag{A.11}$$

where

$$\begin{cases} \lambda_0 \, c_0(\underline{\gamma}) = 0 & \lambda_0' \, c_0'(\underline{\gamma}) = 0 \\ \qquad\vdots & \qquad\vdots \\ \lambda_{N-2} \, c_{N-2}(\underline{\gamma}) = 0 & \lambda_{N-2}' \, c_{N-2}'(\underline{\gamma}) = 0 \\ \lambda_{N-1} \, c_{N-1}(\underline{\gamma}) = 0 & \\ \lambda_N \, c_N(\underline{\gamma}) = 0 & \lambda_N' \, c_N'(\underline{\gamma}) = 0, \end{cases} \tag{A.12}$$

and

$$\begin{cases} \lambda_0 \geq 0 & \lambda_0' \geq 0 \\ \qquad\vdots & \qquad\vdots \\ \lambda_{N-2} \geq 0 & \lambda_{N-2}' \geq 0 \\ \lambda_{N-1} \geq 0 & \\ \lambda_N \geq 0 & \lambda_N' \geq 0, \end{cases} \tag{A.13}$$

with $\lambda_0, \ldots, \lambda_N$ the Lagrange multipliers corresponding to $c_0(\underline{\gamma}), \ldots, c_N(\underline{\gamma})$, and $\lambda'_0, \ldots, \lambda'_{N-2}$ and λ'_N the Lagrange multipliers corresponding to $c'_0(\underline{\gamma}), \ldots, c'_{N-2}(\underline{\gamma})$ and $c'_N(\underline{\gamma})$.

A sufficient condition for a local minimum of problem P to satisfy the KKT equations (A.11), (A.12), and (A.13) is that the so-called Mangasarian–Fromovitz constraint qualification (MFCQ) [NW99; MF67] hold at that local minimum. In the following Lemma, we prove that the MFCQ holds at all feasible points $\underline{\gamma}$ (and thus at all local minima) of problem P:

Lemma A.1
For all practical received CSNR distributions $f(\gamma)$, the MFCQ holds at all feasible points $\underline{\gamma}$ of problem P.

Proof: The proof is deferred to Appendix A. □

As a consequence of the KKT theorem and Lemma A.1, we can thus conclude that any local minimum of problem P must satisfy the KKT equations (A.11), (A.12), and (A.13). We further characterise the possible solutions of problem P with the following three Lemmas:

Lemma A.2
If $\underline{\gamma}^0 = (\gamma_0^0, \ldots, \gamma_{N-1}^0, \bar{\gamma}^0)$ is a solution to problem P, then either $c_N(\underline{\gamma}^0) = 0$ or $c'_N(\underline{\gamma}) = 0$ for all practical received CSNR distributions $f(\gamma)$.

Proof: Let us assume that $\underline{\gamma}^0$ is a solution to problem P, that $f(\gamma)$ is a practical received CSNR distribution, and that both $c_N(\underline{\gamma}^0) > 0$ and $c'_N(\underline{\gamma}^0) > 0$. Observe that $c_N(\underline{\gamma}^0)$ is a continuous, strictly decreasing function of $\bar{\gamma}^0$ for fixed $\gamma_0^0, \ldots, \gamma_{N-1}^0$ (see the argument following equation (A.26) in the proof of Lemma A.1). Hence, $c'_N(\underline{\gamma}^0)$ also being a continuous, strictly decreasing function of $\bar{\gamma}^0$, there exists a $\bar{\gamma}' > \bar{\gamma}^0$ such that either $c_N(\gamma_0^0, \ldots, \gamma_{N-1}^0, \bar{\gamma}') = 0$ and $c'_N(\gamma_0^0, \ldots, \gamma_{N-1}^0, \bar{\gamma}') \geq 0$, or $c_N(\gamma_0^0, \ldots, \gamma_{N-1}^0, \bar{\gamma}') \geq 0$ and $c'_N(\gamma_0^0, \ldots, \gamma_{N-1}^0, \bar{\gamma}') = 0$. However, since $0 < \eta_0 < \cdots < \eta_{N-1}$, it is clear that, for all practical received CSNR distributions $f(\gamma)$, we will have[2] $J(\gamma_0^0, \ldots, \gamma_{N-1}^0, \bar{\gamma}') < J(\gamma_0^0, \ldots, \gamma_{N-1}^0, \bar{\gamma}^0)$ (see Appendix B), and therefore $\underline{\gamma}^0$ cannot be a solution to problem P. We hence must have either $c_N(\underline{\gamma}^0) = 0$ or $c'_N(\underline{\gamma}^0) = 0$. □

The interpretation of Lemma A.2 is clear: either the available power S is used in its totality, or the transmission power S_t is limited by the peak power constraint.

[2] This corresponds to saying that for fixed $\gamma_0^0, \ldots, \gamma_{N-1}^0$ the average spectral efficiency η is a strictly increasing function of $\bar{\gamma}$ (or, equivalently, of the transmitted power $S_t = N_0 B \bar{\gamma} / \bar{g}$), which is intuitively obvious.

Lemma A.3
If $\underline{\gamma}^0 = (\gamma_0^0, \ldots, \gamma_{N-1}^0, \bar{\gamma}^0)$ *is a solution to problem P where* $c_N(\underline{\gamma}^0) > 0$*, then* $(\gamma_0^0, \ldots, \gamma_{N-1}^0, \bar{\gamma}^0) = (\gamma_0^*, \ldots, \gamma_{N-1}^*, \bar{\gamma}^*)$.

Proof: We know by the previous lemma that if $\underline{\gamma}^0$ is a solution to problem P where $c_N(\underline{\gamma}^0) > 0$, then we must have $c'_N(\underline{\gamma}^0) = 0$, i.e. $\bar{\gamma}^0 = \bar{\gamma}^*$. In addition, since $c_N(\underline{\gamma}^0) > 0$, the KKT equations imply that $\lambda_N = 0$. Now, observing that, for $n \in \{0, \ldots, N-2\}$, both c_n and c'_n cannot be active[3] at the same time, and taking into account the fact that $\lambda_N = 0$ in (A.11), we immediately conclude $\lambda_0, \ldots, \lambda_{N-1} > 0$ due to the fact that $\eta_0 f(\gamma_0^0)$ and $(\eta_n - \eta_{n-1}) f(\gamma_n^0)$ for $n \in \{1, \ldots, N-1\}$ are strictly positive. Hence, $(\gamma_0, \ldots, \gamma_{N-1}) = (\gamma_0^*, \ldots, \gamma_{N-1}^*)$. □
If the average power constraint is not active, the solution is thus given by $(\gamma_0^0, \ldots, \gamma_{N-1}^0, \bar{\gamma}^0) = (\gamma_0^*, \ldots, \gamma_{N-1}^*, \bar{\gamma}^*)$.

Lemma A.4
Any $\underline{\gamma}^0 = (\gamma_0^0, \ldots, \gamma_{N-1}^0, \bar{\gamma}^0)$ *such that* $\gamma_0^0 = \gamma_1^0 = \ldots = \gamma_{N-1}^0 > \gamma_{N-1}^*$ *cannot be a solution to problem P.*

Proof: The proof is given in Appendix A. □

5 Constant Peak to Average Power Ratio Transmission Schemes

Using the results of the previous section, we now show how the $N+1$-dimensional optimisation problem presented in Sec. 3 can be reduced to a one-dimensional optimisation problem in the case where the N available transmission schemes have a constant peak to average power ratio (e.g. when using PSK or FSK signal constellations). Since in this case $\xi_0 = \xi_1 = \cdots = \xi_{N-1}$, and hence $\alpha_0 = \alpha_1 = \ldots = \alpha_{N-1}$, we see that the KKT conditions (A.11) are considerably simplified. We can then prove the following Lemma:

Lemma A.5
When $\alpha_0 = \cdots = \alpha_{N-1}$*, any* $\underline{\gamma}^0 = (\gamma_0^0, \ldots, \gamma_{N-1}^0, \bar{\gamma}^0)$ *such that* $\gamma_{n-1}^0 \neq \gamma_n^0 > \gamma_n^*$ *for a given* $n \in \{1, \ldots, N-1\}$ *cannot be a solution to problem P.*

Proof: When $\alpha_0 = \cdots = \alpha_{N-1}$, the equalities in (A.12) show that, since $\gamma_{n-1}^0 \neq \gamma_n^0 > \gamma_n^*$, we must have $\lambda_n = \lambda'_{n-1} = 0$. Hence, the equality

[3] In optimisation theory terminology, an active inequality constraint is a constraint which is satisfied with equality [NW99].

involving $f(\gamma_n)$ in (A.11) becomes

$$-\lambda'_n = (\eta_n - \eta_{n-1})\, f(\gamma_n^0). \tag{A.14}$$

However, since $(\eta_n - \eta_{n-1})\, f(\gamma_n^0) > 0$ (the N available transmission schemes have increasing spectral efficiencies) and $\lambda'_n \geq 0$ (because of (A.13)), it is impossible to find λ'_n such that (A.14) is verified. □

When $\alpha_0 = \cdots = \alpha_{N-1}$, Lemmas A.4 and A.5 thus allow us to conclude that for any solution $\underline{\gamma}$ of problem P, $(\gamma_0, \ldots, \gamma_{N-1})$ can only have one of the following forms:

1. $\gamma_n^* \leq \gamma_0 = \ldots = \gamma_n < \gamma_{n+1}$, and $(\gamma_{n+1}, \ldots, \gamma_{N-1}) = (\gamma_{n+1}^*, \ldots, \gamma_{N-1}^*)$, for a given $n \in \{0, \ldots, N-2\}$, or
2. $\gamma_0 = \gamma_1 = \ldots = \gamma_{N-1} = \gamma_{N-1}^*$.

A minute of thought should now convince the reader that, for each possible value of γ_0, the corresponding values of $\gamma_1, \ldots, \gamma_{N-1}$ are uniquely determined and follow immediately, since for any solution $\underline{\gamma}$ of problem P, $(\gamma_0, \ldots, \gamma_{N-1})$ can only have one of the above two forms. Further, note also that for each possible value of γ_0, the corresponding value of $\bar{\gamma}$ can be directly obtained by applying the results of Lemma A.2 (observe however that solving (A.8) for $\bar{\gamma}$ in general requires numerical root finding techniques).

When $\alpha_0 = \cdots = \alpha_{N-1}$, we thus see that once γ_0 is known, the remaining parameters $\gamma_1, \ldots, \gamma_{N-1}, \bar{\gamma}$ immediately follow. Finding a solution to problem P consequently boils down to finding the $\gamma_0 \in [\gamma_0^*, \gamma_{N-1}^*]$ which minimises $J(\underline{\gamma})$. The $N+1$-dimensional minimisation problem presented in Sec. 3 has thus been reduced to a one-dimensional minimisation problem in the interval $[\gamma_0^*, \gamma_{N-1}^*]$.

6 Variable Peak to Average Power Ratio Transmission Schemes

We now show how to reduce the $N+1$-dimensional optimisation problem presented in Sec. 3 to a one-dimensional optimisation problem in the more general case where the different available transmission schemes have different peak to average power ratios (e.g. when using QAM signal constellations). We will need the following two assumptions:

$$\frac{\alpha_1 - \alpha_0}{\eta_1 - \eta_0} > \frac{\alpha_2 - \alpha_1}{\eta_2 - \eta_1} > \cdots > \frac{\alpha_{N-1} - \alpha_{N-2}}{\eta_{N-1} - \eta_{N-2}} \tag{A.15}$$

and

$$\eta_0 - (\eta_1 - \eta_0)\frac{1 + \alpha_0}{\alpha_1 - \alpha_0} < 0, \tag{A.16}$$

which are verified in numerous practical systems. The assumption made in (A.15) will for example hold if $\eta_1 - \eta_0 = \cdots = \eta_{N-1} - \eta_{N-2}$ (which is the case in many practical transmission schemes [HHØ00; CG01; FSES04; AG97]) and we use square M-ary QAM signal constellations with $M_0 < M_1 < \cdots < M_n$. Indeed, using the expression

$$\xi_n = 3\frac{\sqrt{M_n} - 1}{\sqrt{M_n} + 1} \tag{A.17}$$

provided in [CGB05] for the peak to average power ratio of square M-ary QAM modulations and remembering the relation $\alpha_n = \frac{\xi_n}{\nu} - 1$, it can be easily verified that $\alpha_1 - \alpha_0 > \cdots > \alpha_{N-1} - \alpha_{N-2}$.

Turning now to the assumption in (A.16), note first of all that when $\alpha_n = \frac{\xi_n}{\nu} - 1$, the ratio $\frac{1+\alpha_0}{\alpha_1-\alpha_0} = \frac{\tilde{\xi}_0}{\tilde{\xi}_1-\tilde{\xi}_0}$ is independent of the RF amplifier drain efficiency ν. Whether or not (A.16) is verified thus depends on the values of ξ_0, ξ_1, η_0, and η_1. Using (A.17), it can however be easily checked that (A.16) always holds – whatever be the values of $M_0, M_1 \in \{4, 16, 64, 256, \ldots\}$ (with $M_0 < M_1$) corresponding to transmission schemes 0 and 1 – for uncoded QAM ($\eta_n = \log_2 M_n$), for the trellis codes from [HHØ00] ($\eta_n = \log_2 M_n - \frac{1}{2}$), and for numerous other sets of transmission schemes of practical importance.[4]

Bearing in mind the first N equalities in (A.11), we define the length-N sequence $s_{\underline{\gamma}} = (s_{\underline{\gamma},0}, s_{\underline{\gamma},1}, \ldots, s_{\underline{\gamma},N-1})$ for a given KKT point $\underline{\gamma}$ in the following way:

$$s_{\underline{\gamma},n} = \begin{cases} \operatorname{sign}\left[\lambda_N \left(\rho\bar{\gamma}\left(1+\alpha_0\right) + S_c\right) - \eta_0\right] & \text{if} \quad n = 0, \\ \operatorname{sign}\left[\lambda_N \rho\bar{\gamma}\left(\alpha_n - \alpha_{n-1}\right) - \left(\eta_n - \eta_{n-1}\right)\right] & \text{if} \quad n \in \{1, \ldots, N-1\}. \end{cases} \tag{A.18}$$

By virtue of the assumption made in (A.15), note that if $s_{\tilde{\gamma},n} \in \{0, -1\}$ for a given $n \in \{1, \ldots, N-2\}$, we must have $s_{\tilde{\gamma},k} = -1$ for all $k \in \{n+1, \ldots, N-1\}$.

The set of sequences $s_{\underline{\gamma}}$ such that (A.15) is satisfied has been divided into different subsets in Table A.1. For example, the sequence

[4] Although it is possible to prove results similar to those obtained in this section even in some special cases where (A.15) or (A.16) is not verified, it is impossible, to the best of the authors' knowledge, to do so in full generality using only the ideas presented in this letter. If one considers for example the nested square and cross QAM constellations shown in [HHØ00] (Fig. 1) with $M_n \in \{4, 8, 16, \ldots, 512\}$, it is somewhat surprisingly not even true that $\xi_0 < \xi_1 < \cdots < \xi_7$. It is then a daunting if not impossible task to prove that all possible local minima of problem P have a given simple form (which might not even be the case). Nonetheless, the problem's dimensionality can still be substantially reduced by adequate use of the KKT conditions (A.11), (A.12), and (A.13).

$s_{\underline{\gamma}} = (-1,-1,-1,\ldots,-1)$ is the one and only sequence belonging to subset A_1 (in which case we write $s_{\underline{\gamma}} \in A_1$), and all sequences of the form $s_{\underline{\gamma}} = (-1,1,1,*,\ldots,*)$, where the symbol "$*$" can take the value $-1, 0$, or 1, belong to subset $A_{2,1}$ (in which case we write $s_{\underline{\gamma}} \in A_{2,1}$). We make the definition $A_2 \triangleq A_{2,1} \cup A_{2,2} \cup A_{2,3}$, and obviously have $A = A_1 \cup A_2 \cup A_3$, with similar relations for subsets B and C. For each one of the subsets in Table A.1, the conclusions on the values of $\gamma_0,\ldots,\gamma_{N-1}$ and on those of the Lagrange multipliers $\lambda_0,\ldots,\lambda_{N-1}$ and $\lambda'_0,\ldots,\lambda'_{N-2}$ that can be drawn based on the form of the sequences $s_{\underline{\gamma}}$ belonging to that subset, the fact that for $n \in \{0,\ldots,N-2\}$ both c_n and c'_n cannot be active at the same time, and the KKT conditions (A.11), (A.12), and (A.13) can be found in that subset's entries of the table. We now examine in turn the different subsets appearing in Table A.1.

Subset A_1: We have $s_{\underline{\gamma}} = (-1,-1,-1,\ldots,-1)$, and $(\gamma_0,\ldots,\gamma_{N-1}) = (\gamma_0^*,\ldots,\gamma_{N-1}^*)$. Indeed, since $s_{\underline{\gamma},0} = -1$, we have $\lambda_N(\rho\bar{\gamma}(1+\alpha_0)+S_c) < \eta_0$, and hence (A.11) yields $\lambda_0 > 0$, i.e. the constraint c_0 from (A.7) is active (see (A.12)) and $\gamma_0 = \gamma_0^*$. Therefore, since c_0 and c'_0 cannot be active simultaneously, c'_0 is not active and thus $\lambda'_0 = 0$. Similar arguments can be used to prove the remaining properties given in the table (both for this subset and the remaining subsets), and are henceforth omitted if no difficulties arise.

Subset A_2: $s_{\underline{\gamma}}$ now must have the form $(-1,1,*,\ldots,*,-1)$. Indeed, one can immediately see that $s_{\underline{\gamma},N-1} = -1$ if $s_{\underline{\gamma},N-2} = -1$ by virtue of (A.15), whereas if $s_{\underline{\gamma},N-2} \in \{0,1\}$, Table A.1 shows that $\lambda'_{N-2} > 0$, and $s_{\underline{\gamma},N-1} = -1$ follows from (A.11). Now, let k denote the largest index in the set $\{1,\ldots,N-2\}$ such that $s_{\underline{\gamma},k} = 1$. Table A.1 then shows that we have $\gamma_0 = \gamma_0^*$ and $\gamma_1 = \cdots = \gamma_{k+1}$. In addition, if $k < N-2$ we will also either have $\gamma_n = \gamma_{n+1}$ or $\gamma_{n+1} = \gamma_{n+1}^*$ for all $n \in \{k+1,\ldots,N-2\}$.

Subset A_3: Here, $s_{\underline{\gamma}} = (-1,0,-1,\ldots,-1)$, and $(\gamma_0,\gamma_2,\ldots,\gamma_{N-1}) = (\gamma_0^*,\gamma_2^*,\ldots,\gamma_{N-1}^*)$. A value for $\gamma_1 \in [\gamma_1^*,\gamma_2^*]$ remains to be found.

Subset B_1: $s_{\underline{\gamma}}$ is of the form $(1,-1,-1,\ldots,-1)$, and we have $\gamma_0 = \gamma_1$, and either $\gamma_n = \gamma_{n+1}$ or $\gamma_{n+1} = \gamma_{n+1}^*$ for all $n \in \{1,\ldots,N-2\}$.

Subset B_2: Here, $s_{\underline{\gamma}} = (1,1,*,\ldots,*,-1)$. One can reason exactly as in subset A_2, bearing in mind that we now have $\gamma_0 = \gamma_1$ instead of $\gamma_0 = \gamma_0^*$.

Subset B_3: Now $s_{\underline{\gamma}} = (1,0,-1,\ldots,-1)$, and Table A.1 shows that $\gamma_0 = \gamma_1 = \gamma_2$, and that furthermore either $\gamma_n = \gamma_{n+1}$ or $\gamma_{n+1} = \gamma_{n+1}^*$ for all $n \in \{2,\ldots,N-2\}$.

Subset C_1: We have $s_{\underline{\gamma}} = (0,-1,-1,\ldots,-1)$, and $(\gamma_1,\ldots,\gamma_{N-1}) = (\gamma_1^*,\ldots,\gamma_{N-1}^*)$. A value for $\gamma_0 \in [\gamma_0^*,\gamma_1^*]$ remains to be found.

Subset C_2: We have $s_{\underline{\gamma}} = (0,1,*,\ldots,*,-1)$. One can reason exactly as in

n	A				
$s_{\underline{\gamma},0}$	-1				
0	$\lambda_0 > 0$ $\lambda_0' = 0$ $\gamma_0 = \gamma_0^*$				
$s_{\underline{\gamma},1}$	-1	1			0
1	$\lambda_1 > 0$ $\lambda_1' = 0$ $\gamma_1 = \gamma_1^*$	$\lambda_1 = 0$ $\lambda_1' > 0$ $\gamma_1 = \gamma_2$			$\lambda_1 = 0$ $\lambda_1' = 0$
$s_{\underline{\gamma},2}$	-1	1	-1	0	-1
2	$\lambda_2 > 0$ $\lambda_2' = 0$ $\gamma_2 = \gamma_2^*$	$\lambda_2 = 0$ $\lambda_2' > 0$ $\gamma_2 = \gamma_3$	—	$\lambda_2 = 0$ $\lambda_2' > 0$ $\gamma_2 = \gamma_3$	$\lambda_2 > 0$ $\lambda_2' = 0$ $\gamma_2 = \gamma_2^*$
$s_{\underline{\gamma},3}$	-1		-1	-1	-1
3	$\lambda_3 > 0$ $\lambda_3' = 0$ $\gamma_3 = \gamma_3^*$	Idem	$\lambda_2' > 0$ $\gamma_2 = \gamma_3$ $\vee$ $\lambda_3 > 0$ $\gamma_3 = \gamma_3^*$	—	$\lambda_3 > 0$ $\lambda_3' = 0$ $\gamma_3 = \gamma_3^*$
$s_{\underline{\gamma},4}$	-1		-1	-1	-1
4	$\lambda_4 > 0$ $\lambda_4' = 0$ $\gamma_4 = \gamma_4^*$	Idem	$\lambda_3' > 0$ $\gamma_3 = \gamma_4$ $\vee$ $\lambda_4 > 0$ $\gamma_4 = \gamma_4^*$	$\lambda_3' > 0$ $\gamma_3 = \gamma_4$ $\vee$ $\lambda_4 > 0$ $\gamma_4 = \gamma_4^*$	$\lambda_4 > 0$ $\lambda_4' = 0$ $\gamma_4 = \gamma_4^*$
$\vdots$	$\vdots$	$\vdots$	$\vdots$	$\vdots$	$\vdots$
$s_{\underline{\gamma},N-1}$	-1		-1	-1	-1
$N-1$	$\lambda_{N-1} > 0$ $\gamma_{N-1} = \gamma_{N-1}^*$		$\lambda_{N-2}' > 0$ $\gamma_{N-2} = \gamma_{N-1}$ $\vee$ $\lambda_{N-1} > 0$ $\gamma_{N-1} = \gamma_{N-1}^*$	$\lambda_{N-2}' > 0$ $\gamma_{N-2} = \gamma_{N-1}$ $\vee$ $\lambda_{N-1} > 0$ $\gamma_{N-1} = \gamma_{N-1}^*$	$\lambda_{N-1} > 0$ $\gamma_{N-1} = \gamma_{N-1}^*$
	A_1	$A_{2,1}$	$A_{2,2}$	$A_{2,3}$	A_3

n	B			C		
$s_{\underline{\gamma},0}$	1			0		
0	$\lambda_0 = 0$ $\lambda'_0 > 0$ $\gamma_0 = \gamma_1$			$\lambda_0 = 0$ $\lambda'_0 = 0$		
$s_{\underline{\gamma},1}$	-1	1	0	-1	1	0
1	—	$\lambda_1 = 0$ $\lambda'_1 > 0$ $\gamma_1 = \gamma_2$	$\lambda_1 = 0$ $\lambda'_1 > 0$ $\gamma_1 = \gamma_2$	$\lambda_1 > 0$ $\lambda'_1 = 0$ $\gamma_1 = \gamma_1^*$	$\lambda_1 = 0$ $\lambda'_1 > 0$ $\gamma_1 = \gamma_2$	$\lambda_1 = 0$ $\lambda'_1 = 0$
$s_{\underline{\gamma},2}$	-1		-1	-1		-1
2	$\lambda'_1 > 0$ $\gamma_1 = \gamma_2$ $\vee$ $\lambda_2 > 0$ $\gamma_2 = \gamma_2^*$	See A	—	$\lambda_2 > 0$ $\lambda'_2 = 0$ $\gamma_2 = \gamma_2^*$	See A	$\lambda_2 > 0$ $\lambda'_2 = 0$ $\gamma_2 = \gamma_2^*$
$s_{\underline{\gamma},3}$	-1		-1	-1		-1
3	$\lambda'_2 > 0$ $\gamma_2 = \gamma_3$ $\vee$ $\lambda_3 > 0$ $\gamma_3 = \gamma_3^*$	See A	$\lambda'_2 > 0$ $\gamma_2 = \gamma_3$ $\vee$ $\lambda_3 > 0$ $\gamma_3 = \gamma_3^*$	$\lambda_3 > 0$ $\lambda'_3 = 0$ $\gamma_3 = \gamma_3^*$	See A	$\lambda_3 > 0$ $\lambda'_3 = 0$ $\gamma_3 = \gamma_3^*$
$s_{\underline{\gamma},4}$	-1		-1	-1		-1
4	$\lambda'_3 > 0$ $\gamma_3 = \gamma_4$ $\vee$ $\lambda_4 > 0$ $\gamma_4 = \gamma_4^*$	See A	$\lambda'_3 > 0$ $\gamma_3 = \gamma_4$ $\vee$ $\lambda_2 > 0$ $\gamma_4 = \gamma_4^*$	$\lambda_4 > 0$ $\lambda'_4 = 0$ $\gamma_4 = \gamma_4^*$	See A	$\lambda_4 > 0$ $\lambda'_4 = 0$ $\gamma_4 = \gamma_4^*$
$\vdots$	$\vdots$	$\vdots$	$\vdots$	$\vdots$	$\vdots$	$\vdots$
$s_{\underline{\gamma},N-1}$	-1		-1	-1		-1
$N-1$	$\lambda'_{N-2} > 0$ $\gamma_{N-2} = \gamma_{N-1}$ $\vee$ $\lambda_{N-1} > 0$ $\gamma_{N-1} = \gamma_{N-1}^*$	See A	$\lambda'_{N-2} > 0$ $\gamma_{N-2} = \gamma_{N-1}$ $\vee$ $\lambda_{N-1} > 0$ $\gamma_{N-1} = \gamma_{N-1}^*$	$\lambda_{N-1} > 0$ $\gamma_{N-1} = \gamma_{N-1}^*$	See A	$\lambda_{N-1} > 0$ $\gamma_{N-1} = \gamma_{N-1}^*$
	B_1	B_2	B_3	C_1	C_2	C_3

TABLE A.1: Subsets of sequences $s_{\underline{\gamma}}$ and corresponding properties of $(\gamma_0, \ldots, \gamma_{N-1})$ and the Lagrange multipliers $\lambda_0, \ldots, \lambda_{N-1}$ and $\lambda'_0, \ldots, \lambda'_{N-2}$. Subset A (left-facing page) and subsets B and C (right-facing page).

subset A_2, bearing in mind that now γ_0 is unknown instead of being equal to γ_0^*. A value for $\gamma_0 \in [\gamma_0^*, \gamma_1]$ remains thus to be found.

Subset C_3: Here, $s_{\underline{\gamma}} = (0, 0, -1, \ldots, -1)$, and $(\gamma_2, \ldots, \gamma_{N-1}) = (\gamma_2^*, \ldots, \gamma_{N-1}^*)$. Values for $\gamma_0 \in [\gamma_0^*, \gamma_1]$ and $\gamma_1 \in [\gamma_1^*, \gamma_2^*]$ remain to be found.

Let us now examine the consequences of the assumption in (A.16). Assume that we are at a KKT point $\underline{\gamma}$ such that $s_{\underline{\gamma}} \in A_2 \cup A_3 \cup C_2 \cup C_3$. Consequently, we see that

$$\lambda_N \left(\rho \bar{\gamma} \left(1 + \alpha_0\right) + S_c\right) \leq \eta_0, \tag{A.19}$$

and

$$\lambda_N \rho \bar{\gamma} \left(\alpha_1 - \alpha_0\right) \geq \eta_1 - \eta_0. \tag{A.20}$$

Now, solving for $\bar{\gamma}$ in (A.19) and introducing the result in (A.20) yields

$$\lambda_N S_c \leq \eta_0 - (\eta_1 - \eta_0) \frac{1 + \alpha_0}{\alpha_1 - \alpha_0}, \tag{A.21}$$

which is impossible in view of (A.16) and the non-negativity of λ_N. Therefore, if a given $\underline{\gamma}$ is to be a solution to problem P, we must have $s_{\underline{\gamma}} \in A_1 \cup B \cup C_1$. However, Table A.1 and Lemma A.4 show that for all such $\underline{\gamma}$, $(\gamma_0, \ldots, \gamma_{N-1})$ can only have one of the following forms:

1. $\gamma_n^* \leq \gamma_0 = \ldots = \gamma_n < \gamma_{n+1}$, and $(\gamma_{n+1}, \ldots, \gamma_{N-1}) = (\gamma_{n+1}^*, \ldots, \gamma_{N-1}^*)$, for a given $n \in \{0, \ldots, N-2\}$, or
2. $\gamma_0 = \gamma_1 = \ldots = \gamma_{N-1} = \gamma_{N-1}^*$.

This is exactly the conclusion that was reached in the case of transmission schemes with a constant peak to average power ratio. The remarks made at the end of Section 5 are thus of application and, in the present case as well, finding a solution to problem P boils down to finding the $\gamma_0 \in [\gamma_0^*, \gamma_{N-1}^*]$ which minimises $J(\underline{\gamma})$. The $N+1$-dimensional minimisation problem from Sec. 3 has thus been reduced once again to a one-dimensional minimisation problem in the interval $[\gamma_0^*, \gamma_{N-1}^*]$.

To conclude this discussion, we would like to draw the reader's attention to the fact that although we have succeeded in rigorously showing that the dimensionality of the optimisation problem associated with the design of constant power link adaptation schemes can be reduced from $N+1$ to one both in the special case presented in this section and in the special case presented in the previous section, we by no means intend to suggest that this also could be done for *any* constant power link adaptation scheme, as also mentioned in footnote 4.

n	M_n	η_n	a_n	b_n
0	4	1.5	896.0704	10.7367
1	16	3.5	996.5492	8.7345
2	64	5.5	296.6007	7.9270
3	256	7.5	404.2837	7.8824

TABLE A.2: Parameters a_n and b_n

7 Design Example

We illustrate our methodology by designing a link adaptation system based on the 4-D trellis codes from [HHØ00], considering only the codes for which a square M-ary QAM constellation is used. We hence have $N = 4$ different codes (which we number from $n = 0$ to $n = 3$), with $M_n \in \{4, 16, 64, 256\}$. The nth code has a spectral efficiency given by by $\eta_n = 2n + \frac{3}{2}$ [bits/s/Hz], and a bit-error rate $\mathrm{BER}_n(\gamma)$ on an AWGN channel of CSNR γ which can be approximated by the expression [HHØ00]

$$\mathrm{BER}_n(\gamma) \approx \min\left\{\frac{1}{2}, a_n \exp\left(\frac{-b_n\gamma}{M_n}\right)\right\}, \tag{A.22}$$

where a_n and b_n are given in Table A.2 for $n \in \{0, 1, 2, 3\}$. The system parameters, to a large extent inspired by [CGB05], are given in Table A.3. We assume a Nakagami-m fading channel with $m = 2$, i.e.

$$f(\gamma) = \left(\frac{m}{\bar{\gamma}}\right)^m \frac{\gamma^{m-1}}{\Gamma(m)} \exp\left(-m\frac{\gamma}{\bar{\gamma}}\right), \tag{A.23}$$

where $\Gamma(\cdot)$ is the Gamma function [GR00] and the fading severity parameter $m = 2$.

The optimal value of γ_0 (computed performing a one-dimensional minimisation) and corresponding values of $\gamma_1, \ldots, \gamma_{N-1}$ as a function of the transmitter-receiver distance d are shown in Figs. A.2(a) and A.2(b) respectively with and without the power constraint $S_{\mathrm{maxt}} = 150$ mW (see Table A.3). The values of γ_n^*, $(n = 0, \ldots, 3)$ have also been included for reference. (Recall that the bit-error rate requirement $\mathrm{BER} \leq \mathrm{BER}_0$ was restated as a set of constraints of the form $\gamma_n \geq \gamma_n^*$, $n = 0, \ldots, N-1$; and that once γ_0 is known, the values of $\gamma_1, \ldots, \gamma_{N-1}$ and $\bar{\gamma}$ immediately follow.)

The system's corresponding average spectral efficiency η, transmit power S_{t}, and outage probability $\int_0^{\gamma_0} f(\gamma)\,\mathrm{d}\gamma$ are respectively shown in Figs. A.3, A.4, and A.5 as a function of the transmitter-receiver separation for this optimal value of γ_0; with the peak power constraint $S_{\mathrm{maxt}} =$

$B = 10$ kHz	$N_0/2 = -174$ dBm/Hz
$\mathrm{BER}_0 = 10^{-3}$	$\nu = 0.35$
$T_{\mathrm{tr}} = 5\ \mu$s	$S_{\mathrm{tr}} = 100$ mW
$N_{\mathrm{f}} = 10$ dB	$G_1 = 30$ dB
$M_{\mathrm{link}} = 40$ dB	$T_{\mathrm{f}} = 5$ ms
$r = 3.5$	$S_{\mathrm{c}} = 210.7$ mW
$S_{\mathrm{ct}} = 98.2$ mW	$S = 230$ mW
$S_{\mathrm{maxt}} = 150$ mW	

TABLE A.3: System Parameters

150 mW included in Figs. A.3(a), A.4(a), and A.5(a), and ignored in Figs. A.3(b), A.4(b), and A.5(b). The average spectral efficiency, transmit power, and outage probability that would be obtained by setting $\gamma_0, \ldots, \gamma_3 = \gamma_0^*, \ldots, \gamma_3^*$ have also been plotted for comparison.

A system designer could for example use Fig. A.2 to conclude that, in the present setting, it is only necessary to use codes $n = 2$ and $n = 3$ when the transmitter-receiver separation is between approximately 3.5 m and 11 m in order to maximise the system's average spectral efficiency, both with and without the peak power constraint $S_{\mathrm{maxt}} = 150$ mW. Reaching this kind of conclusion without the results from Secs. 4 and 6 would no doubt require a considerable amount of effort due to the non-linearity and high dimensionality of the associated optimisation problems.

The figures show in addition that, for transmitter-receiver distances between approximately 2.8 m and 23 m when the peak power constraint $S_{\mathrm{maxt}} = 150$ mW is included and between approximately 2.8 m and 34 m when the peak power constraint $S_{\mathrm{maxt}} = 150$ mW is ignored, it is preferable in terms of average spectral efficiency to refrain from transmitting at low CSNR values (which results in an increased outage probability) and to use the resulting power savings to transmit with a higher transmit power at larger CSNR values than to use the transmission scheme that would be obtained by simply setting $\gamma_0, \ldots, \gamma_3 = \gamma_0^*, \ldots, \gamma_3^*$. One of the key reasons for this is the fact that when the system is in sleep mode, one saves not only in transmit power but also in circuit power. This illustrates the importance of taking circuit energy consumption into account when designing link adaptation schemes for short range wireless communication systems, for which circuit and transmit energy consumptions are comparable. (When the transmission distance is long, transmit energy dominates and eventual savings in circuit energy become negligible.)

Furthermore, note that the peak power constraint $S_{\mathrm{maxt}} = 150$ mW cor-

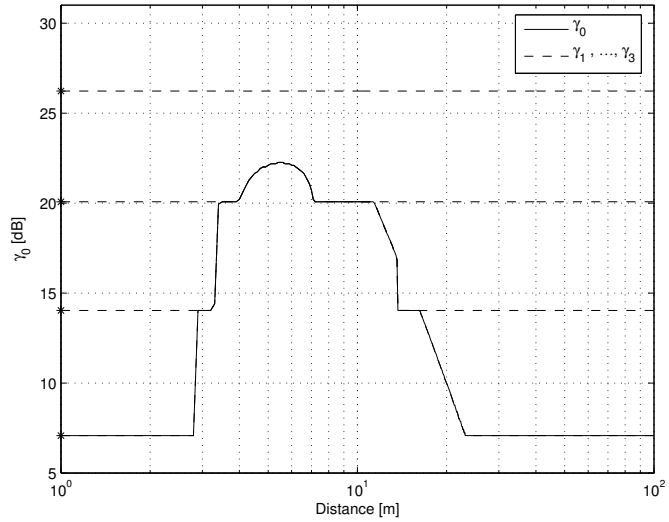

(a)

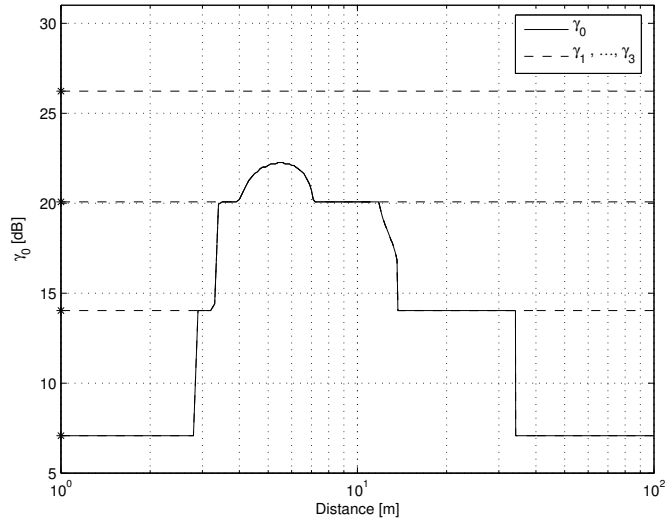

(b)

FIGURE A.2: Optimal value of γ_0 (solid line) and corresponding values of $\gamma_1, \ldots, \gamma_3$ (dashed lines from bottom to top) as a function of the transmitter-receiver distance d; with (a) and without (b) the peak power constraint $S_{\text{maxt}} = 150$ mW. The asterisks on the vertical axis correspond to the values of $\gamma_0^*, \ldots, \gamma_3^*$.

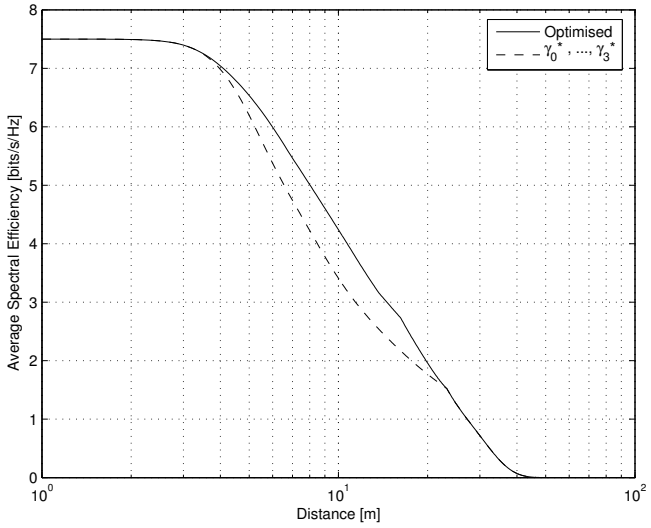

(a)

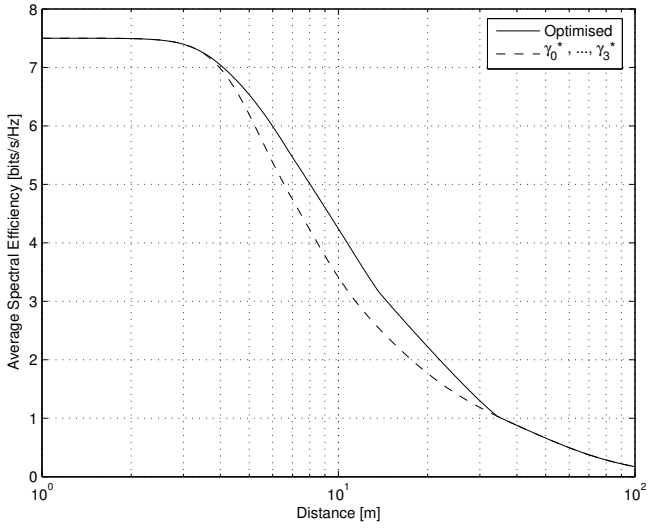

(b)

FIGURE A.3: Average spectral efficiency for the optimal value of γ_0 (solid line), and average spectral efficiency when $\gamma_0, \ldots, \gamma_3 = \gamma_0^*, \ldots, \gamma_3^*$ (dashed line) as a function of the transmitter-receiver distance d; with (a) and without (b) the peak power constraint $S_{\text{maxt}} = 150$ mW.

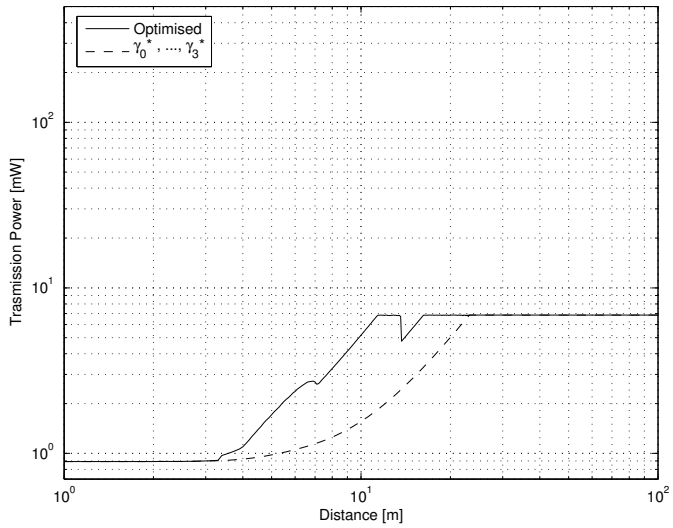

(a)

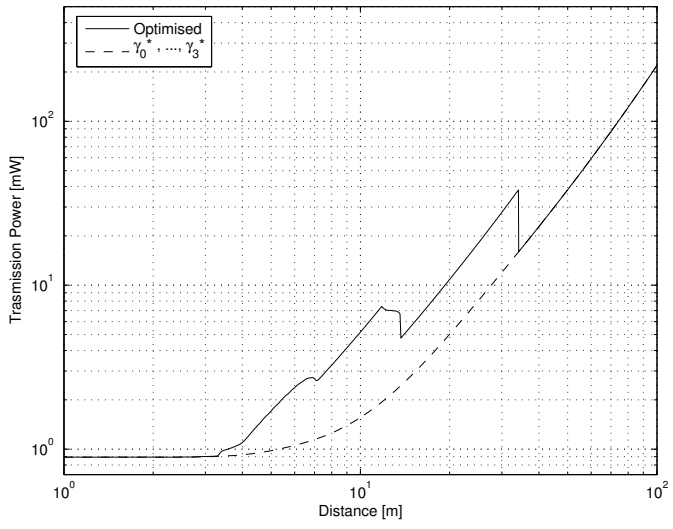

(b)

FIGURE A.4: Transmit power S_t for the optimal value of γ_0 (solid line), and when $\gamma_0, \ldots, \gamma_3 = \gamma_0^*, \ldots, \gamma_3^*$ (dashed line) as a function of the transmitter-receiver distance d; with (a) and without (b) the peak power constraint $S_{\text{maxt}} = 150$ mW.

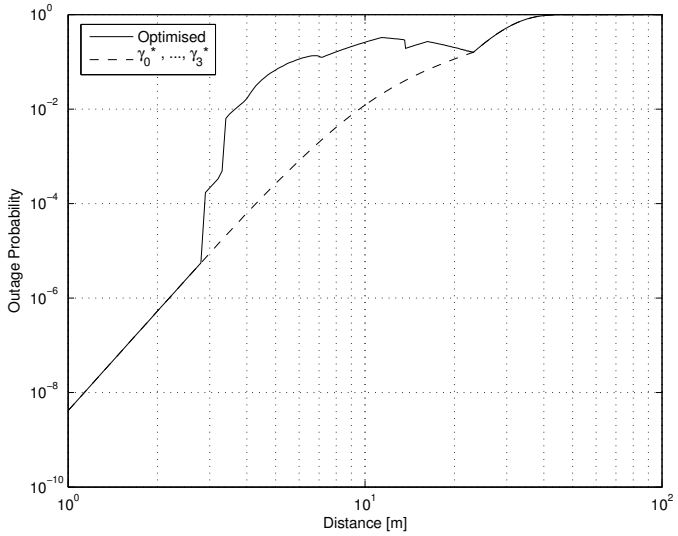

(a)

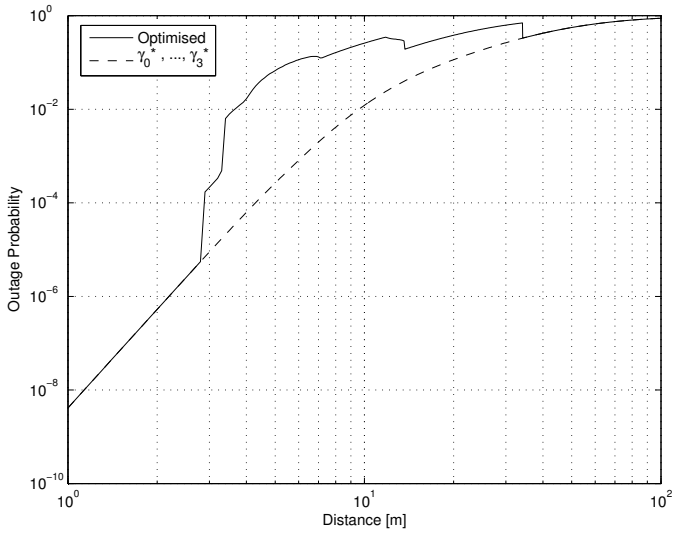

(b)

FIGURE A.5: Outage probability for the optimal value of γ_0 (solid line), and when $\gamma_0, \ldots, \gamma_3 = \gamma_0^*, \ldots, \gamma_3^*$ (dashed line) as a function of the transmitter-receiver distance d; with (a) and without (b) the peak power constraint $S_{\text{maxt}} = 150$ mW.

responds to a maximum transmit power of $S_t = \frac{S_{maxt} - S_{ct}}{\alpha_3} = 6.85$ mW, and is attained at a distance of $d = 11.5$ m as can be seen in Fig. A.4(a). If the peak power constraint had been $S_{maxt} = 500$ mW, the maximum transmit power would be of $S_t = 53.13$ mW, and would be attained at the transmission distance $d = 57.4$ m (see Fig. A.4(b)).

As a final remark, we would like to emphasise that the contribution of this letter lies in the methodology presented in Secs. 4–6 for designing constant power link adaptation schemes, and not in this particular numerical example. The relative performance (characterised by average spectral efficiency, power consumption, outage probability, etc.) of competing system designs will vary greatly with the setting under consideration.

8 Conclusions

In this correspondence, we considered the design of constant power link adaptation schemes in which circuit energy consumption is included in the total energy budget, and in which the system's instantaneous BER must be maintained below a predefined threshold. After stating the associated optimisation problem, we showed how its dimensionality can be reduced – in numerous cases of practical importance – from $N + 1$ to one, where N denotes the number of available transmission schemes. This was done separately for transmission schemes utilising signal constellations of constant and variable peak to average power ratios. The design of such transmission schemes has thus been greatly simplified.

Numerical examples also confirmed the importance of including circuit energy consumption in the global energy budget when designing short-range wireless communication systems.

Appendix A Proofs of Lemmas A.1 and A.4

A.1 Proof of Lemma A.1

Proof: Let us assume a "worst case" scenario, with as many active constraints[5] as possible at a given feasible point $\underline{\gamma}^0$. Noting that, for $n \in \{0, \ldots, N-2\}$, both c_n and c'_n cannot be active at the same time, this amounts to assuming that either c_n or c'_n is active for $n \in \{0, \ldots, N-2\}$,

[5]See the footnote in Sec. 4 regarding active constraints.

and that c_{N-1}, c_N, and c'_N are active. Now, let

$$d_j = \begin{cases} c_j & \text{if } c_j \text{ is active and } j \in \{0,\ldots,N-2\}, \\ c'_j & \text{if } c'_j \text{ is active and } j \in \{0,\ldots,N-2\}, \\ c_j & \text{if } j \in \{N-1, N\}, \\ c'_N & \text{if } j = N+1, \end{cases} \tag{A.24}$$

and define the vectors

$$\nabla d_j = \left(\left.\frac{\partial d_j(\underline{\gamma})}{\partial \gamma_0}\right|_{\underline{\gamma}^0}, \ \cdots, \ \left.\frac{\partial d_j(\underline{\gamma})}{\partial \gamma_{N-1}}\right|_{\underline{\gamma}^0}, \ \left.\frac{\partial d_j(\underline{\gamma})}{\partial \bar{\gamma}}\right|_{\underline{\gamma}^0} \right) \tag{A.25}$$

for all $j \in \{0,\ldots,N+1\}$. $\frac{\partial d_j(\underline{\gamma})}{\partial \gamma_n}$ can be easily evaluated for $j \in \{0,\ldots,N+1\}$ and $n \in \{0,\ldots,N-1\}$. Note that $\frac{\partial d_N(\underline{\gamma})}{\partial \gamma_n} \geq 0$ for all $n \in \{0,\ldots,N-1\}$ since $\alpha_0 \leq \alpha_1 \leq \cdots \leq \alpha_{N-1}$. $\frac{\partial d_j(\underline{\gamma})}{\partial \bar{\gamma}}$ can also be easily evaluated for $j \in \{0,\ldots,N-1,N+1\}$. Evaluation of $\frac{\partial d_N(\underline{\gamma})}{\partial \bar{\gamma}}$ yields

$$\begin{aligned} \frac{\partial d_N(\underline{\gamma})}{\partial \bar{\gamma}} = &-S_c \frac{\partial}{\partial \bar{\gamma}} \int_{\gamma_0}^{\infty} f(\gamma)\mathrm{d}\gamma - \rho \sum_{n=0}^{N-1} (1+\alpha_n) \int_{\gamma_n}^{\gamma_{n+1}} f(\gamma)\mathrm{d}\gamma \\ &-\rho\bar{\gamma} \frac{\partial}{\partial \bar{\gamma}} \sum_{n=0}^{N-1} (1+\alpha_n) \int_{\gamma_n}^{\gamma_{n+1}} f(\gamma)\mathrm{d}\gamma. \end{aligned} \tag{A.26}$$

The first term in the above equation is strictly negative as long as $\frac{\partial}{\partial \bar{\gamma}} \int_{\gamma_0}^{\infty} f(\gamma)\mathrm{d}\gamma > 0$, which is the case for all practical received CSNR distributions (see Appendix B). Moreover, the second term is always strictly negative, and the third term is strictly negative as long as $\frac{\partial}{\partial \bar{\gamma}} \sum_{n=0}^{N-1} (1+\alpha_n) \cdot \int_{\gamma_n}^{\gamma_{n+1}} f(\gamma)\mathrm{d}\gamma > 0$, which is the case for all practical received CSNR distributions since $0 \leq \alpha_0 \leq \alpha_1 \leq \cdots \leq \alpha_{N-1}$ (see Appendix B). Hence, $\left.\frac{\partial d_N(\underline{\gamma})}{\partial \bar{\gamma}}\right|_{\underline{\gamma}^0} < 0$ for all feasible $\underline{\gamma}^0$.

Now, it can easily be seen that if one sets $w \triangleq (1,2,\ldots,N,-1)$, we will always have $\nabla d_j \cdot w > 0$ for all $j \in \{0,\ldots,N+1\}$, whatever be the set of $N+2$ active constraints active at $\underline{\gamma}^0$. (If less than $N+2$ constraints are active at $\underline{\gamma}^0$, the same w will yield $\nabla d_j \cdot w > 0$ for all d_j corresponding to an active constraint.) For all practical received CSNR distributions $f(\gamma)$, the MFCQ thus holds at $\underline{\gamma}^0$ whatever be the set of active constraints at that point. □

A.2 Proof of Lemma A.4

Proof: When $\gamma_0 = \gamma_1 = \cdots = \gamma_{N-1}$, problem P can be rewritten as an optimisation problem in the variables γ_{N-1} and $\bar{\gamma}$ (which we call problem $P^\dagger$): find $\underline{\gamma} = (\gamma_{N-1}, \bar{\gamma})$ such that

$$J^\dagger(\underline{\gamma}) = -\eta_{N-1} \int_{\gamma_{N-1}}^{\infty} f(\gamma) \mathrm{d}\gamma \tag{A.27}$$

is minimum, under the constraints

$$c_\lambda(\underline{\gamma}) = S - [S_\mathrm{c} + \rho\bar{\gamma}(1+\alpha_{N-1})] \int_{\gamma_{N-1}}^{\infty} f(\gamma)\mathrm{d}\gamma \geq 0, \tag{A.28}$$

$$c_\mu(\underline{\gamma}) = \gamma_{N-1} - \gamma^*_{N-1} \geq 0, \tag{A.29}$$

$$c_\tau(\underline{\gamma}) = \bar{\gamma}^* - \bar{\gamma} \geq 0, \tag{A.30}$$

where either $c_\lambda(\underline{\gamma})$ or $c_\tau(\underline{\gamma})$ is active by virtue of Lemma A.2. The KKT equations of problem $P^\dagger$ are

$$\begin{cases} \mu + \lambda\,[S_\mathrm{c} + \rho\bar{\gamma}(1+\alpha_{N-1})]\, f(\gamma_{N-1}) = \eta_{N-1}\, f(\gamma_{N-1}) \\ \lambda \dfrac{\partial}{\partial\bar{\gamma}} \left[S - [S_\mathrm{c} + \rho\bar{\gamma}(1+\alpha_{N-1})] \displaystyle\int_{\gamma_{N-1}}^{\infty} f(\gamma)\mathrm{d}\gamma \right] - \tau \\ \qquad\qquad = -\eta_{N-1} \dfrac{\partial}{\partial\bar{\gamma}} \displaystyle\int_{\gamma_{N-1}}^{\infty} f(\gamma)\mathrm{d}\gamma \\ \lambda\, c_\lambda(\underline{\gamma}) = \mu\, c_\mu(\underline{\gamma}) = \tau\, c_\tau(\underline{\gamma}) = 0 \\ \lambda, \mu, \tau \geq 0, \end{cases} \tag{A.31}$$

where λ, μ, and τ respectively denote the Lagrange multipliers corresponding to $c_\lambda(\underline{\gamma})$, $c_\mu(\underline{\gamma})$, and $c_\tau(\underline{\gamma})$. We hence see that if $\gamma_{N-1} > \gamma^*_{N-1}$, we must have $\mu = 0$. The first equality in (A.31) then becomes $\lambda[S_\mathrm{c} + \rho\bar{\gamma}(1+\alpha_{N-1})] = \eta_{N-1}$. Carrying out the differentiation on the left hand side of the second equality in (A.31) then yields

$$\lambda \left[\rho(1+\alpha_{N-1}) \int_{\gamma_{N-1}}^{\infty} f(\gamma)\mathrm{d}\gamma + [S_\mathrm{c} + \rho\bar{\gamma}(1+\alpha_{N-1})] \frac{\partial}{\partial\bar{\gamma}} \int_{\gamma_{N-1}}^{\infty} f(\gamma)\mathrm{d}\gamma \right] + \tau = \eta_{N-1} \frac{\partial}{\partial\bar{\gamma}} \int_{\gamma_{N-1}}^{\infty} f(\gamma)\mathrm{d}\gamma, \tag{A.32}$$

or $\lambda\rho(1+\alpha_{N-1}) \int_{\gamma_{N-1}}^{\infty} f(\gamma)\mathrm{d}\gamma + \tau = 0$. We hence must have $\lambda = \tau = 0$. This contradicts the first equality in (A.31), since $\eta_{N-1}\, f(\gamma_{N-1}) > 0$. We thus must have $\mu > 0$ and $\gamma_{N-1} = \gamma^*_{N-1}$. □

Appendix B Practical Received CSNR Distributions

It can be verified that each one of the practical received CSNR distributions $f(\gamma)$ arising from one of the channel fading models mentioned in this letter (Rayleigh, Rice, and Nakagami-m) satisfies the property

$$\frac{\partial}{\partial \bar{\gamma}} \int_a^{\infty} f(\gamma) \mathrm{d}\gamma > 0 \tag{A.33}$$

for all $a > 0$. Indeed, let $F(\gamma)$ denote the cumulative distribution function corresponding to $f(\gamma)$. Observe that since the CSNR distributions in question satisfy $f(\gamma) > 0$ for $\gamma \in (0, \infty)$, $F(\gamma)$ has to be a strictly increasing function of γ. The cumulative distribution function of the received CSNR is given by [SA01]

$$F_{\mathrm{nak}}(\gamma) = 1 - \frac{\Gamma(m, \frac{m\gamma}{\bar{\gamma}})}{\Gamma(m)} \tag{A.34}$$

in the case of Nakagami-m fading,[6] and by [SA01]

$$F_{\mathrm{rice}}(\gamma) = 1 - Q_1\left(\sqrt{2K}, \sqrt{\frac{2(1+K)\gamma}{\bar{\gamma}}}\right) \tag{A.35}$$

in the case of Ricean fading; where $\Gamma(\cdot,\cdot)$ is the incomplete Gamma function [GR00], $\Gamma(\cdot)$ is the Gamma function [GR00], m is the fading severity parameter (which ranges from $\frac{1}{2}$ to ∞), $Q_1(\cdot,\cdot)$ is the first order Marcum-Q function [SA01], and K is the Ricean factor. Now, note that both $F_{\mathrm{nak}}(\gamma)$ and $F_{\mathrm{rice}}(\gamma)$ are only functions of the ratio $\frac{\gamma}{\bar{\gamma}}$, and must therefore be strictly decreasing functions of $\bar{\gamma}$ for fixed γ since they are known to be strictly increasing functions of γ for fixed $\bar{\gamma}$. Condition (A.33), which can be rewritten $\frac{\partial[1-F(a)]}{\partial \bar{\gamma}} > 0$ is thus satisfied.

As a consequence of this, it can be seen that for all $0 < \beta_0 \leq \beta_1 \leq \cdots \leq \beta_{N-1}$ and $0 < \gamma_0 \leq \gamma_1 \leq \cdots \leq \gamma_{N-1} < \gamma_N = \infty$, we have

$$\begin{aligned} &\frac{\partial}{\partial \bar{\gamma}} \left[\sum_{n=0}^{N-1} \beta_n \int_{\gamma_n}^{\gamma_{n+1}} f(\gamma) \mathrm{d}\gamma \right] \\ &\qquad = \frac{\partial}{\partial \bar{\gamma}} \left[\beta_0 \int_{\gamma_0}^{\infty} f(\gamma) \mathrm{d}\gamma + \sum_{n=1}^{N-1} (\beta_n - \beta_{n-1}) \int_{\gamma_n}^{\infty} f(\gamma) \mathrm{d}\gamma \right] \\ &\qquad > 0, \end{aligned} \tag{A.36}$$

a property which is used time and again in this document. The same ideas can be used to prove similar properties for other channel fading models as well.

[6] Rayleigh-fading corresponds to the special case $m = 1$.

References

[AG97] M.-S. Alouini and A. Goldsmith. Adaptive M–QAM modulation over Nakagami fading channels. In *Proc. 1997 IEEE Global Communications Conference (Globecom)*, pages 218–223, Phoenix, November 1997.

[CG01] S. T. Chung and A. Goldsmith. Degrees of freedom in adaptive modulation: a unified view. *IEEE Transactions on Communications*, 49(9):1561–1571, September 2001.

[CGB04] S. Cui, A. J. Goldsmith, and A. Bahai. Energy-efficiency of MIMO and cooperative MIMO techniques in sensor networks. *IEEE Journal on Selected Areas in Communications*, 22(6):1089–1098, August 2004.

[CGB05] S. Cui, A. Goldsmith, and A. Bahai. Energy-constrained modulation optimization. *IEEE Transactions on Wireless Communications*, 4(5):2349–2360, September 2005.

[CMGL05] S. Cui, R. Madan, A. J. Goldsmith, and S. Lall. Joint routing, MAC, and link layer optimization in sensor networks with energy constraints. In *Proc. IEEE International Conference on Communications*, May 2005.

[FSES04] S. Falahati, A. Svensson, T. Ekman, and M. Sternad. Adaptive modulation systems for predicted wireless channels. *IEEE Transactions on Communications*, 52(2):307–316, February 2004.

[GC97] A. J. Goldsmith and S.-G. Chua. Variable-rate variable-power MQAM for fading channels. *IEEE Transactions on Communications*, 45(10):1218–1230, October 1997.

[GØO06] A. Gjendemsjø, G. E. Øien, and P. Orten. Optimal discrete-level power control for adaptive modulation schemes with capacity-

approaching component codes. In *Proc. 2006 IEEE International Conference on Communications (ICC)*, Istanbul, June 2006.

[GR00] I. S. Gradshteyn and I. M. Ryzhik. *Table of Integrals, Series, and Products*. Academic Press, sixth edition, 2000.

[GV97] A. J. Goldsmith and P. P. Varaiya. Capacity of fading channels with channel side information. *IEEE Transactions on Information Theory*, 43(6):1986–1992, November 1997.

[HHØ00] K. J. Hole, H. Holm, and G. E. Øien. Adaptive multidimensional coded modulation over flat fading channels. *IEEE Journal on Selected Areas in Communications*, 18(7):1153–1158, July 2000.

[KG00] C. Köse and L. Goeckel. On power adaptation in adaptive signaling systems. *IEEE Transactions on Communications*, 48(11):1769–1773, November 2000.

[KØ05] S. de la Kethulle de Ryhove and G. E. Øien. Energy-optimised coded modulation for short-range wireless communications on Nakagami-*m* fading channels. In *Proc. Norwegian Signal Processing Symposium (NORSIG)*, Stavanger, September 2005.

[MF67] O. L. Mangasarian and S. Fromovitz. The Fritz John necessary optimality conditions in the presence of equality and inequality constraints. *Journal of Mathematical Analysis and Applications*, 17(1):37–47, January 1967.

[Nak60] M. Nakagami. The *m*-distribution: a general formula of intensity distribution of rapid fading. In W. G. Hoffman, editor, *Statistical Methods in Radio Wave Propagation*. Pergamon, Oxford, U.K., 1960.

[NW99] J. Nocedal and S. J. Wright. *Numerical Optimization*. Springer Series in Operations Research, 1999.

[SA01] M. K. Simon and M. S. Alouini. *Digital Communication over Fading Channels*. Wiley Series in Telecommunications and Signal Processing, first edition, 2001.

[SS03] C. Schurgers and M. B. Srivastava. Energy optimal scheduling under average throughput constraint. In *Proc. 2003 IEEE International Conference on Communications (ICC)*, pages 1648–1652, Anchorage, May 2003.

Paper B

On the Statistics and Spectral Efficiency of Dual-Branch MIMO Systems with Link Adaptation and Power Control

Sébastien de la Kethulle de Ryhove, Geir E. Øien, and Frode Bøhagen

Under review for possible publication in *IEEE Transactions on Vehicular Technology* at the time of writing of this dissertation.

Abstract

The capacity of multiple-input multiple-output (MIMO) systems with perfect transmitter and receiver channel state information (CSI) can be attained by decoupling the MIMO channel into a set of independent subchannels, and distributing the power among these subchannels in accordance with the *water-filling* solution. The first contribution of this paper lies in the derivation of expressions for the signal-to-noise ratio (SNR) distributions of the subchannels which arise when decoupling a dual-branch MIMO system (either two transmit or two receive antennæ) according to the above principle; this being done both in the case of short- and long-term transmitter power constraints, and in a Rayleigh-fading environment.

Implementation of the above transmission scheme on a time-varying channel requires however the ability to perform continuous rate adaptation, which is not feasible in any practical system. The second contribution of this paper consists in showing how to maximise the average spectral efficiency (ASE) of dual-branch MIMO systems with perfect transmitter and receiver CSI when using only a fixed, finite number of codes (discrete rate adaptation). This maximum ASE is compared to the system's ergodic capacity, which is found using the subchannel SNR distributions derived in the first part of the paper, and to the maximum ASE that can be attained with discrete rate adaptation if the available power is distributed among the different subchannels in accordance with the water-filling solution. This is done assuming that the transmitter is subject to a short-term power constraint, and that capacity-achieving codes for additive white Gaussian noise (AWGN) channels are available. Knowledge of the subchannel SNR distributions proves necessary to perform this analysis, demonstrating how valuable the knowledge of the subchannel SNR distributions can be for the design of MIMO communication links. The results show that it is possible to come very close to the ergodic capacity with only a few optimal codes, provided that the power distribution is done in an optimal way. Furthermore, they indicate that water-filling is significantly suboptimal when the number of available rates is small.

S. de la Kethulle de Ryhove and G. E. Øien are with the Department of Electronics and Telecommunications, Norwegian University of Science and Technology, N-7491 Trondheim, Norway (e-mails: {delaketh, oien}@iet.ntnu.no).

F. Bøhagen is with UniK/Nera Research, N-1375 Billingstad, Norway (e-mail: frode.bohagen@research.nera.no).

The material in this paper was presented in part at the 2005 International Workshop on Smart Antennas (WSA '05), Duisburg, Germany, April 2005, and at the 2006 International Workshop on Signal Processing Advances in Wireless Communications (SPAWC '06), Cannes, France, July 2006.

1 Introduction

It is nowadays widely known that the use of multiple transmit and receive antennæ (multiple-input multiple-output (MIMO) systems) can considerably increase the performance of wireless systems, both by increasing spectral efficiency and improving link reliability [GSS+03; ZT03]. MIMO technology is seen as a promising means to help satisfy the growing demand for data-intensive wireless applications in today's bandwidth-hungry world, and has been the object of extensive research during recent years (see e.g. [GSS+03; ZT03; JP03; SSP01] and the references therein). In order to attain the capacity of MIMO systems with both transmitter and receiver channel state information (CSI), information theoretic results suggest decoupling such systems into independent subchannels by means of linear precoding, and distributing the available power between these subchannels according to the *water-filling* solution [CT91; JP03; SSP01], in which more power is allocated to subchannels which benefit from better signal-to-noise ratio (SNR) conditions.

The first contribution of this paper lies in the derivation of expressions for the SNR distributions of the subchannels which arise when decoupling a dual-branch MIMO system[1] (either two transmit or two receive antennæ) according to the above principle. This is done both for the case where the average transmit power allocated to the symbol vectors within any one given symbol frame must be kept constant during the transmission of each and every symbol frame (short-term power constraint), and for the more relaxed case where the transmitter is allowed to allocate different average powers to symbol vectors within different symbol frames as long as the average allocated power over multiple symbol frames does not exceed the available power budget (long-term power constraint) [CTB99]. The former scenario is for example relevant in systems where the transmitted power must be kept below a certain level at all times due to e.g. frequency and power regulations, whereas the latter scenario is for instance relevant in systems where the priority is to minimise the total power consumption, or where battery lifetime is an important design parameter.

Achieving capacity using the above scheme (decomposition of the MIMO system into independent subchannels and water-filling for power allocation) on a time-varying channel requires however continuous rate adaptation (i.e. the ability to implement any rate within the continuum covered by the statistical distribution of the channel realisations), and is unfortunately not feasible in a practical system. Indeed, although it is real-

[1] Some authors prefer to speak of dual MIMO systems instead [SG04; MA06].

istic to assume that capacity-achieving codes for additive white Gaussian noise (AWGN) channels of any desired rate can be designed thanks to advances in coding theory (concerning mainly turbo codes [BGT93] and low-density parity-check codes [Gal63]), only a finite number of such codes – and thus rates – will be available in any practical system due to memory and complexity constraints.

Therefore, the second contribution of this work consists in showing how to maximise the average spectral efficiency (ASE) of dual-branch MIMO systems with perfect transmitter and receiver CSI which are subject to a short-term power constraint assuming a given *finite* number n_c of capacity-achieving codes for AWGN channels of different rates are available for use. This is done by first illustrating how to calculate the system's ASE (measured in bits per channel use) when the rates of these codes are fixed and the available power is optimally distributed between the different subchannels, and subsequently discussing how to optimally select the rates of these n_c codes in order to maximise the system's ASE.

We finally also show how to optimally select the rates of these n_c codes in order to maximise the system's ASE when one chooses to distribute the available power among the different subchannels in accordance with the water-filling solution although the number of available rates is finite and this hence is suboptimal. Both in this case and the previous case the resulting maximum ASE is compared – for values of n_c ranging from one to four – to the MIMO system's ergodic capacity. Knowledge of the freshly obtained subchannel SNR distributions is seen to be necessary both to find the optimal rates of the n_c codes under water-filling power allocation and to calculate the system's ergodic capacity – thereby demonstrating how valuable the knowledge of the subchannel SNR distributions can be for the analysis and design of MIMO communication links. The results show that it is possible to approach the ergodic capacity of the MIMO systems under consideration with only a few optimal codes provided that power allocation is done in an optimal way, and additionally illustrate the significant suboptimality of water-filling when the number of available rates is small.

We will assume for simplicity an i.i.d. MIMO Rayleigh flat-fading channel [JP03; Tel95], although we will see that our methodology is general and can be applied to other MIMO channel models (e.g. correlated MIMO Rayleigh-fading channels [CWZ03] or Ricean fading channels [BOØ05]) as well.

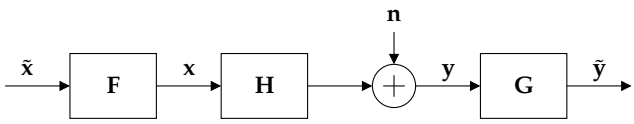

FIGURE B.1: MIMO system model

2 System Model

Let us consider a MIMO link with linear precoding and decoding [SSP01] using N transmitting and M receiving antennæ (see Fig. B.1). We set $m \triangleq \min\{M, N\}$ and $n \triangleq \max\{M, N\}$. Assuming slowly varying, frequency-flat fading, such a MIMO link can be modelled in the complex baseband domain by the expression

$$\tilde{\mathbf{y}} = \mathbf{GHF}\tilde{\mathbf{x}} + \mathbf{Gn}, \tag{B.1}$$

where $\tilde{\mathbf{x}} \in \mathbb{C}^{m\times 1}$ represents the transmitted symbol vector, $\mathbf{H} \in \mathbb{C}^{M\times N}$ is the MIMO channel matrix, assumed to consist of i.i.d. Gaussian entries with independent, variance $1/2$ real and imaginary parts (modelling a spatially uncorrelated Rayleigh-fading environment), $\mathbf{n} \in \mathbb{C}^{M\times 1}$ is a zero-mean circularly symmetric complex Gaussian noise vector with independent, equal variance real and imaginary parts, $\tilde{\mathbf{y}} \in \mathbb{C}^{m\times 1}$ is the receiver estimate for $\tilde{\mathbf{x}}$, and $\mathbf{F} \in \mathbb{C}^{N\times m}$, $\mathbf{G} \in \mathbb{C}^{m\times M}$ respectively represent the linear precoder and decoder matrices. We assume that the channel matrix $\mathbf{H}$ remains constant during the transmission of all the symbol vectors in any given symbol frame (in this paper, a symbol frame consists of a finite number of symbol vectors which are transmitted sequentially), but that the channel matrices corresponding to different symbol frames are mutually independent and identically distributed (this corresponds to an i.i.d. block-fading channel). In addition, $\mathbf{x} \in \mathbb{C}^{N\times 1}$ and $\mathbf{y} \in \mathbb{C}^{M\times 1}$ appearing in Fig. B.1 respectively denote the vector that is transmitted over the N-antenna array and the vector that is received by the M-antenna array. We assume $E[\tilde{\mathbf{x}}\tilde{\mathbf{x}}^\dagger] = I_{m\times m}$, $E[\mathbf{nn}^\dagger] = I_{M\times M}$, and $E[\tilde{\mathbf{x}}\mathbf{n}^\dagger] = \mathbf{0}_{m\times M}$, where † denotes conjugate transposition (for simplicity we assume uncorrelated input sources, each normalised to unit power). For future use, we also define

$$\mathbf{W} = \begin{cases} \mathbf{H}^\dagger\mathbf{H} & \text{if} \quad N \leq M, \text{ and} \\ \mathbf{HH}^\dagger & \text{if} \quad N > M. \end{cases} \tag{B.2}$$

Now, denote the singular value decomposition of the channel matrix $\mathbf{H}$ by

$$\mathbf{H} = \mathbf{U}\mathbf{\Lambda}\mathbf{V}^\dagger, \tag{B.3}$$

where $\mathbf{U} \in \mathbb{C}^{M\times M}$ and $\mathbf{V} \in \mathbb{C}^{N\times N}$ are unitary matrices, and $\mathbf{\Lambda} \in \mathbb{R}^{M\times N}$ is a matrix having the nonnegative square roots of the eigenvalues $\lambda_1, \ldots, \lambda_m$ of $\mathbf{W}$ as entries on its main diagonal and zeros elsewhere. Then, setting $\mathbf{F} = \mathbf{V}\mathbf{\Phi}_f$ and $\mathbf{G} = \mathbf{\Phi}_g\mathbf{V}^\dagger\mathbf{H}^\dagger$, where $\mathbf{\Phi}_g \in \mathbb{R}^{m\times N}$ is such that[2]

$$(\mathbf{\Phi}_g)_{i,j} = \begin{cases} 0 & \text{if} \quad i \neq j \\ \phi_{g,i} & \text{if} \quad i = j, \end{cases} \tag{B.4}$$

with entries $\phi_{g,1}, \ldots, \phi_{g,m}$ chosen arbitrarily under the constraint that $\mathbf{\Phi}_g$ be of full rank, and $\mathbf{\Phi}_f \in \mathbb{R}^{N\times m}$ also has the structure in (B.4) and entries $\phi_{f,1}, \ldots, \phi_{f,m}$, it can be seen that (B.1) becomes

$$\tilde{\mathbf{y}} = \mathbf{\Phi}_g\mathbf{\Lambda}^\dagger\mathbf{\Lambda}\mathbf{\Phi}_f\tilde{\mathbf{x}} + \tilde{\mathbf{n}}, \tag{B.5}$$

where $\tilde{\mathbf{n}} \triangleq \mathbf{G}\mathbf{n}$. The MIMO link has thus been decoupled into m parallel, independent subchannels.

For a given symbol frame (and corresponding channel matrix $\mathbf{H}$), the SNR γ_k on subchannel $k \in \{1, \ldots, m\}$ is then given by [KVRS02]

$$\gamma_k = \frac{E\left[(\mathbf{\Phi}_g\mathbf{\Lambda}^\dagger\mathbf{\Lambda}\mathbf{\Phi}_f\tilde{\mathbf{x}})(\mathbf{\Phi}_g\mathbf{\Lambda}^\dagger\mathbf{\Lambda}\mathbf{\Phi}_f\tilde{\mathbf{x}})^\dagger\right]_{k,k}}{E[\tilde{\mathbf{n}}\tilde{\mathbf{n}}^\dagger]_{k,k}} = \lambda_k\phi_{f,k}^2, \tag{B.6}$$

with $\phi_{f,k}^2$ corresponding to the power that is allocated to subchannel $k \in \{1, \ldots, m\}$. In the case of the *water-filling* solution – advocated by information theory to maximise the information rate of the system – it can be shown that $\phi_{f,1}^2, \ldots, \phi_{f,m}^2$ should satisfy [CT91; KVRS02]

$$\phi_{f,k}^2 = (\mu - \lambda_k^{-1})_+ \qquad \forall k \in \{1, \ldots, m\}, \tag{B.7}$$

where $(\cdot)_+ \triangleq \max(\cdot, 0)$ and μ is a constant which is determined by the power constraint.

We will consider in this work two different power constraints: a *short-term* power constraint and a *long-term* power constraint [CTB99]. For a given power budget P, the short-term power constraint requires that the average transmit power allocated to the symbol vectors within any one symbol frame be less than or equal to P, independently of the channel realisation $\mathbf{H}$ corresponding to this frame; that is, that

$$E[\mathbf{x}^\dagger\mathbf{x}] = \mathrm{tr}\{E[\mathbf{x}\mathbf{x}^\dagger]\} \leq P, \tag{B.8}$$

[2]We use the notation $(\cdot)_{i,j}$ to denote the element in position (i, j) of the matrix in the argument.

where the expectation is taken over the distribution of the symbols $\mathbf{x}$ within any one given symbol frame. This requirement can also be written

$$\mathrm{tr}(\mathbf{F}\mathbf{F}^\dagger) = \sum_{k=1}^{m} \phi_{f,k}^2 \leq P. \tag{B.9}$$

In the case of the less restrictive long-term power constraint, the transmitter is allowed to allocate different average powers to the symbol vectors in frames corresponding to different channel realisations, as long as the average allocated power over multiple symbol frames remains less than or equal to P. This corresponds to the requirement

$$E[\mathrm{tr}(\mathbf{F}\mathbf{F}^\dagger)] \leq P, \tag{B.10}$$

where the expectation is now taken with respect to the distribution of the matrices $\mathbf{F} = \mathbf{V}\mathbf{\Phi}_f$ corresponding to the different symbol frames.

3 Subchannel SNR Distributions

In this section, we establish expressions for the SNR distributions of the independent subchannels obtained by decoupling a MIMO system as described in the previous section, assuming that the available power is distributed among the different subchannels according to the water-filling solution. We restrict our attention to the cases where $m = 1$ (corresponding to single-input single-output (SISO), single-input multiple-output (SIMO) and multiple-input single-output (MISO) systems) or $m = 2$ (two eigenmodes). In this latter case, we assume that $\gamma_1 \geq \gamma_2$, i.e. the subchannel ordering is such that the first subchannel has an SNR which is always greater than or equal to that of the second subchannel.

As mentioned previously, the analysis is done both in the case where the transmitter has a short-term power constraint, and in that where it has a long-term power constraint. It is a simple matter to show that the power constraints (B.9) and (B.10) must be satisfied with equality if the system capacity is to be maximised (this is shown in e.g. [Tel95] for the case of MIMO systems with a deterministic channel matrix $\mathbf{H}$ and perfect transmitter and receiver CSI – an extension to the MIMO systems considered in Sec. 2 is immediate). This result will be used in the derivations that are made in this section.

In the remainder of this document, we use for clarity the notations

$$f_{\gamma_k}^{s,m,n}(\gamma_k), \qquad f_{\gamma_k}^{l,m,n}(\gamma_k) \tag{B.11}$$

to denote the SNR probability density function on the kth among m independent subchannels. Here γ_k ($k \in \{1, \ldots, m\}$) denotes the SNR on the kth among m independent subchannels, the first superscript (s or l) indicates whether the transmitter has a short-term (s) or a long-term (l) power constraint, the second superscript $m = \min\{M, N\}$ denotes the number of independent subchannels (either 1 or 2), and the third superscript is $n = \max\{M, N\}$ as before. Similarly,

$$f_{\lambda_k}^{m,n}(\lambda_k), \tag{B.12}$$

with identical meanings for m and n, denotes the probability density function of the kth largest eigenvalue ($k \leq m$) of the matrix $\mathbf{W} \in \mathbb{C}^{m \times m}$ defined in (B.2). It is also useful to remember that the joint probability density of the ordered eigenvalues ($\lambda_1 \geq \cdots \geq \lambda_m \geq 0$) of matrix $\mathbf{W}$ is given in the case of i.i.d. Rayleigh-fading by [Tel95]

$$f_{\lambda_1,\ldots,\lambda_m}^{m,n}(\lambda_1, \ldots, \lambda_m) = K_{m,n}^{-1} e^{-\sum_{i=1}^{m} \lambda_i} \prod_{i=1}^{m} \lambda_i^{n-m} \prod_{\substack{i<j \\ 1 \leq i,j \leq m}} (\lambda_i - \lambda_j)^2, \tag{B.13}$$

where $K_{m,n}^{-1}$ is a normalising factor,[3] and the superscripts have the same meaning as in (B.12). The distribution law of $\mathbf{W}$ is called the *Wishart* distribution with parameters m and n [Tel95].

Since both the SNR γ_k on the kth among m independent subchannels and the kth eigenvalue of matrix $\mathbf{W}$ are nonnegative quantities, probability density functions such as $f_{\gamma_k}^{s,m,n}(\cdot)$, $f_{\gamma_k}^{l,m,n}(\cdot)$, and $f_{\lambda_k}^{m,n}(\cdot)$ always vanish for strictly negative values of γ_k or λ_k. The analytical expressions for such probability density functions provided throughout this document are *only* valid for nonnegative values of the argument, although this is not always explicitly stated. We choose to adopt this convention rather than to unnecessarily complicate the analytical expressions for these probability density functions by multiplying them by unit step functions.

3.1 SISO, SIMO, and MISO Systems

We consider for the sake of completeness the case where $n \geq m = 1$, which corresponds to SISO, SIMO, or MISO systems.

[3] The normalisation constraints $\int_0^\infty f_{\lambda_1}^{1,n}(\lambda_1)\, \mathrm{d}\lambda_1 = 1$ and $\int_0^\infty \int_0^{\lambda_1} f_{\lambda_1,\lambda_2}^{2,n}(\lambda_1, \lambda_2)\, \mathrm{d}\lambda_2\, \mathrm{d}\lambda_1 = 1$ respectively imply that $K_{1,n} = (n-1)!$ and that $K_{2,n} = (n-1)!(n-2)!$.

3.1.1 Short-Term Power Constraint

In this case, the average transmit power allocated to the symbol vectors within any one given symbol frame must be equal to P. The parameter μ in equation (B.7) is chosen such that

$$(\mu - \lambda_1^{-1})_+ = P, \tag{B.14}$$

corresponding to the short-term power constraint $\mathrm{tr}(\mathbf{F}\mathbf{F}^\dagger) = P$. This yields $\mu = P + \frac{1}{\lambda_1}$ since $P > 0$. Combining this with equations (B.6) and (B.7), we deduce that $\gamma_1 = \mu\lambda_1 - 1 = P\lambda_1$. We hence have

$$f_{\gamma_1}^{s,1,n}(\gamma_1) = \frac{1}{P} f_{\lambda_1}^{1,n}\left(\frac{\gamma_1}{P}\right). \tag{B.15}$$

The probability distribution of the unique eigenvalue λ_1 of $\mathbf{W}$ can be obtained by setting $m = 1$ in (B.13). This yields

$$f_{\lambda_1}^{1,n}(\lambda_1) = \frac{e^{-\lambda_1}}{(n-1)!}\,\lambda_1^{n-1}, \tag{B.16}$$

where we have used the fact that $K_{1,n} = (n-1)!$ as mentioned in footnote 3. The final expression for $f_{\gamma_1}^{s,1,n}(\gamma_1)$ thus reads

$$f_{\gamma_1}^{s,1,n}(\gamma_1) = \frac{1}{P^n}\frac{e^{-\gamma_1/P}}{(n-1)!}\,\gamma_1^{n-1}, \tag{B.17}$$

which corresponds to the SNR distribution on the equivalent channel representing the SISO, SIMO, or MISO system.

3.1.2 Long-Term Power Constraint

The transmitter is now allowed to allocate different average powers to the symbol vectors in frames corresponding to different channel realisations, as long as the long-term power constraint $E[\mathrm{tr}(\mathbf{F}\mathbf{F}^\dagger)] = P$ is respected. In this case, it can be shown [JP03] that μ in equation (B.7) is the solution of

$$\frac{1}{(n-1)!}\int_{1/\mu}^{\infty}\left(\mu - \frac{1}{\gamma}\right) e^{-\gamma}\gamma^{n-1}\,\mathrm{d}\gamma = P. \tag{B.18}$$

Finding an exact value for μ requires the use of numerical root finding techniques. The SNR probability function on the equivalent channel is then given by

$$f_{\gamma_1}^{l,1,n}(\gamma_1) = \frac{1}{\mu} f_{\lambda_1}^{1,n}(z_1) + \delta(\gamma_1)\cdot\int_0^{1/\mu} f_{\lambda_1}^{1,n}(x)\,\mathrm{d}x, \tag{B.19}$$

where $\delta(\cdot)$ denotes the Dirac delta function, $z_1 \triangleq (\gamma_1 + 1)/\mu$, and $f_{\lambda_1}^{1,n}(\lambda_1)$ represents the distribution of the unique eigenvalue λ_1 of $\mathbf{W}$, given in (B.16). The proof of Theorem B.2 (stated in Sec. 3.2), which is given in Appendix A, can be used almost verbatim to establish this result. The integral $\int_0^{1/\mu} f_{\lambda_1}^{1,n}(x)\mathrm{d}x$ admits a closed form solution which is given in Appendix B.

3.2 Dual-Branch MIMO Systems

In this section, we assume that $m = 2$, which corresponds to dual-branch MIMO systems.

3.2.1 Short-Term Power Constraint

Once again, the average transmit power allocated to the symbol vectors within any one given symbol frame must be equal to P. The parameter μ in equation (B.7) must likewise satisfy

$$(\mu - \lambda_1^{-1})_+ + (\mu - \lambda_2^{-1})_+ = P, \tag{B.20}$$

corresponding to the short-term power constraint $\mathrm{tr}(\mathbf{F}\mathbf{F}^\dagger) = \phi_{f,1}^2 + \phi_{f,2}^2 = P$.

Theorem B.1
Under the present assumptions and short-term power budget P, the subchannel SNR probability density functions $f_{\gamma_1}^{s,2,n}(\gamma_1)$ and $f_{\gamma_2}^{s,2,n}(\gamma_2)$ are given by

$$f_{\gamma_1}^{s,2,n}(\gamma_1) = \frac{K_{2,n}^{-1}}{P}\int_0^{\frac{\gamma_1}{P\gamma_1+P}} \Big(\frac{\gamma_1}{P} - x\Big)^2 \exp\Big(-\frac{\gamma_1}{P} - x\Big)\Big(\frac{\gamma_1}{P}x\Big)^{n-2}\mathrm{d}x \quad + \\ K_{2,n}^{-1}\int_{\frac{\gamma_1}{P}}^{\frac{2\gamma_1}{P}} \frac{2x^{2n-1}(2\gamma_1 - Px)^2}{(2\gamma_1 - Px + 1)^{n+2}} \exp\Big(-x\,\frac{2\gamma_1 - Px + 2}{2\gamma_1 - Px + 1}\Big)\,\mathrm{d}x \tag{B.21}$$

and

$$f_{\gamma_2}^{s,2,n}(\gamma_2) = \delta(\gamma_2)\cdot K_{2,n}^{-1} h_n(P) + K_{2,n}^{-1}(2\gamma_2 + 1)^{n-2} \quad \times \\ \int_{\frac{2\gamma_2}{P}}^{\infty} \frac{2x^{2n-1}(2\gamma_2 - Px)^2}{(Px+1)^{n+1}} \exp\Big(-x\,\frac{2\gamma_2 + Px + 2}{Px+1}\Big)\,\mathrm{d}x, \tag{B.22}$$

where $\delta(\cdot)$ is the Dirac delta function and

$$h_n(P) \triangleq \int_0^{\infty}\int_0^{\frac{x}{Px+1}} (x-y)^2 \exp(-x-y)(xy)^{n-2}\,\mathrm{d}y\,\mathrm{d}x. \tag{B.23}$$

Proof: The proof is given in Appendix A. □

Note that some of the definite integrals appearing in the theorem statement do not admit closed form solutions. This is discussed in detail in Appendix B, where closed form expressions are given whenever possible. Moreover, a simple approximation for $f_{\gamma_1}^{s,2,2}(\gamma_1)$ is proposed in Sec. 3.3.

3.2.2 Long-Term Power Constraint

As in Sec. 3.1.2, the transmitter is now allowed to allocate different average powers to the symbol vectors in frames corresponding to different channel realisations, but must respect the long-term power constraint $E[\mathrm{tr}(\mathbf{F}\mathbf{F}^\dagger)] = P$. It is shown in [JP03] that μ in equation (B.7) must then be the solution of

$$\sum_{q=1}^{2} \frac{(q-1)!}{(n+q-3)!} \int_{1/\mu}^{\infty} \left(\mu - \frac{1}{\gamma}\right) e^{-\gamma} \gamma^{n-2} \left[L_{q-1}^{n-2}(\gamma)\right]^2 \mathrm{d}\gamma = P, \tag{B.24}$$

where $L_q^a(x) = \frac{1}{q!} e^x x^{-a} \frac{\mathrm{d}^q}{\mathrm{d}x^q}(e^{-x} x^{a+q})$ is the associated Laguerre polynomial of order q. We must resort to numerical methods to obtain an exact value for μ.

Theorem B.2
Under the present assumptions, long-term power budget P, and corresponding μ obtained by solving (B.24), the subchannel SNR probability density functions $f_{\gamma_k}^{l,2,n}(\gamma_k)$, for all $k \in \{1,2\}$, are given by

$$f_{\gamma_k}^{l,2,n}(\gamma_k) = \frac{1}{\mu} f_{\lambda_k}^{2,n}(z_k) + \delta(\gamma_k) \cdot \int_0^{1/\mu} f_{\lambda_k}^{2,n}(x)\, \mathrm{d}x, \qquad k \in \{1,2\} \tag{B.25}$$

where $\delta(\cdot)$ denotes the Dirac delta function, $z_k \triangleq (\gamma_k + 1)/\mu$, and

$$f_{\lambda_2}^{2,n}(\lambda_2) = K_{2,n}^{-1}(n-2)! e^{-2\lambda_2} \lambda_2^{n-2} \sum_{q=0}^{n-2} \frac{(n-q)(n-q-1)}{q!} \lambda_2^q \tag{B.26}$$

and

$$f_{\lambda_1}^{2,n}(\lambda_1) = \frac{e^{-\lambda_1} \lambda_1^{n-2} \left[\lambda_1^2 (n-2)! - 2\lambda_1 (n-1)! + n!\right]}{K_{2,n}} - f_{\lambda_2}^{2,n}(\lambda_1) \tag{B.27}$$

respectively denote the probability density functions of the smallest and largest eigenvalue of $\mathbf{W} \in \mathbb{C}^{2\times 2}$.

Proof: The proof is given in Appendix A. □

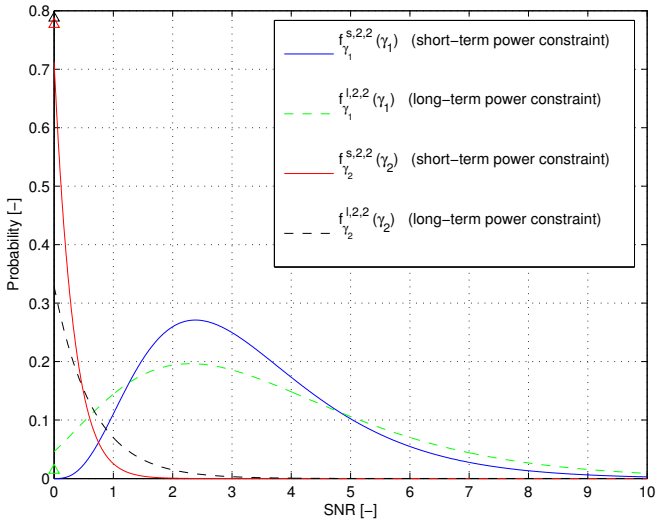

FIGURE B.2: Probability density functions appearing in Theorems 1 and 2 for $P = 0$ dB and $m = n = 2$ (SNR in linear scale). Dirac pulses are represented by triangles.

The integrals $\int_0^{1/\mu} f_{\lambda_2}^{2,n}(x)\mathrm{d}x$ and $\int_0^{1/\mu} f_{\lambda_1}^{2,n}(x)\mathrm{d}x$ admit closed form solutions which are given in Appendix B. Plots of the probability density functions $f_{\gamma_1}^{s,2,2}(\gamma_1)$, $f_{\gamma_1}^{l,2,2}(\gamma_1)$, $f_{\gamma_2}^{s,2,2}(\gamma_2)$, and $f_{\gamma_2}^{l,2,2}(\gamma_2)$ as obtained in Theorems 1 and 2 are shown in Fig. B.2 for $P = 0$ dB.

The validity of the results presented in Theorems 1 and 2 have been verified by comparing the cumulative distribution functions

$$F_{\gamma_k}^{s,m,n}(z) \triangleq \int_0^z f_{\gamma_k}^{s,m,n}(\gamma_k)\ \mathrm{d}\gamma_k \tag{B.28}$$

and

$$F_{\gamma_k}^{l,m,n}(z) \triangleq \int_0^z f_{\gamma_k}^{l,m,n}(\gamma_k)\ \mathrm{d}\gamma_k, \tag{B.29}$$

where $k \in \{1, \ldots, m\}$, to the output of Monte Carlo simulations (10^6 samples). The agreement between theoretical and simulated cumulative distribution functions was perfect in all cases. A plot of $F_{\gamma_1}^{s,2,4}(z)$, $F_{\gamma_1}^{l,2,4}(z)$, $F_{\gamma_2}^{s,2,4}(z)$, and $F_{\gamma_2}^{l,2,4}(z)$ together with the output of the corresponding Monte Carlo simulations is shown in Fig. B.3 for $P = 0$ dB.

Note that it is simple to extend the results obtained in Theorems B.1 and B.2 to other dual-branch MIMO channel models (e.g. correlated MIMO

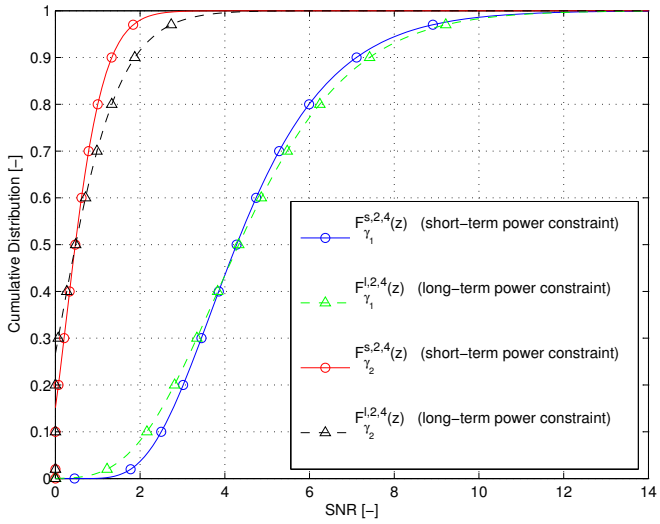

FIGURE B.3: Cumulative distribution functions $F^{s,2,4}_{\gamma_1}(z)$, $F^{l,2,4}_{\gamma_1}(z)$, $F^{s,2,4}_{\gamma_2}(z)$, and $F^{l,2,4}_{\gamma_2}(z)$ for $P = 0$ dB (SNR in linear scale). The circles and triangles correspond to the results of Monte Carlo simulations (10^6 samples), whereas the solid and dashed lines were computed using the results presented in Theorems 1 and 2.

Rayleigh-fading channels [CWZ03] or Ricean fading channels [BOØ05]) simply by using the appropriate expression for the eigenvalue distribution $f^{2,n}_{\lambda_1,\lambda_2}(\lambda_1,\lambda_2)$: this expression can be introduced in e.g. (B.78) and (B.81) to obtain $f^{s,2,n}_{\gamma_1}(\gamma_1)$, or in (B.25) after marginalisation to obtain $f^{l,m,n}_{\gamma_k}(\gamma_k)$.

3.3 Approximations for the case $m = n = 2$

When $m = 2$, the expressions for $f^{s,2,n}_{\gamma_1}(\gamma_1)$ and $f^{s,2,n}_{\gamma_2}(\gamma_2)$ (short-term power constraint case) depend on definite integrals, some of which do not admit closed form solutions (see Appendix B for details). In this section, we consider the important special case where $n = m = 2$ and propose a simple approximation for $f^{s,2,2}_{\gamma_1}(\gamma_1)$. Comparable ideas could also be used to derive similar approximations when $n > 2$ although we have chosen not to explore this issue any further in this document.

Let us consider

$$\widehat{f}^{s,2,2}_{\gamma_1}(\gamma_1) = be^{-b\gamma_1}[(b\gamma_1)^2 - 2b\gamma_1 + 2] - 2be^{-2b\gamma_1}, \tag{B.30}$$

as a candidate to approximate $f_{\gamma_1}^{s,2,2}(\gamma_1)$, where b is a parameter that can be adjusted. This expression presents the advantage of satisfying the normalisation constraint

$$\int_0^\infty \widehat{f}_{\gamma_1}^{s,2,2}(\gamma_1)\,\mathrm{d}\gamma_1 = 1 \tag{B.31}$$

and the requirement

$$\widehat{f}_{\gamma_1}^{s,2,2}(0) = 0 \tag{B.32}$$

for all b, both of which are also met by $f_{\gamma_1}^{s,2,2}(\gamma_1)$.

The approximation for $f_{\gamma_1}^{s,2,2}(\gamma_1)$ suggested in (B.30) was inspired by the corresponding SNR distribution $f_{\gamma_1}^{l,2,2}(\gamma_1)$ in the long-term power constraint case, which is given by

$$f_{\gamma_1}^{l,2,2}(\gamma_1) = \delta(\gamma_1)\cdot\left[1-\frac{e^{-1/\mu}}{\mu^2}\left(1+\mu^2(2-e^{-1/\mu})\right)\right] \quad + \\ \frac{1}{\mu}\left[e^{-z_1}(z_1^2-2z_1+2)-2e^{-2z_1}\right], \tag{B.33}$$

with $z_1 = (\gamma_1+1)/\mu$ as before. Since the short-term version $f_{\gamma_1}^{s,2,2}(\gamma_1)$ has no discrete components (Dirac pulses) as can be seen by examining (B.21), we simply chose to ignore the first term of (B.33). We also chose to set $z_1 = b\cdot\gamma_1$ instead of $z_1 = (\gamma_1+1)/\mu$ in order to satisfy (B.32). The final expression was multiplied by $b\mu$ in order to also satisfy (B.31), yielding (B.30).

For values of P at intervals of 0.5 dB between -15 dB and 20 dB, we selected b such that the square of the L^2-norm

$$\|e(\gamma_1)\|_2^2 = \int_0^\infty |f_{\gamma_1}^{s,2,2}(\gamma_1) - \widehat{f}_{\gamma_1}^{s,2,2}(\gamma_1)|^2\,\mathrm{d}\gamma_1 \tag{B.34}$$

of the error $e(\gamma_1) = f_{\gamma_1}^{s,2,2}(\gamma_1) - \widehat{f}_{\gamma_1}^{s,2,2}(\gamma_1)$ be minimised. $\|e(\gamma_1)\|_2^2$ is plotted in Fig. B.4 as a function of P. As can be seen from the figure, the norm of the approximation error is maximum when $P \approx 5.5$ dB, in which case $\|e(\gamma_1)\|_2^2 \approx 6.628\times10^{-5}$. Nevertheless, the actual probability density function $f_{\gamma_1}^{s,2,2}(\gamma_1)$ and its approximation $\widehat{f}_{\gamma_1}^{s,2,2}(\gamma_1)$ are remarkably close even in this worst case, as shown in Fig. B.5.

4 System Capacity and Continuous Rate Adaptation

In order to maximise the information rate of the system described in Sec. 2 for $m \in \{1,2\}$ by applying the water-filling solution (see Sec. 2), continuous rate adaptation is required both in the case of a short-term power constraint

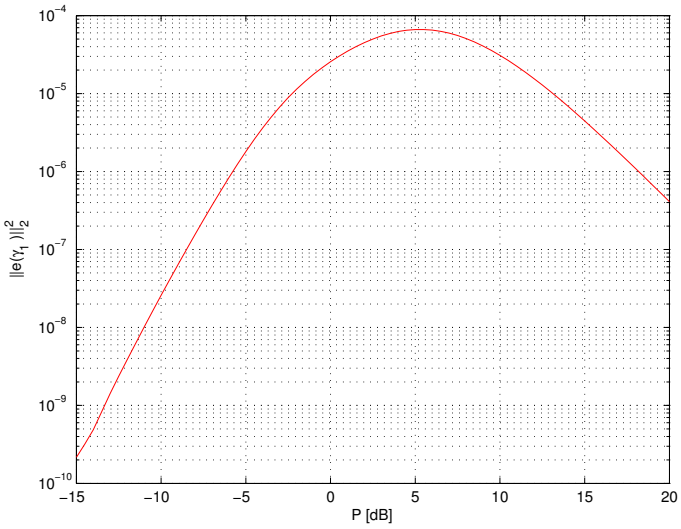

FIGURE B.4: Squared L^2-norm of the approximation error $\|e(\gamma_1)\|_2^2$ as a function of P. The maximum value is attained when $P \approx 5.5$ dB.

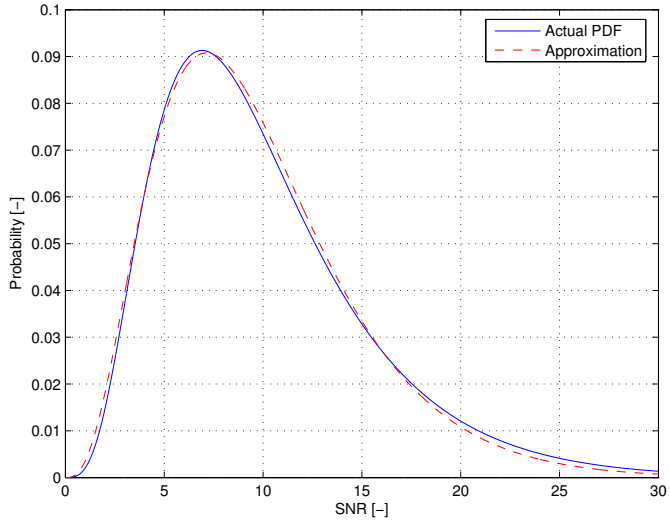

FIGURE B.5: $f_{\gamma_1}^{s,2,2}(\gamma_1)$ and $\widehat{f}_{\gamma_1}^{s,2,2,\prime}(\gamma_1)$ when $P = 5.5$ dB. SNR in linear scale.

and in the case of a long-term power constraint. Indeed, if this maximum information rate (or *capacity* C) is to be attained, a capacity achieving code designed to operate at the information rate $\log_2(1+\gamma_k)$ has to be utilised whenever the SNR on subchannel k is γ_k – this having to be done for every symbol frame and each one of the k among m subchannels. Since both in the short-term and long-term power constraint cases the subchannel SNR distributions have a continuous component for any $m \in \{1,2\}$ and any $k \in \{1,\ldots,m\}$ as shown in Sec. 3, an infinite number of such capacity-achieving codes is required if the whole SNR range is to be covered.

The system's ergodic capacity C is given by the sum of the capacities of each one of the m subchannels. In the short-term power constraint case, we have

$$C = \sum_{k=1}^{m} \int_0^\infty \log_2(1+\gamma_k) f_{\gamma_k}^{s,m,n}(\gamma_k)\,\mathrm{d}\gamma_k, \quad \text{[bits/channel use]} \tag{B.35}$$

where the capacity of each subchannel is calculated as in [GV97, Eq. (2)] using the newly found SNR distributions. A similar identity – which can simply be obtained by replacing $f_{\gamma_k}^{s,m,n}(\gamma_k)$ by $f_{\gamma_k}^{l,m,n}(\gamma_k)$ in the above expression – obviously also holds in the long-term power constraint case.

5 Maximum ASE of Discrete Rate Dual-Branch MIMO Systems with a Short-Term Power Constraint

In the case of discrete rate adaptation, only a finite number n_c of capacity-achieving codes for AWGN channels is available for use. In this section, we first show how to calculate the ASE of a dual-branch MIMO system when the rates $\{R_i\}_{i=1}^{n_c}$ of these n_c codes are fixed and the available power is optimally distributed between the $m=2$ subchannels. We then discuss how to find the values $\{R_i^*\}_{i=1}^{n_c}$ of the rates for which such a system's ASE is maximised. We restrict our attention to the case of dual-branch MIMO systems with a short-term power constraint, since performing a similar optimisation in the case discrete rate dual-branch MIMO systems with a long-term power constraint is a problem of a mathematically different nature to which the methods employed in this section cannot be directly applied.

5.1 Optimal power allocation and ASE calculation for fixed $R_{n_c}, \ldots, R_1$

Let us define the *rate vector* $\mathbf{R}_{n_c} \triangleq (R_{n_c}, \ldots, R_1, R_0 = 0)$ (we set $R_0 = 0$ for convenience although R_0 *is not* an optimisation variable), the *power allocation vector* $\mathbf{P}_m \triangleq (\phi^2_{f,1}, \ldots, \phi^2_{f,m})$, and the *vector of eigenvalues* $\mathbf{L}_m \triangleq (\lambda_1, \ldots, \lambda_m)$. All these will be potentially different for every realisation of the channel matrix $\mathbf{H}$. Now, for any given $\mathbf{R}_{n_c}$, $\mathbf{L}_m$, and $\mathbf{P}_m$, we define the *instantaneous information rate* $\nu(\mathbf{R}_{n_c}, \mathbf{L}_m, \mathbf{P}_m)$ by

$$\nu(\mathbf{R}_{n_c}, \mathbf{L}_m, \mathbf{P}_m) \triangleq \sum_{k=1}^{m} \log_2(1 + \lambda_k \phi^2_{f,k}), \tag{B.36}$$

where the short-term power constraint $\sum_{k=1}^{m} \phi^2_{f,k} \leq P$, and the rate constraints $\log_2(1 + \lambda_k \phi^2_{f,k}) \in \mathbf{R}_{n_c}\ \forall k \in \{1, \ldots m\}$, must be satisfied in order for $\mathbf{P}_m$ to be a valid power allocation vector.

For any given $\mathbf{R}_{n_c}$ and $\mathbf{L}_m$, the optimal power allocation vector $\mathbf{P}^*_m \triangleq (\phi^{*2}_{f,1}, \ldots, \phi^{*2}_{f,m})$ is given by

$$\mathbf{P}^*_m = \arg\max_{\mathbf{P}_m} \nu(\mathbf{R}_{n_c}, \mathbf{L}_m, \mathbf{P}_m), \tag{B.37}$$

where the power and rate constraints mentioned above must obviously still be satisfied. For fixed $\mathbf{R}_{n_c}$, the maximal ASE $\eta_{\mathrm{op}}(\mathbf{R}_{n_c})$ is then simply given by

$$\eta_{\mathrm{op}}(\mathbf{R}_{n_c}) = \int_{\Omega_m} \nu(\mathbf{R}_{n_c}, \mathbf{L}_m, \mathbf{P}^*_m) f^{m,n}_{\lambda_1,\ldots,\lambda_m}(\lambda_1, \ldots, \lambda_m)\, \mathrm{d}\Lambda_m, \tag{B.38}$$

where

$$\Omega_m \triangleq \{(\lambda_1, \ldots, \lambda_m) | \lambda_1 \geq \cdots \geq \lambda_m \geq 0\} \subset \mathbb{R}^m, \tag{B.39}$$

$\mathrm{d}\Lambda_m \triangleq \mathrm{d}\lambda_m \cdots \mathrm{d}\lambda_1$, $f^{m,n}_{\lambda_1,\ldots,\lambda_m}(\lambda_1, \ldots, \lambda_m)$ was defined in (B.13), and the subscript *op* is used to indicate that the available power has been optimally distributed between the m subchannels. For convenience, we also define

$$\nu^*(\mathbf{R}_{n_c}, \mathbf{L}_m) \triangleq \nu(\mathbf{R}_{n_c}, \mathbf{L}_m, \mathbf{P}^*_m). \tag{B.40}$$

In the remainder of this section, we show how to calculate the ASE $\eta_{\mathrm{op}}(\mathbf{R}_{n_c})$ for dual-branch MIMO systems and $n_c \in \{1, 2, 3, 4\}$. We assume without loss of generality that $R_{n_c} > \cdots > R_1 > R_0 = 0$.[4]

[4] If the strict inequalities were to be replaced with non-strict inequalities in the relation $R_{n_c} > \cdots > R_1 > R_0 = 0$, the results of this section would still apply. However, in this case it is obvious that whenever $\mathbf{R}_{n_c}$ is such that k of these non-strict inequalities are satisfied with equality, the calculation of $\eta_{\mathrm{op}}(\mathbf{R}_{n_c})$ can be reduced to that of $\eta_{\mathrm{op}}(\mathbf{R}'_{n_c-k})$, where $\mathbf{R}'_{n_c-k}$ is obtained from $\mathbf{R}_{n_c}$ by removing any repeated components and renumbering.

We first calculate $\nu^*(\mathbf{R}_{n_c}, \mathbf{L}_2)$ and then obtain $\eta_{\text{op}}(\mathbf{R}_{n_c})$ via (B.38). For $i \in \{0, \ldots, n_c\}$, let $\gamma_i^* \triangleq 2^{R_i} - 1$, and let

$$A_{ij} \triangleq \left\{ (\lambda_1, \lambda_2) \in \Omega_2 \middle| \frac{\gamma_i^*}{\lambda_1} + \frac{\gamma_j^*}{\lambda_2} \leq P \right\}, \tag{B.41}$$

where $i \in \{0, \ldots, n_c\}$ and $j \in \{0, \ldots, i\}$. We also define

$$r(A_{ij}) \triangleq R_i + R_j \tag{B.42}$$

for each A_{ij}. For every set Q of points of Ω_2, we can consider the event "observing a channel matrix $\mathbf{H}$ such that the corresponding $(\lambda_1, \lambda_2) \in Q$". The probability that this event take place is given by

$$\Pr(Q) = \iint_Q f^{2,n}_{\lambda_1,\lambda_2}(\lambda_1, \lambda_2)\, \mathrm{d}\lambda_2\, \mathrm{d}\lambda_1. \tag{B.43}$$

where we have chosen to use the same letter for the set of points of Ω_2 and the event defined by this set, the meaning being clear from the context. For simplicity, we refer to this quantity as the *probability of set* Q. It is important at this point to note that the probability of any finite intersection of the form $I = \bigcap_k A_{i_k j_k}$ can be easily obtained as

$$\Pr(I) = \int_{\max_k \xi_k}^{\infty} \int_{\max_k \eta_k}^{\lambda_1} f^{2,n}_{\lambda_1,\lambda_2}(\lambda_1, \lambda_2)\, \mathrm{d}\lambda_2\, \mathrm{d}\lambda_1, \tag{B.44}$$

where $\xi_k = \frac{\gamma_{i_k}^* + \gamma_{j_k}^*}{P}$ and $\eta_k = \frac{\gamma_{j_k}^* \lambda_1}{\lambda_1 P - \gamma_{i_k}^*}$. This is illustrated in Fig. B.6 for $I = A_{42} \cap A_{33}$, where the shaded area corresponds to $\{(\lambda_1, \lambda_2) \in A_{42} \cap A_{33}\}$. Furthermore, we can use mathematical induction to prove that

$$\begin{aligned} \Pr\left(Q \setminus \bigcup_{k=1}^{\kappa} Q_k \right) = \Pr(Q) - \sum_{k=1}^{\kappa} \Pr(Q \cap Q_k) + \sum_{k,l \,|\, k<l} \Pr(Q \cap Q_k \cap Q_l) \\ + \cdots + (-1)^{\kappa} \Pr\left(Q \cap \bigcap_{k=1}^{\kappa} Q_k \right). \end{aligned} \tag{B.45}$$

This identity allows us to evaluate any expression of the form $\Pr(I \setminus J)$, with I defined as above and J a finite union of the form $J = \bigcup_l A_{i_l j_l}$. Indeed, each one of the terms in the expression which is obtained by applying (B.45) to $\Pr(I \setminus J)$ is a finite intersection of A_{ij}s which can be computed using (B.44). We now separately consider the cases $n_c = 1$ and $n_c \in \{2, 3, 4\}$.

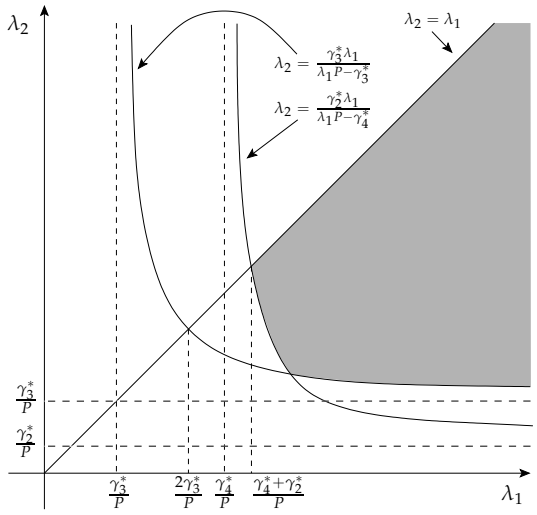

FIGURE B.6: Calculation of $\Pr(\mathrm{A}_{42} \cap \mathrm{A}_{33})$ using (B.44). The shaded area corresponds to $\{(\lambda_1, \lambda_2) \in A_{42} \cap A_{33}\}$.

5.1.1 $n_c = 1$

In this case, we have a single code of rate R_1. For a given channel matrix $\mathbf{H}$ and corresponding λ_1 and λ_2, $\nu^*(\mathbf{R}_1, \mathbf{L}_2)$ will be equal to $2R_1$ if the power budget is large enough to support a code of rate R_1 on both subchannels, i.e. if

$$\begin{cases} \frac{\gamma_1^*}{\lambda_1} \leq P \\ \frac{\gamma_1^*}{\lambda_2} \leq P \\ \frac{\gamma_1^*}{\lambda_1} + \frac{\gamma_1^*}{\lambda_2} \leq P. \end{cases} \tag{B.46}$$

The first and second inequalities respectively state that the available power must be sufficient to support a rate R_1 on the first (best) and second (worst) subchannels. The third inequality states that the sum of the powers that is allocated to both subchannels must not exceed the total available power P. Since $\lambda_1 \geq \lambda_2 \geq 0$, it can easily be seen that the first inequality is automatically verified if the second is, and that the first two are whenever the third is. Consequently, if $\frac{\gamma_1^*}{\lambda_1} + \frac{\gamma_1^*}{\lambda_2} \leq P$, i.e. if $(\lambda_1, \lambda_2) \in A_{11}$, the optimal power distribution is characterised by $\phi_{f,k}^{*2} = \frac{\gamma_1^*}{\lambda_k}$ ($k \in \{1, 2\}$), and $\nu^*(\mathbf{R}_1, \mathbf{L}_2) = r(A_{11}) = 2R_1$.

If λ_1 and λ_2 are such that – given the available power budget P – only one subchannel can support transmission at a rate R_1, we will have

$\nu^*(\mathbf{R}_1, \mathbf{L}_2) = R_1$. It can be verified that this happens if and only if

$$\begin{cases} \frac{\gamma_1^*}{\lambda_1} \leq P \\ \frac{\gamma_1^*}{\lambda_1} + \frac{\gamma_1^*}{\lambda_2} > P, \end{cases} \tag{B.47}$$

i.e. if $(\lambda_1, \lambda_2) \in A_{10} \backslash A_{11}$. Finally, $\nu^*(\mathbf{R}_1, \mathbf{L}_2) = 0$ if none of the subchannels can support transmission at a rate R_1, which is the case if $\frac{\gamma_1^*}{\lambda_1} > P$, i.e. if $(\lambda_1, \lambda_2) \in \Omega_2 \backslash A_{10}$.

Bearing in mind the above results, $\eta_{\text{op}}(\mathbf{R}_1)$ can be calculated using (B.38). This yields

$$\eta_{\text{op}}(\mathbf{R}_1) = r(A_{11}) \cdot \Pr(A_{11}) + r(A_{10}) \cdot \Pr(A_{10} \backslash A_{11}), \tag{B.48}$$

where $\Pr(A_{11})$ and $\Pr(A_{10} \backslash A_{11})$ can be calculated using (B.44) and (B.45).

5.1.2 $n_c = 2$, $n_c = 3$, and $n_c = 4$

Proceeding exactly as in the case $n_c = 1$, it is possible to derive expressions for $\eta_{\text{op}}(\mathbf{R}_2)$, $\eta_{\text{op}}(\mathbf{R}_3)$, and $\eta_{\text{op}}(\mathbf{R}_4)$. (The details are somewhat tedious and hence not included here.) This yields

$$\eta_{\text{op}}(\mathbf{R}_{n_c}) = \sum_{k=1}^{2(2^{n_c}-1)} S_{n_c,k} \cdot T_{n_c,k}, \qquad n_c \in \{2, 3, 4\} \tag{B.49}$$

where $S_{n_c,k}$ and $T_{n_c,k}$ are given in Tables B.1, B.2, and B.3 respectively when $n_c = 2$, $n_c = 3$, and $n_c = 4$. Note that $T_{n_c,k}$ can be computed using (B.44) and (B.45) for all $n_c \in \{2, 3, 4\}$ and $k \in \{1, \ldots, 2(2^{n_c} - 1)\}$.

A Venn diagram representing the different sets that appear in Table B.3 is depicted in Fig. B.7, where each closed contour corresponds to a set A_{ij} and the numbers 1 to 30 correspond to the results of the set operations in the argument of $T_{4,1}$ to $T_{4,30}$. It is also interesting to remark that the expression for $\eta_{\text{op}}(\mathbf{R}_4)$ given in (B.49) can be used to compute $\eta_{\text{op}}(\mathbf{R}_1)$, $\eta_{\text{op}}(\mathbf{R}_2)$, and $\eta_{\text{op}}(\mathbf{R}_3)$. Indeed, we have e.g. $\eta_{\text{op}}((x, y, 0, 0, 0)) = \eta_{\text{op}}((x, y, 0))$ for all $x > y > 0$.

Note that the methodology presented in this section can also be used to evaluate $\eta_{\text{op}}(\mathbf{R}_{n_c})$ for other dual-branch MIMO channel models simply by using the appropriate expression for the eigenvalue distribution $f^{2,n}_{\lambda_1,\lambda_2}(\lambda_1, \lambda_2)$ in (B.44).

5.2 Maximising the ASE with respect to the component rates

In this section, we discuss how to find the rate vector $\mathbf{R}^*_{n_c} = \arg\max_{\mathbf{R}_{n_c}} \eta_{\text{op}}(\mathbf{R}_{n_c})$ resulting in the maximum ASE $\eta_{\text{op}}(\mathbf{R}^*_{n_c})$ when $n_c \in$

k	$S_{2,k}$	$T_{2,k}$
1	$r(A_{22})$	$\Pr(A_{22})$
2	$r(A_{21})$	$\Pr(A_{21} \backslash A_{22})$
3	$r(A_{20})$	$\Pr(A_{20} \backslash A_{11})$
4	$r(A_{11})$	$\Pr(A_{11} \backslash A_{20})$
5	$r(A_{10})$	$\Pr(A_{10} \backslash (A_{11} \cup A_{20}))$
6	$\max\{r(A_{11}), r(A_{20})\}$	$\Pr((A_{11} \cap A_{20}) \backslash A_{21})$

TABLE B.1: Expressions for $S_{2,k}$ and $T_{2,k}$

k	$S_{3,k}$	$T_{3,k}$
1	$r(A_{33})$	$\Pr(A_{33})$
2	$r(A_{32})$	$\Pr(A_{32} \backslash A_{33})$
3	$r(A_{31})$	$\Pr(A_{31} \backslash A_{22})$
4	$r(A_{30})$	$\Pr(A_{30} \backslash A_{11})$
5	$r(A_{22})$	$\Pr(A_{22} \backslash A_{30})$
6	$r(A_{21})$	$\Pr(A_{21} \backslash (A_{22} \cup A_{30}))$
7	$r(A_{20})$	$\Pr(A_{20} \backslash (A_{11} \cup A_{30}))$
8	$r(A_{11})$	$\Pr(A_{11} \backslash A_{20})$
9	$r(A_{10})$	$\Pr(A_{10} \backslash (A_{11} \cup A_{20}))$
10	$\max\{r(A_{22}), r(A_{31})\}$	$\Pr((A_{22} \cap A_{31}) \backslash A_{32})$
11	$\max\{r(A_{22}), r(A_{30})\}$	$\Pr((A_{22} \cap A_{30}) \backslash A_{31})$
12	$\max\{r(A_{21}), r(A_{30})\}$	$\Pr((A_{21} \cap A_{30}) \backslash (A_{22} \cup A_{31}))$
13	$\max\{r(A_{20}), r(A_{11})\}$	$\Pr((A_{20} \cap A_{11}) \backslash (A_{21} \cup A_{30}))$
14	$\max\{r(A_{30}), r(A_{11})\}$	$\Pr((A_{30} \cap A_{11}) \backslash A_{21})$

TABLE B.2: Expressions for $S_{3,k}$ and $T_{3,k}$

k	$S_{4,k}$	$T_{4,k}$
1	$r(A_{44})$	$\Pr(A_{44})$
2	$r(A_{43})$	$\Pr(A_{43} \backslash A_{44})$
3	$r(A_{42})$	$\Pr(A_{42} \backslash A_{33})$
4	$r(A_{41})$	$\Pr(A_{41} \backslash A_{22})$
5	$r(A_{40})$	$\Pr(A_{40} \backslash A_{11})$
6	$r(A_{33})$	$\Pr(A_{33} \backslash A_{40})$
7	$r(A_{32})$	$\Pr(A_{32} \backslash (A_{33} \cup A_{40}))$
8	$r(A_{31})$	$\Pr(A_{31} \backslash (A_{22} \cup A_{40}))$
9	$r(A_{30})$	$\Pr(A_{30} \backslash (A_{11} \cup A_{40}))$
10	$r(A_{22})$	$\Pr(A_{22} \backslash A_{30})$
11	$r(A_{21})$	$\Pr(A_{21} \backslash (A_{22} \cup A_{30}))$
12	$r(A_{20})$	$\Pr(A_{20} \backslash (A_{11} \cup A_{30}))$
13	$r(A_{11})$	$\Pr(A_{11} \backslash A_{20})$
14	$r(A_{10})$	$\Pr(A_{10} \backslash (A_{11} \cup A_{20}))$
15	$\max\{r(A_{33}), r(A_{42})\}$	$\Pr((A_{33} \cap A_{42}) \backslash A_{43})$
16	$\max\{r(A_{33}), r(A_{41})\}$	$\Pr((A_{33} \cap A_{41}) \backslash A_{42})$
17	$\max\{r(A_{33}), r(A_{40})\}$	$\Pr((A_{33} \cap A_{40}) \backslash A_{41})$
18	$\max\{r(A_{32}), r(A_{41})\}$	$\Pr((A_{32} \cap A_{41}) \backslash (A_{33} \cup A_{42}))$
19	$\max\{r(A_{32}), r(A_{40})\}$	$\Pr((A_{32} \cap A_{40}) \backslash (A_{33} \cup A_{41}))$
20	$\max\{r(A_{31}), r(A_{40}), r(A_{22})\}$	$\Pr((A_{31} \cap A_{40} \cap A_{22}) \backslash (A_{32} \cup A_{41}))$
21	$\max\{r(A_{40}), r(A_{22})\}$	$\Pr((A_{40} \cap A_{22}) \backslash A_{31})$
22	$\max\{r(A_{31}), r(A_{40})\}$	$\Pr((A_{31} \cap A_{40}) \backslash (A_{22} \cup A_{41}))$
23	$\max\{r(A_{22}), r(A_{41})\}$	$\Pr((A_{41} \cap A_{22}) \backslash A_{32})$
24	$\max\{r(A_{22}), r(A_{31})\}$	$\Pr((A_{22} \cap A_{31}) \backslash (A_{32} \cup A_{40}))$
25	$\max\{r(A_{22}), r(A_{30})\}$	$\Pr((A_{22} \cap A_{30}) \backslash (A_{31} \cup A_{40}))$
26	$\max\{r(A_{21}), r(A_{40})\}$	$\Pr((A_{21} \cap A_{40}) \backslash (A_{31} \cup A_{22}))$
27	$\max\{r(A_{21}), r(A_{30})\}$	$\Pr((A_{21} \cap A_{30}) \backslash (A_{31} \cup A_{40} \cup A_{22}))$
28	$\max\{r(A_{11}), r(A_{40})\}$	$\Pr((A_{11} \cap A_{40}) \backslash A_{21})$
29	$\max\{r(A_{11}), r(A_{30})\}$	$\Pr((A_{11} \cap A_{30}) \backslash (A_{21} \cup A_{40}))$
30	$\max\{r(A_{11}), r(A_{20})\}$	$\Pr((A_{11} \cap A_{20}) \backslash (A_{21} \cup A_{30}))$

TABLE B.3: Expressions for $S_{4,k}$ and $T_{4,k}$

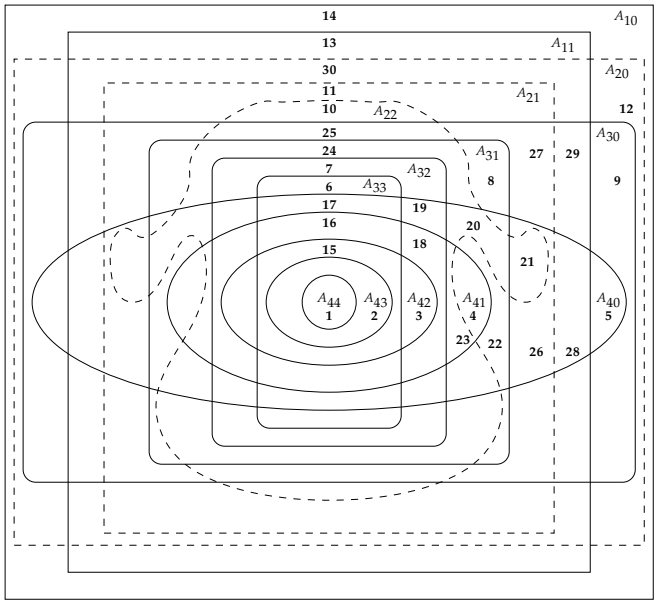

FIGURE B.7: Venn diagram representing the different sets appearing in Table B.3 and the relations between them. The closed contours correspond to the different A_{ij}s, whereas the numbers 1 to 30 correspond to the results of the set operations in the argument of $T_{4,1}$ to $T_{4,30}$.

$\{1,2,3,4\}$. (Note that for every $\mathbf{L}_m$, the values of $\mathbf{R}_{n_c}^*$ and $\mathbf{P}_m^*$ – the latter quantity being obtained via Eq. (B.37) with $\mathbf{R}_{n_c} = \mathbf{R}_{n_c}^*$ – will be *jointly* optimal. However, whereas $\mathbf{R}_{n_c}^*$ remains fixed, the value of $\mathbf{P}_m^*$ changes as a function of $\mathbf{L}_m$.) This is an n_c-dimensional optimisation problem. The most straightforward approach to solve it would be to compute the points where the gradient $\nabla_{\mathbf{R}_{n_c}} \eta_{\mathrm{op}}(\mathbf{R}_{n_c})$ vanishes. It is unfortunately not practical to do this analytically since the expressions for $\eta_{\mathrm{op}}(\mathbf{R}_{n_c})$ are quite involved for all values of $n_c \in \{1,2,3,4\}$.

A plot of $\eta_{\mathrm{op}}(\mathbf{R}_1)$ as a function of R_1 reveals that this function can have several local maxima (see Fig. B.8(a)). Further numerical experiments reveal that the total number of local maxima increases rapidly with n_c. It is thus necessary to explore the whole n_c-dimensional space to find the optimal $\mathbf{R}_{n_c}$. When $n_c = 1$ or $n_c = 2$ this can be done by plotting $\eta_{\mathrm{op}}(\mathbf{R}_{n_c})$ as a function of $(R_{n_c}, \ldots, R_1)$ for $M_{n_c} > R_{n_c} > \cdots > R_1 > 0$, where M_{n_c} is a suitably chosen number whose value helps to limit the search space. (How to choose M_{n_c} is discussed in Appendix C.) The approximate positions of all the local maxima then become apparent, and it is possible to find the value of $\eta_{\mathrm{op}}(\mathbf{R}_{n_c})$ at each local maximum by using a steepest-descent like algo-

rithm [NW99] with a starting point sufficiently close to the local maximum in question. The values of $\mathbf{R}_{n_c}^*$ and $\eta_{\text{op}}(\mathbf{R}_{n_c}^*)$ immediately follow.

When $n_c \geq 3$, it becomes more difficult to plot $\eta_{\text{op}}(\mathbf{R}_{n_c})$ as a function of $\{R_i\}_{i=1}^{n_c}$ for $M_{n_c} > R_{n_c} > \cdots > R_1 > 0$. We therefore proceed by evaluating $\eta_{\text{op}}(\mathbf{R}_{n_c})$ at all points of the form $(i_{n_c} \cdot \Delta, \ldots, i_1 \cdot \Delta)$, where $i_{n_c} > \cdots > i_1 > 0$ are integers, $(i_{n_c} + 1) \cdot \Delta > M_{n_c} > i_{n_c} \cdot \Delta$, and Δ is a suitably chosen quantity (see Sec. 7).[5] The resulting values can then be sorted, and a steepest-descent like algorithm can be used (starting from each one of the rate vectors $\mathbf{R}_{n_c}$ resulting in one of the top N_p ASE values $\eta_{\text{op}}(\mathbf{R}_{n_c})$) to attempt to find the local maxima which are in the neighbourhood of each one of these N_p points, where N_p is a sufficiently large integer (see Sec. 7). One of the local maxima obtained in this way will then hopefully be the global maximum, although rigorously proving this is difficult and beyond the scope of this paper. The results presented in Sec. 7 can thus be considered as lower bounds for the maximum ASE $\eta_{\text{op}}(\mathbf{R}_{n_c}^*)$ when $n_c = 3$ and $n_c = 4$.

We conclude this section with some additional remarks regarding the maximisation of $\eta_{\text{op}}(\mathbf{R}_{n_c})$. Note first of all (see Tables B.1, B.2, and B.3) that due to the presence of terms of the form $\max_l\{r(A_{i_l j_l})\}$ in the expression for $S_{n_c,k}$, $\eta_{\text{op}}(\mathbf{R}_{n_c})$ is not differentiable at all points $\mathbf{R}_{n_c} \in \mathcal{R}_{n_c}^\circ$ when $n_c \geq 2$, where $\mathcal{R}_{n_c}^\circ$ denotes the interior of the set $\mathcal{R}_{n_c} \triangleq \{(R_{n_c}, \ldots, R_1, 0) | M_{n_c} > R_{n_c} > \cdots > R_1 > 0\}$. Strictly speaking, this precludes the use of steepest-descent like algorithms to maximise $\eta_{\text{op}}(\mathbf{R}_{n_c})$. To avoid this problem, one can for example consider writing $\mathcal{R}_{n_c} = \bigcup_l \mathcal{R}_{n_c,l}$, where $\mathcal{R}_{n_c,k}^\circ \cap \mathcal{R}_{n_c,l}^\circ = \emptyset$ for all $k \neq l$ and $\eta_{\text{op}}(\mathbf{R}_{n_c})$ is differentiable on $\mathcal{R}_{n_c,l}^\circ$ for all l. Constrained optimisation algorithms can then be used to maximise $\eta_{\text{op}}(\mathbf{R}_{n_c})$ on $\mathcal{R}_{n_c,l}$ for all l. It can however be verified that when $n_c = 4$, at least 286 different such sets are required, and that this number rapidly increases with n_c. Furthermore, numerical simulations show that $\eta_{\text{op}}(\mathbf{R}_{n_c})$ can have more than one local maximum on some of these sets. This approach was thus considered impractical and not followed here.

Another possibility is to use optimisation algorithms which do not require that the function to be optimised be differentiable, like for example the Nelder-Mead simplex algorithm [NM65]. Nevertheless, numerical simulations show that in practice good results can be obtained by simply ignoring this problem and using steepest-descent like algorithms as described above, which is the approach that was followed here.

We would also like to point the reader's attention to the fact that although the ASE computation as presented in Sec. 5.1 can be extended with-

[5] Genetic algorithms provide an interesting alternative which has not been explored by the authors in this context [Gol89].

out too much difficulty to $n_c > 4$, the problem of finding $\mathbf{R}_{n_c}^*$ and $\eta_{\text{op}}(\mathbf{R}_{n_c}^*)$ becomes increasingly complex and quickly becomes intractable. However, the results from Sec. 7 show that for when $n_c = 4$ and $P < 20$ dB, the maximum attainable ASE is within less than 2 dB of the ergodic capacity for $n = 2$, and within less than 0.5 dB of the ergodic capacity when $n = 8$. The gain that can be achieved by increasing the value of n_c is thus small.

6 Maximum ASE of Discrete Rate Dual-Branch MIMO Systems With a Short-Term Power Constraint and Power Allocation Done by Water-Filling

In this section, we discuss how to find the maximum ASE of dual-branch MIMO systems operating in a Rayleigh-fading environment such as the one described in Sec. 2 when power allocation is done in accordance with the water-filling solution but only a finite number n_c of capacity achieving codes of rates $R_{n_c} > \cdots > R_1 > 0$ are available for use. We again choose to restrict our attention to the case of dual-branch MIMO systems where the transmitter is subject to a short-term power constraint.

It is important to observe that although distributing the available power in accordance with the water-filling solution is optimal when an *infinite* number of capacity-achieving codes is available for use (see Sec. 4), choosing to distribute the available power in this manner when only a *finite* set of capacity achieving codes is available in general is strictly suboptimal, as will be illustrated by the numerical results presented in Sec. 7. The motivation for the study of the water-filling solution in this setting is thus first to clearly demonstrate its suboptimality, and second to quantify the rate loss which is incurred by choosing to utilise it. An advantage of the water-filling solution is however that – as we will show below – it is significantly easier to compute the optimal rate vector (denoted $\mathbf{R}_{n_c}^{**}$ to distinguish it from the vector $\mathbf{R}_{n_c}^* = \arg\max_{\mathbf{R}_{n_c}} \eta_{\text{op}}(\mathbf{R}_{n_c})$ which was introduced in Sec. 5) when choosing to distribute the power between the different subchannels in the manner it advocates.

When power allocation is done in accordance with the water-filling solution in a dual-branch MIMO system operating in a Rayleigh-fading environment such as the one described in Sec. 2, it was shown in Sec. 3 that the resulting subchannel SNR distributions are given by (B.21)–(B.22) in the case of a short-term power constraint. Now, let us assume that n_c capacity-achieving codes of rates $R_{n_c} > \cdots > R_1 > 0$ are available for use. Defining

the rate vector $\mathbf{R}_{n_c} \triangleq (R_{n_c}, \ldots, R_1, R_0 = 0)$ (we again set $R_0 = 0$ for convenience although R_0 still *is not* an optimisation variable), and $\gamma_i^* \triangleq 2^{R_i} - 1$ for $i \in \{0, \ldots, n_c\}$ as in Sec. 5.1, the system's ASE becomes

$$\eta_{\text{wf}}(\mathbf{R}_c) = \sum_{k=1}^{2} \sum_{i=1}^{n_c} \log_2(1+\gamma_i^*) \int_{\gamma_i^*}^{\gamma_{i+1}^*} f_{\gamma_k}^{s,2,n}(\gamma_k)\, \mathrm{d}\gamma_k, \tag{B.50}$$

where we have defined $\gamma_{n_c+1}^* \triangleq \infty$, and the subscript *wf* is used to indicate that the available power has been distributed among the subchannels in accordance with the water-filling solution. The code of rate R_i is used on subchannel k whenever the subchannel SNR γ_k is such that

$$\gamma_{i+1}^* > \gamma_k > \gamma_i^* \tag{B.51}$$

as in any adaptive coded modulation system [GV97; HHØ00].

The methodology we use to find the rates $R_{n_c}^{**}, \ldots, R_1^{**}$ for which the ASE $\eta_{\text{wf}}(\mathbf{R}_c)$ is maximum is based on a slight generalisation of [HØA+03] and is presented hereafter. Let $f_{\gamma_{1,2}}^{s,2,n}(\gamma) \triangleq f_{\gamma_1}^{s,2,n}(\gamma) + f_{\gamma_2}^{s,2,n}(\gamma)$ for $\gamma \in [0, \infty)$, and let

$$F_{\gamma_{1,2}}^{s,2,n}(z) \triangleq \int_0^z f_{\gamma_{1,2}}^{s,2,n}(\gamma)\, \mathrm{d}\gamma. \tag{B.52}$$

In order to find the optimal rate vector $\mathbf{R}_{n_c}^{**} \triangleq (R_{n_c}^{**}, \ldots, R_1^{**}, 0)$, we first calculate the gradient of $\eta_{\text{wf}}(\mathbf{R}_c)$ with respect to $\{\gamma_i^*\}_{i=1}^{n_c}$. This gradient is then set to zero, and the resulting set of equations solved with respect to $\{\gamma_i^*\}_{i=1}^{n_c}$. This yields

$$F_{\gamma_{1,2}}^{s,2,n}(\gamma_{i+1}^*) - F_{\gamma_{1,2}}^{s,2,n}(\gamma_i^*) - (1+\gamma_i^*) \log\left(\frac{1+\gamma_i^*}{1+\gamma_{i-1}^*}\right) f_{\gamma_{1,2}}^{s,2,n}(\gamma_i^*) = 0 \tag{B.53}$$

$\forall i \in \{1, \ldots, n_c\}$, where $\log(\cdot)$ denotes the natural logarithm. Noting that γ_{i+1}^* appears only in one place in this equation, it is trivial to rearrange the $n_c - 1$ first equations into a recursive set of equations where γ_{i+1}^* is written as a function of γ_i^* and γ_{i-1}^*

$$\gamma_{i+1}^* = \left(F_{\gamma_{1,2}}^{s,2,n}\right)^{-1} \left[F_{\gamma_{1,2}}^{s,2,n}(\gamma_i^*) + (1+\gamma_i^*) \log\left(\frac{1+\gamma_i^*}{1+\gamma_{i-1}^*}\right) f_{\gamma_{1,2}}^{s,2,n}(\gamma_i^*)\right] \tag{B.54}$$

$\forall i \in \{1, \ldots, n_c - 1\}$, where $\left(F_{\gamma_{1,2}}^{s,2,n}\right)^{-1}(\cdot)$ is the inverse of the injective function $F_{\gamma_{1,2}}^{s,2,n}(\cdot)$. For any given γ_1^*, (B.54) can be used to find the corresponding optimal $\{\gamma_i^*\}_2^{n_c}$. The ASE $\eta_{\text{wf}}(\mathbf{R}_c)$ can then be maximised with respect to

γ_1^* only. Once this maximisation has been completed, the corresponding optimal rates $\{R_i^{**}\}_{i=1}^{n_c}$ and maximum ASE $\eta_{\text{wf}}(\mathbf{R}_c^{**})$ immediately follow.

To conclude this section, we would like to draw the reader's attention to the fact that these ideas can be used to compute the optimal rate vector and maximum ASE under water-filling power allocation for dual-branch MIMO systems operating in other fading environments as well, as long as expressions for the corresponding subchannel SNR distributions can be obtained as described in Sec. 3.

7 Numerical Results

We use the notation $\widehat{\mathbf{R}}_{n_c}^*$ for the approximation for $\mathbf{R}_{n_c}^*$ obtained via numerical simulations as described in Sec. 5 when $n_c \in \{3,4\}$. We also find it convenient to introduce

$$\widetilde{\mathbf{R}}_{n_c}^* = \begin{cases} \mathbf{R}_{n_c}^* & \text{if} \quad n_c \in \{1,2\} \\ \widehat{\mathbf{R}}_{n_c}^* & \text{if} \quad n_c \in \{3,4\}. \end{cases} \tag{B.55}$$

We calculated the ergodic capacity C (given in Eq. (B.35)), and maximum ASEs $\eta_{\text{op}}(\widetilde{\mathbf{R}}_{n_c}^*)$ and $\eta_{\text{wf}}(\mathbf{R}_{n_c}^{**})$ (together with the corresponding vectors $\widetilde{\mathbf{R}}_{n_c}^*$ and $\mathbf{R}_{n_c}^{**}$) using the methods described in Sec. 5 and Sec. 6. Numerical integration algorithms were used whenever required (e.g. to evaluate integrals of the form (B.44) and the integrals appearing in (B.35)), and routines from the CFSQP source code [LZT97] were used to find the local maxima of $\eta_{\text{op}}(\mathbf{R}_{n_c})$. This was done for $n_c \in \{1,2,3,4\}$, $m = 2$, $n \in \{2,4,8\}$, and a power budget $P \in [-10\,\text{dB}, 20\,\text{dB}]$. When computing $\eta_{\text{op}}(\widehat{\mathbf{R}}_{n_c}^*)$ for $n_c \in \{3,4\}$, we set $\Delta = M_{n_c}/22$ to keep computational complexity at an acceptable level. (For each value of P and n, this corresponds to 9109 evaluations of $\eta_{\text{op}}(\mathbf{R}_4)$ and to 1794 evaluations of $\eta_{\text{op}}(\mathbf{R}_3)$.) We also set $N_p = 500$ when $n_c = 4$, and $N_p = 100$ when $n_c = 3$.

The effect of the presence of several local maxima in $\eta_{\text{op}}(\mathbf{R}_{n_c})$ is illustrated in Fig. B.8. Fig. B.8(a) shows the ASE $\eta_{\text{op}}(\mathbf{R}_1)$ as a function of R_1 for $n = 8$ and $P = -6\,\text{dB}$, and for $n = 8$ and $P = -3\,\text{dB}$. There are two distinct local maxima, and it can be seen that when $P = -6\,\text{dB}$ the global maximum is situated at the local maximum with the largest value of R_1, whereas it is situated at the local maximum with the smallest value of R_1 when $P = -3\,\text{dB}$. This creates a discontinuity in the value of R_1^* maximising $\eta_{\text{op}}(\mathbf{R}_1)$ as P increases from $-6\,\text{dB}$ to $-3\,\text{dB}$, although $\eta_{\text{op}}(\mathbf{R}_1^*)$ itself remains continuous. Such discontinuities are illustrated in Fig. B.8(b) for $n = 2$ and $n_c = 4$ (solid curves). A similar phenomenon is observed when

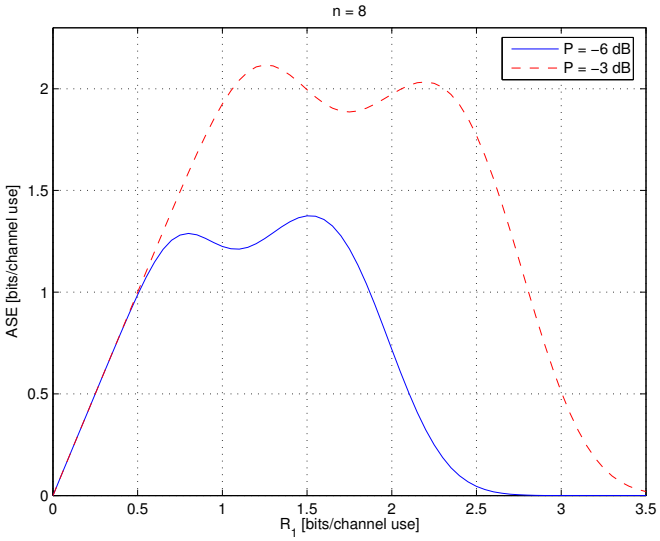

(a)

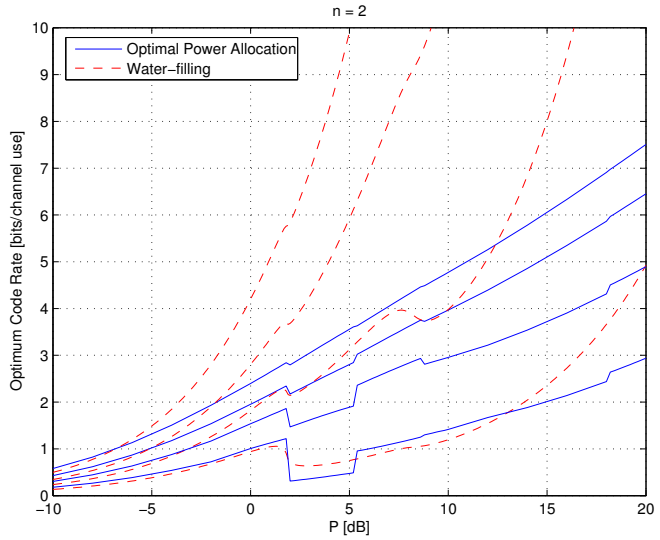

(b)

FIGURE B.8: Fig. B.8(a) shows the ASE $\eta_{\mathrm{op}}(\mathbf{R}_1)$ as a function of R_1 for $n = 8$ and $P = -6\,\mathrm{dB}$ (solid curve) and for $n = 8$ and $P = -3\,\mathrm{dB}$ (dashed curve). In Fig B.8(b), the code rates $\{\widehat{R}_i^*\}_{i=1}^4$ which (approximately) maximise $\eta_{\mathrm{op}}(\mathbf{R}_4)$ (solid curves), and the code rates $\{R_i^{**}\}_{i=1}^4$ which maximise $\eta_{\mathrm{wf}}(\mathbf{R}_4)$ (dashed curves) are plotted as a function of the power budget P for $n = 2$.

computing the code rates $\{R_i^{**}\}_{i=1}^{n_c}$ which maximise $\eta_{\text{wf}}(\mathbf{R}_{n_c})$, although it does not take place in the case illustrated in Fig. B.8(b) (dashed curves).

The system's ergodic capacity and maximum ASEs $\eta_{\text{op}}(\widetilde{\mathbf{R}}_{n_c}^{*})$ and $\eta_{\text{wf}}(\mathbf{R}_{n_c}^{**})$ for $n_c = 1$, $n_c = 2$, $n_c = 3$, and $n_c = 4$ are respectively shown in Figs. B.9(a), B.9(b), and B.9(c) for $n = 2$, $n = 4$, and $n = 8$. As expected, both $\eta_{\text{op}}(\mathbf{R}_{n_c}^{*})$ and $\eta_{\text{wf}}(\mathbf{R}_{n_c}^{**})$ approach the system's ergodic capacity C as n_c increases. The figures also show that the gap between $\eta_{\text{op}}(\widetilde{\mathbf{R}}_{n_c}^{*})$ and $\eta_{\text{wf}}(\mathbf{R}_{n_c}^{**})$ widens as the power budget P increases, and narrows as n_c increases as could be expected. It is also apparent that the larger the value of n, the lower the value of the power budget P at which the gap between $\eta_{\text{op}}(\mathbf{R}_{n_c}^{*})$ and $\eta_{\text{wf}}(\mathbf{R}_{n_c}^{**})$ starts to become noticeable. It is our belief that results such as those presented in Fig. B.9 can be a very valuable tool when seeking to maximise the ASE during the design of MIMO communication systems.

8 Conclusions

We established expressions for the subchannel SNR distributions which arise from (i) the decomposition of dual-branch MIMO systems into independent subchannels and (ii) applying the *water-filling* principle for distributing the available power between these subchannels. This was done both in the case of short- and long-term transmitter power constraints. We thereafter considered the problem of maximising the ASE of dual-branch MIMO communication systems with perfect transmitter and receiver CSI when using a fixed number of codes, assuming there is a short-term power constraint that the transmitter must respect during the transmission of every symbol frame, and assuming the availability of capacity-achieving codes for AWGN channels. This maximum ASE was then compared to the system's ergodic capacity, and to the maximum ASE that can be attained if the available power is distributed among the different subchannels in accordance with the water-filling solution although only discrete rate adaptation is possible. The newly established expressions for the subchannel SNR distributions were seen to be necessary to perform this analysis. The results revealed that it is possible to closely approach the ergodic capacity of such MIMO systems with only a small number of capacity-achieving codes, and additionally demonstrated the significant suboptimality of water-filling when the number of available rates is small.

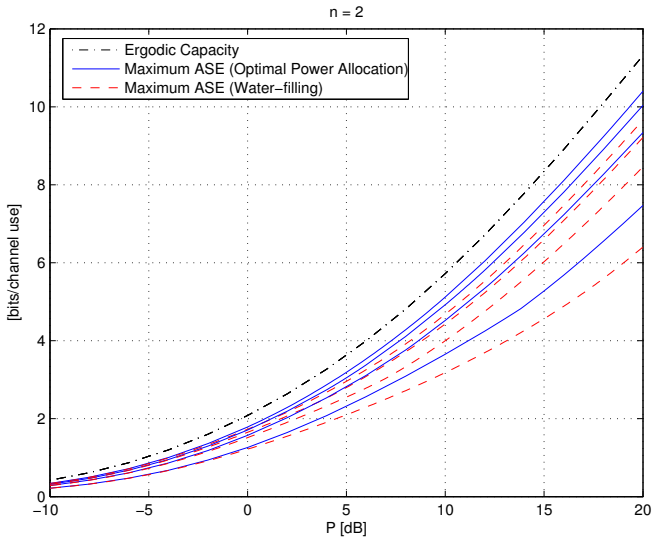
n = 2
Ergodic Capacity
Maximum ASE (Optimal Power Allocation)
Maximum ASE (Water−filling)
[bits/channel use]
P [dB]
0
2
4
6
8
10
12
−10
−5
0
5
10
15
20

(a)

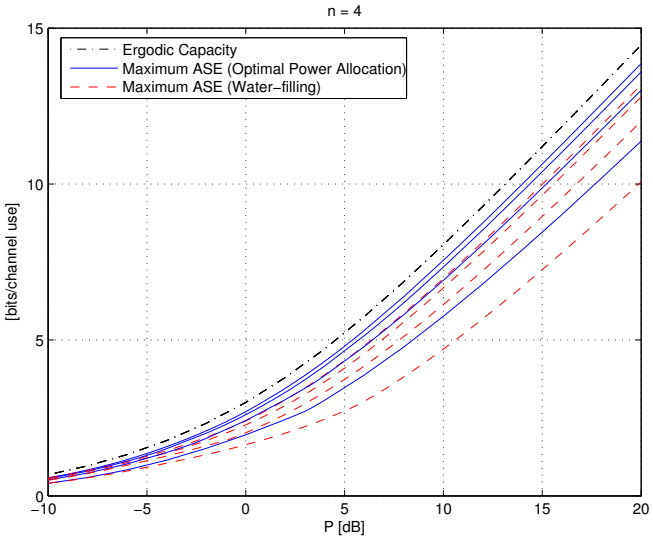
n = 4
Ergodic Capacity
Maximum ASE (Optimal Power Allocation)
Maximum ASE (Water−filling)
[bits/channel use]
P [dB]
0
5
10
15
−10
−5
0
5
10
15
20

(b)

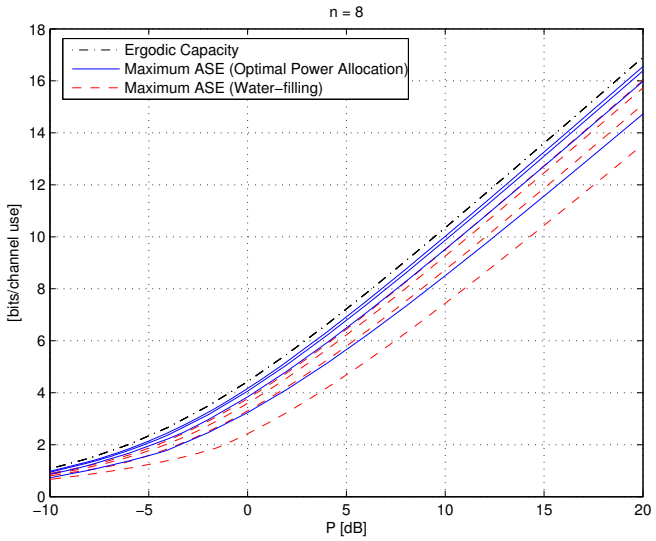

(c)

FIGURE B.9: The figures show – for $n = 2$ (a), $n = 4$ (b), and $n = 8$ (c) – the system's ergodic capacity and the maximum ASEs $\eta_{\text{op}}(\widetilde{\mathbf{R}}^{*}_{n_c})$ and $\eta_{\text{wf}}(\mathbf{R}^{**}_{n_c})$ for $n_c \in \{1, 2, 3, 4\}$ as a function of the power budget P.

Appendix A Proofs of Theorems B.1 and B.2

A.1 Proof of Theorem B.1

Proof: In this proof, for notational simplicity we omit the superscripts introduced in equations (B.11) and (B.12). It is thus implicitly understood that $m = 2$ and that we are in the presence of a short-term power constraint.

The joint distribution of the ordered eigenvalues λ_1, λ_2 of the matrix $\mathbf{W}$ is obtained by setting $m = 2$ in (B.13), which yields

$$f_{\lambda_1,\lambda_2}(\lambda_1, \lambda_2) = \frac{e^{-\lambda_1-\lambda_2}}{(n-1)!(n-2)!}(\lambda_1 - \lambda_2)^2(\lambda_1\lambda_2)^{n-2}, \tag{B.56}$$

where $\lambda_1 \geq \lambda_2 \geq 0$ and we have used the fact that $K_{2,n} = (n-1)!(n-2)!$ as mentioned in footnote 3. We begin by proving the result for $f_{\gamma_1}(\gamma_1)$. Remembering that the first channel always benefits from the best SNR conditions, and that the transmitter is constrained to use a non-zero power budget P at all times, it is straightforward to conclude that the SNR ratio on this first channel will always be strictly positive. This allows us to write

$$\gamma_1 = (\mu\lambda_1 - 1)_+ = \mu\lambda_1 - 1, \tag{B.57}$$

where the first equality is obtained by combining equations (B.6) and (B.7). Note that, for given λ_1 and λ_2, the solution μ of equation (B.20) is given by

$$\mu = \begin{cases} \dfrac{1}{2}\left(P + \dfrac{1}{\lambda_1} + \dfrac{1}{\lambda_2}\right) & \text{if} \quad \lambda_2 \geq \lambda_{1P} \\ P + \dfrac{1}{\lambda_1} & \text{if} \quad \lambda_2 < \lambda_{1P}, \end{cases} \tag{B.58}$$

where we have introduced the notation $\lambda_{1P} \triangleq \frac{\lambda_1}{P\lambda_1+1}$ for clarity. This yields

$$\gamma_1 = \begin{cases} \dfrac{1}{2}\left(P\lambda_1 - 1 + \dfrac{\lambda_1}{\lambda_2}\right) & \text{if} \quad \lambda_2 \geq \lambda_{1P} \\ P\lambda_1 & \text{if} \quad \lambda_2 < \lambda_{1P}. \end{cases} \tag{B.59}$$

We therefore write

$$f_{\gamma_1}(\gamma_1) = \underbrace{f_{\gamma_1}\left(\frac{1}{2}\left(P\lambda_1 - 1 + \frac{\lambda_1}{\lambda_2}\right)\middle|\lambda_2 \geq \lambda_{1P}\right)}_{A}\underbrace{\Pr(\lambda_2 \geq \lambda_{1P})}_{B} \quad + \\ \underbrace{f_{\gamma_1}(P\lambda_1|\lambda_2 < \lambda_{1P})}_{C} \cdot \underbrace{\Pr(\lambda_2 < \lambda_{1P})}_{D}, \tag{B.60}$$

where $\Pr(\cdot)$ denotes the probability that the event in the argument take place. We now successively evaluate each one of the four quantities A, B, C, and D appearing above.

To evaluate A, let us define the cumulative distribution function

$$\widetilde{F}_{\gamma_1}(z) = \int_0^z f_{\gamma_1}\left(\gamma_1 \mid \lambda_2 \geq \lambda_{1P}\right) \, \mathrm{d}\gamma_1. \tag{B.61}$$

This quantity can also be written as

$$\widetilde{F}_{\gamma_1}(z) = \int_0^{\frac{z}{P}} \int_{\lambda_{1P}}^{\lambda_1} f_{\lambda_1,\lambda_2}\left(\lambda_1, \lambda_2 | \lambda_2 \geq \lambda_{1P}\right) \mathrm{d}\lambda_2 \mathrm{d}\lambda_1 \quad + \int_{\frac{z}{P}}^{\frac{2z}{P}} \int_{\frac{\lambda_1}{2z - P\lambda_1 + 1}}^{\lambda_1} f_{\lambda_1,\lambda_2}\left(\lambda_1, \lambda_2 | \lambda_2 \geq \lambda_{1P}\right) \mathrm{d}\lambda_2 \mathrm{d}\lambda_1, \tag{B.62}$$

where $f_{\lambda_1,\lambda_2}(\lambda_1, \lambda_2)$ is given in (B.56). Indeed, remembering that when $\lambda_2 \geq \lambda_{1P}$ then $\gamma_1 = \frac{1}{2}\left(P\lambda_1 - 1 + \frac{\lambda_1}{\lambda_2}\right)$, and that (B.56) corresponds to the distribution of the ordered eigenvalues of the matrix $\mathbf{W}$ (i.e. $\lambda_1 \geq \lambda_2 \geq 0$), one can see that equation (B.62), which results from the integration of $f_{\lambda_1,\lambda_2}(\lambda_1, \lambda_2 \mid \lambda_2 \geq \lambda_{1P})$ over the region $Y = Y_1 \cap Y_2 \cap Y_3 \subset \mathbb{R}^2$, with

$$Y_1 = \{\lambda_1, \lambda_2 \mid \lambda_1 \geq \lambda_2\}, \tag{B.63}$$

$$Y_2 = \{\lambda_1, \lambda_2 \mid \lambda_2 \geq \lambda_{1P}\}, \tag{B.64}$$

$$Y_3 = \left\{\lambda_1, \lambda_2 \;\middle|\; \frac{1}{2}\left(P\lambda_1 - 1 + \frac{\lambda_1}{\lambda_2}\right) \leq z\right\}, \tag{B.65}$$

corresponds exactly to the definition of $\widetilde{F}_{\gamma_1}(z)$ given in (B.61). The region Y is depicted in Fig. B.10.

Now, since $\forall(\lambda_1, \lambda_2) \in Y_2$, we have

$$f_{\lambda_1,\lambda_2}\left(\lambda_1, \lambda_2 \mid \lambda_2 \geq \lambda_{1P}\right) = \frac{f_{\lambda_1,\lambda_2}(\lambda_1, \lambda_2)}{B}, \tag{B.66}$$

with B as defined in (B.60), we can write

$$\widetilde{F}_{\gamma_1}(z) = \frac{1}{B}\int_0^{\frac{z}{P}} \int_{\lambda_{1P}}^{\lambda_1} f_{\lambda_1,\lambda_2}(\lambda_1, \lambda_2) \, \mathrm{d}\lambda_2 \, \mathrm{d}\lambda_1 \quad + \frac{1}{B}\int_{\frac{z}{P}}^{\frac{2z}{P}} \int_{\frac{\lambda_1}{2z - P\lambda_1 + 1}}^{\lambda_1} f_{\lambda_1,\lambda_2}(\lambda_1, \lambda_2) \, \mathrm{d}\lambda_2 \, \mathrm{d}\lambda_1. \tag{B.67}$$

A can now be obtained without difficulty by evaluating

$$A = f_{\gamma_1}\left(\gamma_1 | \lambda_2 \geq \lambda_{1P}\right) = \left.\frac{\mathrm{d}\widetilde{F}_{\gamma_1}(z)}{\mathrm{d}z}\right|_{z=\gamma_1}. \tag{B.68}$$

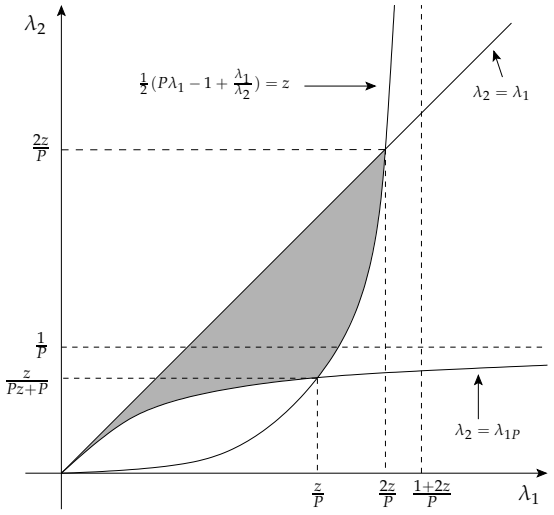

FIGURE B.10: Graphical representation of $Y = Y_1 \cap Y_2 \cap Y_3$. Y corresponds to the shaded area.

In order to do this, let us define $f_{\lambda_2}(\lambda_1, \lambda_2)$ such that

$$\frac{\partial f_{\lambda_2}(\lambda_1, \lambda_2)}{\partial \lambda_2} = f_{\lambda_1, \lambda_2}(\lambda_1, \lambda_2), \tag{B.69}$$

as well as $g_0(\lambda_1)$, $g_1(\lambda_1)$, $g_2(\lambda_1, z)$ and $G_0(\lambda_1)$, $G_1(\lambda_1)$, $G_2(\lambda_1, z)$ such that

$$\frac{\mathrm{d}G_0(\lambda_1)}{\mathrm{d}\lambda_1} = g_0(\lambda_1) \triangleq f_{\lambda_2}(\lambda_1, \lambda_1), \tag{B.70}$$

$$\frac{\mathrm{d}G_1(\lambda_1)}{\mathrm{d}\lambda_1} = g_1(\lambda_1) \triangleq f_{\lambda_2}\left(\lambda_1, \lambda_{1P}\right), \tag{B.71}$$

$$\frac{\partial G_2(\lambda_1, z)}{\partial \lambda_1} = g_2(\lambda_1, z) \triangleq f_{\lambda_2}\left(\lambda_1, \frac{\lambda_1}{2z - P\lambda_1 + 1}\right). \tag{B.72}$$

Then,

$$\begin{aligned}
&\frac{\mathrm{d}}{\mathrm{d}z} \int_0^{\frac{z}{P}} \int_{\lambda_{1P}}^{\lambda_1} f_{\lambda_1, \lambda_2}(\lambda_1, \lambda_2)\, \mathrm{d}\lambda_2\, \mathrm{d}\lambda_1 \Big|_{z=\gamma_1} \\
&\quad = \frac{\mathrm{d}}{\mathrm{d}z} \int_0^{\frac{z}{P}} g_0(\lambda_1) - g_1(\lambda_1)\, \mathrm{d}\lambda_1 \Big|_{z=\gamma_1} \\
&\quad = \frac{\mathrm{d}}{\mathrm{d}z} \left[G_0\left(\frac{z}{P}\right) - G_0(0) - G_1\left(\frac{z}{P}\right) + G_1(0) \right] \Big|_{z=\gamma_1} \\
&\quad = \frac{1}{P} f_{\lambda_2}\left(\frac{\gamma_1}{P}, \frac{\gamma_1}{P}\right) - \frac{1}{P} f_{\lambda_2}\left(\frac{\gamma_1}{P}, \frac{\gamma_1}{P\gamma_1 + P}\right).
\end{aligned} \tag{B.73}$$

We also have

$$\begin{aligned}
&\frac{\mathrm{d}}{\mathrm{d}z}\int_{\frac{z}{P}}^{\frac{2z}{P}}\int_{\frac{\lambda_1}{2z-P\lambda_1+1}}^{\lambda_1} f_{\lambda_1,\lambda_2}(\lambda_1,\lambda_2)\,\mathrm{d}\lambda_2\,\mathrm{d}\lambda_1\Big|_{z=\gamma_1}\\
&\quad=\frac{\mathrm{d}}{\mathrm{d}z}\int_{\frac{z}{P}}^{\frac{2z}{P}} g_0(\lambda_1)-g_2(\lambda_1,z)\,\mathrm{d}\lambda_1\Big|_{z=\gamma_1}\\
&\quad=\frac{\mathrm{d}}{\mathrm{d}z}\left[G_0\left(\frac{2z}{P}\right)-G_0\left(\frac{z}{P}\right)\right]\Big|_{z=\gamma_1}-\frac{\mathrm{d}}{\mathrm{d}z}\left[G_2\left(\frac{2z}{P},z\right)-G_2\left(\frac{z}{P},z\right)\right]\Big|_{z=\gamma_1}\\
&\quad=\frac{2}{P}\,f_{\lambda_2}\left(\frac{2\gamma_1}{P},\frac{2\gamma_1}{P}\right)-\frac{1}{P}\,f_{\lambda_2}\left(\frac{\gamma_1}{P},\frac{\gamma_1}{P}\right)\\
&\qquad-\frac{\mathrm{d}}{\mathrm{d}z}\,G_2\left(\frac{2z}{P},z\right)\Big|_{z=\gamma_1}-\frac{\mathrm{d}}{\mathrm{d}z}\,G_2\left(\frac{z}{P},z\right)\Big|_{z=\gamma_1}. \qquad \text{(B.74)}
\end{aligned}$$

The evaluation of $\frac{\mathrm{d}}{\mathrm{d}z}\,G_2(\frac{2z}{P},z)\big|_{z=\gamma_1}$ yields

$$\begin{aligned}
\frac{\mathrm{d}G_2\left(\frac{2z}{P},z\right)}{\mathrm{d}z}\Big|_{z=\gamma_1}&=\frac{2}{P}\,g_2\Big(\frac{2\gamma_1}{P},\gamma_1\Big)+\left[\frac{\partial G_2\left(\frac{2z}{P},t\right)}{\partial t}\Big|_{t=z}\right]\Big|_{z=\gamma_1}\\
&=\frac{2}{P}\,g_2\Big(\frac{2\gamma_1}{P},\gamma_1\Big)+\int_{\eta}^{\frac{2z}{P}}\frac{\partial g_2(\lambda_1,z)}{\partial z}\,\mathrm{d}\lambda_1\Big|_{z=\gamma_1}, \qquad \text{(B.75)}
\end{aligned}$$

where η is an arbitrary real constant and we have used the fact that

$$\frac{\partial^2 G_2(\lambda_1,z)}{\partial\lambda_1\partial z}=\frac{\partial^2 G_2(\lambda_1,z)}{\partial z\partial\lambda_1} \qquad \text{(B.76)}$$

to obtain the last equality. $\frac{\mathrm{d}}{\mathrm{d}z}\,G_2(\frac{z}{P},z)\big|_{z=\gamma_1}$ can be obtained by similar means. By combining equations (B.67), (B.73), (B.74), and (B.75) with the expression obtained for $\frac{\mathrm{d}}{\mathrm{d}z}\,G_2(\frac{z}{P},z)\big|_{z=\gamma_1}$ and rearranging the terms, we obtain

$$\frac{\mathrm{d}\widetilde{F}_{\gamma_1}(z)}{\mathrm{d}z}\Big|_{z=\gamma_1}=-\frac{1}{B}\int_{\frac{z}{P}}^{\frac{2z}{P}}\frac{\partial}{\partial z}\,g_2(\lambda_1,z)\,\mathrm{d}\lambda_1\Big|_{z=\gamma_1}. \qquad \text{(B.77)}$$

This finally yields

$$\frac{\mathrm{d}\widetilde{F}_{\gamma_1}(z)}{\mathrm{d}z}\Big|_{z=\gamma_1}=\frac{2}{B}\int_{\frac{\gamma_1}{P}}^{\frac{2\gamma_1}{P}}\frac{\lambda_1 f_{\lambda_1,\lambda_2}\left(\lambda_1,\frac{\lambda_1}{2\gamma_1-P\lambda_1+1}\right)}{(2\gamma_1-P\lambda_1+1)^2}\,\mathrm{d}\lambda_1=A \qquad \text{(B.78)}$$

by using (B.69) and (B.72).

Let us now proceed with the evaluation of B, C, and D. The value of B need in fact not be computed since B will cancel out with the factor $\frac{1}{B}$ appearing in (B.78).

To calculate C, we start by remarking that that if $\lambda_2 < \lambda_{1P}$, then

$$f_{\lambda_1,\lambda_2}(\lambda_1, \lambda_2 \mid \lambda_2 < \lambda_{1P}) = \frac{f_{\lambda_1,\lambda_2}(\lambda_1, \lambda_2)}{D}, \tag{B.79}$$

with D defined in (B.60). Therefore,

$$f_{\lambda_1}(\lambda_1 | \lambda_2 < \lambda_{1P}) = \frac{1}{D} \int_0^{\lambda_{1P}} f_{\lambda_1,\lambda_2}(\lambda_1, \lambda_2)\, \mathrm{d}\lambda_2, \tag{B.80}$$

and hence, since if $\lambda_2 < \lambda_{1P}$ then $\gamma_1 = P\lambda_1$, we finally obtain

$$f_{\gamma_1}(\gamma_1 | \lambda_2 < \lambda_{1P}) = \frac{1}{D \cdot P} \int_0^{\lambda_{1P}} f_{\lambda_1,\lambda_2}\Big(\frac{\gamma_1}{P}, \lambda_2\Big)\, \mathrm{d}\lambda_2. \tag{B.81}$$

Finally, the value of D need not be computed either since D will cancel out with the factor $\frac{1}{D}$ appearing in (B.81).

$f_{\gamma_1}(\gamma_1)$ is obtained by combining equations (B.60), (B.78) and (B.81), and introducing the expression for $f_{\lambda_1,\lambda_2}(\lambda_1, \lambda_2)$ given in (B.56).

We proceed in a similar way to prove the result for $f_{\gamma_2}(\gamma_2)$. □

A.2 Proof of Theorem B.2

Proof: The values of the superscripts introduced in equations (B.11) and (B.12) being clear from the context, they are once again omitted in this proof for the sake of notational simplicity. First of all, let us show that $f_{\lambda_1}(\lambda_1)$ and $f_{\lambda_2}(\lambda_2)$, which respectively denote the probability density functions of the largest and smallest eigenvalue of $\mathbf{W}$, indeed correspond to the expressions given in the theorem statement. We have

$$f_{\lambda_1}(\lambda_1) = \int_0^{\lambda_1} f_{\lambda_1,\lambda_2}(\lambda_1, \lambda_2)\, \mathrm{d}\lambda_2 \tag{B.82}$$

and

$$f_{\lambda_2}(\lambda_2) = \int_{\lambda_2}^{\infty} f_{\lambda_1,\lambda_2}(\lambda_1, \lambda_2)\, \mathrm{d}\lambda_1, \tag{B.83}$$

where $f_{\lambda_1,\lambda_2}(\lambda_1, \lambda_2)$ (given in (B.56)) denotes the joint distribution of the ordered eigenvalues λ_1, λ_2 of matrix $\mathbf{W}$.

The above expressions can be evaluated by making use of the indefinite integral [GR00]

$$\int x^n e^{-x}\, \mathrm{d}x = -n! e^{-x} \sum_{q=0}^{n} \frac{x^q}{q!} \tag{B.84}$$

valid for integer n, after having expanded $(\lambda_1 - \lambda_2)^2$ in (B.82) and (B.83). Equations (B.26) and (B.27) are obtained after performing some manipulations and rearranging the terms.

We now proceed to prove (B.25). By combining equations (B.6) and (B.7), it can easily be seen that the SNR γ_k on the kth subchannel ($k \in \{1, 2\}$) is given by

$$\gamma_k = (\mu\lambda_k - 1)_+. \tag{B.85}$$

Bearing this in mind, $f_{\gamma_k}(\gamma_k)$ can be expressed as

$$\begin{aligned} f_{\gamma_k}(\gamma_k) = {} & f_{\gamma_k}(\mu\lambda_k - 1 \mid \mu\lambda_k - 1 \geq 0) \cdot \Pr\,(\mu\lambda_k - 1 \geq 0) \\ & + f_{\gamma_k}(0 \mid \mu\lambda_k - 1 < 0) \cdot \Pr\,(\mu\lambda_k - 1 < 0), \end{aligned} \tag{B.86}$$

Now, noting that for $\gamma_k = \mu\lambda_k - 1 \geq 0$,

$$f_{\gamma_k}(\mu\lambda_k - 1 \mid \mu\lambda_k - 1 \geq 0) = \frac{f_{\gamma_k}(\mu\lambda_k - 1)}{\Pr\,(\mu\lambda_k - 1 \geq 0)}, \tag{B.87}$$

and that $f_{\gamma_k}(0 \mid \mu\lambda_k - 1 < 0) = \delta(\gamma_k)$, we can rewrite (B.86) as

$$f_{\gamma_k}(\gamma_k) = \begin{cases} f_{\gamma_k}(\mu\lambda_k - 1) + \delta(\gamma_k) \cdot \Pr\,(\mu\lambda_k - 1 < 0) & \text{if } \gamma_k \geq 0 \\ 0 & \text{otherwise.} \end{cases} \tag{B.88}$$

Finally, since $\Pr\,(\mu\lambda_k - 1 < 0) = \Pr\,(\lambda_k < \frac{1}{\mu})$, and since for $\gamma_k = \mu\lambda_k - 1 \geq 0$, we have

$$f_{\gamma_k}(\mu\lambda_k - 1) = \frac{1}{\mu}\, f_{\lambda_k}(z_k), \tag{B.89}$$

where z_k is defined as in the theorem statement, we can rewrite (B.88) as

$$f_{\gamma_k}(\gamma_k) = \begin{cases} \dfrac{1}{\mu}\, f_{\lambda_k}(z_k) + \delta(\gamma_k) \displaystyle\int_0^{1/\mu} f_{\lambda_k}(x)\, \mathrm{d}x & \text{if } \gamma_k \geq 0 \\ 0 & \text{otherwise.} \end{cases} \tag{B.90}$$

However, γ_k can never take negative values because it represents a signal-to-noise ratio (see also Sec. 3). Therefore, we make a slight abuse in notation by rewriting (B.90) as

$$f_{\gamma_k}(\gamma_k) = \frac{1}{\mu}\, f_{\lambda_k}(z_k) + \delta(\gamma_k) \cdot \int_0^{1/\mu} f_{\lambda_k}(\lambda_k)\, \mathrm{d}\lambda_k, \tag{B.91}$$

where it is implicitly understood that $\gamma_k \geq 0$ as explained in Sec. 3. □

Appendix B Closed Form Expressions

In this appendix we give expressions for the definite integrals appearing in Theorems B.1 and B.2 whenever possible.

B.1 SISO, SIMO, and MISO Systems

Although the integral in (B.18) admits a closed form solution, numerical methods are still required to obtain the value of μ. We therefore choose not to include it here.

The integral appearing in (B.19) can be simply evaluated using (B.84) to obtain

$$\int_0^{1/\mu} \lambda_1^{n-1} e^{-\lambda_1} \, \mathrm{d}\lambda_1 = (n-1)! \left[1 - e^{-1/\mu} \sum_{q=0}^{n-1} \frac{1}{\mu^q q!} \right]. \tag{B.92}$$

B.2 Dual-Branch MIMO Systems

When $k = 2$, the integral appearing in (B.25) can be easily evaluated using (B.84) to obtain

$$\begin{aligned} \int_0^{1/\mu} f_{\lambda_2}^{2,n}(\lambda_2) \, \mathrm{d}\lambda_2 &= \frac{1}{(n-1)!} \int_0^{1/\mu} e^{-2\lambda_2} \lambda_2^{n-2} \sum_{q=0}^{n-2} \frac{(n-q)(n-q-1)}{q!} \lambda_2^q \, \mathrm{d}\lambda_2 \\ &= \frac{1}{(n-1)!} \sum_{q=0}^{n-2} \frac{(n-q)(n-q-1)}{q!} \int_0^{1/\mu} e^{-2\lambda_2} \lambda_2^{n+q-2} \, \mathrm{d}\lambda_2 \\ &= 1 - \frac{e^{-2/\mu}}{(n-1)!} \sum_{q=0}^{n-2} \frac{(n-q)(n-q-1)(n+q-2)!}{q! \, 2^{n+q-1}} \sum_{p=0}^{n+q-2} \frac{2^p}{\mu^p p!}. \end{aligned} \tag{B.93}$$

When $k = 1$, this integral becomes

$$\int_0^{1/\mu} f_{\lambda_1}^{2,n}(\lambda_1) \, \mathrm{d}\lambda_1 = - \int_0^{1/\mu} f_{\lambda_2}^{2,n}(\lambda_1) \, \mathrm{d}\lambda_1 \quad + \tag{B.94}$$

$$\underbrace{K_{2,n}^{-1} \int_0^{1/\mu} e^{-\lambda_1} \lambda_1^{n-2} [\lambda_1^2 (n-2)! - 2\lambda_1 (n-1)! + n!] \, \mathrm{d}\lambda_1}_{\zeta}.$$

The integral $\int_0^{1/\mu} f_{\lambda_2}^{2,n}(\lambda_1) \, \mathrm{d}\lambda_1$ was evaluated in (B.93). Evaluation of the remaining integral yields

$$\zeta = 2 - 2e^{-1/\mu} \left[\frac{2-n}{2(n-1)!\mu^{n-1}} + \frac{1}{2(n-1)!\mu^n} + \sum_{q=0}^{n-2} \frac{1}{q!\mu^q} \right], \tag{B.95}$$

which is obtained by repeated application of (B.84) and rearrangement of the terms.

Evaluation of the first integral in (B.21) yields

$$\begin{aligned}\int_0^b (a-x)^2 \exp(-a-x)(ax)^{n-2}\,\mathrm{d}x \\ = e^{-a}a^{n-2}\left[a^2(n-2)! - 2a(n-1)! + n!\right] \quad - \\ n!e^{-a-b}a^{n-2}\left[\sum_{q=0}^{n}\frac{b^q}{q!} - \frac{2a}{n}\sum_{q=0}^{n-1}\frac{b^q}{q!} + \frac{a^2}{n(n-1)}\sum_{q=0}^{n-2}\frac{b^q}{q!}\right], \end{aligned} \tag{B.96}$$

obtained again by using (B.84), and by setting $a = \frac{\gamma_1}{P}$ and $b = \frac{\gamma_1}{P\gamma_1+P}$ for notational simplicity.

Finally, the double integral corresponding to $h_n(P)$ in (B.23) can be reduced to a single integral by using (B.96) with x replaced by y, a replaced by x, and b replaced by $\frac{x}{Px+1}$.

To the best of the authors' knowledge, neither the second integral appearing in (B.21) nor the second integral in (B.22) admit closed form solutions.

Appendix C Obtaining a Value for M_{n_c}

A value for M_{n_c} can for example be obtained as follows: let us assume that a lower bound η_{lb} for $\eta_{\mathrm{op}}(\mathbf{R}^*_{n_c})$ is known (such a lower bound can for example be obtained by evaluating $\eta_{\mathrm{op}}(\mathbf{R}_{n_c})$ for different values of $\mathbf{R}_{n_c}$), and that the value of $\eta_{\mathrm{op}}(\mathbf{R}^*_{n_c-1})$ is known as well. Let us define $g(R_{n_c}) \triangleq 2R_{n_c}\cdot\Pr(A_{n_c0})$, where $\gamma^*_{n_c} = 2^{R_{n_c}} - 1$ in the definition of A_{n_c0} (see (B.41)), and let M_{n_c} be the largest value such that

$$\eta_{\mathrm{lb}} = \eta_{\mathrm{op}}(\mathbf{R}^*_{n_c-1}) + g(M_{n_c}), \tag{B.97}$$

which can be found by utilising numerical root-finding algorithms. It can be verified that $g(R_{n_c})$ decreases with increasing R_{n_c} for all $R_{n_c} > M_{n_c}$. Therefore, for all $\mathbf{R}_{n_c}$ such that $R_{n_c} > M_{n_c}$, we have

$$\eta_{\mathrm{op}}(\mathbf{R}_{n_c}) \leq \eta_{\mathrm{op}}(\mathbf{R}^*_{n_c-1}) + g(R_{n_c}) < \eta_{\mathrm{lb}}, \tag{B.98}$$

and thus we must have $R_{n_c} \leq M_{n_c}$ if η_{lb} is to be attained.

The first inequality in (B.98) follows from the following fact: noting that $(\lambda_1, \lambda_2) \in A_{n_c0}$ if and only if event E – defined as "transmission at a rate

R_{n_c} is done on at least one of the $m = 2$ subchannels" – takes place, we have

$$\begin{aligned}\eta_{\text{op}}(\mathbf{R}_{n_c}) &= \eta_{\text{op}}(\mathbf{R}_{n_c}|\neg E)\Pr(\neg E) + \eta_{\text{op}}(\mathbf{R}_{n_c}|E)\Pr(E) \\ &\leq \eta_{\text{op}}(\mathbf{R}_{n_c}|\neg E) + \eta_{\text{op}}(\mathbf{R}_{n_c}|E)\Pr(E) \\ &= \eta_{\text{op}}(\mathbf{R}_{n_c}|\neg E) + \eta_{\text{op}}(\mathbf{R}_{n_c}|E)\Pr(A_{n_c 0}) \\ &\leq \eta_{\text{op}}(\mathbf{R}^*_{n_c-1}) + 2R_{n_c} \cdot \Pr(A_{n_c 0}),\end{aligned} \tag{B.99}$$

where $\eta_{\text{op}}(\mathbf{R}_{n_c}|E)$ ($\eta_{\text{op}}(\mathbf{R}_{n_c}|\neg E)$) denotes the ASE when the rate vector is $\mathbf{R}_{n_c}$ and event E takes (does not take) place, and $\Pr(E)$ ($\Pr(\neg E)$) denotes the probability that event E (not) take place.

References

[BGT93] C. Berrou, A. Glavieux, and P. Thitimajshima. Near Shannon limit error-correcting coding and decoding: Turbo-codes. In *Proc. 1993 IEEE International Conference on Communications (ICC)*, pages 1064–1070, Geneva, May 1993.

[BOØ05] F. Bøhagen, P. Orten, and G. E. Øien. On the Shannon capacity of dual MIMO systems in Ricean fading. In *Proc. sixth IEEE Workshop on Signal Processing Advances in Wireless Communications (SPAWC)*, pages 114–118, New York, June 2005.

[CT91] T. Cover and J. Thomas. *Elements of Information Theory*. John Wiley & Sons, 1991.

[CTB99] G. Caire, G. Taricco, and E. Biglieri. Optimum power control over fading channels. *IEEE Transactions on Information Theory*, 45(5):1468–1489, July 1999.

[CWZ03] M. Chiani, M. Win, and A. Zanella. On the capacity of spatially correlated MIMO Rayleigh-fading channels. *IEEE Transactions on Information Theory*, 49(10):2263–2371, October 2003.

[Gal63] R. Gallager. *Low-density parity-check codes*. PhD thesis, MIT Press, Cambridge, MA, 1963.

[Gol89] D. Goldberg. *Genetic Algorithms in Search, Optimization, and Machine Learning*. Addison Wesley Publishing Company, 1989.

[GR00] I. S. Gradshteyn and I. M. Ryzhik. *Table of Integrals, Series, and Products*. Academic Press, sixth edition, 2000.

[GSS+03] D. Gesbert, M. Shafi, D. Shiu, P. J. Smith, and A. Naguib. From theory to practice: an overview of MIMO space-time coded wireless systems. *IEEE Journal on Selected Areas in Communications*, 21(3):281–302, April 2003.

[GV97] A. J. Goldsmith and P. P. Varaiya. Capacity of fading channels with channel side information. *IEEE Transactions on Information Theory*, 43(6):1986–1992, November 1997.

[HHØ00] K. J. Hole, H. Holm, and G. E. Øien. Adaptive multidimensional coded modulation over flat fading channels. *IEEE Journal on Selected Areas in Communications*, 18(7):1153–1158, July 2000.

[HØA+03] H. Holm, G. E. Øien, M. S. Alouini, D. Gesbert, and K. J. Hole. Optimal design of adaptive coded modulation schemes for maximum average spectral efficiency. In *Proc. fourth IEEE Workshop on Signal Processing Advances in Wireless Communications (SPAWC)*, pages 403–407, Rome, June 2003.

[JP03] S. K. Jayaweera and H. V. Poor. Capacity of multiple-antenna systems with both receiver and transmitter channel state information. *IEEE Transactions on Information Theory*, 49(10):2697–2709, October 2003.

[KVRS02] M. Kiessling, I. Viering, M. Reinhardt, and J. Speidel. Short-term and long-term diagonalization of correlated MIMO channels with adaptive modulation. In *Proc. 2002 IEEE International Symposium on Personal, Indoor and Mobile Radio Communications (PIMRC)*, pages 593–597, Lisbon, September 2002.

[LZT97] C. Lawrence, J. Zhou, and A. Tits. User's guide for CFSQP version 2.5d. AEM Design, Inc., 1997.

[MA06] A. Maaref and S. Aïssa. Mutual information statistics for dual MIMO systems in correlated Rayleigh fading. *IEEE Communications Letters*, 10(8):591–593, August 2006.

[NM65] J. A. Nelder and R. Mead. A simplex method for function minimization. *The Computer Journal*, 7(4):308–313, 1965.

[NW99] J. Nocedal and S. J. Wright. *Numerical Optimization*. Springer Series in Operations Research, 1999.

[SG04] P. J. Smith and L. M. Garth. Exact capacity distribution for dual MIMO systems in Ricean fading. *IEEE Communications Letters*, 8(1):18–20, January 2004.

[SSP01] H. Sampath, P. Stoica, and A. Paulraj. Generalized linear precoder and decoder design for MIMO channels using the weighted MMSE criterion. *IEEE Transactions on Communications*, 49(12):2198–2206, December 2001.

[Tel95] E. Telatar. Capacity of multi-antenna Gaussian channels. Technical report, AT&T Bell Laboratories, June 1995.

[ZT03] L. Zheng and D. N. C. Tse. Diversity and multiplexing: a fundamental tradeoff in multiple-antenna channels. *IEEE Transactions on Information Theory*, 49(5):1073–1096, May 2003.

Paper C

Rate-Optimal Power Adaptation in Average and Peak Power Constrained Fading Channels

Sébastien de la Kethulle de Ryhove and Geir E. Øien

Accepted for publication in *Proc. 2007 IEEE Wireless Communications & Networking Conference (WCNC),* Hong Kong, March 2007

Abstract

The power adaptation strategy which maximises the average information rate that can be reliably transmitted over average and peak power constrained block-fading single-user discrete-time channels, in which perfect transmitter and receiver channel state information (CSI) are available and in which any transmitted codeword spans a single fading block, is characterised by means of a theorem and subsequently computed numerically in different scenarios. The results reveal striking differences between the well known water-pouring power adaptation strategy which is optimal from a capacity point of view in the case of stationary and ergodic fading channels where the input is subject to an average power constraint only, and the rate-optimal power adaptation strategy of the average and peak power constrained block-fading channels studied in this document.

1 Introduction

The capacity of single-user, discrete-time communication channels subject to different constraints on the input signal has been extensively studied since the dawn of information theory [Sha48; Smi71; SBD95; GV97; CS99], the most commonly used input constraint being the average power constraint. The capacity of the Gaussian channel – in which the input signal is subject to such a constraint – was originally derived by Shannon [Sha48]. Smith [Smi71] later studied the scalar Gaussian channel subject simultaneously to average and peak power constraints, and proved that the capacity-achieving distribution in this case is discrete with a finite number of mass points. These results were subsequently extended to the quadrature (two-dimensional) additive Gaussian channel by Shamai and Bar-David [SBD95]. They showed that the capacity-achieving distribution of such channels subject to average and peak power constraints has a uniformly distributed phase, and a magnitude which is discrete with a finite number of mass points; that is, that it consists of a finite number of concentric circles which are centred about the origin in the complex plane.

The capacity of average power constrained stationary and ergodic fading channels with perfect channel state information (CSI) at the transmitter and the receiver was studied by Goldsmith and Varaiya [GV97]. They showed that the optimal power adaptation strategy is water-pouring in time, and proposed a variable-rate, variable-power (multiple codebook) coding scheme to achieve capacity. These results were subsequently generalised to the case of imperfect transmitter CSI by Caire and Shamai [CS99]. They additionally proved that a conventional constant-rate, constant-power codebook is sufficient to achieve capacity provided that the codebook symbols are dynamically scaled by an appropriate power allocation function (which depends on the transmitter CSI only) before transmission.

In this paper, we study block-fading channels in which the input symbols are subject simultaneously to average and peak power constraints, and in which perfect CSI is available both at the transmitter and at the receiver. After characterising, by means of a theorem, the power allocation strategy which maximises the average information rate that can be transmitted over such channels with an arbitrarily low probability of error – assuming any transmitted codeword spans a single fading block – we numerically compute it in different scenarios. For simplicity, we hereafter refer to this power allocation strategy as the *rate-optimal* power allocation strategy.

Our results reveal striking differences between the rate-optimal power allocation strategy for block-fading channels where the input is subject to an average power constraint only (which also is the capacity-achieving

power allocation strategy for the stationary and ergodic fading channel studied in [GV97] and thereafter in [CS99], as we will show), and the rate-optimal power allocation strategy for the average and peak power constrained block-fading channels studied in this document.

The remainder of this document is organised as follows: the system model is introduced in Sec. 2, and a theorem which characterises the corresponding rate-optimal power allocation strategy is subsequently proved in Sec. 3. The methodology we use to numerically compute this rate-optimal power allocation strategy is then discussed in Sec. 4, where numerical results are also presented. Conclusions are finally drawn in Sec. 5.

2 System Model

We consider a frequency-flat fading, discrete-time channel with time-varying channel gain denoted by $h_k \in \mathbb{C}$ at time $k \in \{0, 1, 2, \ldots\}$. Let the transmitted signal have complex baseband representation $X_k \in \mathbb{C}$. The received baseband signal $Y_k \in \mathbb{C}$ can then be written

$$Y_k = h_k X_k + W_k, \tag{C.1}$$

where the elements of the sequence $\{W_k\}$ are assumed to be zero mean, unit variance i.i.d. circularly symmetric complex Gaussian random variables, viz. $W_k \sim \mathcal{N}_{\mathbb{C}}(0, 1)$.

The channel gain h_k is assumed to be nonzero and perfectly estimated at the receiver (high-quality channel gain estimates can for example be achieved by the transmission of a known sequence of pilot symbols), and subsequently fed back to the transmitter via a delay and error free feedback channel. The CSI h_k will hence be perfectly known to the transmitter and the receiver at all times $k \in \{0, 1, 2, \ldots\}$, provided that it remains constant between successive estimations. To ensure that this is true in our case, we will assume a block-fading scenario throughout this document – that is, that h_k remains constant for blocks of N consecutive symbols – and therefore that h_k is perfectly known to both the transmitter and the receiver at all times. We furthermore assume that the sequence $\{h_0, h_N, h_{2N}, \ldots\}$ of channel gains corresponding to successive blocks is stationary and ergodic, and that the block-length N is sufficiently long to allow for capacity-achieving coding within each block (we exclusively consider the case where any transmitted codeword spans a single fading block). In addition to the generic time index k, it is convenient for future use to introduce a block index $q \in \{0, 1, 2, \ldots\}$, and an index $j \in \{0, 1, \ldots, N-1\}$ to designate the elements within each block. We thus have $k = Nq + j$.

3 Maximum Average Information Rate and Rate-Optimal Power Adaptation Strategy

Let $C(P_{\text{av}}, P_{\text{peak}})$ denote the operational capacity [CT91] of a non-fading complex additive white Gaussian noise channel with unit noise power, and input samples which are subject to an average power constraint P_{av} and a peak power constraint P_{peak}. The *information* capacity [CT91] $C_{\text{info}}(P_{\text{av}}, P_{\text{peak}})$ of such a channel was studied in [SBD95], where it was shown that the capacity-achieving distribution has a uniformly distributed phase, and that its magnitude is discrete with a finite number of mass points. It can be shown using a time-sharing argument detailed in Appendix A (see also [SH05]) that $C_{\text{info}}(P_{\text{av}}, P_{\text{peak}})$ is a concave function of P_{av} for fixed P_{peak}. Bearing this in mind, it becomes a simple matter to adapt the proofs for the coding theorem and the converse to the coding theorem – given respectively in [CT91, Sec. 10.1] and [CT91, Sec. 10.2] for the case of the scalar discrete-time additive white Gaussian noise channel in which the input is subject to an average power constraint only – to establish equality between $C_{\text{info}}(P_{\text{av}}, P_{\text{peak}})$ and $C(P_{\text{av}}, P_{\text{peak}})$.

For given average and peak powers P_{av} and P_{peak}, let us introduce the *pre-adaptation* SNR

$$\gamma_q \triangleq P_{\text{av}} \, |h_q|^2 \tag{C.2}$$

for block q, let $f_\gamma(\gamma) = f_\gamma(\gamma = \gamma_q)$ denote the corresponding pre-adaptation SNR probability density function (which will be assumed to be nonzero for all $\gamma \in (0, \infty)$), and let in addition

$$p_{\text{peak}} \triangleq \frac{P_{\text{peak}}}{P_{\text{av}}}. \tag{C.3}$$

Let us now suppose we allow the transmit power $P(\gamma)$ to change as a function of $\gamma = \gamma_q$ (the block index q will be omitted in the remainder of this document for simplicity). The *post-adaptation* SNR is then given by

$$\frac{\gamma \cdot P(\gamma)}{P_{\text{av}}} = \gamma \cdot p(\gamma), \tag{C.4}$$

where we have defined $p(\gamma) \triangleq P(\gamma)/P_{\text{av}}$.

For a given power allocation function $p(\gamma)$, the maximum information rate that can be transmitted through channel (C.1) with arbitrarily small probability of error during a fading block with pre-adaptation SNR γ is thus given by $C\left(\gamma \cdot p(\gamma), \, \gamma \cdot p_{\text{peak}}\right)$. Moreover, for a given power allocation

function $p(\gamma)$, the maximum *average* information rate that can be transmitted through channel (C.1) with arbitrarily small probability of error is simply the average of the maximum information rates than can be transmitted via channel (C.1) during each fading block, i.e.

$$\int_0^\infty C\left(\gamma \cdot p(\gamma),\, \gamma \cdot p_{\text{peak}}\right)\, f_\gamma(\gamma)\, \mathrm{d}\gamma. \tag{C.5}$$

We have the following theorem:

Theorem C.1
The maximum average information rate that can be transmitted through channel (C.1) with arbitrarily low probability of error under the assumptions of Sec. 2, with the input samples subject to the average and peak power constraints

$$E\left\{|X_k|^2\right\} \leq P_{\text{av}} \tag{C.6}$$

and

$$|X_k|^2 \leq P_{\text{peak}} \qquad \forall k \in \{0, 1, 2, \ldots\}, \tag{C.7}$$

where[1] $P_{\text{av}} \leq P_{\text{peak}}$, is given by

$$\sup_{p(\gamma)} \int_0^\infty C\left(\gamma \cdot p(\gamma),\, \gamma \cdot p_{\text{peak}}\right)\, f_\gamma(\gamma)\, \mathrm{d}\gamma, \tag{C.8}$$

with p_{peak} having been defined in (C.3) and the supremum being taken over all power allocation functions $p(\gamma)$ such that

$$\int_0^\infty p(\gamma)\, f_\gamma(\gamma)\, \mathrm{d}\gamma \leq 1 \tag{C.9}$$

and

$$0 \leq p(\gamma) \leq p_{\text{peak}}. \tag{C.10}$$

Proof: It can easily be seen that the maximum average information rate that can be reliably transmitted through channel (C.1) under the assumptions of Sec. 2 is given by (C.8) provided that the average and peak power constraints on the input samples (C.6) and (C.7) are satisfied if and only if the power allocation function $p(\gamma)$ satisfies constraints (C.9) and (A.10). We now proceed to prove this. For a given fading block with pre-adaptation SNR γ, and for fixed $p(\gamma)$ and p_{peak}, let

$$g_{R,\Theta}(r, \theta) = \frac{1}{2\pi} \sum_{i=1}^{s} a_i\, \delta(r - r_i), \tag{C.11}$$

[1] We do not consider the case $P_{\text{av}} > P_{\text{peak}}$ since in this case the supremum in (C.8) is trivially achieved by setting $p(\gamma) = p_{\text{peak}}$ for all $\gamma \in (0, \infty)$.

where $\delta(\cdot)$ is the Dirac delta function and $\{a_1, \ldots, a_s\}$ and $\{r_1, \ldots, r_s\}$ respectively denote the weights and radii of s concentric circles (all of which depend on γ, $p(\gamma)$, and p_{peak}), be the input distribution (in polar coordinates) achieving the capacity $C\left(\gamma \cdot p(\gamma),\, \gamma \cdot p_{\text{peak}}\right)$ of a non-fading quadrature additive white Gaussian noise channel with unit power gain, unit noise power, average power constraint $\gamma \cdot p(\gamma) = |h|^2 P(\gamma)$, and peak power constraint $\gamma \cdot p_{\text{peak}} = |h|^2 P_{\text{peak}}$. Transmission on a non-fading quadrature additive white Gaussian noise channel with power gain $|h|^2$, unit noise power, average power constraint $\gamma \cdot p(\gamma)/|h|^2 = P(\gamma)$ and peak power constraint $\gamma \cdot p_{\text{peak}}/|h|^2 = P_{\text{peak}}$ – corresponding to channel (C.1) during the given fading block with pre-adaptation SNR γ – should then be performed using a codebook with elements which are i.i.d. [CT91] according to the distribution

$$g^*_{R,\Theta}(r,\theta) = \frac{1}{2\pi} \sum_{i=1}^{s} a_i \, \delta\left(r - \frac{r_i}{|h|}\right) \tag{C.12}$$

in order to achieve the information rate $C\left(\gamma \cdot p(\gamma), \gamma \cdot p_{\text{peak}}\right)$ during this fading block. When using such a codebook, we have that

$$E\{|X_j|^2\} \leq P(\gamma) \tag{C.13}$$

and

$$|X_j|^2 \leq P_{\text{peak}} \qquad \forall j \in \{0, 1, \ldots, N-1\}, \tag{C.14}$$

where the expectation in (C.13) is taken over all the elements of the codebook used during the fading block under consideration. By averaging (C.13) over all fading blocks, it is easy to see that constraint (C.6) on the input samples will be satisfied if and only if the power allocation function $p(\gamma)$ satisfies (C.9). Moreover, since (C.14) must be satisfied during all fading blocks, we also see that condition (C.7) is equivalent to condition (C.10). □

Remark: One could consider as in [GV97; CS99] a scenario without the restriction to block-fading introduced in Sec. 2, but still with perfect transmitter and receiver CSI (with e.g. h_k i.i.d.). We conjecture that the capacity of channel (C.1) under such fading assumptions and average and peak power constraints (C.6) and (C.7) is given by (C.8) with $p(\gamma)$ having to satisfy constraints (C.9) and (C.10). In order to establish this, one would have to extend the coding theorem and corresponding converse from [GV97] or [CS99] to the case where the input signal is also subject to a peak power constraint. Although we believe this can be done without any particular

difficulties, we have chosen not to do so because in our opinion such a scenario is less realistic than the one considered in this paper for the reasons given in Sec. 2.

We outline in Appendix B the arguments needed to prove that if $p^*(\gamma)$ is to be a supremum of (C.8) subject to constraints (C.9) and (C.10), it must be continuous and such that

$$\begin{cases} p^*(\gamma) = 0 & \text{if } \gamma \leq \lambda^* \\ \gamma \cdot C'\big(\gamma \cdot p^*(\gamma), \gamma \cdot p_{\text{peak}}\big) = \lambda^* & \text{if } \gamma > \lambda^* \text{ and } C'_{\gamma \cdot p_{\text{peak}}} < \frac{\lambda^*}{\gamma} \\ p^*(\gamma) = p_{\text{peak}} & \text{if } \gamma > \lambda^* \text{ and } C'_{\gamma \cdot p_{\text{peak}}} \geq \frac{\lambda^*}{\gamma} \end{cases} \tag{C.15}$$

for all $\gamma \in (0, \infty)$, where $C'(\rho, \gamma \cdot p_{\text{peak}}) \triangleq \frac{\partial}{\partial \rho} C(\rho, \gamma \cdot p_{\text{peak}})$, $C'_{\gamma \cdot p_{\text{peak}}} \triangleq C'\big(\gamma \cdot p_{\text{peak}}, \gamma \cdot p_{\text{peak}}\big)$, and λ^* is such that $\int_{\lambda^*}^{\infty} p^*(\gamma) f_\gamma(\gamma)\, \mathrm{d}\gamma = 1$.

It is also important to observe that

$$C'(0, \gamma \cdot p_{\text{peak}}) = 1, \tag{C.16}$$

since when $\rho \ll \gamma \cdot p_{\text{peak}}$, $C(\rho, \gamma \cdot p_{\text{peak}})$ is approximately equal to the capacity $\log(1 + \rho)$ [nats/channel use] of a non-fading quadrature additive Gaussian noise channel with unit average noise power and average input power constraint ρ. Note additionally that the concavity of $C(\rho, \gamma \cdot p_{\text{peak}})$ implies that $C'(\rho, \gamma \cdot p_{\text{peak}})$ is decreasing in ρ.

Finally, note that in the special case where the peak power constraint is absent (i.e. when $p_{\text{peak}} = \infty$ and $C'(\gamma \cdot p(\gamma), \infty) = \frac{1}{1+\gamma \cdot p(\gamma)}$), the solution $p^*(\gamma)$ satisfying (C.15) becomes simply

$$p^*(\gamma) = \max\left(\tfrac{1}{\lambda^*} - \tfrac{1}{\gamma}, 0\right) \tag{C.17}$$

for all $\gamma \in (0, \infty)$, where λ^* is such that $\int_{\lambda^*}^{\infty} (\frac{1}{\lambda^*} - \frac{1}{\gamma}) f_\gamma(\gamma)\, \mathrm{d}\gamma = 1$. This is exactly the water-pouring solution established in [GV97], which is capacity-optimal in the case of stationary and ergodic fading channels with perfect transmitter and receiver CSI (the constant λ^* corresponds to the cutoff SNR value γ_0 from [GV97]).

4 Numerical Simulations

By using (C.15), we numerically calculated an approximation for the rate-optimal normalised allocated power $p^*(\gamma)$ which achieves the supremum in (C.8) subject to constraints (C.9) and (C.10) in different cases. A

Nakagami-m block-fading channel [SA04] was assumed, resulting in a pre-adaptation SNR γ per block distributed according to the law

$$f_\gamma(\gamma) = \left(\frac{m}{\gamma_{\text{av}}}\right)^m \frac{\gamma^{m-1}}{\Gamma(m)} \exp\left(-m\frac{\gamma}{\gamma_{\text{av}}}\right), \tag{C.18}$$

where m is the fading severity parameter (the special case $m = 1$ corresponds to a Rayleigh-fading channel), γ_{av} is the average pre-adaptation SNR, and $\Gamma(\cdot)$ denotes the Gamma function [GR00].

We now briefly describe the details of the numerical optimisation procedure. The main difficulty lies in the computation of $C'(P_{\text{av}}, P_{\text{peak}})$ for different values of P_{av} and P_{peak}. An approximation for this quantity can be obtained via the centred finite difference

$$C'(P_{\text{av}}, P_{\text{peak}}) \simeq \frac{C(P_{\text{av}} + \Delta, P_{\text{peak}}) - C(P_{\text{av}} - \Delta, P_{\text{peak}})}{2\Delta}, \tag{C.19}$$

where we chose to set $\Delta = 10^{-5}$ after some experimentation. Note that in order for (C.19) to yield a good approximation for $C'(P_{\text{av}}, P_{\text{peak}})$, it is imperative that $C(P_{\text{av}} + \Delta, P_{\text{peak}})$ and $C(P_{\text{av}} - \Delta, P_{\text{peak}})$ be computed with good accuracy.

In order to evaluate $C(P_{\text{av}}, P_{\text{peak}})$ for given P_{av} and P_{peak}, one needs to find the positions and probabilities of the mass points of the capacity-achieving magnitude distribution [SBD95]. This can be done by using steepest descent-like algorithms (routines from the CFSQP optimisation software [LZT97] were used to obtain the results presented in this section) together with the necessary and sufficient optimality condition provided in [SBD95, p. 1064]. Numerical experimentation showed that this can only be done with sufficient accuracy for our purposes when the capacity-achieving magnitude distribution possesses up to six or seven mass points. The reason for this is that as the number of mass points in the capacity-achieving magnitude distribution increases, the optimality condition from [SBD95] becomes more difficult to verify due to the growing effect of numerical inaccuracies.

The number of mass points in the capacity-achieving magnitude distribution increases as $P_{\text{av}} \to 0$ for fixed P_{peak}, and as P_{av} and P_{peak} approach infinity while the ratio $P_{\text{av}}/P_{\text{peak}}$ remains constant. The approximations

$$C(P_{\text{av}}, P_{\text{peak}}) \simeq \log(1 + P_{\text{av}}), \tag{C.20}$$

$$C'(P_{\text{av}}, P_{\text{peak}}) \simeq 1/(1 + P_{\text{av}}), \tag{C.21}$$

corresponding to a quadrature additive Gaussian channel which is subject to an average power constraint only, can often prove useful in cases where

$P_{\text{av}} \ll P_{\text{peak}}$ and the number of mass points of the capacity-achieving distribution is too large to use steepest descent-like algorithms in conjunction with the condition from [SBD95].

In order to find an approximation for $p^*(\gamma)$ for given $f_\gamma(\gamma)$ and p_{peak}, we proceed by first tabulating approximations for $\gamma \cdot C'(\gamma \cdot p(\gamma), \gamma \cdot p_{\text{peak}})$ for a number of different $\gamma \in [0, 30]$ belonging to a suitably chosen set[2] G, and for $p(\gamma) \in \{0, \frac{p_{\text{peak}}}{100}, \frac{2p_{\text{peak}}}{100}, \ldots, p_{\text{peak}}\}$. This can be done by using (C.19)–(C.21) and following the procedure described above. Fig. C.1 shows plots of this quantity for $p_{\text{peak}} = 2$ and $\gamma \in \{1, 2, 6\}$. For comparison, plots of $\gamma \cdot C'(\gamma \cdot p(\gamma), \infty)$ (corresponding to a quadrature additive Gaussian channel which is subject to an average power constraint only) have been included as well. Fig. C.1 confirms that $\gamma \cdot C'(\gamma \cdot p(\gamma), \gamma \cdot p_{\text{peak}})$ is a monotonously decreasing function of $p(\gamma)$ (this is to be expected since $C(P_{\text{av}}, P_{\text{peak}})$ is concave in P_{av} for fixed P_{peak} as explained in Sec. 3), and also shows that $\gamma \cdot C'(\gamma \cdot p(\gamma), \infty)$ is a good approximation for $\gamma \cdot C'(\gamma \cdot p(\gamma), \gamma \cdot p_{\text{peak}})$ when $\frac{p(\gamma)}{p_{\text{peak}}}$ is small.

Once this has been done, one can find an approximation for the solution $p^*(\gamma)$ of (C.15) $\forall \gamma \in G$ and any given λ^*, and subsequently an approximation for $\int_{\lambda^*}^{\infty} p^*(\gamma) f_\gamma(\gamma)\, \mathrm{d}\gamma$. The latter approximation can be computed by assuming that $p^*(\gamma)$ varies linearly between the values $\gamma \in G$ for which it is approximately known, and by neglecting $\int_{\max_{\gamma \in G}}^{\infty} p^*(\gamma) f_\gamma(\gamma)\, \mathrm{d}\gamma$. (The value of the latter integral is always negligible in the case of the results presented in this section.) Numerical root-finding techniques can therefore be used to find an approximation for the value of λ^* such that $\int_{\lambda^*}^{\infty} p^*(\gamma) f_\gamma(\gamma)\, \mathrm{d}\gamma = 1$, and an approximation for the corresponding rate-optimal normalised power allocation function $p^*(\gamma)$ follows.

The resulting $p^*(\gamma)$ has been plotted in Fig. C.2 for $p_{\text{peak}} = 2$, values of the fading severity parameter $m \in \{1, 2\}$, and values of the average pre-adaptation SNR $\gamma_{\text{av}} \in \{\frac{1}{2}, 1, 2\} = \{-3.01\ldots\ \text{dB}, 0\,\text{dB}, 3.01\ldots\ \text{dB}\}$; and in Fig. C.3 for $p_{\text{peak}} = 3$, values of the fading severity parameter $m \in \{1, 2\}$, and values of the average pre-adaptation SNR $\gamma_{\text{av}} \in \{-3.01\ldots\ \text{dB}, 0\,\text{dB}\}$. For comparison, the normalised rate-optimal power allocation function when $p_{\text{peak}} = \infty$ (given by $p^*(\gamma) = \max(\frac{1}{\lambda^*} - \frac{1}{\gamma}, 0)$ as explained in Sec. 3) has also been plotted in Fig. C.4 for $m \in \{1, 2\}$ and

[2] We set $G = G_0 \triangleq \{0.0, 0.1, 0.2, 0.3, 0.4, 0.5, 0.6, 0.7, 0.8, 0.9, 1.0, 1.1, 1.2, 1.3, 1.4, 1.5, 1.6, 1.7, 1.8, 1.9, 2.0, 2.1, 2.2, 2.3, 2.4, 2.5, 3.0, 3.5, 4.0, 4.5, 5.0, 6.0, 7.0, 8.0, 9.0, 10.0, 11.0, 12.0, 13.0, 14.0, 15.0, 16.0, 17.0, 18.0, 19.0, 20.0, 25.0, 30.0\}$ when $p_{\text{peak}} = 2$, and $G = G_0 \backslash \{20.0, 25.0, 30.0\}$ when $p_{\text{peak}} = 3$. The points in set G are chosen in a way which is approximately such that they be closer to each other in intervals where $p^*(\gamma)$ changes significantly than in intervals where $p^*(\gamma)$ does not change as much.

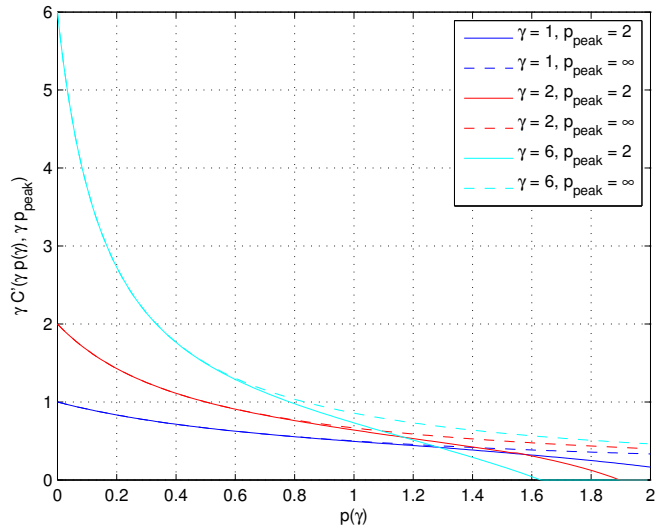

FIGURE C.1: Approximations for $\gamma \cdot C'(\gamma \cdot p(\gamma), \gamma \cdot p_{\text{peak}})$ and $\gamma \cdot C'(\gamma \cdot p(\gamma), \infty)$ as a function of $p(\gamma)$ when $p_{\text{peak}} = 2$ and $\gamma \in \{1, 2, 6\}$.

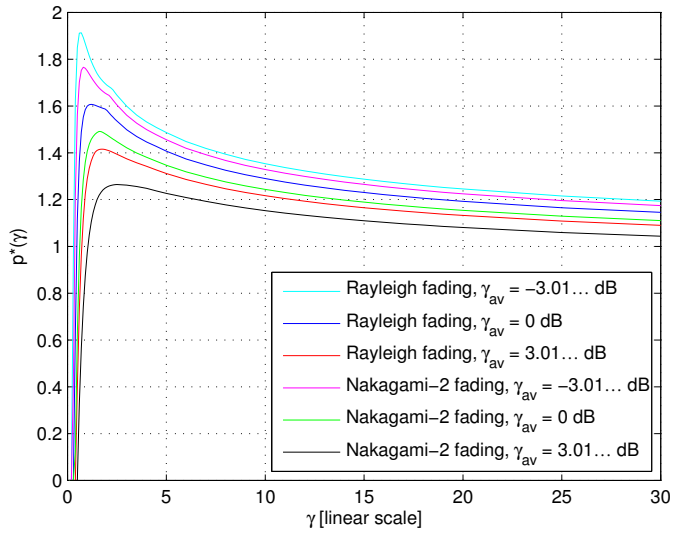

FIGURE C.2: Approximation for the rate-optimal normalised allocated power $p^*(\gamma)$ as a function of the pre-adaptation SNR γ when $p_{\text{peak}} = 2$ for Rayleigh-fading (fading severity parameter $m = 1$) and Nakagami-m fading with $m = 2$. The average pre-adaptation SNR γ_{av} takes values in $\{-3.01\ldots \text{ dB}, 0 \text{ dB}, 3.01\ldots \text{ dB}\}$.

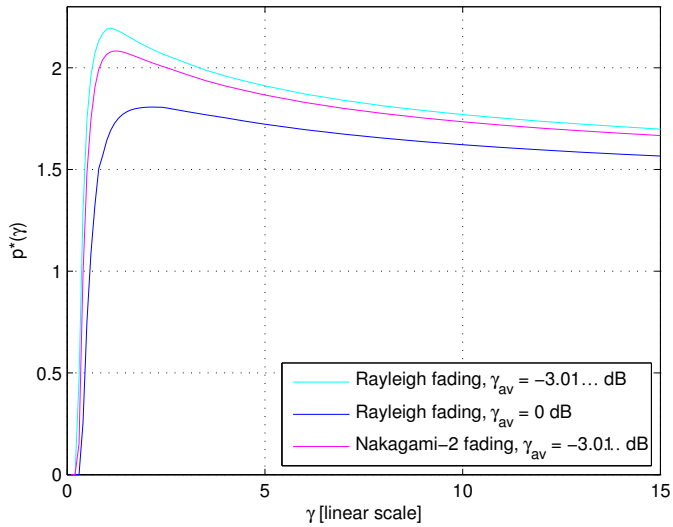

FIGURE C.3: Approximation for the rate-optimal normalised allocated power $p^*(\gamma)$ as a function of the pre-adaptation SNR γ when $p_{\text{peak}} = 3$ for Rayleigh-fading (fading severity parameter $m = 1$) and Nakagami-m fading with $m = 2$. The average pre-adaptation SNR γ_{av} takes values in $\{-3.01\ldots \text{ dB}, 0 \text{ dB}\}$.

$\gamma_{\text{av}} \in \{-3.01\ldots \text{ dB}, 0\,\text{dB}, 3.01\ldots \text{ dB}\}$.

The results presented in these figures show that for all the examples in this section (with $p_{\text{peak}} \in \{2, 3\}$) the optimal normalised power allocation function $p^*(\gamma)$ is identically zero for pre-adaptation SNR values in the neighbourhood of zero, then suddenly increases very quickly with γ until a maximum value is reached, and finally decreases gradually as $\gamma \to \infty$. These figures also show that the behaviour of $p^*(\gamma)$ is highly dependent on the characteristics of the pre-adaptation SNR probability density function $f_\gamma(\gamma)$. As the severity of the fading increases (i.e. as γ_{av} or m decreases, and low pre-adaptation SNR values become more probable), we see that an increasing amount of power is allocated to fading blocks with low pre-adaptation SNRs. A comparison of Figs. C.2 and C.3 also reveals that for a fixed pre-adaptation SNR probability density function $f_\gamma(\gamma)$, the sharpness of the peak in the rate-optimal normalised power allocation function $p^*(\gamma)$ becomes less pronounced as p_{peak} increases.

A striking and important difference between the rate-optimal power adaptation strategy when the input is subject to an average power constraint only (see Fig. C.4) – also corresponding to the water-pouring solu-

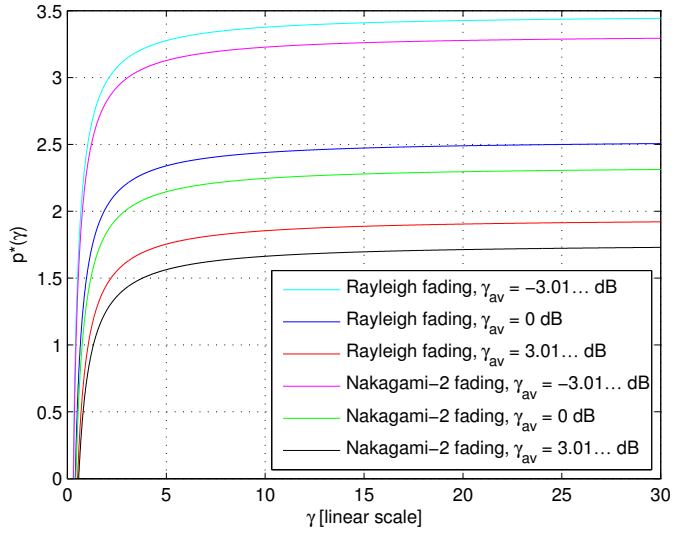

FIGURE C.4: Rate-optimal normalised allocated power $p^*(\gamma) = \max(\frac{1}{\lambda^*} - \frac{1}{\gamma}, 0)$ as a function of the pre-adaptation SNR γ in the average power constrained only case ($p_{\text{peak}} = \infty$) for Rayleigh-fading (fading severity parameter $m = 1$) and Nakagami-m fading with $m = 2$. The average pre-adaptation SNR γ_{av} takes values in $\{-3.01\ldots \text{ dB}, 0 \text{ dB}, 3.01\ldots \text{ dB}\}$.

tion from [GV97] – and the rate-optimal power adaptation strategy when the input is simultaneously subject to average and peak power constraints is the fact that in the latter case the rate-optimal power allocation function is not necessarily a monotonously increasing function of γ (see Figs. C.2 and C.3). This can also be seen by observing in Fig. C.1 that the solid lines corresponding to $\gamma \cdot C'(\gamma \cdot p(\gamma), \gamma \cdot 2)$ for $\gamma \in \{1, 2, 6\}$ cross, whereas the dashed lines corresponding to $\gamma \cdot C'(\gamma \cdot p(\gamma), \infty)$ for $\gamma \in \{1, 2, 6\}$ do not.

5 Conclusions

In this paper, we characterised by means of a theorem the power adaptation strategy which maximises the average information rate that can be reliably transmitted over average and peak power constrained block-fading Gaussian channels in which perfect transmitter and receiver channel state information (CSI) are available, and in which any transmitted codeword spans a single fading block. We subsequently numerically computed it under different block-fading scenarios and different values of the normalised peak

power p_{peak}. Our results reveal that, as opposed to the case of Gaussian stationary and ergodic fading channels with perfect transmitter and receiver CSI and an input which is only subject to an average power constraint (when the well known water-pouring solution is capacity-achieving), the rate-optimal power allocation function is not necessarily a monotonously increasing function of the pre-adaptation SNR.

Appendix A Concavity of $C_{\text{info}}(P_{\text{av}}, P_{\text{peak}})$ for Fixed P_{peak}

Consider the discrete-time quadrature additive Gaussian noise channel

$$Y_k = X_k + W_k, \tag{C.22}$$

where Y_k, X_k, and W_k respectively denote the channel output, input, and additive noise at time k. The sequence $\{W_k\}$ is assumed to consist of zero mean, unit variance i.i.d. circularly symmetric complex Gaussian random variables. In this appendix, we show that the information capacity

$$C_{\text{info}}(P_{\text{av}}, P_{\text{peak}}) = \lim_{n\to\infty} \sup_{\phi_{X^n}(x^n)} \frac{1}{n} I(X^n; Y^n) \tag{C.23}$$

of channel (C.22), with $X^n \triangleq \{X_1, \ldots, X_n\}$, $Y^n \triangleq \{Y_1, \ldots, Y_n\}$, and where the supremum is taken over all probability density functions $\phi_{X^n}(x^n)$ such that

$$\frac{1}{n} \sum_{i=1}^{n} \int_{\mathbb{C}} |x_i|^2 \phi_{X_i}(x_i)\, \mathrm{d}x_i \leq P_{\text{av}} \tag{C.24}$$

and

$$\phi_{X_i}(x_i) = 0 \text{ if } |x_i|^2 > P_{\text{peak}} \qquad \forall i \in \{1, \ldots, n\}, \tag{C.25}$$

is a concave function of P_{av} for fixed P_{peak}. (Note that for memoryless channels, definition (C.23) reduces to

$$C_{\text{info}}(P_{\text{av}}, P_{\text{peak}}) = \sup_{\phi_X(x)} I(X; Y), \tag{C.26}$$

where the supremum is now taken over all probability density functions $\phi_X(x)$ such that $\int_{\mathbb{C}} |x|^2 \phi_X(x)\, \mathrm{d}x \leq P_{\text{av}}$ and $\phi_X(x) = 0$ if $|x|^2 > P_{\text{peak}}$.) We need to show that for any $P_{\text{av}_1}, P_{\text{av}_2} \geq 0$ and any $0 \leq \lambda \leq 1$, we have

$$C_{\text{info}}(P_\lambda, P_{\text{peak}}) \geq \lambda\, C_{\text{info}}(P_{\text{av}_1}, P_{\text{peak}}) + (1-\lambda)\, C_{\text{info}}(P_{\text{av}_2}, P_{\text{peak}}), \tag{C.27}$$

where $P_\lambda = \lambda P_{\text{av}_1} + (1-\lambda)P_{\text{av}_2}$. Let $\phi_{1,X^n}(x^n)$ and $\phi_{2,X^n}(x^n)$ be the distributions achieving the supremum in (C.23) respectively when $P_{\text{av}} = P_{\text{av}_1}$ and $P_{\text{av}} = P_{\text{av}_2}$. Since channel (C.22) is memoryless, we have that $\phi_{k,X_1}(x_1) = \phi_{k,X_2}(x_2) = \cdots = \phi_{k,X_n}(x_n)$ for $k \in \{1,2\}$, i.e. $X_1, \ldots, X_n$ are i.i.d according to $\phi_{k,X_1}(x_1)$ for $k \in \{1,2\}$. Let us now define

$$\phi_{\lambda,X^n}(x^n) = \prod_{i=1}^{\lfloor n\lambda \rfloor} \phi_{1,X_i}(x_i) \prod_{i=\lfloor n\lambda \rfloor+1}^{n} \phi_{2,X_i}(x_i). \tag{C.28}$$

Note that $\lfloor n\lambda \rfloor = n\lambda$ for n sufficiently large. We then have

$$\begin{aligned}\lim_{n\to\infty} \frac{1}{n} \sum_{i=1}^{n} \int_{\mathbb{C}} |x_i|^2 \phi_{\lambda,X_i}(x_i)\, \mathrm{d}x_i &\leq \lim_{n\to\infty} \frac{\lfloor n\lambda \rfloor P_{\text{av}_1} + (n - \lfloor n\lambda \rfloor) P_{\text{av}_2}}{n} \\ &= \lambda P_{\text{av}_1} + (1-\lambda) P_{\text{av}_2} = P_\lambda, \end{aligned} \tag{C.29}$$

which means that the average power constraint is satisfied. Note that the peak power constraint is also trivially satisfied when X^n is distributed according to $\phi_{\lambda,X^n}(x^n)$.

Moreover, when $X^n \sim \phi_{\lambda,X^n}(x^n)$, we have that

$$\begin{aligned}\lim_{n\to\infty} \frac{1}{n} I(X^n; Y^n) &= \lim_{n\to\infty} \frac{1}{n} \left[\sum_{i=1}^{\lfloor n\lambda \rfloor} I(X_i, Y_i) + \sum_{i=\lfloor n\lambda \rfloor+1}^{n} I(X_i, Y_i) \right] \\ &= \lim_{n\to\infty} \frac{1}{n} \Big[\lfloor n\lambda \rfloor C_{\text{info}}(P_{\text{av}_1}, P_{\text{peak}}) \\ &\qquad + (n - \lfloor n\lambda \rfloor)\, C_{\text{info}}(P_{\text{av}_2}, P_{\text{peak}}) \Big] \\ &= \lambda C_{\text{info}}(P_{\text{av}_1}, P_{\text{peak}}) + (1-\lambda) C_{\text{info}}(P_{\text{av}_2}, P_{\text{peak}}), \end{aligned} \tag{C.30}$$

and (C.27) follows immediately.

Appendix B Characterisation of $p^*(\gamma)$

In this appendix, we discuss how to find a $p(\gamma)$ for which the supremum in (C.8), subject to constraints (C.9) and (A.10), is attained. This is equivalent to finding a $p(\gamma)$ minimising

$$-\int_0^\infty C\left(\gamma \cdot p(\gamma),\, \gamma \cdot p_{\text{peak}}\right)\, f_\gamma(\gamma)\, \mathrm{d}\gamma \tag{C.31}$$

subject to

$$\int_0^\infty p(\gamma)\, f_\gamma(\gamma)\, \mathrm{d}\gamma = 1, \tag{C.32}$$

$$-p(\gamma) \leq 0, \tag{C.33}$$

and

$$p(\gamma) - p_{\text{peak}} \leq 0, \tag{C.34}$$

where, as assumed in Sec. 3, $f_\gamma(\gamma) \neq 0$ for all $\gamma \in (0, \infty)$. (It is elementary to show that (C.9) must be satisfied with equality whenever $P_{\text{av}} \leq P_{\text{peak}}$.) Note that $J_1(p) \triangleq p(\gamma) f_\gamma(\gamma)$, $J_2(p) \triangleq -p(\gamma)$, and $J_3(p) \triangleq p(\gamma) - p_{\text{peak}}$ are convex in p [Tro96, p. 63]. In addition, since $C(\rho, \gamma \cdot p_{\text{peak}})$ is a concave function of ρ for fixed $\gamma \cdot p_{\text{peak}}$ as explained in Sec. 3, it follows [Tro96, p. 63] that $-C\left(\gamma \cdot p, \gamma \cdot p_{\text{peak}}\right) f_\gamma(\gamma)$ is convex in p. Consequently [Tro96], we can solve this problem by minimising

$$J(p) = \int_0^\infty \Big[- C\left(\gamma \cdot p(\gamma), \gamma \cdot p_{\text{peak}}\right) f_\gamma(\gamma) + \lambda p(\gamma) f_\gamma(\gamma) \\ - \mu_1(\gamma) p(\gamma) + \mu_2(\gamma)\left(p(\gamma) - p_{\text{peak}}\right)\Big] \, \mathrm{d}\gamma, \tag{C.35}$$

where $\lambda \in \mathbb{R}$ is such that condition (C.32) is satisfied, and $\mu_1(\gamma)$ and $\mu_2(\gamma)$ are nonnegative and such that, for all $\gamma \in (0, \infty)$,

$$-\mu_1(\gamma) p(\gamma) = 0 \tag{C.36}$$

and

$$\mu_2(\gamma)\left[p(\gamma) - p_{\text{peak}}\right] = 0. \tag{C.37}$$

In order to minimise (C.35), it can be shown that $p(\gamma)$ should satisfy the Euler-Lagrange equation [Tro96]

$$\left[\gamma \cdot C'(\gamma \cdot p(\gamma), \gamma \cdot p_{\text{peak}}) - \lambda\right] f_\gamma(\gamma) = -\mu_1(\gamma) + \mu_2(\gamma) \tag{C.38}$$

in all intervals excluding a corner point [Tro96], where we have introduced the notation $C'(\rho, \gamma \cdot p_{\text{peak}}) \triangleq \frac{\partial}{\partial \rho} C(\rho, \gamma \cdot p_{\text{peak}})$. Furthermore, it can also be shown that $p(\gamma)$ should be continuous at each corner point [Tro96, p. 207] if it is to minimise (C.35).

By analysing (C.32)–(C.34) together with (C.36)–(C.38), we find after a minute of thought that any solution $p^*(\gamma)$ minimising (C.31) subject to the constraints (C.32)–(C.34) should be such that

$$\begin{cases} p^*(\gamma) = 0 & \text{if } \gamma \leq \lambda^* \\ \gamma \cdot C'\left(\gamma \cdot p^*(\gamma), \gamma \cdot p_{\text{peak}}\right) = \lambda^* & \text{if } \gamma > \lambda^* \text{ and } C'_{\gamma \cdot p_{\text{peak}}} < \frac{\lambda^*}{\gamma} \\ p^*(\gamma) = p_{\text{peak}} & \text{if } \gamma > \lambda^* \text{ and } C'_{\gamma \cdot p_{\text{peak}}} \geq \frac{\lambda^*}{\gamma} \end{cases} \tag{C.39}$$

for all $\gamma \in (0, \infty)$, where $C'_{\gamma \cdot p_{\text{peak}}} \triangleq C'\left(\gamma \cdot p_{\text{peak}}, \gamma \cdot p_{\text{peak}}\right)$, and λ^* is such that $\int_{\lambda^*}^\infty p^*(\gamma) f_\gamma(\gamma) \, \mathrm{d}\gamma = 1$.

This can be seen by observing that $C'(\gamma \cdot p(\gamma), \gamma \cdot p_{\text{peak}}) \leq 1$ by virtue of the fact that $C'(0, \gamma \cdot p_{\text{peak}}) = 1$ and that $C'(\rho, \gamma \cdot p_{\text{peak}})$ is decreasing in ρ as explained in Sec. 3, and combining this with the fact that $\mu_1(\gamma) = 0$ ($\mu_2(\gamma) = 0$) whenever $p(\gamma) > 0$ ($p(\gamma) < p_{\text{peak}}$).

References

[CS99] G. Caire and S. Shamai (Shitz). On the capacity of some channels with channel state information. *IEEE Transactions on Information Theory*, 45(6):2007–2019, September 1999.

[CT91] T. Cover and J. Thomas. *Elements of Information Theory*. John Wiley & Sons, 1991.

[GR00] I. S. Gradshteyn and I. M. Ryzhik. *Table of Integrals, Series, and Products*. Academic Press, sixth edition, 2000.

[GV97] A. J. Goldsmith and P. P. Varaiya. Capacity of fading channels with channel side information. *IEEE Transactions on Information Theory*, 43(6):1986–1992, November 1997.

[LZT97] C. Lawrence, J. Zhou, and A. Tits. User's guide for CFSQP version 2.5d. AEM Design, Inc., 1997.

[SA04] M. K. Simon and M. S. Alouini. *Digital Communication over Fading Channels*. Wiley Series in Telecommunications and Signal Processing, second edition, 2004.

[SBD95] S. Shamai (Shitz) and I. Bar-David. The capacity of average and peak-power-limited quadrature Gaussian channels. *IEEE Transactions on Information Theory*, 41(4):1060–1071, July 1995.

[SH05] V. Sethuraman and B. Hajek. Capacity per unit energy of fading channels with a peak constraint. *IEEE Transactions on Information Theory*, 51(9):3102–3120, September 2005.

[Sha48] C. E. Shannon. A mathematical theory of communication. *Bell System Technical Journal*, 27:379–423, 623–656, 1948.

[Smi71] J. Smith. The information capacity of amplitude- and variance-constrained scalar Gaussian channels. *Information and Control*, 18(3):203–219, April 1971.

[Tro96] J. Troutman. *Variational Calculus and Optimal Control*. Springer, second edition, 1996.

Paper D

On the Capacity and Mutual Information of Memoryless Noncoherent Rayleigh-Fading Channels

Sébastien de la Kethulle de Ryhove, Ninoslav Marina, and Geir E. Øien

Under review for possible publication in *IEEE Transactions on Information Theory* at the time of writing of this dissertation.

Abstract

The memoryless noncoherent single-input single-output (SISO) Rayleigh-fading channel is considered. Closed-form expressions for the mutual information between the output and the input of this channel when the input magnitude distribution is discrete and restricted to having two mass points are derived, and it is subsequently shown how these expressions can be used to obtain closed-form expressions for the capacity of this channel for signal to noise ratio (SNR) values of up to approximately 0 dB, and a tight capacity lower bound for SNR values between 0 dB and 10 dB. The expressions for the channel capacity and its lower bound are given as functions of a parameter which can be obtained via numerical root-finding algorithms.

Part of the material in this letter was presented by N. Marina at the 2004 International Conference on Telecommunications, Fortaleza, Brazil.

S. de la Kethulle de Ryhove and G. E. Øien are with the Department of Electronics and Telecommunications, Norwegian University of Science and Technology, N–7491 Trondheim, Norway (e-mails: {delaketh, oien}@iet.ntnu.no).

N. Marina was with the Swiss Federal Institute of Technology (EPFL), CH–1015 Lausanne, Switzerland, and is currently with Sowoon Technologies, PSE Technology Park, CH–1015 Lausanne, Switzerland (e-mail: ninoslav.marina@sowoon.com).

1 Introduction

Wireless communication channels in which neither the transmitter nor the receiver possess any knowledge of the channel propagation coefficients (also known as noncoherent channels) have recently been receiving a considerable amount of attention [MH99; ZT02; LV04; AFTS01; TE97; LM03]. Such channels arise whenever the channel coherence time is too short to obtain a reliable estimate of the propagation coefficients via the standard pilot symbol technique (high mobility wireless systems are a typical example of such a scenario). They are currently less well understood than coherent channels, in which the channel state is assumed to be known to the receiver (and sometimes also the transmitter).

In this correspondence, we consider the memoryless noncoherent single-input single-output (SISO) Rayleigh-fading channel, which was studied under the assumption of an average power constrained input in e.g. [AFTS01; TE97; LM03]. In [AFTS01], Abou-Faycal *et al.* rigorously proved (in the average power constrained input case) that the magnitude of the capacity-achieving distribution is discrete with a finite number of mass points, one of these mass points being necessarily located at the origin (zero magnitude). Using numerical optimisation algorithms, the authors also empirically found that a magnitude distribution with two mass points achieves capacity at low signal to noise ratio (SNR) values, and that the required number of mass points to achieve capacity increases monotonically with the SNR. Numerical optimisation algorithms remain however the only way to find the number of mass points of the capacity-achieving magnitude distribution for a given SNR.

Another important reference on the average power constrained memoryless noncoherent SISO Rayleigh-fading channel is the work of Taricco and Elia [TE97], where lower and upper capacity bounds were established, and it was also proved that for high SNR values the capacity only grows double-logarithmically in the SNR. The upper bound from [TE97] was subsequently tightened by Lapidoth and Moser [LM03] in the framework of a more general study on capacity bounds and multiple-antenna systems on flat-fading channels.

The problem of finding the capacity-achieving magnitude distribution of the memoryless noncoherent SISO Rayleigh-fading channel in the average power constrained input case can be solved for low SNR values by using numerical optimisation algorithms as in [AFTS01], but the optimisation problem becomes intractable for high SNR values due to its high dimensionality. An additional difficulty arises due to the fact that closed-form solutions for the integrals appearing in the expression for the channel

mutual information when the input magnitude distribution is discrete are not available in the literature. Consequently, numerical integration algorithms must be repeatedly used when performing such an optimisation.

In this letter, we derive closed-form expressions for the mutual information of the noncoherent Rayleigh-fading channel when the input magnitude distribution is discrete and has two mass points, thus completely eliminating the need for numerical integration in order to compute the mutual information in such a case. For low SNR values (of up to approximately 0 dB) and an average power constrained input, in which case the capacity-achieving magnitude distribution is discrete with two mass points, these closed-form expressions additionally enable us to write the channel capacity as a function of a single parameter which can be obtained via numerical root-finding techniques. This capacity expression also becomes a tight capacity lower bound when the SNR takes values between 0 dB and 10 dB.

Part of the material in this correspondence can also be found in [Mar04a; Mar04b], where an expression for the mutual information of the noncoherent Rayleigh-fading channel, when the input magnitude distribution is discrete and restricted to having only two mass points, was presented in the framework of a study regarding the capacity region of a two-user multiple-access channel in which the channel state is known neither to the transmitters nor to the receiver. The most important additional contributions of this letter lie firstly in a fully detailed and rigorous proof of the validity of this expression, secondly in the derivation of alternative analytical expressions for the same quantity (which naturally follow from the structure of our proof), thirdly in the discussion of a special case in which the expression provided in [Mar04a; Mar04b] can be simplified, fourthly in noting that the hypergeometric functions [GR00] appearing in the expression from [Mar04a; Mar04b] can also be expressed in terms of the incomplete beta function [GR00], and fifthly in showing how to obtain analytical expressions for the derivative of the mutual information of the noncoherent Rayleigh-fading channel (when the input magnitude distribution is discrete with two mass points) with respect to parameters of interest, with applications to capacity calculations and the derivation of a capacity lower bound.

The remainder of this letter is organised as follows: the channel model is introduced in Sec. 2, closed-form expressions for the mutual information when the channel input magnitude distribution is discrete and has two mass points being subsequently derived in Sec. 3. Applications to capacity calculations (for SNR values of up to approximately 0 dB) and the derivation of a capacity lower bound (for SNR values between 0 dB and 10 dB) in the average power constrained input case are then discussed in Sec. 4, and

conclusions finally drawn in Sec. 5.

2 Channel Model

We consider discrete-time memoryless noncoherent SISO Rayleigh-fading channels of the form [AFTS01]

$$V_k = A_k U_k + W_k, \tag{D.1}$$

where for each time instant $k \in \mathbb{N}$, $A_k \in \mathbb{C}$, $U_k \in \mathbb{C}$, $V_k \in \mathbb{C}$, and $W_k \in \mathbb{C}$ respectively represent the channel fading coefficient, the transmitted symbol, the received symbol, and the channel noise. The elements of the sequences $\{A_k\}$ and $\{W_k\}$ are assumed to be zero mean i.i.d. circularly symmetric complex Gaussian random variables with variances respectively equal to 1 and $\sigma^2 > 0$, i.e. $A_k \sim \mathcal{N}_{\mathbb{C}}(0,1)$ and $W_k \sim \mathcal{N}_{\mathbb{C}}(0,\sigma^2)$. It is also assumed that the elements of the sequences $\{A_k\}$ and $\{W_k\}$ are mutually independent. The channel (D.1) being stationary and memoryless, we henceforth omit the notation of the time index k.

A and W being circularly symmetric complex Gaussian distributed, it follows that conditioned on a value u of U, the channel output V also is circularly symmetric complex Gaussian distributed, with mean value zero and variance $|u|^2 + \sigma^2$. Consequently, conditioned on the input U, the channel output V is distributed according to the law

$$f_{V|U}(v|u) = \frac{1}{\pi(|u|^2 + \sigma^2)}\, e^{\frac{-|v|^2}{|u|^2+\sigma^2}}. \tag{D.2}$$

Note that since $f_{V|U}(v|u)$ is independent of the phase $\arg u$ of the input signal, the latter quantity cannot carry any information. If we now make the variable transformations

$$\begin{cases} X = |U| \\ Y = |V| \end{cases}, \qquad X, Y \geq 0, \tag{D.3}$$

we obtain an equivalent channel, the probability density of the output Y of which, conditioned on a value x of its input X, is given by

$$f_{Y|X}(y|x) = \frac{2y}{x^2 + \sigma^2}\, e^{\frac{-y^2}{x^2+\sigma^2}} \qquad X, Y \geq 0. \tag{D.4}$$

Let $I(X;Y)$ denote the mutual information [CT91] between the input and output of the channel with transition probability (D.4), and let $f_X(x)$ and $f_Y(y)$ respectively denote the channel input and output probability density

functions. Note that since $f_{V|U}(v|u)$ is independent of $\arg u$ and $\arg v$ we always have $I(X;Y) = I(U;V)$, where $I(U;V)$ denotes the mutual information between the input and output of the channel with transition probability (D.2).

3 Closed-Form Expressions For $I(X;Y)$ When The Input Distribution Has Two Mass Points

For a given input probability density function $f_X(x)$, the mutual information $I(X;Y)$ of the channel with transition probability (D.4) is given by[1]

$$I(X;Y) = \int_0^\infty \int_0^\infty f_{Y|X}(y|x) f_X(x) \log \frac{f_{Y|X}(y|x)}{f_Y(y)} \, \mathrm{d}y \, \mathrm{d}x, \tag{D.5}$$

with $f_Y(y) = \int_0^\infty f_{Y|X}(y|x) f_X(x) \, \mathrm{d}x$. In this section, we derive a closed-form expression for $I(X;Y)$ when the input probability density function $f_X(x)$ has the form

$$f_X(x) = a_1 \delta(x - x_1) + a_2 \delta(x - x_2), \tag{D.6}$$

where $\delta(\cdot)$ denotes the Dirac distribution, a_1 and a_2 are constants which, $f_X(x)$ being a probability density function, must be such that $0 \leq a_1, a_2 \leq 1$ and $a_1 + a_2 = 1$, $x_1, x_2 \geq 0$ by virtue of the fact that $X = |U| \geq 0$, and we assume without loss of generality that $x_1 \leq x_2$.

We will in addition assume that $0 < a_1, a_2 < 1$, that $x_1 \neq x_2$, and that $x_1 = 0$. The reason for the first two assumptions is that the case where either $a_1 = 0$, $a_1 = 1$, or $x_1 = x_2$ is of little interest since $f_X(x)$ then reduces to a probability density function with only one mass point and the mutual information vanishes. The reason for assuming that $x_1 = 0$ is that – when the input probability distribution must satisfy an average power constraint of the form $E\left[X^2\right] \leq P$ for a given power budget P – the capacity-achieving input distribution of the channel with transition probability $f_{Y|X}(y|x)$ given in (D.4) always has one mass point located at the origin [AFTS01], and consequently the case $x_1 = 0$ is one of great practical importance. We however would like to point out that the case $x_1 \neq 0$ can be treated in exactly the same manner as below and that we choose not do so in order to keep all equations as simple as possible.

[1] In this letter, logarithms will be taken in base e, and mutual information will be measured in nats.

With this choice for $f_X(x)$, the mutual information (D.5) becomes

$$I(X;Y) = -a_1 - a_1 \log \sigma^2 - a_2 - a_2 \log(x_2^2 + \sigma^2) - \sum_{k=1}^{2} \int_0^\infty \frac{2y\, a_k}{x_k^2 + \sigma^2} e^{\frac{-y^2}{x_k^2+\sigma^2}} \log \left(\sum_{l=1}^{2} \frac{a_l}{x_l^2 + \sigma^2} e^{\frac{-y^2}{x_l^2+\sigma^2}} \right) \mathrm{d}y. \tag{D.7}$$

The difficulty to find a closed-form expression for $I(X;Y)$ lies in finding an expression for integrals of the form (with $x \in \{0, x_2\}$)

$$J(x) \triangleq \int_0^\infty \frac{2y}{x^2+\sigma^2} e^{\frac{-y^2}{x^2+\sigma^2}} \log \left(\frac{a_1}{\sigma^2} e^{\frac{-y^2}{\sigma^2}} + \frac{a_2}{x_2^2+\sigma^2} e^{\frac{-y^2}{x_2^2+\sigma^2}} \right) \mathrm{d}y, \tag{D.8}$$

which appear in (D.7). Integrals resembling $J(x)$ do not appear in tables such as [GR00], and to the best of the authors' knowledge no closed-form expression is currently available in the literature. How to derive such closed-form expressions for $J(x)$, which can then be used to obtain closed-form expressions for the mutual information $I(X;Y)$ when the input probability density function $f_X(x)$ is of the form (D.6), is shown in Sec. 3.1 below.

3.1 Closed-Form Expressions for $J(x)$

Let us define

$$\alpha \triangleq \frac{x_2^2}{x_2^2+\sigma^2} \frac{x^2+\sigma^2}{\sigma^2}, \qquad \beta \triangleq \frac{a_2}{a_1} \frac{\sigma^2}{x_2^2+\sigma^2}, \tag{D.9}$$

which remembering the above assumptions can be seen to be always strictly positive, and let us in addition introduce the strictly positive quantity

$$y_*^2 \triangleq -\frac{\sigma^2(x_2^2+\sigma^2)}{x_2^2} \log \beta \tag{D.10}$$

whenever $\log \beta < 0$ (i.e. when $0 < \beta < 1$). Note that when this is the case, we have

$$\frac{a_1}{\sigma^2} e^{\frac{-y_*^2}{\sigma^2}} = \frac{a_2}{x_2^2+\sigma^2} e^{\frac{-y_*^2}{x_2^2+\sigma^2}} \tag{D.11}$$

for the $y_*^2 > 0$ defined in (D.10). We now provide expressions for $J(x)$ in three different cases.

3.1.1 Case I: $\alpha \in \{1, \frac{1}{2}, \frac{1}{3}, \ldots\}$

Noting that

$$\log\left(\frac{a_1}{\sigma^2}e^{\frac{-y^2}{\sigma^2}} + \frac{a_2}{x_2^2+\sigma^2}e^{\frac{-y^2}{x_2^2+\sigma^2}}\right) \tag{D.12}$$
$$= \frac{-y^2}{x_2^2+\sigma^2} + \log\frac{a_2}{x_2^2+\sigma^2} + \log\left(1+\beta^{-1}e^{\frac{-\alpha y^2}{x^2+\sigma^2}}\right),$$

it is easy to see that $J(x) = J_{11}(x) + J_{12}(x) + J_{13}(x)$, with

$$J_{11}(x) = \int_0^\infty \frac{-2y^3}{(x^2+\sigma^2)(x_2^2+\sigma^2)}e^{\frac{-y^2}{x^2+\sigma^2}}\mathrm{d}y = -\frac{x^2+\sigma^2}{x_2^2+\sigma^2}, \tag{D.13}$$

$$J_{12}(x) = \log\frac{a_2}{x_2^2+\sigma^2}\int_0^\infty \frac{2y}{x^2+\sigma^2}e^{\frac{-y^2}{x^2+\sigma^2}}\mathrm{d}y = \log\frac{a_2}{x_2^2+\sigma^2}, \tag{D.14}$$

and

$$J_{13}(x) = \int_0^\infty \frac{2y}{x^2+\sigma^2}e^{\frac{-y^2}{x^2+\sigma^2}}\log\left(1+\beta^{-1}e^{\frac{-\alpha y^2}{x^2+\sigma^2}}\right)\mathrm{d}y \tag{D.15}$$
$$= \left(1-(-\beta)^{-\frac{1}{\alpha}}\right)\log\left(1+\beta^{-1}\right) - \sum_{k=1}^{1/\alpha}\frac{1}{k(-\beta)^{k-\frac{1}{\alpha}}}. \tag{D.16}$$

The last equality is a direct consequence of the fact that, for any $a, b > 0$ we have, omitting the integration constant,

$$\int \frac{2y}{a}\,e^{-y^2/a}\log\left(1+b\,e^{-\alpha y^2/a}\right)\mathrm{d}y \tag{D.17}$$
$$= \sum_{k=1}^{1/\alpha}\frac{1}{k}(-b)^{k-\frac{1}{\alpha}}e^{-k\alpha y^2/a} - \left(e^{-y^2/a} + (-b)^{-\frac{1}{\alpha}}\log b\right)\log\left(1+b\,e^{-\alpha y^2/a}\right),$$

which can be verified by differentiating the expression on the right-hand side of the equality sign with respect to y and remembering that for any $q \neq 1$ and any positive integer n, we have $\sum_{k=1}^{n} q^k = (q - q^{n+1})/(1-q)$.

3.1.2 Case II: $0 < \beta < 1$ and $\alpha \notin \{1, \frac{1}{2}, \frac{1}{3}, \ldots\}$

In this case, we have $J(x) = J_{21}(x) + J_{22}(x) + J_{23}(x) + J_{24}(x) + J_{25}(x) + J_{26}(x)$, with

$$J_{21}(x) = \int_0^{y_*} \frac{-2y^3}{\sigma^2(x^2+\sigma^2)} e^{\frac{-y^2}{x^2+\sigma^2}} \mathrm{d}y, \tag{D.18}$$

$$J_{22}(x) = \log \frac{a_1}{\sigma^2} \int_0^{y_*} \frac{2y}{x^2+\sigma^2} e^{\frac{-y^2}{x^2+\sigma^2}} \mathrm{d}y, \tag{D.19}$$

$$J_{23}(x) = \int_0^{y_*} \frac{2y}{x^2+\sigma^2} e^{\frac{-y^2}{x^2+\sigma^2}} \log\left(1 + \beta e^{\frac{\alpha y^2}{x^2+\sigma^2}}\right) \mathrm{d}y, \tag{D.20}$$

$$J_{24}(x) = \int_{y_*}^{\infty} \frac{-2y^3}{(x^2+\sigma^2)(x_2^2+\sigma^2)} e^{\frac{-y^2}{x^2+\sigma^2}} \mathrm{d}y, \tag{D.21}$$

$$J_{25}(x) = \log \frac{a_2}{x_2^2+\sigma^2} \int_{y_*}^{\infty} \frac{2y}{x^2+\sigma^2} e^{\frac{-y^2}{x^2+\sigma^2}} \mathrm{d}y, \tag{D.22}$$

and

$$J_{26}(x) = \int_{y_*}^{\infty} \frac{2y}{x^2+\sigma^2} e^{\frac{-y^2}{x^2+\sigma^2}} \log\left(1 + \beta^{-1} e^{\frac{-\alpha y^2}{x^2+\sigma^2}}\right) \mathrm{d}y. \tag{D.23}$$

This can be seen by remembering (D.12), observing that we furthermore also have

$$\log\left(\frac{a_1}{\sigma^2} e^{\frac{-y^2}{\sigma^2}} + \frac{a_2}{x_2^2+\sigma^2} e^{\frac{-y^2}{x_2^2+\sigma^2}}\right) = \frac{-y^2}{\sigma^2} + \log\frac{a_1}{\sigma^2} + \log\left(1 + \beta e^{\frac{\alpha y^2}{x^2+\sigma^2}}\right), \tag{D.24}$$

and by writing the integration interval in the expression (D.8) for $J(x)$ in the form $[0, y_*) \cup [y_*, \infty)$. Noting that $e^{-y_*^2/(x^2+\sigma^2)} = \beta^{\frac{1}{\alpha}}$, it is straightforward to compute $J_{21}(x)$, $J_{22}(x)$, $J_{24}(x)$, and $J_{25}(x)$ to obtain

$$J_{21}(x) = \frac{\beta^{\frac{1}{\alpha}}}{\sigma^2}\left(x^2 + \sigma^2 + y_*^2\right) - 1 - \frac{x^2}{\sigma^2}, \tag{D.25}$$

$$J_{22}(x) = \left(1 - \beta^{\frac{1}{\alpha}}\right) \log\frac{a_1}{\sigma^2}, \tag{D.26}$$

$$J_{24}(x) = -\left(\frac{x^2+\sigma^2+y_*^2}{x_2^2+\sigma^2}\right) \beta^{\frac{1}{\alpha}}, \tag{D.27}$$

and

$$J_{25}(x) = \left(\log\frac{a_2}{x_2^2+\sigma^2}\right) \beta^{\frac{1}{\alpha}}. \tag{D.28}$$

We now turn our attention to $J_{23}(x)$ and $J_{26}(x)$, which are more delicate to compute. To find an expression for $J_{23}(x)$, note that for all $y \in [0, y_*)$ we have $0 < \beta e^{\alpha y^2/(x^2+\sigma^2)} < 1$. Therefore, the identity [GR00]

$$\log(1+a) = \sum_{k=1}^{\infty} \frac{(-1)^{k+1}}{k} a^k, \tag{D.29}$$

which is valid for $-1 < a \leq 1$, can be used to obtain

$$J_{23}(x) = \int_0^{y_*} \frac{2y}{x^2+\sigma^2} e^{\frac{-y^2}{x^2+\sigma^2}} \log\left(1 + \beta e^{\frac{\alpha y^2}{x^2+\sigma^2}}\right) \mathrm{d}y \tag{D.30}$$

$$= \int_0^{y_*} \frac{2y}{x^2+\sigma^2} e^{\frac{-y^2}{x^2+\sigma^2}} \sum_{k=1}^{\infty} \frac{(-1)^{k+1}}{k} \beta^k e^{\frac{k\alpha y^2}{x^2+\sigma^2}} \mathrm{d}y \tag{D.31}$$

$$= \sum_{k=1}^{\infty} \int_0^{y_*} \frac{(-1)^{k+1}}{k} \frac{2y\,\beta^k}{x^2+\sigma^2} e^{\frac{-y^2(1-k\alpha)}{x^2+\sigma^2}} \mathrm{d}y \tag{D.32}$$

$$= \sum_{k=1}^{\infty} \frac{(-\beta)^k}{k(k\alpha-1)} - \beta^{\frac{1}{\alpha}} \sum_{k=1}^{\infty} \frac{(-1)^k}{k(k\alpha-1)}, \tag{D.33}$$

where the order of integration and summation can be inverted in (D.32) by virtue of Lebesgue's dominated convergence theorem [Wei96]. Indeed, defining for $n \in \{1, 2, \ldots\}$

$$\phi_n(y) \triangleq \frac{2y}{x^2+\sigma^2} e^{\frac{-y^2}{x^2+\sigma^2}} \sum_{k=1}^{n} \frac{(-1)^{k+1}}{k} \beta^k e^{\frac{k\alpha y^2}{x^2+\sigma^2}}, \tag{D.34}$$

we see referring to Lemma D.1 in Appendix A that $|\phi_n(y)| \leq \phi_1(y)$ for all $y \in [0, y_*)$, and since $\int_0^{y_*} \phi_1(y)\mathrm{d}y < \infty$ the assumptions of Lebesgue's dominated convergence theorem are verified. Evaluating the sums appearing in (D.33) then yields, remembering that $0 < \beta < 1$ and that $\alpha \notin \{1, \frac{1}{2}, \frac{1}{3}, \ldots\}$,

$$J_{23}(x) = \sum_{k=1}^{\infty} \frac{(-1)^{k+1}}{k} \beta^k + \sum_{k=1}^{\infty} \frac{\alpha}{k\alpha-1} (-\beta)^k - \beta^{\frac{1}{\alpha}} \sum_{k=1}^{\infty} \frac{(-1)^k}{k(k\alpha-1)} \tag{D.35}$$

$$= \log(1+\beta) - \frac{\alpha\beta}{\alpha-1}\, {}_2F_1\left(\begin{matrix}1, \frac{\alpha-1}{\alpha} \\ \frac{2\alpha-1}{\alpha}\end{matrix}; -\beta\right) + \frac{\beta^{\frac{1}{\alpha}}}{\alpha-1}\, {}_3F_2\left(\begin{matrix}1, 1, \frac{\alpha-1}{\alpha} \\ 2, \frac{2\alpha-1}{\alpha}\end{matrix}; -1\right), \tag{D.36}$$

where

$${}_pF_q\left(\begin{matrix}\xi_1, \xi_2, \ldots, \xi_p \\ \eta_1, \eta_2, \ldots, \eta_q\end{matrix}; z\right) = \sum_{k=0}^{\infty} \frac{(\xi_1)_k (\xi_2)_k \ldots (\xi_p)_k}{(\eta_1)_k (\eta_2)_k \ldots (\eta_q)_k} \frac{z^k}{k!} \tag{D.37}$$

denotes the generalised hypergeometric series [Bai72; Luk69; GR00], with $(a)_k \triangleq a(a+1)\cdots(a+k-1)$ the Pochhammer symbol [GR00] and $z \in \mathbb{C}$. In the special case where $p = 2$ and $q = 1$, the above series reduces to the extensively studied Gauss hypergeometric series, which is often also denoted $F(\xi_1, \xi_2; \eta_1; z)$[Bai72; Luk69; GR00]. Although the ${}_3F_2$ appearing in (D.36) can be reduced to a ${}_2F_1$ by splitting the second sum appearing in (D.33) into partial fractions before summing, we do not do so because subsequent simplifications in the final expression for $J(x)$ then become less apparent (this remark also applies to (D.38) below).

Using a similar procedure to evaluate $J_{26}(x)$ yields

$$J_{26}(x) = \frac{\beta^{\frac{1}{\alpha}}}{\alpha+1} {}_3F_2\left(\begin{matrix}1, 1, \frac{\alpha+1}{\alpha} \\ 2, \frac{2\alpha+1}{\alpha}\end{matrix}; -1\right). \tag{D.38}$$

Putting the above results together, we obtain after some elementary manipulations

$$\begin{aligned} J(x) = -1 - \frac{x^2}{\sigma^2} + \log\frac{a_1}{\sigma^2} + \log(1+\beta) - \frac{\alpha\beta}{\alpha-1} {}_2F_1\left(\begin{matrix}1, \frac{\alpha-1}{\alpha} \\ \frac{2\alpha-1}{\alpha}\end{matrix}; -\beta\right) \\ + \beta^{\frac{1}{\alpha}}\left[\alpha + \frac{1}{\alpha-1} {}_3F_2\left(\begin{matrix}1, 1, \frac{\alpha-1}{\alpha} \\ 2, \frac{2\alpha-1}{\alpha}\end{matrix}; -1\right) + \frac{1}{\alpha+1} {}_3F_2\left(\begin{matrix}1, 1, \frac{\alpha+1}{\alpha} \\ 2, \frac{2\alpha+1}{\alpha}\end{matrix}; -1\right)\right], \end{aligned} \tag{D.39}$$

which can be further simplified to obtain

$$J(x) = -1 - \frac{x^2}{\sigma^2} + \log\frac{a_1}{\sigma^2} + \log(1+\beta) - \frac{\alpha\beta}{\alpha-1} {}_2F_1\left(\begin{matrix}1, \frac{\alpha-1}{\alpha} \\ \frac{2\alpha-1}{\alpha}\end{matrix}; -\beta\right) + \frac{\pi\beta^{\frac{1}{\alpha}}}{\sin\frac{\pi}{\alpha}} \tag{D.40}$$

as shown in Appendix B.

Note that the reason for splitting the integration interval $[0, \infty)$ into $[0, y_*) \cup [y_*, \infty)$ and evaluating the resulting integrals in different ways is the fact that the series expansion (D.29) only is valid for $-1 < a \leq 1$.

3.1.3 Case III: $\beta \geq 1$

We now have

$$\frac{a_2}{x_2^2+\sigma^2} e^{\frac{-y^2}{x_2^2+\sigma^2}} \geq \frac{a_1}{\sigma^2} e^{\frac{-y^2}{\sigma^2}} \tag{D.41}$$

for all $y > 0$, and consequently $J(x)$ can be evaluated by using (D.12) together with (D.29) over the whole integration range $[0, \infty)$. This yields, using the same technique as in Sec. 3.1.2, $J(x) = J_{31}(x) + J_{32}(x) + J_{33}(x)$, with

$J_{31}(x) = J_{11}(x)$ and $J_{32}(x) = J_{12}(x)$ respectively given in (D.13) and (D.14), and

$$J_{33}(x) = \int_0^\infty \frac{2y}{x^2+\sigma^2} e^{\frac{-y^2}{x^2+\sigma^2}} \log\left(1+\beta^{-1} e^{\frac{-\alpha y^2}{x^2+\sigma^2}}\right) \mathrm{d}y \tag{D.42}$$

$$= \log(1+\beta^{-1}) - \frac{\alpha\beta^{-1}}{\alpha+1}\, {}_2F_1\left(\begin{matrix}1, \frac{\alpha+1}{\alpha} \\ \frac{2\alpha+1}{\alpha}\end{matrix}; -\beta^{-1}\right). \tag{D.43}$$

$J(x)$ hence reads

$$J(x) = -\frac{x^2+\sigma^2}{x_2^2+\sigma^2} + \log\frac{a_2}{x_2^2+\sigma^2} + \log(1+\beta^{-1}) - \frac{\alpha\beta^{-1}}{\alpha+1}\, {}_2F_1\left(\begin{matrix}1, \frac{\alpha+1}{\alpha} \\ \frac{2\alpha+1}{\alpha}\end{matrix}; -\beta^{-1}\right). \tag{D.44}$$

We now give some comments regarding the expressions for $J(x)$ obtained in (D.40) when $0 < \beta < 1$ and $\alpha \notin \{1, \frac{1}{2}, \frac{1}{3}, \ldots\}$, and in (D.44) when $\beta \geq 1$.

First of all, we recall that in the case when $p = q+1$, the series ${}_pF_q$ defined in (D.37) converges for $|z| < 1$, also when $z = 1$ provided that $\mathrm{Re}\,(\sum\eta - \sum\xi) > 0$, and when $z = -1$ provided that $\mathrm{Re}\,(\sum\eta - \sum\xi) > -1$ [Bai72]. (In our case, when $p = q+1 = 2$ and $\sum\eta - \sum\xi = 0$ the series converges for $z = -1$ as well as for $|z| < 1$, whereas when $p = q+1 = 3$ and $\sum\eta - \sum\xi = 1$ the series converges for $z = \pm 1$ as well as for $|z| < 1$.) However, ${}_{p+1}F_p$ can be extended to a single-valued analytic function of z on the domain $\mathbb{C}\backslash(1,\infty)$ [Luk69; IH87a; IH87b], and it is common practise to use the symbol ${}_{p+1}F_p$ to denote both the resulting generalised hypergeometric function and the generalised hypergeometric series on the right hand side of (D.37) which represents the function inside the unit circle.

In Appendix C, we show that the functions $G(z) : \mathbb{C} \to \mathbb{C}$ and $G_2(z) : \mathbb{C} \to \mathbb{C}$, which are respectively defined in (D.76) and (D.101), are analytic for all $z \in \mathbb{C}\backslash(-\infty, -1]$. Although the proof we have is somewhat technical, the consequences are far-reaching. Indeed, if we consider the expression on the right hand side of (D.42) as a function of $z = \beta^{-1}$, then we immediately see that this function is analytic for all $z \in \mathbb{C}\backslash(-\infty, -1]$ by comparing it to the definition of $G(z)$ in (D.76). Additionally, the discussion in the previous paragraph shows that the right hand side of (D.43), when considered as a function of $z = \beta^{-1}$ (with $\log(\cdot)$ denoting the principal branch of the logarithm [Con73], which is analytic on $\mathbb{C}\backslash(-\infty, 0)$) also is analytic for all $z \in \mathbb{C}\backslash(-\infty, -1]$. It then follows from the theory of complex analysis [Con73] that equality between the right hand sides of (D.42) and (D.43) not only holds for $\beta \geq 1$, but actually whenever $\beta^{-1} \in \mathbb{C}\backslash(-\infty, -1]$, and thus in particular for all $\beta > 0$.

When $\alpha \notin \{1, \frac{1}{2}, \frac{1}{3}, \ldots\}$, we can consider the right hand side of (D.30) as a function of $z = \beta$, compare it to the definition of $G_2(z)$ in (D.101) to see that it is analytic for all $z \in \mathbb{C}\backslash(-\infty, -1]$, and conclude as above that equality with the expression in (D.36) is assured not only for $0 < \beta < 1$ but for all $\beta \in \mathbb{C}\backslash(-\infty, -1]$, and thus whenever $\beta > 0$. We can also show, using the same arguments and working with $G(z)$ in (D.76), that when $\alpha \notin \{1, \frac{1}{2}, \frac{1}{3}, \ldots\}$, equality between the right hand sides of (D.23) and (D.38) not only holds for $0 < \beta < 1$ but actually for all $\beta \in \mathbb{C}\backslash(-\infty, -1]$, and hence whenever $\beta > 0$. We have therefore proved that, when $\alpha \notin \{1, \frac{1}{2}, \frac{1}{3}, \ldots\}$, (D.40) in fact holds for all $\beta \in \mathbb{C}\backslash(-\infty, -1]$, and as a consequence in particular when $\beta > 0$.

We also would like to discuss in some more detail the restriction $\alpha \notin \{1, \frac{1}{2}, \frac{1}{3}, \ldots\}$ which was made in Sec. 3.1.2. We see that

$$\frac{\alpha}{\alpha - 1} \, {}_2F_1\left(\begin{matrix} 1, \frac{\alpha-1}{\alpha} \\ \frac{2\alpha-1}{\alpha} \end{matrix}; -\beta\right) \tag{D.45}$$

is defined neither when $\alpha = 1$ because of the factor $\frac{1}{\alpha-1}$, nor when $\alpha \in \{\frac{1}{2}, \frac{1}{3}, \ldots\}$ because in such a case $\frac{2\alpha-1}{\alpha}$ is a negative integer or zero, $|\frac{\alpha-1}{\alpha}| > |\frac{2\alpha-1}{\alpha}|$, and then the hypergeometric function ${}_2F_1$ itself is not defined [GR00; Luk69]. Nonetheless, if we let d belong to the set $\{1, \frac{1}{2}, \frac{1}{3}, \ldots\}$, we still have for all $\beta > 0$ that

$$\begin{aligned}
&\lim_{\alpha \to d} \left\{ \log(1+\beta) - \frac{\alpha\beta}{\alpha - 1} \, {}_2F_1\left(\begin{matrix} 1, \frac{\alpha-1}{\alpha} \\ \frac{2\alpha-1}{\alpha} \end{matrix}; -\beta\right) + \frac{\beta^{\frac{1}{\alpha}}}{\alpha - 1} \, {}_3F_2\left(\begin{matrix} 1, 1, \frac{\alpha-1}{\alpha} \\ 2, \frac{2\alpha-1}{\alpha} \end{matrix}; -1\right) \right\} \\
&= \lim_{\alpha \to d} \int_0^{y_*} \frac{2y}{x^2 + \sigma^2} e^{\frac{-y^2}{x^2+\sigma^2}} \log\left(1 + \beta e^{\frac{\alpha y^2}{x^2+\sigma^2}}\right) \mathrm{d}y \qquad \text{(D.46)} \\
&= \int_0^{y_*} \frac{2y}{x^2 + \sigma^2} e^{\frac{-y^2}{x^2+\sigma^2}} \log\left(1 + \beta e^{\frac{dy^2}{x^2+\sigma^2}}\right) \mathrm{d}y < \infty, \qquad \text{(D.47)}
\end{aligned}$$

where the exchange of the order of the limit and integration operations again follows from Lebesgue's dominated convergence theorem (it is easy to verify that the assumptions are met). The last integral can be evaluated using the identity

$$\begin{aligned}
\int \frac{2y}{a} \, e^{-y^2/a} \log\left(1 + b \, e^{dy^2/a}\right) \mathrm{d}y &= e^{-y^2/a} \sum_{k=0}^{1/d-1} \frac{(-b)^k}{\frac{1}{d} - k} e^{kdy^2/a} \qquad \text{(D.48)} \\
&\quad + \left((-b)^{\frac{1}{d}} - e^{-y^2/a}\right) \log\left(1 + b \, e^{dy^2/a}\right) - \frac{d(-b)^{\frac{1}{d}} y^2}{a} - d e^{-y^2/a}
\end{aligned}$$

which is valid for any $a, b > 0$ and $d \in \{1, \frac{1}{2}, \frac{1}{3}, \ldots\}$ (this can be verified by differentiating the expression on the right-hand side of the equality sign

with respect to y), and where the integration constant has been omitted. For convenience we therefore will consider (D.36) and (D.40) to be valid also when $\alpha \in \{1, \frac{1}{2}, \frac{1}{3}, \ldots\}$, it being understood that the value at such points is to be obtained by a limiting process, and that any necessary numerical evaluations can for example be performed using relations such as (D.48).

We now point the reader's attention to the fact that by setting $x = x_2$ in (D.40) and (D.44), and noting that then $\alpha = x_2^2/\sigma^2$ as can be seen from (D.9), we obtain the continuation formula

$$\frac{\alpha\beta}{\alpha-1}{}_2F_1\left(\begin{matrix}1, \frac{\alpha-1}{\alpha} \\ \frac{2\alpha-1}{\alpha}\end{matrix}; -\beta\right) + \alpha - \frac{\pi\beta^{\frac{1}{\alpha}}}{\sin\frac{\pi}{\alpha}} = \frac{\alpha\beta^{-1}}{\alpha+1}{}_2F_1\left(\begin{matrix}1, \frac{\alpha+1}{\alpha} \\ \frac{2\alpha+1}{\alpha}\end{matrix}; -\beta^{-1}\right). \tag{D.49}$$

Bearing in mind the remarks in the previous paragraph, this is valid in particular when $\alpha, \beta > 0$, the case we are interested in. (Evaluating integrals in more than one way is a technique that has already been successfully used to derive identities involving the generalised hypergeometric function ${}_3F_2$ [IH87a; IH87b].)

To conclude this section, we note that the hypergeometric functions appearing in (D.40) and (D.44) can also be expressed in terms of the incomplete beta function $B_z(a, b)$ by virtue of the relation [GR00]

$${}_2F_1\left(\begin{matrix}a, b \\ b+1\end{matrix}; z\right) = bz^{-b}B_z(b, 1-a), \tag{D.50}$$

which is valid whenever the left hand side is defined.

3.2 Closed-Form Expressions for $I(X;Y)$

In Sec. 3.1, a closed-form expression for $J(x)$ was provided in (D.13)–(D.16) for the case where $\alpha \in \{1, \frac{1}{2}, \frac{1}{3}, \ldots\}$ and $\beta > 0$, and two closed-form expressions for $J(x)$ were provided in (D.40) and (D.44) for the case where $\alpha, \beta > 0$.

In order to obtain an expression for $I(X;Y)$ which is valid in the general case where $\alpha, \beta > 0$, the two integrals appearing in (D.7) must be evaluated using (D.40) or (D.44). There are four different possibilities for how to do this, each with its own advantages and disadvantages. For example, if one is seeking an analytical expression which does not present indeterminations that must be lifted by a limiting process for values of $\alpha \in \{1, \frac{1}{2}, \frac{1}{3}, \ldots\}$, one should use (D.44) to evaluate both integrals in (D.7). One might on the other hand be interested in an expression where the series representation (D.37) of the hypergeometric function always converges. One then should use (D.40) if $\beta < 1$, and (D.44) if $\beta \geq 1$ to evaluate the integrals in (D.7).

Another criterion to decide when to use (D.40) and when to use (D.44) to evaluate the integrals in (D.7) is the simplicity of the resulting expression for $I(X;Y)$: simple analytical expressions will generally be easier to analyse and provide more insight than more complex ones. For example, if we choose to evaluate the integrals in (D.7) by using (D.40) and (D.44) respectively when $k = 1$ and $k = 2$, we obtain the expression

$$\begin{aligned} I(X;Y) = &-(1-a_2)\log(1-a_2) - a_2\log a_2 - (1-a_2)\log(1+\beta) \\ &-\frac{a_2 x_2^2}{x_2^2+\sigma^2}\,{}_2F_1\left(\begin{matrix}1, -\frac{\sigma^2}{x_2^2}\\ -\frac{\sigma^2}{x_2^2}+1\end{matrix}; -\beta\right) + (1-a_2)\frac{\pi\beta^{1+\frac{\sigma^2}{x_2^2}}}{\sin\frac{\pi\sigma^2}{x_2^2}} \\ &-a_2\log(1+\beta^{-1}) + \frac{(1-a_2)\,x_2^2}{\sigma^2}\,{}_2F_1\left(\begin{matrix}1, \frac{\sigma^2}{x_2^2}+1\\ \frac{\sigma^2}{x_2^2}+2\end{matrix}; -\beta^{-1}\right), \end{aligned} \tag{D.51}$$

where we have used the relation $a_1 = 1 - a_2$ to eliminate a_1, and one recognises the entropy $H(X)$ of the channel input X, which is distributed according to the law $f_X(x)$ given in (D.6). We do not list here all the possible expressions for $I(X;Y)$ which arise from the different ways of evaluating the integrals in (D.7), but instead conclude this section with a discussion of the properties of $I(X;Y)$ as $x_2 \to \infty$ which can be deduced from (D.51).

If we let $x_2 \to \infty$ in (D.51), one can immediately see that

$$-(1-a_2)\log(1+\beta) - \frac{a_2\,x_2^2}{x_2^2+\sigma^2}\,{}_2F_1\left(\begin{matrix}1, -\frac{\sigma^2}{x_2^2}\\ -\frac{\sigma^2}{x_2^2}+1\end{matrix}; -\beta\right) \longrightarrow -a_2,$$

by remembering (D.9) and (D.37). By use of (D.9), (D.37), (D.49), and L'Hospital's rule, it furthermore follows that

$$(1-a_2)\frac{\pi\beta^{1+\frac{\sigma^2}{x_2^2}}}{\sin\frac{\pi\sigma^2}{x_2^2}} \longrightarrow a_2$$

and

$$-a_2\log(1+\beta^{-1}) + \frac{(1-a_2)\,x_2^2}{\sigma^2}\,{}_2F_1\left(\begin{matrix}1, \frac{\sigma^2}{x_2^2}+1\\ \frac{\sigma^2}{x_2^2}+2\end{matrix}; -\beta^{-1}\right) \longrightarrow 0,$$

although some effort is required here. As $x_2 \to \infty$, we thus see that

$$I(X;Y) \longrightarrow -(1-a_2)\log(1-a_2) - a_2\log a_2 = H(X). \tag{D.52}$$

This can be intuitively understood if one remembers that the mutual information can be written [CT91]

$$I(X;Y) = H(X) - H(X|Y), \tag{D.53}$$

with $H(X|Y)$ the conditional entropy of the channel input X given the channel output Y. As $x_2 \to \infty$, the mass points of the channel input distribution $f_X(x)$ grow more and more separated, and it is to be expected that it will be more and more difficult to make a wrong decision on the value of the channel input X if the channel output Y were to be known, and hence that $H(X|Y) \to 0$ as we just proved.

Note in passing that we also have found an exact expression for $H(X|Y)$ as can be seen by comparing (D.51) with (D.52) and (D.53).

4 Maximum Attainable Mutual Information and Application to Capacity Calculations

We now consider the calculation of the capacity of the channel with transition probability $f_{Y|X}(y|x)$ given in (D.4) when the input X must satisfy the average power constraint $E[X^2] \leq P$ for a given power budget P. Let the signal to noise ratio (SNR) then be defined by

$$\text{SNR} \triangleq P/\sigma^2, \tag{D.54}$$

where σ^2 denotes the noise power (introduced in Sec. 2). In this case, it has been proved [AFTS01] that the capacity-achieving probability density function $f_X(x)$ is discrete and has a finite number of mass points, one of these mass points being located at the origin ($x = 0$). It has also been empirically found (by means of numerical simulations) that a probability density function $f_X(x)$ with two mass points achieves capacity for low SNR values, and that the required number of mass points to achieve capacity increases monotonically with the SNR.

Referring to the results from [AFTS01], we see that a distribution with two mass points achieves capacity for SNR values below approximately 0 dB, and that the maximum mutual information that can be achieved by using such an input distribution is within 0.02 nats of the channel capacity whenever SNR $\leq$ 10 dB.

Following [AFTS01], let $x_1 = 0$ and $x_2^2 = P/a_2$ in $f_X(x)$ (see (D.6)). For any given power budget P, the input probability density function $f_X(x)$ is thus uniquely determined by the value of a_2. Furthermore, let[2] $I_{a_2}(\text{SNR})$

[2]Note by referring to (D.9) and (D.51) that $I_{a_2}(\text{SNR})$ only depends on P and σ^2 via the ratio SNR $= P/\sigma^2$.

denote the value taken by the mutual information $I(X;Y)$ for given values of a_2, P, and σ^2 (with $x_2^2 = P/a_2$ in (D.6)), and let

$$I^*(\mathrm{SNR}) \triangleq \max_{0 \leq a_2 \leq 1} I_{a_2}(\mathrm{SNR}) \tag{D.55}$$

and

$$a_2^*(\mathrm{SNR}) \triangleq \arg \max_{0 \leq a_2 \leq 1} I_{a_2}(\mathrm{SNR}). \tag{D.56}$$

$I^*(\mathrm{SNR})$ hence corresponds to the maximum attainable value of the mutual information $I(X;Y)$ when the input probability density function $f_X(x)$ has two mass points, and $a_2^*(\mathrm{SNR})$ corresponds to the probability of the nonzero mass point for which $I_{a_2}(\mathrm{SNR}) = I^*(\mathrm{SNR})$. The channel capacity $C(\mathrm{SNR})$ is thus equal to $I^*(\mathrm{SNR})$ for SNR values below approximately 0 dB, and exceeds $I^*(\mathrm{SNR})$ by less than 0.02 nats whenever $\mathrm{SNR} \leq 10$ dB.

Although $a_2^*(\mathrm{SNR})$ can be obtained by solving a one-dimensional optimisation problem, it must also satisfy the equation

$$\frac{\partial I_{a_2}(\mathrm{SNR})}{\partial a_2} = 0. \tag{D.57}$$

An expression for $\partial I_{a_2}/\partial a_2$ can be obtained by noting that

$$\begin{aligned} &\frac{\mathrm{d}}{\mathrm{d}a}\, {}_2F_1\left(\begin{matrix}1, h_1(a)\\ 1+h_1(a)\end{matrix}; h_2(a)\right) \\ &\quad = \frac{\mathrm{d}h_2(a)}{\mathrm{d}a}\frac{h_1(a)}{1+h_1(a)}\, {}_2F_1\left(\begin{matrix}2, 1+h_1(a)\\ 2+h_1(a)\end{matrix}; h_2(a)\right) \\ &\qquad + \frac{\mathrm{d}h_1(a)}{\mathrm{d}a}\frac{h_2(a)}{(1+h_1(a))^2}\, {}_3F_2\left(\begin{matrix}2, 1+h_1(a), 1+h_1(a)\\ 2+h_1(a), 2+h_1(a)\end{matrix}; h_2(a)\right) \end{aligned} \tag{D.58}$$

for any given differentiable functions $h_1(\cdot)$ and $h_2(\cdot)$ whenever the left hand-side is defined, and using this expression together with the expression for $I(X;Y)$ that is obtained by evaluating both integrals in (D.7) with the help of (D.44). (Relation (D.58) can be established for values of $h_2(\cdot)$ inside the unit circle by using the series representation (D.37), and subsequently for all other values of $h_2(\cdot) \in \mathbb{C}\backslash(1,\infty)$ by using analytic continuation arguments.)[3]

It is clear that (D.57) must be satisfied by at least one value $0 < a_2 < 1$: this can be seen by observing that $I_{a_2}(\mathrm{SNR}) = 0$, when $a_2 = 0$ or $a_2 = 1$,

[3]Note that (D.58) also could be used to obtain expressions for e.g. $\partial I_{a_2}(\mathrm{SNR})/\partial\,\mathrm{SNR}$, or for the derivative of $I(X;Y)$ (when the distribution of X is discrete and has two mass points) with respect to any other parameter of interest.

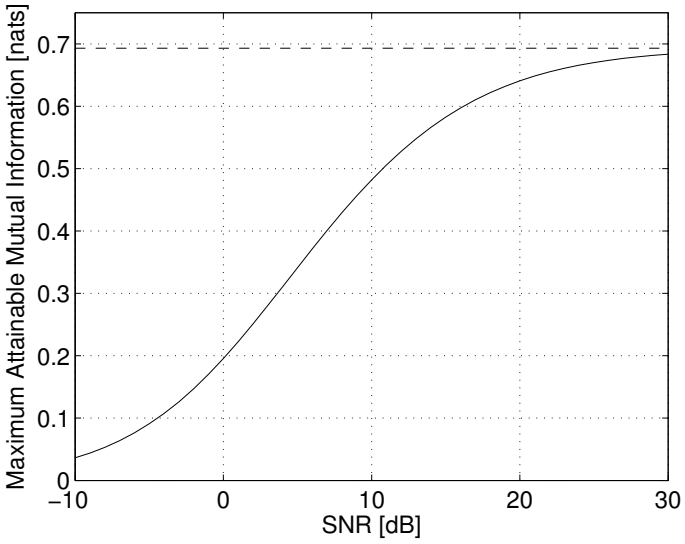

FIGURE D.1: Maximum attainable mutual information $I^*_{a_2}(\mathrm{SNR})$ [nats] as a function of the SNR [dB] when the input probability density function $f_X(x)$ is discrete and restricted to having two mass points. The constant $\log 2 = 0.693\ldots$ has also been plotted for reference (dashed line).

and that $I_{a_2}(\mathrm{SNR}) \geq 0$ when $0 < a_2 < 1$. Indeed, $I_{a_2}(\mathrm{SNR})$ being a continuous and differentiable function of a_2 in this range, it follows that there is at least one value $0 < a_2 < 1$ which satisfies (D.57). Moreover, numerical experiments also seem to indicate that the solution of (D.57) always is unique although we presently do not have a proof of this property.

For SNR values of up to approximately 0 dB, we have thus found a closed-form expression for the capacity $C(\mathrm{SNR})$ of the channel with transition probability (D.4) as a function of a single parameter which can be obtained via numerical root-finding algorithms.

Figs. D.1 and D.2 respectively show the maximum attainable mutual information $I^*_{a_2}(\mathrm{SNR})$ when the input probability density function $f_X(x)$ is discrete and restricted to having two mass points, and the corresponding optimal probability $a_2^*(\mathrm{SNR})$ of the nonzero mass point as a function of the SNR. These figures were obtained by numerically solving (D.57) for SNR values between -10 dB and 30 dB, which proved to be by far the simplest method. In Fig. D.1 we have also plotted the constant $\log 2 = 0.693\ldots$ for reference, and it can be seen as expected that $\lim_{\mathrm{SNR}\to\infty} I^*_{a_2}(\mathrm{SNR}) = \log 2$, and that $\lim_{\mathrm{SNR}\to\infty} a_2^*(\mathrm{SNR}) = \frac{1}{2}$.

Fig. D.3 shows the mutual information $I_{a_2}(\mathrm{SNR})$ as a function of the

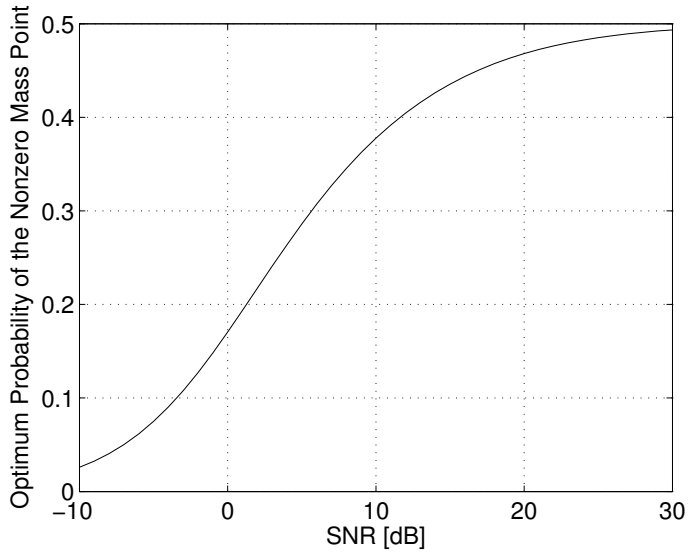

FIGURE D.2: Optimal probability $a_2^*(\mathrm{SNR})$ of the nonzero mass point as a function of the SNR [dB].

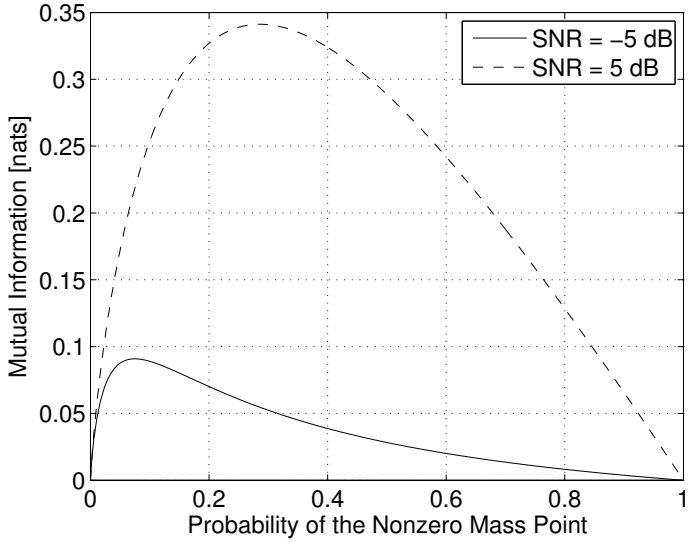

FIGURE D.3: Mutual Information $I_{a_2}(\mathrm{SNR})$ [nats] as a function of the probability a_2 of the nonzero mass point for $\mathrm{SNR} \in \{-5\,\mathrm{dB}, 5\,\mathrm{dB}\}$.

probability a_2 of the nonzero mass point when SNR $\in \{-5\,\text{dB}, 5\,\text{dB}\}$. It is interesting to observe that $I_{a_2}(\text{SNR})$ ceases to be concave in a_2 for sufficiently low SNR values, and that as SNR $\to \infty$, the figure suggests that $I_{a_2}(\text{SNR})$ indeed approaches the entropy $H(X)$ of the channel input X as also mentioned earlier.[4] Note additionally that in both cases shown in the figure the equation $\partial I_{a_2}(\text{SNR})/\partial a_2 = 0$ only has one solution $a_2 \in (0,1)$.

5 Conclusions

In this correspondence, we considered the memoryless noncoherent SISO Rayleigh-fading channel. We first derived closed-form expressions for the mutual information between the output and input signals of this channel when the input magnitude distribution is discrete and restricted to having two mass points, and subsequently showed how these expressions can be used to derive closed-form expressions for the capacity of this channel for SNR values below approximately 0 dB, and a tight capacity lower bound for SNR values between 0 dB and 10 dB. The expressions for the channel capacity and its lower bound are given as functions of a parameter which can be obtained via numerical root-finding algorithms.

Appendix A Exchange of the Order of Integration and Summation in (D.32)

In this appendix, we state and prove a lemma which will be used to show that it is legitimate to exchange the order of integration and summation in (D.32).

Lemma D.1
Let n be a positive integer, let $0 \leq q \leq 1$, and let $T_n \triangleq \sum_{k=1}^{n} \frac{(-1)^{k+1}}{k} q^k$. Then $0 \leq T_n \leq q$ for all n.

Proof: Let n and p be positive integers. The result is trivial if $q = 0$. We thus assume $0 < q \leq 1$ in the remainder of this proof. For all such q, we always have $T_1 = q$, and $T_{2n} < T_{2n+1}$. The lemma will thus be proved if we show that $0 \leq T_{2n}$ and $T_{2n+1} \leq q$ for any positive integer n. Now, noting that

$$c_p \triangleq \frac{q^p}{p} - \frac{q^{p+1}}{p+1} = \frac{q^p}{p} - \frac{q^p}{p}\frac{qp}{p+1} > 0, \tag{D.59}$$

[4] Note that since X is distributed according to the law $f_X(x)$ given in (D.6), $H(X)$ is nothing more than the binary entropy function [nats], which attains its maximum value of $\log 2 = 0.693\ldots$ when $a_1 = a_2 = \frac{1}{2}$.

we see that $T_{2n} = \sum_{k=0}^{n-1} c_{2k+1} > 0$ and that $T_{2n+1} = q - \sum_{k=1}^{n} c_{2k} < q$. □

Appendix B Simplification of (D.39)

In this appendix, we show how the expression for $J(x)$ given in (D.39) can be reduced to the simpler equivalent expression given in (D.40). Let

$$\begin{aligned} S &\triangleq \alpha + \frac{1}{\alpha-1}{}_3F_2\left(\begin{matrix}1,1,\frac{\alpha-1}{\alpha}\\ 2,\frac{2\alpha-1}{\alpha}\end{matrix};-1\right) + \frac{1}{\alpha+1}{}_3F_2\left(\begin{matrix}1,1,\frac{\alpha+1}{\alpha}\\ 2,\frac{2\alpha+1}{\alpha}\end{matrix};-1\right) \\ &= \alpha + \sum_{k=1}^{\infty} \frac{(-1)^{k+1}}{k(k\alpha-1)} + \sum_{k=1}^{\infty} \frac{(-1)^{k+1}}{k(k\alpha+1)} \\ &= \alpha + \sum_{k=0}^{\infty} \frac{1}{(2k+1)((2k+1)\alpha-1)} - \sum_{k=1}^{\infty} \frac{1}{2k(2k\alpha-1)} \\ &\quad + \sum_{k=0}^{\infty} \frac{1}{(2k+1)((2k+1)\alpha+1)} - \sum_{k=1}^{\infty} \frac{1}{2k(2k\alpha+1)} \\ &\triangleq \alpha + S_1 - S_2 + S_3 - S_4. \end{aligned} \tag{D.60}$$

with obvious definitions for S_1, S_2, S_3, and S_4, and the assumptions of Sec 3.1.2 still applying. These sums can be evaluated in terms of the psi function $\psi(\cdot)$ [GR00], which admits the series representation

$$\psi(q+1) = -\gamma + \sum_{k=0}^{\infty} \frac{q}{(k+1)(k+1+q)} \tag{D.61}$$

$$= -\gamma + \sum_{k=1}^{\infty} \frac{q}{k(k+q)}, \tag{D.62}$$

with $\gamma = 0.577\ldots$ denoting Euler's constant [GR00], as can easily be deduced from [GR00, 8.362 (1)]. This yields

$$S_1 = -\frac{\gamma}{2} - \log 2 - \frac{1}{2}\psi\Big(\frac{\alpha-1}{2\alpha}\Big), \tag{D.63}$$

$$S_2 = -\frac{\gamma}{2} - \frac{1}{2}\psi\Big(\frac{2\alpha-1}{2\alpha}\Big), \tag{D.64}$$

$$S_3 = \frac{\gamma}{2} + \log 2 + \frac{1}{2}\psi\Big(\frac{\alpha+1}{2\alpha}\Big), \tag{D.65}$$

and

$$S_4 = \frac{\gamma}{2} + \alpha + \frac{1}{2}\psi\Big(\frac{1}{2\alpha}\Big). \tag{D.66}$$

Here, (D.63) can be verified by setting $q = -\frac{1}{2\alpha} - \frac{1}{2}$ in (D.61) to evaluate $S_1 + \frac{\gamma}{2} + \frac{1}{2}\psi(\frac{\alpha-1}{2\alpha})$, and noting that

$$\log 2 = (1 - \tfrac{1}{2}) + (\tfrac{1}{3} - \tfrac{1}{4}) + (\tfrac{1}{5} - \tfrac{1}{6}) + \cdots \tag{D.67}$$

$$= \sum_{k=1}^{\infty} \frac{1}{(2k+1)(2k+2)}, \tag{D.68}$$

with (D.67) following from (D.29) at $a = 1$; (D.64) follows directly by setting $q = -\frac{1}{2\alpha}$ in (D.62); (D.65) can be obtained by using (D.61) with $q = \frac{1}{2\alpha} - \frac{1}{2}$ to evaluate $\frac{\gamma}{2} + \frac{1}{2}\psi(\frac{\alpha+1}{2\alpha}) - S_3$ and remembering (D.68); and (D.66) can be proved by setting $q = \frac{1}{2\alpha} - 1$ in the identity

$$\psi(q+1) = -\gamma + \frac{q}{q+1} + \sum_{k=1}^{\infty} \frac{q}{(k+1)(k+1+q)}, \tag{D.69}$$

which can easily be obtained starting from (D.61), to find an expression for $\frac{\gamma}{2} + \frac{1}{2}\psi(\frac{1}{2\alpha}) + \alpha - S_4$ and observing that

$$1 = (1 - \tfrac{1}{2}) + (\tfrac{1}{2} - \tfrac{1}{3}) + (\tfrac{1}{3} - \tfrac{1}{4}) + \cdots = \sum_{k=1}^{\infty} \frac{1}{k(k+1)}. \tag{D.70}$$

Combining (D.60) with (D.63)–(D.66) yields

$$S = \tfrac{1}{2}\left[\psi(1 - \tfrac{1}{2\alpha}) - \psi(\tfrac{1}{2\alpha}) + \psi(\tfrac{1}{2} + \tfrac{1}{2\alpha}) - \psi(\tfrac{1}{2} - \tfrac{1}{2\alpha})\right] \tag{D.71}$$

$$= \tfrac{1}{2}\left[\pi \cot \tfrac{\pi}{2\alpha} + \pi \tan \tfrac{\pi}{2\alpha}\right] \tag{D.72}$$

$$= \frac{\pi}{\sin \frac{\pi}{\alpha}}, \tag{D.73}$$

where (D.72) follows from the relations [GR00]

$$\psi(1-q) = \psi(q) + \pi \cot \pi q \tag{D.74}$$

$$\psi(\tfrac{1}{2} + q) = \psi(\tfrac{1}{2} - q) + \pi \tan \pi q. \tag{D.75}$$

The simplification in (D.39) now follows immediately from (D.60) and (D.73).

Appendix C Analytic Character of $G(z)$ and $G_2(z)$

In this appendix, we show that the functions $G(z)$ and $G_2(z)$, defined respectively in (D.76) and (D.101), are analytic for all $z \in \mathbb{C}\backslash(-\infty, -1]$. This fact is used in Sec. 3.1 to prove additional properties of the expressions for $J(x)$ given in (D.40) and (D.44).

Let us consider the function $G : \mathbb{C} \to \mathbb{C}$ defined by

$$G(z) = \int_c^\infty 2ay\, e^{-ay^2} \log\left(1 + z\, e^{-by^2}\right) \mathrm{d}y, \tag{D.76}$$

with a, b positive real constants, c a nonnegative real constant, and where $\log(\cdot)$ denotes the principal branch of the logarithm [Con73].

To prove that $G(z)$ is analytic for all $z \in \mathbb{C}\backslash(-\infty, -1]$, consider the function $g : \mathbb{C} \times \mathbb{R}^+ \to \mathbb{C}$ defined by

$$g(z, y) = 2ay\, e^{-ay^2} \log\left(1 + z\, e^{-by^2}\right). \tag{D.77}$$

For any fixed y it is clear that $g(z, y)$, when considered as a function of z only, is analytic on the domain $z \in \mathbb{C}\backslash(-\infty, -1]$ since the principal branch of the logarithm is analytic on $\mathbb{C}\backslash(-\infty, 0]$. It hence satisfies the Cauchy-Riemann equations (which are a necessary and sufficient condition for a complex function to be analytic) [Con73]

$$\frac{\partial u_g}{\partial z_r} = \frac{\partial v_g}{\partial z_i} \quad \text{and} \quad \frac{\partial u_g}{\partial z_i} = -\frac{\partial v_g}{\partial z_r} \tag{D.78}$$

for all $z \in \mathbb{C}\backslash(-\infty, -1]$, where $u_g(z_r, z_i, y) = \operatorname{Re} g(z_r + iz_i, y)$ and $v_g(z_r, z_i, y) = \operatorname{Im} g(z_r + iz_i, y)$.

In order to show that $G(z)$ is analytic on $\mathbb{C}\backslash(-\infty, -1]$, we will show that the Cauchy-Riemann equations

$$\frac{\partial u_G}{\partial z_r} = \frac{\partial v_G}{\partial z_i} \quad \text{and} \quad \frac{\partial u_G}{\partial z_i} = -\frac{\partial v_G}{\partial z_r} \tag{D.79}$$

are satisfied for all $z \in \mathbb{C}\backslash(-\infty, -1]$, where $u_G(z_r, z_i) = \operatorname{Re}\ G(z_r + iz_i)$ and $v_G(z_r, z_i) = \operatorname{Im}\ G(z_r + iz_i)$. (We will sometimes write $u_G(z)$ instead of $u_G(z_r, z_i)$, $v_G(z)$ instead of $v_G(z_r, z_i)$, $u_g(z, y)$ instead of $u_g(z_r, z_i, y)$, and $v_g(z, y)$ instead of $v_g(z_r, z_i, y)$ for convenience.) Since obviously

$$u_G(z) = \int_c^\infty u_g(z, y)\, \mathrm{d}y \quad \text{and} \quad v_G(z) = \int_c^\infty v_g(z, y)\, \mathrm{d}y, \tag{D.80}$$

it is sufficient to show that

$$\frac{\partial}{\partial z_r} \int_c^\infty u_g(z, y)\, \mathrm{d}y = \int_c^\infty \frac{\partial u_g(z, y)}{\partial z_r}\, \mathrm{d}y, \tag{D.81}$$

together with similar conditions for

$$\frac{\partial}{\partial z_i} \int_c^\infty u_g(z, y)\, \mathrm{d}y, \quad \frac{\partial}{\partial z_r} \int_c^\infty v_g(z, y)\, \mathrm{d}y, \quad \frac{\partial}{\partial z_i} \int_c^\infty v_g(z, y)\, \mathrm{d}y \tag{D.82}$$

by virtue of (D.78). In order to do so, we will use the following result [Wei96]:

Theorem D.1
Let $(\mathcal{Y}, \mathcal{A}, \mu)$ (with $\mathcal{Y}$ a set, $\mathcal{A}$ a σ-algebra on $\mathcal{Y}$, and μ a measure on $\mathcal{A}$) be a measure space, let (b_0, b_1) be a (possibly infinite) interval of $\mathbb{R}$, and let $h : (b_0, b_1) \times \mathcal{Y} \to \mathbb{R} \cup \infty$. For all $x \in (b_0, b_1)$, let

$$\mathcal{J}(x) = \int_{\mathcal{Y}} h(x, y)\, \mathrm{d}\mu \tag{D.83}$$

which is assumed to be always finite. Let $\mathcal{V}$ be a neighbourhood of $x^* \in (b_0, b_1)$ such that:

(i) *For almost all $y \in \mathcal{Y}$, $h(x, y)$ is continuously differentiable with respect to x on $\mathcal{V}$.*
(ii) *There exists an integrable function $\mathcal{H} : \mathcal{Y} \to \mathbb{R} \cup \infty$ such that for all $x \in \mathcal{V}$*

$$\left| \frac{\partial h}{\partial x}(x, y) \right| \leq \mathcal{H}(y) \quad \textit{almost everywhere.} \tag{D.84}$$

Then $\mathcal{J}(x)$ is differentiable at x^*, and

$$\frac{\mathrm{d}\mathcal{J}(x^*)}{\mathrm{d}x} = \int_{\mathcal{Y}} \frac{\partial h}{\partial x}(x^*, y)\, \mathrm{d}\mu. \tag{D.85}$$

Proof: See standard texts on Lebesgue integration such as [Wei96]. □

In our case, $\mathcal{Y}$ is the interval $[c, \infty)$, $\mathcal{A}$ is the Borel σ-algebra on $\mathcal{Y}$, and μ is the standard Lebesgue measure on $\mathcal{A}$. The function $h(z_r, y) = u_g(z_r, z_i, y)$ with z_i fixed when proving (D.81), and similar definitions when proving the conditions in (D.82).

Now, for the $g(z, y)$ defined in (D.77), we have

$$\begin{aligned} u_g(z_r, z_i, y) &= 2aye^{-ay^2} \log \left| 1 + (z_r + iz_i)e^{by^2} \right| \\ &= aye^{-ay^2} \log \left(\left(1 + z_r e^{-by^2}\right)^2 + \left(z_i e^{-by^2}\right)^2 \right), \end{aligned} \tag{D.86}$$

and hence

$$\frac{\partial u_g}{\partial z_r} = \frac{2aye^{-(a+b)y^2}\left(1 + z_r e^{-by^2}\right)}{\left(1 + z_r e^{-by^2}\right)^2 + \left(z_i e^{-by^2}\right)^2} = \frac{\partial v_g}{\partial z_i}. \tag{D.87}$$

In the sequel, we will need to upper bound the absolute value of (D.87) in different settings. This will always be accomplished by obtaining an upper bound $M < \infty$ for $\left|1 + z_r e^{-by^2}\right|$ and a lower bound $m > 0$ for $\left|\left(1 + z_r e^{-by^2}\right)^2 + \left(z_i e^{-by^2}\right)^2\right|$.

Let z_r^* and z_i be such that $z_r^* + iz_i \in \mathbb{C}\backslash(-\infty, -1]$, and let the neighbourhood $\mathcal{V}$ of z_r^* be defined by

$$\mathcal{V} = \begin{cases} (z_r^* - \varepsilon, z_r^* + \varepsilon) & \text{if } z_i = 0 \text{ and } z_r^* \in (-1, \infty) \\ (z_r^* - 1, z_r^* + 1) & \text{if } z_i \neq 0, \end{cases} \tag{D.88}$$

with $\varepsilon \triangleq \frac{z_r^*+1}{2} > 0$ when $z_i = 0$ and $z_r^* \in (-1, \infty)$. Then,

$$\left|1 + z_r e^{-by^2}\right| \leq 1 + |z_r| \leq 1 + |z_r^*| + \max\{1, \varepsilon\} \triangleq M, \tag{D.89}$$

for any $z_r \in \mathcal{V}$, any given z_i, and any $y \in [c, \infty)$; whereas if $z_i = 0$,

$$\begin{aligned}\left(1 + z_r e^{-by^2}\right)^2 + \left(z_i e^{-by^2}\right)^2 &= \left(1 + z_r e^{-by^2}\right)^2 \\ &\geq \left(1 + \tfrac{z_r^*-1}{2} e^{-by^2}\right)^2 \\ &\geq \min\left\{1, \left(1 + \tfrac{z_r^*-1}{2}\right)^2\right\} \triangleq m_1\end{aligned} \tag{D.90}$$

for any $z_r \in \mathcal{V}$ and any $y \in [c, \infty)$, and if $z_i \neq 0$ we have for any $z_r \in \mathcal{V}$ and any $y \in [c, \infty)$

$$\begin{aligned}&\left(1 + z_r e^{-by^2}\right)^2 + \left(z_i e^{-by^2}\right)^2 \\ &\qquad \geq \min\left\{\left(1 + z_r e^{-bc^2}\right)^2 + \left(z_i e^{-bc^2}\right)^2, 1, \tfrac{z_i^2}{z_r^2 + z_i^2}\right\} \\ &\qquad \geq \min\left\{\left(z_i e^{-bc^2}\right)^2, 1, \tfrac{z_i^2}{\max\{(z_r^*-1)^2, (z_r^*+1)^2\} + z_i^2}\right\} \\ &\qquad \triangleq m_2,\end{aligned} \tag{D.91}$$

as one can see by noting that

$$\inf_{y \in [c, \infty)} \left(1 + z_r e^{-by^2}\right)^2 + \left(z_i e^{-by^2}\right)^2 \tag{D.92}$$

must either be attained when $y = c$, when $y \to \infty$, or when

$$\frac{\partial}{\partial y}\left\{\left(1 + z_r e^{-by^2}\right)^2 + \left(z_i e^{-by^2}\right)^2\right\} = 0. \tag{D.93}$$

Consequently, if we set $m \triangleq \min\{m_1, m_2\} > 0$, we see that for all $z_r \in \mathcal{V}$ and any $y \in [c, \infty)$,

$$\left|\frac{\partial u_g}{\partial z_r}(z_r, z_i, y)\right| \leq \frac{2May\, e^{-(a+b)y^2}}{m}, \tag{D.94}$$

which is integrable on $[c, \infty)$ for any $a, b, m, M > 0$ and any $c \geq 0$. Noting in addition that for any $z_r \in \mathcal{V}$ and any z_i, $\frac{\partial u_g}{\partial z_r}$ given in (D.87) is continuous in z_r, we have proved that (D.81) holds for all $z = z_r^* + iz_i \in \mathbb{C}\backslash(-\infty, -1]$ by virtue of Theorem D.1.

Similarly, let z_r and z_i^* be such that $z_r + iz_i^* \in \mathbb{C}\backslash(-\infty, -1]$, and let the neighbourhood $\mathcal{V}$ of z_i^* be defined by

$$\mathcal{V} = \begin{cases} (z_i^* - 1, z_i^* + 1) & \text{if } z_r \in (-1, \infty) \\ (z_i^* - \varepsilon, z_i^* + \varepsilon) & \text{if } z_r \in (-\infty, -1] \text{ and } z_i^* \neq 0, \end{cases} \tag{D.95}$$

with $\varepsilon = \frac{|z_i^*|}{2} > 0$ when $z_i^* \neq 0$. Then,

$$\left|1 + z_r e^{-by^2}\right| \leq 1 + |z_r| \triangleq M', \tag{D.96}$$

for any $z_i \in \mathcal{V}$ and any $y \in [c, \infty)$; whereas if $z_r \in (-1, \infty)$,

$$\begin{aligned}\left(1 + z_r e^{-by^2}\right)^2 + \left(z_i e^{-by^2}\right)^2 &\geq \left(1 + z_r e^{-by^2}\right)^2 \\ &\geq \min\left\{1, \left(1 + z_r\right)^2\right\} \triangleq m_1',\end{aligned} \tag{D.97}$$

for all $z_i \in \mathcal{V}$ and any $y \in [c, \infty)$, and if $z_i^* \neq 0$

$$\begin{aligned}&\left(1 + z_r e^{-by^2}\right)^2 + \left(z_i e^{-by^2}\right)^2 \\ &\quad \geq \min\left\{\left(1 + z_r e^{-bc^2}\right)^2 + \left(z_i e^{-bc^2}\right)^2, 1, \tfrac{z_i^2}{z_r^2 + z_i^2}\right\} \\ &\quad \geq \min\left\{\left((z_i^* - \varepsilon) e^{-bc^2}\right)^2, 1, \tfrac{\min\{(z_i^* - \varepsilon)^2, (z_i^* + \varepsilon)^2\}}{z_r^2 + \min\{(z_i^* - \varepsilon)^2, (z_i^* + \varepsilon)^2\}}\right\} \\ &\quad \triangleq m_2',\end{aligned} \tag{D.98}$$

for all $z_i \in \mathcal{V}$ and any $y \in [c, \infty)$. Consequently, if we set $m' \triangleq \min\{m_1', m_2'\} > 0$, we see that for all $z_i \in \mathcal{V}$ and any $y \in [c, \infty)$,

$$\left|\frac{\partial v_g}{\partial z_i}(z_r, z_i, y)\right| \leq \frac{2M' a y\, e^{-(a+b)y^2}}{m'}, \tag{D.99}$$

which is integrable on $[c, \infty)$ for any $a, b, m', M' > 0$ and any $c \geq 0$. Noting in addition that for any $z_i \in \mathcal{V}$ and any z_r, $\frac{\partial v_g}{\partial z_i}$ given in (D.87) is continuous in z_i, we have proved that the order of integration and derivation can be exchanged in the last expression appearing in (D.82) for all $z = z_r + i z_i^* \in \mathbb{C}\backslash(-\infty, -1]$.

Noting now that

$$\frac{\partial u_g}{\partial z_i} = \frac{2aye^{-(a+b)y^2}\left(z_i e^{-by^2}\right)}{\left(1 + z_r e^{-by^2}\right)^2 + \left(z_i e^{-by^2}\right)^2} = -\frac{\partial v_g}{\partial z_r}, \tag{D.100}$$

it is easy to transpose the above arguments to prove that exchanging the order of differentiation and integration is legitimate for all $z \in \mathbb{C}\backslash(-\infty, -1]$ also in the case of the first and second expressions appearing in (D.82), and we have thus established the analytic character of the function $G(z)$ defined in (D.76) on the domain $\mathbb{C}\backslash(-\infty, -1]$.

Let us now consider the function $G_2 : \mathbb{C} \to \mathbb{C}$ defined by

$$G_2(z) = \int_0^c 2ay\, e^{-ay^2} \log\left(1 + z\, e^{-by^2}\right) \mathrm{d}y, \tag{D.101}$$

with a a positive real constant, $b \in \mathbb{R}$, and c a nonnegative real constant. The arguments from this appendix can be used verbatim to prove that $G_2(z)$ also is analytic on $\mathbb{C}\backslash(-\infty, -1]$ – and the proof can even be simplified due to the fact that the integration interval $[0, c)$ now being finite, it is sufficient that the corresponding functions $u_{g_2}(z_r, z_i, y)$ and $v_{g_2}(z_r, z_i, y)$ be differentiable functions of z_r and z_i on $\mathbb{C}\backslash(-\infty, -1]$ for all $y \in [0, c)$ to guarantee that the order in which integration and differentiation are performed in (D.81) and in the expressions given in (D.82) (with $u_g(z, y)$ and $v_g(z, y)$ respectively replaced by $u_{g_2}(z, y)$ and $v_{g_2}(z, y)$, and the integration interval $[c, \infty)$ replaced by $[0, c)$) can be exchanged [GR00, Sec. 12.211].

References

[AFTS01] I. Abou-Faycal, M. Trott, and S. Shamai (Shitz). The capacity of discrete-time memoryless Rayleigh-fading channels. *IEEE Transactions on Information Theory*, 47(4):1290–1301, May 2001.

[Bai72] W. N. Bailey. *Generalized Hypergeometric Series*. Hafner Publishing Company, New York, 1972.

[Con73] J. B. Conway. *Functions of One Complex Variable*. Springer, first edition, 1973.

[CT91] T. Cover and J. Thomas. *Elements of Information Theory*. John Wiley & Sons, 1991.

[GR00] I. S. Gradshteyn and I. M. Ryzhik. *Table of Integrals, Series, and Products*. Academic Press, sixth edition, 2000.

[IH87a] A. A. Inayat-Hussain. New properties of hypergeometric series derivable from Feynman integrals. I. Transformation and reduction formulae. *Journal of Physics A: Mathematical and General*, 20(13):4109–4117, September 1987.

[IH87b] A. A. Inayat-Hussain. New properties of hypergeometric series derivable from Feynman integrals. II. A generalisation of the H function. *Journal of Physics A: Mathematical and General*, 20(13):4119–4128, September 1987.

[LM03] A. Lapidoth and S. Moser. Capacity bounds via duality with applications to multiple-antenna systems on flat-fading channels. *IEEE Transactions on Information Theory*, 49(10):2426–2467, October 2003.

[Luk69] Y. L. Luke. *The Special Functions and Their Approximations*, volume 1. Academic Press, New York, 1969.

[LV04] Y. Liang and V. Veeravalli. Capacity of noncoherent time-selective Rayleigh-fading channels. *IEEE Transactions on Information Theory*, 50(12):3095–3110, December 2004.

[Mar04a] N. Marina. Rayleigh fading multiple access channel without channel state information. In *Proc. eleventh International Conference on Telecommunications (ICT)*, pages 128–133, Fortaleza, August 2004.

[Mar04b] N. Marina. *Successive Decoding*. PhD thesis, Swiss Federal Institute of Technology, 2004.

[MH99] T. Marzetta and B. Hochwald. Capacity of a mobile multiple-antenna communication link in Rayleigh flat fading. *IEEE Transactions on Information Theory*, 45(1):139–157, January 1999.

[TE97] G. Taricco and M. Elia. Capacity of fading channel with no side information. *Electronics Letters*, 33(16):1368–1370, July 1997.

[Wei96] A. J. Weir. *Lebesgue Integration & Measure*. Cambridge University Press, 1996.

[ZT02] L. Zheng and D. Tse. Communication on the Grassmann manifold: A geometric approach to the noncoherent multiple-antenna channel. *IEEE Transactions on Information Theory*, 48(2):359–383, February 2002.

Paper E

Capacity-Achieving Input Phase Distributions for Noncoherent Rayleigh-Fading Channels with Memory

Sébastien de la Kethulle de Ryhove, Ralf R. Müller, and Geir E. Øien

Under review for possible publication in *IEEE Transactions on Information Theory* at the time of writing of this dissertation.

Abstract

The present correspondence considers single-input single-output noncoherent Rayleigh-fading channels in which the memory is modelled by an autoregressive process of arbitrary order p and in which the magnitude of the input signal is constrained in an arbitrary manner. A contribution is made to the understanding of such channels by proving that, for any given input magnitude distribution, it is optimum from a capacity perspective to choose the phase of the input independent and identically distributed, with a distribution which is uniform over the interval $[0, 2\pi)$. In particular, if the capacity of such a channel can be achieved with an input distribution f, then it is also achievable by an input distribution f' having the same magnitude distribution and a phase distribution with the above property.

Part of the material in this letter was presented at the 2006 International Workshop on Signal Processing Advances for Wireless Communications (SPAWC '06), Cannes, France, July 2006.

S. de la Kethulle de Ryhove, R. R. Müller, and G. E. Øien are with the Department of Electronics and Telecommunications, Norwegian University of Science and Technology, N–7491 Trondheim, Norway (e-mails: {delaketh, mueller, oien}@iet.ntnu.no).

1 Introduction

Wireless communication channels in which neither the transmitter nor the receiver possess any knowledge of the channel propagation coefficients (also known as noncoherent channels) have recently been receiving a considerable amount of attention [MH99; ZT02; LV04; LM03; TE97; AFTS01; CHM04; Zha05]. Such channels arise whenever the channel coherence time is too short to obtain a reliable estimate of the propagation coefficients via the standard pilot symbol technique (high mobility wireless systems are a typical example of such a scenario). Noncoherent channels are currently less well understood than coherent channels, in which the channel state is assumed to be known to the receiver (and maybe also the transmitter).

In [MH99], Marzetta and Hochwald studied multiple-antenna systems over noncoherent Rayleigh-fading channels, assuming that the channel remains constant during blocks consisting of several symbol periods, and that the channel coefficients corresponding to different blocks are mutually independent. In addition to giving useful design criteria and characterising the capacity-achieving distribution, they derived asymptotic expressions for the capacity in the special case of single-input single-output (SISO) channels. These results were then extended to the multiple-antenna case by Zheng and Tse in [ZT02]. Further progress in this area was made by Liang and Veeravalli [LV04], who also studied the multiple-antenna noncoherent Rayleigh-fading channel under block fading assumptions. However, while continuing to assume that the channel coefficients corresponding to different blocks are mutually independent, their model allows for correlation (in time) between the different propagation coefficients within a block. They showed that the ratio between the rank of the block correlation matrix and the block length plays a crucial role when determining channel capacity, and obtained asymptotic capacity expressions in several different cases.

Noncoherent channels without the restriction to block fading were studied in [LM03] by Lapidoth and Moser. They do not make the restriction to Rayleigh or Rice fading, and allow for channel memory and partial side information at the receiver. Assuming that the fading process is stationary, ergodic, and has finite differential entropy rate, they showed that the capacity of such channels typically only grows double-logarithmically in the SNR. They also introduced the *fading number*, which is the second-order term in the high-SNR asymptotic expansion of capacity, and showed that in the case of noncoherent SISO channels with memory under the above assumptions, the fading number is achievable by independent, identically distributed (i.i.d.) distributions with uniformly distributed phase.

The special case of average power constrained, memoryless non-

coherent Rayleigh-fading SISO channels was studied by Taricco and Elia in [TE97], where capacity bounds were derived, and subsequently in [AFTS01] by Abou-Faycal *et al.*, where it was proved that the capacity-achieving distribution has a discrete magnitude with a finite number of mass points. The bounds from [TE97] were then tightened in [LM03].

Average power constrained, noncoherent Rayleigh-fading SISO channels with memory, in which the memory is modelled by a first order autoregressive process [AR(1)], were studied by Chen *et al.* [CHM04], who showed that a Gaussian input distribution generates bounded mutual information as the SNR approaches infinity, and then gave necessary and sufficient conditions for an input distribution to achieve unbounded mutual information as the SNR approaches infinity. Subsequently, Zhang [Zha05] derived upper and lower bounds for the capacity of this channel, and showed that the amount of information carried by the phase is bounded by a constant as the SNR approaches infinity.

In this letter, we consider SISO noncoherent Rayleigh-fading channels in which the memory is modelled by an autoregressive process of arbitrary order p [AR(p)]. If p is sufficiently large, this enables us to accurately model the bandlimited Rayleigh-fading process [BB04], which has a zero power spectral density past the maximum Doppler frequency and appears in many physical models of mobile radio channels.

We contribute to the understanding of such channels by proving that, for any given input magnitude distribution, it is optimum from a capacity perspective to choose the input phase i.i.d. and uniformly distributed on $[0, 2\pi)$, thus complementing the results from [CHM04; Zha05; LM03].[1] An immediate consequence of this result is that if the capacity of any such channel is achievable using a given input probability distribution f, then it is also achievable by an input probability distribution f' with the same magnitude distribution and a phase distribution which possesses the above property.

2 System Model

We consider discrete-time SISO noncoherent fading channels of the form

$$\begin{aligned} H_k &= -\sum_{j=1}^{p} \alpha_j H_{k-j} + W_k \\ Y_k &= H_k X_k + Z_k, \end{aligned} \tag{E.1}$$

[1] Note that the results from [LM03] concerning input distributions for noncoherent fading-channels with memory only are valid for asymptotically high SNR values.

where $p \in \mathbb{Z}^+$, and for each time instant $k \in \{1, 2, \ldots\}$, $H_k \in \mathbb{C}$, $X_k \in \mathbb{C}$, $Y_k \in \mathbb{C}$, and $Z_k \in \mathbb{C}$ respectively represent the channel fading coefficient, the transmitted symbol, the received symbol, and the channel noise. The elements of the sequences $\{W_k\}$ and $\{Z_k\}$ are assumed to be zero mean i.i.d. circularly symmetric complex Gaussian random variables, with variances respectively equal to $\sigma_w^2 > 0$ and $\sigma_z^2 > 0$ (we hence write $W_k \sim \mathcal{N}_{\mathbb{C}}(0, \sigma_w^2)$ and $Z_k \sim \mathcal{N}_{\mathbb{C}}(0, \sigma_z^2)$). It is also assumed that the elements of the sequences $\{W_k\}$ and $\{Z_k\}$ are mutually independent, and that the random variables in the sequence $\{H_k\}_{k=-p+1}^{0}$ are i.i.d. and $\mathcal{N}_{\mathbb{C}}(0, \sigma_w^2)$ distributed for initialisation purposes. As one can see from (E.1), the fading process $\{H_k\}$ is generated by an autoregressive process of order p, the parameters of which consist of the complex coefficients $\{\alpha_1, \alpha_2, \ldots, \alpha_p\}$ and the variance σ_w^2 of the driving noise process. As explained in [BB04], AR(p) processes are commonly used to approximate discrete-time random processes, and an autoregressive (AR) model can approximate any arbitrary spectrum if the order p is taken sufficiently large. Among others, the bandlimited Rayleigh-fading process – the power spectral density of which is zero past the maximum Doppler frequency – which appears in many physical models of mobile radio channels can be closely approximated by such a process. Note also that both nonisotropic [BB04; ABK02] and isotropic [Cla68; CK97] Rayleigh-fading channels can be modelled by communication channels of the form (E.1). A wide variety of practical scenarios can hence be accurately represented by communication channels of this form.

If $\{X_k\}$ is a sequence of random variables, let the notation X_a^b designate the sequence $\{X_a, \ldots, X_b\}$. Furthermore, let $I(X_a^b; Y_a^b)$ denote the mutual information between the random sequences X_a^b and Y_a^b. Then, given a set of arbitrary constraints

$$\begin{cases} \mu_1(|X_1|, \ldots, |X_n|) \leq 0 \\ \mu_2(|X_1|, \ldots, |X_n|) \leq 0 \\ \qquad\qquad\qquad \vdots \\ \mu_m(|X_1|, \ldots, |X_n|) \leq 0 \end{cases} \tag{E.2}$$

on the magnitude of the input signal (for simplicity, we write the constraints in the compact form $\boldsymbol{\mu}(|X_1|, \ldots, |X_n|) \preceq \mathbf{0}$), the capacity of the channel described by (E.1) is simply

$$C(\boldsymbol{\mu}) = \lim_{n \to \infty} \frac{1}{n} \sup I(X_1^n; Y_1^n), \tag{E.3}$$

where the supremum is taken over all joint distributions on X_1^n such that $\boldsymbol{\mu}(|X_1|, \ldots, |X_n|) \preceq \mathbf{0}$. The set of constraints $\boldsymbol{\mu}(|X_1|, \ldots, |X_n|) \preceq \mathbf{0}$ can consist of deterministic and/or stochastic constraints. Given a power budget

P, both the average power constraint

$$\frac{1}{n}\sum_{k=1}^{n} E\left\{|X_k|^2\right\} - P \leq 0 \tag{E.4}$$

and peak power constraint

$$|X_k|^2 - P \leq 0, \qquad \forall k \in \{1, \ldots, n\} \tag{E.5}$$

are examples of possible choices for the set of constraints $\boldsymbol{\mu}(|X_1|, \ldots, |X_n|) \preceq \mathbf{0}$.

3 Structure of the Optimal Input Phase Distributions

If X is a random variable, let the notation $h(X)$ designate the differential entropy of X if X is continuous, and the entropy of X if X is discrete. The mutual information $I(X;Y)$ between two random variables X and Y is then given by

$$I(X;Y) = h(Y) - h(Y|X). \tag{E.6}$$

Remembering the channel model (E.1), let us now define

$$\begin{aligned} C_n(\boldsymbol{\mu}) &\triangleq \frac{1}{n}\sup I(X_1^n; Y_1^n) \\ &= \frac{1}{n}\sup\left[h(Y_1^n) - h(Y_1^n|X_1^n)\right], \end{aligned} \tag{E.7}$$

where the supremum is taken over all input distributions on X_1^n satisfying the constraints (E.2). Note that $C_n(\boldsymbol{\mu})$ is nothing more than the supremum, over all allowed input distributions, of the average mutual information achieved by the input signals X_1^n over n channel uses, and that due to the presence of the additive Gaussian noise in (E.1) the random variables in the sequence Y_1^n will always be continuous.

For any given value of n in (E.7), if $\{X_1, \ldots, X_n\}$ is a sequence of random variables, let us define the random vector $\boldsymbol{X} \triangleq (X_1, \ldots, X_n)^{\mathsf{T}}$, where $(\cdot)^{\mathsf{T}}$ denotes transposition. (We henceforth will use the notations X_1^n and $\boldsymbol{X}$ interchangeably.) Moreover, and again bearing in mind the channel model (E.1), let us introduce the polar coordinates

$$\begin{cases} X_k = Q_k e^{i\Theta_k}, & Q_k \geq 0,\ \Theta_k \in [0, 2\pi), \\ Y_k = R_k e^{i\Psi_k}, & R_k \geq 0,\ \Psi_k \in [0, 2\pi), \end{cases} \tag{E.8}$$

for all $k \in \{1, \ldots, n\}$. One can apply the above transformation to $h(Y_1^n)$ and $h(Y_1^n|X_1^n)$ to show that

$$I(X_1^n; Y_1^n) = I(Q_1^n, \Theta_1^n; R_1^n, \Psi_1^n) \tag{E.9}$$

as one would expect. (However, since for the same random object, the differential entropies computed in different coordinate systems differ by the expectation of the logarithm of the Jacobian of the coordinate change [ZT02], we have e.g. $h(Y_1^n) = h(R_1^n, \Psi_1^n) + E\{\log \prod_{k=1}^n R_k\}$, where R_1^n and Ψ_1^n are viewed as sequences of real random variables and $h(Y_1^n)$ is computed in rectangular coordinates.) We are now in a position to state the main result of this correspondence.

Theorem E.1
Consider the channel model given in (E.1) and, for any given input magnitude probability distribution $f_Q^0(\boldsymbol{q})$ satisfying the constraints (E.2),

$$C_n(\boldsymbol{\mu}, f_Q^0) \triangleq \frac{1}{n} \sup_{f_{\Theta|Q}(\boldsymbol{\theta}|\boldsymbol{q})} I(Q_1^n, \Theta_1^n; R_1^n, \Psi_1^n), \tag{E.10}$$

where the supremum is taken over all conditional phase probability distributions $f_{\boldsymbol{\Theta}|Q}(\boldsymbol{\theta}|\boldsymbol{q})$, and the mutual information is taken with respect to input probability distributions of the form $f_{\boldsymbol{\Theta}|Q}(\boldsymbol{\theta}|\boldsymbol{q}) f_Q^0(\boldsymbol{q})$. Then, for any given n and $f_Q^0(\boldsymbol{q})$, the supremum in (E.10) is achievable by the conditional phase probability distribution

$$f_{\boldsymbol{\Theta}|Q}^0(\boldsymbol{\theta}|\boldsymbol{q}) = \prod_{i=1}^n f_{\Theta_i}^0(\theta_i), \tag{E.11}$$

with $f_{\Theta_i}^0(\theta_i)$ i.i.d. and uniform on $[0, 2\pi)$. In particular, if $f_X(\boldsymbol{x})$ ($f_Q(\boldsymbol{q}) f_{\boldsymbol{\Theta}|Q}(\boldsymbol{\theta}|\boldsymbol{q})$ in polar coordinates) achieves the supremum in (E.7), then this supremum can also be achieved by a probability distribution $f'_X(\boldsymbol{x})$ which can be expressed in polar coordinates as $f_Q(\boldsymbol{q}) f_{\boldsymbol{\Theta}|Q}^0(\boldsymbol{\theta}|\boldsymbol{q})$, with $f_{\boldsymbol{\Theta}|Q}^0(\boldsymbol{\theta}|\boldsymbol{q})$ of the form (E.11) and $f_{\Theta_i}^0(\theta_i)$ i.i.d. and uniform on $[0, 2\pi)$.

4 Proof of the Main Result

4.1 Preliminaries

Note first of all that since $\boldsymbol{W}$ is circularly symmetric complex Gaussian distributed, and since linear transformations of circularly symmetric complex Gaussian random vectors remain circularly symmetric complex Gaussian [Tel95], it follows that $\boldsymbol{H}$ is circularly symmetric complex Gaussian

distributed. In addition, $\boldsymbol{Z}$ also being circularly symmetric complex Gaussian distributed, it follows that conditioned on a value $\boldsymbol{x} = (x_1, \ldots, x_n)$ of $\boldsymbol{X}$, the random vector $\boldsymbol{Y}$ also is circularly symmetric complex Gaussian distributed (see [Tel95] for a rigorous proof of this fact), with mean value zero and covariance matrix $\Sigma_{\boldsymbol{Y}|\boldsymbol{X}} = E\{\boldsymbol{Y}\boldsymbol{Y}^\dagger|\boldsymbol{X}\}$ given by

$$\Sigma_{\boldsymbol{Y}|\boldsymbol{X}} = \begin{pmatrix} v_0|x_1|^2 + \sigma_z^2 & v_1^* x_1 x_2^* & \cdots & v_{n-1}^* x_1 x_n^* \\ v_1 x_2 x_1^* & v_0|x_2|^2 + \sigma_z^2 & \cdots & v_{n-2}^* x_2 x_n^* \\ \vdots & \vdots & \ddots & \vdots \\ v_{n-1} x_n x_1^* & v_{n-2} x_n x_2^* & \cdots & v_0|x_n|^2 + \sigma_z^2 \end{pmatrix}, \tag{E.12}$$

where $(\cdot)^*$ denotes complex conjugation, $(\cdot)^\dagger$ denotes conjugate transposition, and the coefficients $v_k \triangleq E\{H_l H_{l-k}^*\}$ can be obtained from the AR parameters $\{\alpha_1, \ldots, \alpha_p\}$ and σ_w^2 via the procedure described in [BJR94, pp. 55–56]. Conversely, the AR parameters $\{\alpha_1, \ldots, \alpha_p\}$ and σ_w^2 which match any desired autocorrelation function up to lag p (i.e. any desired $\{v_0, \ldots, v_p\}$) can be obtained from the Yule-Walker equations [BB04; BJR94], which can be expressed in matrix form as

$$\begin{pmatrix} v_0 & v_1^* & \cdots & v_p^* \\ v_1 & v_0 & \cdots & v_{p-1}^* \\ \vdots & \vdots & \ddots & \vdots \\ v_p & v_{p-1} & \cdots & v_0 \end{pmatrix} \begin{pmatrix} 1 \\ \alpha_1 \\ \vdots \\ \alpha_p \end{pmatrix} = \begin{pmatrix} \sigma_w^2 \\ 0 \\ \vdots \\ 0 \end{pmatrix}. \tag{E.13}$$

The coefficients v_k for $k > p$ then follow from [BB04]

$$v_k = -\sum_{j=1}^{p} \alpha_j v_{k-j}, \qquad k > p. \tag{E.14}$$

Note that $\Sigma_{\boldsymbol{Y}|\boldsymbol{X}}$ is invertible if $\sigma_z^2 > 0$. Indeed, if we define $S_k \triangleq H_k X_k$ for all $k \in \{1, \ldots, n\}$, we can write $\Sigma_{\boldsymbol{Y}|\boldsymbol{X}} = \Sigma_{\boldsymbol{S}|\boldsymbol{X}} + \sigma_z^2 I_{n\times n}$, where $\Sigma_{\boldsymbol{S}|\boldsymbol{X}}$ is the covariance matrix of $\boldsymbol{S}$ conditioned on $\boldsymbol{X}$, and $I_{n\times n}$ denotes the $n \times n$ identity matrix. $\Sigma_{\boldsymbol{Y}|\boldsymbol{X}}$ being the sum of the positive semidefinite matrix $\Sigma_{\boldsymbol{S}|\boldsymbol{X}}$ and the positive definite matrix $\sigma_z^2 I_{n\times n}$, it is positive definite and hence invertible.

The above arguments show that conditioned on the input $\boldsymbol{X}$, the probability density function of the channel output $\boldsymbol{Y}$ can be expressed as

$$f_{\boldsymbol{Y}|\boldsymbol{X}}(\boldsymbol{y}|\boldsymbol{x}) = \frac{1}{\det \pi\Sigma_{\boldsymbol{Y}|\boldsymbol{X}}} \exp\left(-\boldsymbol{y}^\dagger \Sigma_{\boldsymbol{Y}|\boldsymbol{X}}^{-1} \boldsymbol{y}\right). \tag{E.15}$$

In order to prove Theorem E.1, we will need the following preliminary Lemma.

Lemma E.1
The inverse $\Sigma^{-1}_{\boldsymbol{Y}|\boldsymbol{X}}$ of the matrix $\Sigma_{\boldsymbol{Y}|\boldsymbol{X}}$ given in (E.12) can be written in the form

$$\Sigma^{-1}_{\boldsymbol{Y}|\boldsymbol{X}} = \begin{pmatrix} p_{11} & x_1 x_2^* p_{12} & \cdots & x_1 x_n^* p_{1n} \\ x_2 x_1^* p_{21} & p_{22} & \cdots & x_2 x_n^* p_{2n} \\ \vdots & \vdots & \ddots & \vdots \\ x_n x_1^* p_{n1} & x_n x_2^* p_{n2} & \cdots & p_{nn} \end{pmatrix}, \tag{E.16}$$

where $p_{ij} = p_{ji}^*$ are constants which are independent of the values of $\{\theta_k = \arg x_k\}_{k=1}^n$ for all $1 \leq i, j \leq n$.

Proof: The proof is given in Appendix A. □

Utilising (E.16) we can rewrite the product $\boldsymbol{y}^\dagger \Sigma^{-1}_{\boldsymbol{Y}|\boldsymbol{X}} \boldsymbol{y}$ which appears in the density (E.15) as

$$\boldsymbol{y}^\dagger \Sigma^{-1}_{\boldsymbol{Y}|\boldsymbol{X}} \boldsymbol{y} = \sum_{i=1}^n p_{ii} |y_i|^2 + 2 \sum_{i=1}^{n-1} \sum_{j=i+1}^n \mathrm{Re}\left[p_{ij} x_i y_j (x_j y_i)^* \right]. \tag{E.17}$$

We now express the density (E.15) using the polar coordinates introduced in (E.8), which yields, bearing in mind (E.17),

$$\begin{aligned} f_{\boldsymbol{R},\boldsymbol{\Psi}|\boldsymbol{Q},\boldsymbol{\Theta}}(\boldsymbol{r},\boldsymbol{\psi}|\boldsymbol{q},\boldsymbol{\theta}) = \frac{\prod_{i=1}^n r_i}{\det \pi \Sigma_{\boldsymbol{R},\boldsymbol{\Psi}|\boldsymbol{Q},\boldsymbol{\Theta}}} \exp\left[-\sum_{i=1}^n \rho_{ii} r_i^2 \right] \\ \times \exp\left[-2 \sum_{i=1}^{n-1} \sum_{j=i+1}^n \rho_{ij} q_i q_j r_i r_j \cos\left[(\theta_j - \theta_i) - (\psi_j - \psi_i) - \phi_{ij} \right] \right], \end{aligned} \tag{E.18}$$

where the product $\prod_{i=1}^n r_i$ is the Jacobian of the coordinate transformation, $\Sigma_{\boldsymbol{R},\boldsymbol{\Psi}|\boldsymbol{Q},\boldsymbol{\Theta}}$ is the matrix $\Sigma_{\boldsymbol{Y}|\boldsymbol{X}}$ expressed in the new coordinates (as shown in Appendix A, its determinant does not depend on $\{\arg x_k\}_{k=1}^n$), and we have set $\rho_{ij} \triangleq |p_{ij}|$ and $\phi_{ij} \triangleq \arg p_{ij}$, both of which do not depend on $\{\arg x_k\}_{k=1}^n$ for all $1 \leq i, j \leq n$.

It is convenient for the sequel to make the transformation

$$\begin{cases} \Theta_1' = [\Theta_1]_{2\pi} \\ \Theta_2' = [\Theta_2 - \Theta_1]_{2\pi} \\ \quad \vdots \\ \Theta_n' = [\Theta_n - \Theta_{n-1}]_{2\pi}, \end{cases} \qquad \begin{cases} \Psi_1' = [\Psi_1]_{2\pi} \\ \Psi_2' = [\Psi_2 - \Psi_1]_{2\pi} \\ \quad \vdots \\ \Psi_n' = [\Psi_n - \Psi_{n-1}]_{2\pi}, \end{cases} \tag{E.19}$$

where we have introduced the notation $[\Xi]_{2\pi} \triangleq \Xi \mod 2\pi$ for the sake of compactness. If we observe that the coordinate change (E.19) is bijective

and has Jacobian equal to 1; and that furthermore, for all $j \leq n$, $\Theta_j = \left[\sum_{k=1}^{j} \Theta'_k\right]_{2\pi}$ and $\Psi_j = \left[\sum_{k=1}^{j} \Psi'_k\right]_{2\pi}$, then it becomes a simple matter to use (E.18) to obtain the expression

$$f_{\boldsymbol{R},\boldsymbol{\Psi}'|\boldsymbol{Q},\boldsymbol{\Theta}'}(\boldsymbol{r},\boldsymbol{\psi}'|\boldsymbol{q},\boldsymbol{\theta}') = \frac{\prod_{i=1}^{n} r_i}{\det \pi\Sigma_{\boldsymbol{R},\boldsymbol{\Psi}'|\boldsymbol{Q},\boldsymbol{\Theta}'}} \exp\left[-\sum_{i=1}^{n} \rho_{ii} r_i^2\right] \tag{E.20}$$
$$\times \exp\left[-2\sum_{i=1}^{n-1}\sum_{j=i+1}^{n} \rho_{ij} q_i q_j r_i r_j \cos\left[-\phi_{ij} + \textstyle\sum_{k=i+1}^{j}(\theta'_k - \psi'_k)\right]\right],$$

where $\det \pi\Sigma_{\boldsymbol{R},\boldsymbol{\Psi}'|\boldsymbol{Q},\boldsymbol{\Theta}'} = \det \pi\Sigma_{\boldsymbol{R},\boldsymbol{\Psi}|\boldsymbol{Q},\boldsymbol{\Theta}}$ does not depend on $\{\arg x_k\}_{k=1}^{n}$. We are now ready to prove Theorem E.1.

4.2 Proof of Theorem E.1

Proof: Since

$$C_n(\boldsymbol{\mu}, f_Q^0) = \frac{1}{n} \sup_{f_{\boldsymbol{\Theta}|\boldsymbol{Q}}(\boldsymbol{\theta}|\boldsymbol{q})} I(Q_1^n, \Theta_1^n; R_1^n, \Psi_1^n) \tag{E.21}$$
$$= \frac{1}{n} \sup_{f_{\boldsymbol{\Theta}'|\boldsymbol{Q}}(\boldsymbol{\theta}'|\boldsymbol{q})} I(Q_1^n, \Theta'^n_1; R_1^n, \Psi'^n_1) \tag{E.22}$$
$$= \frac{1}{n} \sup_{f_{\boldsymbol{\Theta}'|\boldsymbol{Q}}(\boldsymbol{\theta}'|\boldsymbol{q})} [h(R_1^n, \Psi'^n_1) - h(R_1^n, \Psi'^n_1|Q_1^n, \Theta'^n_1)], \tag{E.23}$$

where the mutual information in (E.21) is to be calculated using input probability distributions of the form $f_Q^0(\boldsymbol{q}) f_{\boldsymbol{\Theta}|\boldsymbol{Q}}(\boldsymbol{\theta}|\boldsymbol{q})$, and the mutual information and differential entropies in (E.22) and (E.23) are to be calculated using input probability distributions of the form $f_Q^0(\boldsymbol{q}) f_{\boldsymbol{\Theta}'|\boldsymbol{Q}}(\boldsymbol{\theta}'|\boldsymbol{q})$, the Theorem will be proved if we show that the supremum in (E.23) can be achieved by the probability distribution

$$f^0_{\boldsymbol{\Theta}'|\boldsymbol{Q}}(\boldsymbol{\theta}'|\boldsymbol{q}) = \prod_{i=1}^{n} f^0_{\Theta'_i}(\theta'_i), \tag{E.24}$$

with $f^0_{\Theta'_i}(\theta'_i)$ i.i.d. and uniform on $[0, 2\pi)$, since if Θ'^n_1 is i.i.d. and uniformly distributed on $[0, 2\pi)$, then so is Θ_1^n. In order to do this, we will prove that for any given n and $f_Q^0(\boldsymbol{q})$, $h(R_1^n, \Psi'^n_1|Q_1^n, \Theta'^n_1)$ is independent of $f_{\boldsymbol{\Theta}'|\boldsymbol{Q}}(\boldsymbol{\theta}'|\boldsymbol{q})$, whereas $h(R_1^n, \Psi'^n_1)$ is maximised by choosing $f_{\boldsymbol{\Theta}'|\boldsymbol{Q}}(\boldsymbol{\theta}'|\boldsymbol{q}) = f^0_{\boldsymbol{\Theta}'|\boldsymbol{Q}}(\boldsymbol{\theta}'|\boldsymbol{q})$.

At this stage, it is important to make the following two observations. First, the set of constraints (E.2) being independent of Θ_1^n (and consequently

also of Θ'^n_1), one need not be concerned with them when seeking the probability distribution $f_{\boldsymbol{\Theta}'|\boldsymbol{Q}}(\boldsymbol{\theta}'|\boldsymbol{q})$ which achieves the supremum in (E.23). Second, it is easy to see by direct examination of (E.20) that $f_{\boldsymbol{R},\boldsymbol{\Psi}'|\boldsymbol{Q},\boldsymbol{\Theta}'}(\boldsymbol{r},\boldsymbol{\psi}'|\boldsymbol{q},\boldsymbol{\theta}')$ depends neither on Θ'_1 nor on Ψ'_1. (This was the reason for making the coordinate change (E.19).) Consequently, $I(Q^n_1,\Theta'^n_1;R^n_1,\Psi'^n_1)$ is independent of $f_{\Theta'_1|Q,\Theta'_2,\ldots\Theta'_n}(\theta'_1|\boldsymbol{q},\theta'_2,\ldots,\theta'_n)$. We are thus free to choose $f_{\Theta'_1}(\theta'_1)$ independent of $\boldsymbol{Q}$ and $\Theta'_2,\ldots\Theta'_n$, uniformly distributed on $[0,2\pi)$.

Now, we have that

$$h(R^n_1,\Psi'^n_1|Q^n_1,\Theta'^n_1) = -\iiint f_{\boldsymbol{Q},\boldsymbol{\Theta}'}(\boldsymbol{q},\boldsymbol{\theta}')\ \times \underbrace{\left[\int f_{\boldsymbol{R},\boldsymbol{\Psi}'|\boldsymbol{Q},\boldsymbol{\Theta}'}(\boldsymbol{r},\boldsymbol{\psi}'|\boldsymbol{q},\boldsymbol{\theta}')\ \log f_{\boldsymbol{R},\boldsymbol{\Psi}'|\boldsymbol{Q},\boldsymbol{\Theta}'}(\boldsymbol{r},\boldsymbol{\psi}'|\boldsymbol{q},\boldsymbol{\theta}')\,\mathrm{d}\boldsymbol{\psi}'\right]}_{B}\,\mathrm{d}\boldsymbol{r}\,\mathrm{d}\boldsymbol{\theta}'\,\mathrm{d}\boldsymbol{q} \tag{E.25}$$

with $\mathrm{d}\boldsymbol{\psi}' \triangleq \mathrm{d}\psi'_1\cdots\mathrm{d}\psi'_n$, similar definitions for $\mathrm{d}\boldsymbol{r}$, $\mathrm{d}\boldsymbol{\theta}'$, and $\mathrm{d}\boldsymbol{q}$, integration with respect to θ'_i and ψ'_i being performed over the interval $[0,2\pi)$ for all $1\le i\le n$, and integration with respect to r_i and q_i being performed over the interval $[0,\infty)$ for $1\le i\le n$. To prove that $h(R^n_1,\Psi'^n_1|Q^n_1,\Theta'^n_1)$ is independent of $f_{\boldsymbol{\Theta}'|\boldsymbol{Q}}(\boldsymbol{\theta}'|\boldsymbol{q})$, the key lies in noting that the term labelled B in (E.25) becomes independent of $\boldsymbol{\theta}'$ once the integrals between square brackets have been performed. This is a direct consequence of the fact that expressions of the form

$$\int_0^{2\pi} g(f_{\boldsymbol{R},\boldsymbol{\Psi}'|\boldsymbol{Q},\boldsymbol{\Theta}'}(\boldsymbol{r},\boldsymbol{\psi}'|\boldsymbol{q},\boldsymbol{\theta}'))\,\mathrm{d}\psi'_k, \tag{E.26}$$

with $f_{\boldsymbol{R},\boldsymbol{\Psi}'|\boldsymbol{Q},\boldsymbol{\Theta}'}(\boldsymbol{r},\boldsymbol{\psi}'|\boldsymbol{q},\boldsymbol{\theta}')$ given in (E.20), $k\in\{1,\ldots,n\}$, and $g:\mathbb{R}\to\mathbb{R}$ any continuous function, are independent of the value of θ'_k. Indeed, it can be seen by looking at (E.20) that $f_{\boldsymbol{R},\boldsymbol{\Psi}'|\boldsymbol{Q},\boldsymbol{\Theta}'}(\boldsymbol{r},\boldsymbol{\psi}'|\boldsymbol{q},\boldsymbol{\theta}')$ is a periodic function of ψ'_k (with period 2π) for all $k\in\{1,\ldots,n\}$; and thus the fact that (E.26) is independent of θ'_k becomes obvious if one sets for example $\psi''_k=\psi'_k-\theta'_k$ before performing the integration. $h(R^n_1,\Psi'^n_1|Q^n_1,\Theta'^n_1)$ is therefore independent of $f_{\boldsymbol{\Theta}'|\boldsymbol{Q}}(\boldsymbol{\theta}'|\boldsymbol{q})$ as we claimed above.

We now turn our attention to the term $h(R^n_1,\Psi'^n_1)$. We have

$$\begin{aligned} h(R^n_1,\Psi'^n_1) &= h(R^n_1)+h(\Psi'^n_1|R^n_1) && \text{(E.27)}\\ &\le h(R^n_1)+h(\Psi'^n_1) && \text{(E.28)}\\ &\le h(R^n_1)+\sum_{i=1}^n h(\Psi'_i) && \text{(E.29)}\\ &\le h(R^n_1)+n\log 2\pi && \text{(E.30)} \end{aligned}$$

where inequality (E.28) is satisfied with equality if Ψ'^n_1 is independent from R^n_1, inequality (E.29) is satisfied with equality if the random variables in the sequence Ψ'^n_1 are mutually independent, and inequality (E.30) is satisfied with equality if Ψ'_i is uniformly distributed on $[0, 2\pi)$ for all $i \in \{1, \ldots, n\}$. We now show that these conditions are met if one chooses $f_{\boldsymbol{\Theta}'|Q}(\boldsymbol{\theta}'|\boldsymbol{q}) = f^0_{\boldsymbol{\Theta}'|Q}(\boldsymbol{\theta}'|\boldsymbol{q})$, which is given in (E.24). We then have

$$f_{\boldsymbol{R},\boldsymbol{\Psi}'}(\boldsymbol{r},\boldsymbol{\psi}') = \frac{1}{(2\pi)^n} \quad \times \tag{E.31}$$
$$\int_0^\infty \cdots \int_0^\infty f^0_Q(\boldsymbol{q}) \left[\int_0^{2\pi} \cdots \int_0^{2\pi} f_{\boldsymbol{R},\boldsymbol{\Psi}'|Q,\boldsymbol{\Theta}'}(\boldsymbol{r},\boldsymbol{\psi}'|\boldsymbol{q},\boldsymbol{\theta}')\, \mathrm{d}\boldsymbol{\theta}' \right] \mathrm{d}\boldsymbol{q},$$

with $\mathrm{d}\boldsymbol{\theta}' = \mathrm{d}\theta'_1 \cdots \mathrm{d}\theta'_n$ and $\mathrm{d}\boldsymbol{q} = \mathrm{d}q_1 \cdots \mathrm{d}q_n$. Now, using an argument identical to that used when discussing $h(R^n_1, \Psi'^n_1|Q^n_1, \Theta'^n_1)$, it can be seen that the expression in square brackets in (E.31) is independent of $\boldsymbol{\psi}'$. This implies that $f_{\boldsymbol{R},\boldsymbol{\Psi}'}(\boldsymbol{r},\boldsymbol{\psi}')$ can be written in the form

$$f_{\boldsymbol{R},\boldsymbol{\Psi}'}(\boldsymbol{r},\boldsymbol{\psi}') = \frac{1}{(2\pi)^n}\, f_{\boldsymbol{R}}(\boldsymbol{r}). \tag{E.32}$$

The above expression can now be used to verify that the conditions which are required for inequalities (E.28), (E.29), and (E.30) to hold with equality indeed are met. □

The problem of finding the distribution $f_X(\boldsymbol{x})$ ($f_{Q,\Theta}(\boldsymbol{q},\boldsymbol{\theta})$ in polar coordinates) which achieves the supremum in (E.7) has thus been reduced to finding the magnitude distribution $f_Q(\boldsymbol{q})$ such that $f_Q(\boldsymbol{q}) f^0_{\boldsymbol{\Theta}|Q}(\boldsymbol{\theta}|\boldsymbol{q})$, with $f^0_{\boldsymbol{\Theta}|Q}(\boldsymbol{\theta}|\boldsymbol{q})$ chosen as suggested in Theorem E.1, achieves the supremum in (E.7).

5 Discussion

In this section, we would like to make a few remarks concerning $I(Q^n_1, \Theta^n_1; R^n_1, \Psi^n_1)$. If we select $f_{Q,\boldsymbol{\Theta}}(\boldsymbol{q},\boldsymbol{\theta}) = f_Q(\boldsymbol{q})/(2\pi)^n$, the results from Sec. 3 show that we can write

$$\begin{aligned} I(Q^n_1, \Theta^n_1; R^n_1, \Psi^n_1) &= h(R^n_1, \Psi^n_1) - h(R^n_1, \Psi^n_1|Q^n_1, \Theta^n_1) && \text{(E.33)}\\ &= h(R^n_1) + h(\Psi^n_1|R^n_1) - h(R^n_1|Q^n_1, \Theta^n_1) \\ &\quad - h(\Psi^n_1|R^n_1, Q^n_1, \Theta^n_1) && \text{(E.34)}\\ &= h(R^n_1) - h(R^n_1|Q^n_1) \\ &\quad + h(\Psi^n_1) - h(\Psi^n_1|R^n_1, Q^n_1, \Theta^n_1), && \text{(E.35)} \end{aligned}$$

where the equality $h(R_1^n|Q_1^n,\Theta_1^n) = h(R_1^n|Q_1^n)$ follows from the fact that $f_{\boldsymbol{R}|Q,\boldsymbol{\Theta}}(\boldsymbol{r}|\boldsymbol{q},\boldsymbol{\theta}) = f_{\boldsymbol{R}|Q}(\boldsymbol{r}|\boldsymbol{q})$, which can be proved using arguments similar to those employed in the proof of Theorem E.1. Moreover, note that although, when selecting $f_{Q,\boldsymbol{\Theta}}(\boldsymbol{q},\boldsymbol{\theta}) = f_Q(\boldsymbol{q})/(2\pi)^n$, the random sequences Ψ_1^n and R_1^n are independent as shown in Sec. 3, Ψ_1^n and R_1^n are *not* conditionally independent[2] given (Q_1^n,Θ_1^n). For example, when $p = 1$, $n = 2$, $\sigma_w^2 = \sigma_z^2 = 1$, and $\alpha_1 \in \mathbb{R}$, a routine computation (bearing in mind the fact that $\int_0^{2\pi} \exp(a\cos\xi)\,\mathrm{d}\xi = 2\pi I_0(a)$, where $I_0(\cdot)$ is the zeroth order modified Bessel function of the first kind [GR00]) shows that in such a case

$$f_{\boldsymbol{\Psi}|\boldsymbol{R},Q,\boldsymbol{\Theta}}(\boldsymbol{\psi}|\boldsymbol{r},\boldsymbol{q},\boldsymbol{\theta}) = \frac{\exp\left[\dfrac{2\alpha_1 r_1 r_2 q_1 q_2 \cos(\theta_1-\theta_2+\psi_2-\psi_1)}{q_1^2 q_2^2(1-\alpha_1^2)+q_1^2+q_2^2+1}\right]}{4\pi^2 I_0\left[\dfrac{2\alpha_1 r_1 r_2 q_1 q_2}{q_1^2 q_2^2(1-\alpha_1^2)+q_1^2+q_2^2+1}\right]}, \tag{E.36}$$

which clearly depends on r_1 and r_2.

We can interpret

$$h(R_1^n) - h(R_1^n|Q_1^n) \tag{E.37}$$

as the information carried by the magnitude of the input signal, and

$$h(\Psi_1^n) - h(\Psi_1^n|R_1^n,Q_1^n,\Theta_1^n) \tag{E.38}$$

as the information carried by the phase of the input signal. It is interesting to remark that although $f_{\boldsymbol{\Theta}|Q}(\boldsymbol{\theta}|\boldsymbol{q})$ can be chosen independently of $f_Q(\boldsymbol{q})$ in order to maximise the information which can be carried by X_1^n, one apparently has to take into account the minimisation of the value of $h(\Psi_1^n|R_1^n,Q_1^n,\Theta_1^n)$ (in addition to maximising $h(R_1^n) - h(R_1^n|Q_1^n)$) when seeking $f_Q(\boldsymbol{q})$.

One can for example see this by examining the channel (E.1) under the average power constraint (E.4), with $p = 1$, $\alpha_1 = \frac{1}{3}$ and $P = \sigma_w^2 = \sigma_z^2 = 1$. By considering for the case $n = 2$ (with $f_{\boldsymbol{\Theta}|Q}(\boldsymbol{\theta}|\boldsymbol{q})$ chosen as suggested in Theorem E.1) the family of probability mass functions

$$f_Q(\boldsymbol{q}) = \beta_1\delta(q_1)\delta(q_2) + (1-\beta_1)\delta(q_1-\beta_2)\delta(q_2-\beta_2), \tag{E.39}$$

where $\delta(\cdot)$ is the Dirac delta function, and $1 \geq \beta_1 \geq 0$ and $\beta_2 \geq 0$ can be freely chosen as long as the constraint (E.4) is satisfied, one can verify using numerical integration that $h(\Psi_1^2|R_1^2,Q_1^2,\Theta_1^2)$ depends on $f_Q(\boldsymbol{q})$ via the values of β_1 and β_2.

[2] A similar phenomenon occurs for example if, given two independent random variables Ω_1, Ω_2 which are uniformly distributed over $[0,1)$, one considers the random variable $\Omega_3 = (\Omega_1 + \Omega_2) \mod 1$, which also is uniformly distributed over $[0,1)$. Then Ω_3 and Ω_2 are independent, but they are not conditionally independent given Ω_1.

6 Conclusions

In this correspondence, we considered single-input single-output noncoherent Rayleigh-fading channels in which the memory is modelled by an autoregressive process of arbitrary order p, and in which the magnitude of the input signal is constrained in an arbitrary manner. For such channels – which can model a wide variety of practical scenarios – we proved that, for any given input magnitude probability distribution, it is optimum from a capacity perspective to choose the phase of the input distribution independent and identically distributed, with a uniform distribution over the interval $[0, 2\pi)$. This is an interesting complement to previous work on such channels.

Investigating whether or not our results will continue to hold under even more general assumptions than the ones made in this correspondence is a challenging subject for future exploration. For example, the case of Ricean fading and that of single-input multiple-output systems are worthy of consideration.

Appendix A Proof of Lemma E.1

Proof of Lemma E.1: If $\Sigma_{\boldsymbol{Y}|\boldsymbol{X}}^{-1}$ can be written in the form (E.16) – with p_{ij} independent of the values of $\{\arg x_k\}_{k=1}^n$ – the fact that $p_{ij} = p_{ji}^*$ (and hence that $p_{ii} \in \mathbb{R}$) can easily be seen by remembering that the inverse of any invertible Hermitian matrix also is Hermitian. (Indeed, if A is an $n \times n$ invertible Hermitian matrix, we have $AA^{-1} = I_{n\times n} = I_{n\times n}^\dagger = (A^{-1})^\dagger A^\dagger = (A^{-1})^\dagger A$, and consequently $(A^{-1})^\dagger = A^{-1}$.)

The remainder of the proof relies on the identity [AH99]

$$A^{-1} = \frac{1}{\det A} (\operatorname{cof} A)^\mathsf{T} \tag{E.40}$$

valid for any invertible square matrix A, where $\operatorname{cof} A$ designates the cofactor matrix of A, which satisfies[3]

$$(\operatorname{cof} A)_{ij} = (-1)^{i+j} \det A_{ij}^M, \tag{E.41}$$

with A_{ij}^M the minor of matrix A, obtained by deleting the ith row and the jth column of A.

[3]The notation $(\cdot)_{ij}$ is used to designate the element located in position (i, j) of the matrix in the argument. (However, the notation $(\cdot)_{ij}^M$ has a completely different meaning.)

Let us now prove that the elements of $\Sigma^{-1}_{\boldsymbol{Y}|\boldsymbol{X}}$ indeed satisfy the properties stated in Lemma E.1. By (E.40) and (E.41), we have that

$$(\Sigma^{-1}_{\boldsymbol{Y}|\boldsymbol{X}})_{ij} = \frac{1}{\det \Sigma_{\boldsymbol{Y}|\boldsymbol{X}}} \, (-1)^{i+j} \det (\Sigma_{\boldsymbol{Y}|\boldsymbol{X}})^{M}_{ji}. \tag{E.42}$$

For given i and j, we now construct the matrix[4] $(\Sigma_{\boldsymbol{Y}|\boldsymbol{X}})^{M'}_{ji}$ starting from $(\Sigma_{\boldsymbol{Y}|\boldsymbol{X}})^{M}_{ji}$ as follows: for all $k \in \{1, \ldots, n-1\}$,

- if $k < j$, the kth row of $(\Sigma_{\boldsymbol{Y}|\boldsymbol{X}})^{M'}_{ji}$ is taken equal to the kth row of $(\Sigma_{\boldsymbol{Y}|\boldsymbol{X}})^{M}_{ji}$ if $x_k = 0$, and is taken equal to the kth row of $(\Sigma_{\boldsymbol{Y}|\boldsymbol{X}})^{M}_{ji}$ divided by x_k if $x_k \neq 0$.
- if $k \geq j$, the kth row of $(\Sigma_{\boldsymbol{Y}|\boldsymbol{X}})^{M'}_{ji}$ is taken equal to the kth row of $(\Sigma_{\boldsymbol{Y}|\boldsymbol{X}})^{M}_{ji}$ if $x_{k+1} = 0$, and is taken equal to the kth row of $(\Sigma_{\boldsymbol{Y}|\boldsymbol{X}})^{M}_{ji}$ divided by x_{k+1} if $x_{k+1} \neq 0$.

We then construct the matrix $(\Sigma_{\boldsymbol{Y}|\boldsymbol{X}})^{M''}_{ji}$ starting from $(\Sigma_{\boldsymbol{Y}|\boldsymbol{X}})^{M'}_{ji}$ as follows: for all $k \in \{1, \ldots, n-1\}$,

- if $k < i$, the kth column of $(\Sigma_{\boldsymbol{Y}|\boldsymbol{X}})^{M''}_{ji}$ is taken equal to the kth column of $(\Sigma_{\boldsymbol{Y}|\boldsymbol{X}})^{M'}_{ji}$ if $x_k = 0$, and is taken equal to the kth column of $(\Sigma_{\boldsymbol{Y}|\boldsymbol{X}})^{M'}_{ji}$ divided by x^*_k if $x_k \neq 0$.
- if $k \geq i$, the kth column of $(\Sigma_{\boldsymbol{Y}|\boldsymbol{X}})^{M''}_{ji}$ is taken equal to the kth column of $(\Sigma_{\boldsymbol{Y}|\boldsymbol{X}})^{M'}_{ji}$ if $x_{k+1} = 0$, and is taken equal to the kth column of $(\Sigma_{\boldsymbol{Y}|\boldsymbol{X}})^{M'}_{ji}$ divided by x^*_{k+1} if $x_{k+1} \neq 0$.

Referring to the structure of $\Sigma_{\boldsymbol{Y}|\boldsymbol{X}}$ shown in (E.12), a minute of thought should now convince the reader of the fact that for all i, j the matrix $(\Sigma_{\boldsymbol{Y}|\boldsymbol{X}})^{M''}_{ji}$ constructed using the above procedure only has elements which are independent of $\{\arg x_k\}_{k=1}^n$, and hence also has a determinant which is independent of $\{\arg x_k\}_{k=1}^n$. We now distinguish between two different cases:

(i) if $i \neq j$, and $x_i = 0$ or $x_j = 0$, $(\Sigma_{\boldsymbol{Y}|\boldsymbol{X}})^{M}_{ji}$ either possesses a row of zeros or a column of zeros, and hence $\det (\Sigma_{\boldsymbol{Y}|\boldsymbol{X}})^{M}_{ji} = 0$. Consequently, it follows from (E.42) that $(\Sigma^{-1}_{\boldsymbol{Y}|\boldsymbol{X}})_{ij} = 0$. By setting $p_{ij} = 0$, it is easy to see that the properties stated in Lemma E.1 are satisfied for all such elements $(\Sigma^{-1}_{\boldsymbol{Y}|\boldsymbol{X}})_{ij}$.

[4] An example illustrating how this is done is given after the proof.

(ii) if $i = j$, or if $i \neq j$, $x_i \neq 0$, and $x_j \neq 0$, the scaling property of the determinant implies that

$$\det\left(\Sigma_{\boldsymbol{Y}|\boldsymbol{X}}\right)_{ji}^{M} = \det\left(\Sigma_{\boldsymbol{Y}|\boldsymbol{X}}\right)_{ji}^{M''} x_i x_j^* \prod_{\substack{k=1 \\ k\neq i,j;\ x_k\neq 0}}^{n} |x_k|^2, \tag{E.43}$$

when $i \neq j$, and that

$$\det\left(\Sigma_{\boldsymbol{Y}|\boldsymbol{X}}\right)_{ii}^{M} = \det\left(\Sigma_{\boldsymbol{Y}|\boldsymbol{X}}\right)_{ii}^{M''} \prod_{\substack{k=1 \\ k\neq i;\ x_k\neq 0}}^{n} |x_k|^2. \tag{E.44}$$

Bearing in mind (E.42), we see that, when $i \neq j$, $(\Sigma_{\boldsymbol{Y}|\boldsymbol{X}}^{-1})_{ij}$ can be written in the form $x_i x_j^* p_{ij}$, where

$$p_{ij} = \frac{1}{\det \Sigma_{\boldsymbol{Y}|\boldsymbol{X}}} (-1)^{i+j} \det\left(\Sigma_{\boldsymbol{Y}|\boldsymbol{X}}\right)_{ji}^{M''} \prod_{\substack{k=1 \\ k\neq i,j;\ x_k\neq 0}}^{n} |x_k|^2, \tag{E.45}$$

and that $(\Sigma_{\boldsymbol{Y}|\boldsymbol{X}}^{-1})_{ii} = p_{ii}$, with

$$p_{ii} = \frac{1}{\det \Sigma_{\boldsymbol{Y}|\boldsymbol{X}}} \det\left(\Sigma_{\boldsymbol{Y}|\boldsymbol{X}}\right)_{ii}^{M''} \prod_{\substack{k=1 \\ k\neq i;\ x_k\neq 0}}^{n} |x_k|^2. \tag{E.46}$$

A construction similar to the one used to obtain $(\Sigma_{\boldsymbol{Y}|\boldsymbol{X}})_{ji}^{M''}$ from $(\Sigma_{\boldsymbol{Y}|\boldsymbol{X}})_{ji}^{M}$ can be applied to $\Sigma_{\boldsymbol{Y}|\boldsymbol{X}}$ to prove that $\det \Sigma_{\boldsymbol{Y}|\boldsymbol{X}}$ is independent of $\{\arg x_k\}_{k=1}^{n}$ (the procedure is almost identical and hence not included here). Consequently, all elements $(\Sigma_{\boldsymbol{Y}|\boldsymbol{X}}^{-1})_{ij}$ such that $i = j$, or such that $i \neq j$, $x_i \neq 0$, and $x_j \neq 0$ possess the properties stated in Lemma E.1. □

To facilitate the understanding of the main ideas in the proof of Lemma E.1, the following equations illustrate how the calculation of $(\Sigma^{-1}_{\boldsymbol{Y}|\boldsymbol{X}})_{41}$ can be performed. It is assumed that $n = 4$ and that $x_k \neq 0$ for all $k \in \{1, \ldots, n\}$. We then have

$$
\begin{aligned}
(\Sigma^{-1}_{\boldsymbol{Y}|\boldsymbol{X}})_{41} &= -\frac{1}{\det \Sigma_{\boldsymbol{Y}|\boldsymbol{X}}} \cdot \det(\Sigma_{\boldsymbol{Y}|\boldsymbol{X}})^{M}_{14} \\
&= -\frac{1}{\det \Sigma_{\boldsymbol{Y}|\boldsymbol{X}}} \cdot \det \underbrace{\begin{pmatrix} v_1 x_2 x_1^* & v_0|x_2|^2 + \sigma_z^2 & v_1^* x_2 x_3^* \\ v_2 x_3 x_1^* & v_1 x_3 x_2^* & v_0|x_3|^2 + \sigma_z^2 \\ v_3 x_4 x_1^* & v_2 x_4 x_2^* & v_1 x_4 x_3^* \end{pmatrix}}_{(\Sigma_{\boldsymbol{Y}|\boldsymbol{X}})^{M}_{14}} \\
&= -\frac{x_2 x_3 x_4}{\det \Sigma_{\boldsymbol{Y}|\boldsymbol{X}}} \cdot \det \underbrace{\begin{pmatrix} v_1 x_1^* & \frac{v_0|x_2|^2 + \sigma_z^2}{x_2} & v_1^* x_3^* \\ v_2 x_1^* & v_1 x_2^* & \frac{v_0|x_3|^2 + \sigma_z^2}{x_3} \\ v_3 x_1^* & v_2 x_2^* & v_1 x_3^* \end{pmatrix}}_{(\Sigma_{\boldsymbol{Y}|\boldsymbol{X}})^{M'}_{14}} \\
&= -\frac{x_1^* |x_2|^2 |x_3|^2 x_4}{\det \Sigma_{\boldsymbol{Y}|\boldsymbol{X}}} \cdot \det \underbrace{\begin{pmatrix} v_1 & \frac{v_0|x_2|^2 + \sigma_z^2}{|x_2|^2} & v_1^* \\ v_2 & v_1 & \frac{v_0|x_3|^2 + \sigma_z^2}{|x_3|^2} \\ v_3 & v_2 & v_1 \end{pmatrix}}_{(\Sigma_{\boldsymbol{Y}|\boldsymbol{X}})^{M''}_{14}}.
\end{aligned}
$$

References

[ABK02] A. Abdi, J. Barger, and M. Kaveh. A parametric model for the distribution of the angle of arrival and the associated correlation function and power spectrum at the mobile station. *IEEE Transactions on Vehicular Technology*, 51(1):425–434, February 2002.

[AFTS01] I. Abou-Faycal, M. Trott, and S. Shamai (Shitz). The capacity of discrete-time memoryless Rayleigh-fading channels. *IEEE Transactions on Information Theory*, 47(4):1290–1301, May 2001.

[AH99] S. Andrilli and D. Hecker. *Elementary Linear Algebra*. Academic Press, second edition, 1999.

[BB04] K. E. Baddour and N. C. Beaulieu. Autoregressive modeling for fading channel simulation. *IEEE Transactions on Wireless Communications*, 4(4):1650–1662, July 2004.

[BJR94] G. E. P. Box, G. M. Jenkins, and G. C. Reinsel. *Time Series Analysis: Forecasting and Control*. Prentice Hall, third edition, 1994.

[CHM04] R. Chen, B. Hajek, and U. Madhow. On fixed input distributions for noncoherent communication over high-SNR Rayleigh-fading channels. *IEEE Transactions on Information Theory*, 50(12):3390–3396, December 2004.

[CK97] R. H. Clarke and W. L. Khoo. 3-D mobile radio channel statistics. *IEEE Transactions on Vehicular Technology*, 46(3):798–799, August 1997.

[Cla68] R. H. Clarke. A statistical theory of mobile-radio reception. *Bell System Technical Journal*, 47(6):957–1000, July-August 1968.

[GR00] I. S. Gradshteyn and I. M. Ryzhik. *Table of Integrals, Series, and Products*. Academic Press, sixth edition, 2000.

[LM03] A. Lapidoth and S. Moser. Capacity bounds via duality with applications to multiple-antenna systems on flat-fading channels. *IEEE Transactions on Information Theory*, 49(10):2426–2467, October 2003.

[LV04] Y. Liang and V. Veeravalli. Capacity of noncoherent time-selective Rayleigh-fading channels. *IEEE Transactions on Information Theory*, 50(12):3095–3110, December 2004.

[MH99] T. Marzetta and B. Hochwald. Capacity of a mobile multiple-antenna communication link in Rayleigh flat fading. *IEEE Transactions on Information Theory*, 45(1):139–157, January 1999.

[TE97] G. Taricco and M. Elia. Capacity of fading channel with no side information. *Electronics Letters*, 33(16):1368–1370, July 1997.

[Tel95] E. Telatar. Capacity of multi-antenna Gaussian channels. Technical report, AT&T Bell Laboratories, June 1995.

[Zha05] J. Zhang. On the bounds of the non-coherent capacity of Gauss-Markov fading channels. In *Proc. 2005 IEEE International Conference on Acoustics, Speech, and Signal Processing (ICASSP)*, pages 757–760, Philadelphia, March 2005.

[ZT02] L. Zheng and D. Tse. Communication on the Grassmann manifold: A geometric approach to the noncoherent multiple-antenna channel. *IEEE Transactions on Information Theory*, 48(2):359–383, February 2002.